

Modeling and Simulation of Linear and Branched Polysaccharides having Diverse Linkage Patterns by Molecular Dynamics Approach

THESIS

Submitted in partial fulfilment
of the requirements for the degree of
DOCTOR OF PHILOSOPHY

by

P SRUTHI

ID No.: 2018PHXF0014H

Under the supervision of

Prof. Durba Roy



BIRLA INSTITUTE OF TECHNOLOGY AND SCIENCE, PILANI

2024

CERTIFICATE

This is to certify that the thesis entitled “**Modeling and Simulation of Linear and Branched Polysaccharides having Diverse Linkage Patterns by Molecular Dynamics Approach** ” submitted by Miss. **P SRUTHI**, ID No: **2018PHXF0014H** for the award of Ph.D. of the Institute embodies original work done by her under my supervision.

Signature of the supervisor :



Name

: Prof. DURBA ROY

Designation

: Associate Professor

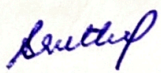
Department of Chemistry

Date

: Jan 17, 2024

DECLARATION

The research work embodied in this thesis entitled “**Modeling and Simulation of Linear and Branched Polysaccharides having Diverse Linkage Patterns by Molecular Dynamics Approach**” has been carried out by me under the supervision of **Prof. Durba Roy**, Department of Chemistry, BITS-Pilani, Hyderabad Campus, India. This work is original and has not been submitted in part or full for any degree to this or any other University.

Signature : 
Name : P Sruthi
Date : 17 JAN 2024

Acknowledgements

In the wise words of a famous saying, “We all have dreams. But in order to make dreams come to reality, it takes an awful lot of determination, self discipline, dedication, effort and support from people around”.

The past five years have been a transformative experience for me, and I owe much of my success to the guidance and support of numerous individuals. First and foremost, I would like to express my gratitude to **God** for the divine guidance, blessings, and good health that enabled me to pursue my dreams.

I am deeply grateful to my mentor, **Prof. Durba Roy**, for her unwavering support and mentorship throughout my research work. It has been a privilege to work in her lab, and I am grateful for the countless opportunities she has presented me. The skills I have acquired by observing her work are truly invaluable and are indeed life lessons. Her dedication, expertise and passion for research has profound impact on my personal and professional growth. I consider it as a fortunate stroke of serendipity to be part of her lab.

I would also like to extend my sincere thanks to my Doctoral Advisory Committee (DAC) members, **Prof. Amit Nag** and **Prof. Manab Chakravarty** for their invaluable suggestions, guidance throughout the tenure. They have been approachable and ready to help. I wish to extend my gratitude to **Prof. Sounak Roy**, Head, Department of Chemistry and the Doctoral Research Committee (DRC) members for their consistent and constructive feedback during the research work.

I thank my fellow labmates **Dr. Karuna Anna S., Sravani N, Sidhanth K P, Rituparna Hazra, Jayapriya V, Dinesh Kumar J** for their stimulating discussions, patience and camaraderie.

I am thankful to the administrative personnel of **Birla Institute of Technology and Science-Pilani**, Hyderabad Campus for their services towards the smooth progress of my research work. I would also like to acknowledge BITS-Pilani, Hyderabad for the fellowship and infrastructure facilities.

Expressing my gratitude towards my family feels insufficient, as words cannot fully capture the depth of my appreciation for their unwavering love, care, sacrifices, and understanding, which have been the bedrock of my success. My parents, **Vijay Shekar & Satya Kameswari P**, and grandparents, **Subramanyam & Sita Y**, have been instrumental in

my journey, believing in me and providing me with unwavering support. Their belief in me has been a constant source of motivation, pushing me to reach new heights and persevere through challenges. Their love and support has been my driving force, and I am truly blessed to have them by my side. I am deeply indebted to them for their constant support and encouragement. I am also immensely grateful to my husband, **Krishna Kiriti N**, for believing in my dreams and helping me turn them into reality. Special thanks to my uncle, **Sai Phani Y**, for always having my back. Lastly, this journey would have been incomplete without the persistent support of my brother, **Abhishek P**, and my loving daughter, **Sirisha N**. Without each of you, this journey would have been incomplete, and I am honoured to have such incredible individuals in my life.

Abstract

Polysaccharides known for their diverse functional attributes, hold immense promise across various domains, from biomedical applications to food technology. This thesis delves into the comprehensive investigation of structural, dynamical, and mechanical properties of α and β -glucans.

The primary focus of this thesis revolves around elucidating the behavior of α and β -glucan strands within aqueous environments, mirroring the prevalent conditions in biological systems. Structural characterization involves meticulous analyses of intermolecular and intramolecular hydrogen bonding, end-to-end distance determination, and root mean square deviation, unravelling the intricacies of individual strands. Employing principal component analysis, the dynamics of these glucan strands are scrutinized, offering insights into their conformational variability and behavior. Particularly intriguing is the study of the interaction between bile acid clusters and polysaccharides, especially β -glucans known for their potential in mitigating dyslipidemia and metabolic syndromes. Spectroscopic signatures, such as ^1H NMR chemical shifts and small-angle scattering profiles, are computed and compared with experimental data to enrich our understanding of this interaction.

Furthermore, the thesis illuminates mechanical attributes of polysaccharides take center stage, focusing on delineating the influence of glycosidic linkage type and anomericity of monomers on elasticity. Employing steered molecular dynamics (SMD) simulations, force-extension (F-E) curves are generated and validated against atomic force microscopy (AFM) results. Density functional theory (DFT) calculations complement the SMD simulations by estimating single-point energies of conformers during polysaccharide stretching.

The unique synergy between computational modelling and experimental validation in this thesis lays a solid foundation for future advancements in designing novel polysaccharide-based materials, drug delivery systems, and therapeutic interventions, poised to significantly impact diverse industries and biomedical domains.

Contents

Certificate	ii
Declaration	iii
Acknowledgements	iv
Abstract	vi
Contents	vii
List of Tables	x
List of Figures	xi
List of Abbreviations	xvii
1 Introduction	1
1.1 Introduction to carbohydrates	2
1.2 Extraction of polysaccharides	5
1.3 Synthesis of polysaccharides	6
1.3.1 Chemical synthesis of polysaccharides	6
1.3.2 Enzymatic synthesis of polysaccharides	7
1.4 Analysis techniques	8
1.5 Simulation studies on saccharides	8
1.5.1 Structure and energetics of <i>D</i> -glucose	9
1.5.2 Studies on glucose based disaccharides and beyond	13
1.6 β -glucan bile acid interactions	15
1.7 Force spectroscopy of polysaccharides	17
1.8 Polysaccharide membranes	19
1.9 Thesis overview	21
2 Methodology	22
2.1 Molecular Dynamics	23
2.2 Steered Molecular Dynamics Simulations	25
2.3 Modelling of initial configurations	27
2.4 Simulation details	28
2.5 Analysis techniques	31

2.5.1	Principal component analysis (PCA)	31
2.5.2	3x3x3 Simulation cell to account for boundary crossing artefacts of soft clusters	33
2.5.3	Moment of inertia and shape anisotropy	33
2.5.4	Small angle scattering profiles	34
3	Relation between glycosidic linkage, structure and dynamics of α and β-glucans in water	36
3.1	Introduction	37
3.2	Methodology	39
3.2.1	Modeling of oligosaccharides	39
3.2.2	Simulation software, parameters and force fields	40
3.3	Results and discussion	40
3.4	Conclusion	52
4	Structural and spectroscopic details of polysaccharide–bile acid composites from molecular dynamics simulations	53
4.1	Introduction	54
4.2	Methodology	56
4.2.1	Modelling of the polysaccharide, cholic acid and sodium cholate	56
4.2.2	Simulation parameters and force field	56
4.2.3	Software and data analysis	57
4.3	Results and discussions	57
4.3.1	Molecular arrangements of Ch and NaCh in water and impact of polysaccharide	58
4.3.2	Time evolution of the shape and size of the bile acid and β -glucan composites	59
4.3.3	Moment of inertia and shape anisotropy	61
4.3.4	Small angle scattering profiles of the Ch self-assembly and other biliary components	63
4.3.5	NMR chemical shifts of Ch in absence and presence of β -glucan	64
4.4	Conclusion	68
5	Control of anomericity and glycosidic linkage on the mechanics of polysaccharides	69
5.1	Introduction	70
5.2	Simulation methodology	72
5.3	Results and discussion	73
5.3.1	Monosaccharide variants and the glycosidic linkages	73
5.3.2	Force-extension (F-E) curves: comparison of SMD and AFM data	74
5.3.3	Glycosidic dihedrals and Cremer-pople pyranose ring puckering parameters	77
5.3.4	Structure and energetics of the monosaccharide conformers along an SMD trajectory	81
5.4	Conclusion	84

6	Characterizing the mechanical properties of natural polysaccharides through steered molecular dynamics	86
6.1	Introduction	87
6.2	Simulation methodology	89
6.3	Results and discussion	90
6.3.1	Structural properties of the variants	90
6.3.2	Force-extension curves, comparison of SMD and AFM	92
6.3.3	Glycosidic dihedrals and Cremer Pople puckering under stretched conditions	95
6.3.4	Structure and energetics of the monosaccharide conformers across the SMD trajectory	96
6.4	Temperature varying SMD simulations of Chitin, Galactose and Pectin	100
6.5	Conclusion	100
7	Conclusions and Future Perspectives	102
	Bibliography	108
A	Appendix	132
A.1	GROMACS input file	133
A.2	NAMD input file	134
A.3	SMD input file	135
A.4	SMD tcl script	136
A.5	Matlab script for ‘big-box’ calculation	138
A.6	Coordination number calculation	140
A.7	Radius of gyration of the biggest cluster	142
A.8	Scattering profile calculation	143
	List of Publications	145
	List of Conferences	146
	Biography	147

List of Figures

1.1	Some examples of everyday carbohydrates. Images source: www.lecturio.com , wikipedia.org , www.cnbc.com , www.vectorstock.com	2
1.2	Representation of glycosidic bond formation from two β - <i>D</i> -glucose monosaccharides. Numbering (in green) is for ring carbons.	3
1.3	Glycosidic linkages formed by α and β glucose molecules.	4
1.4	Different configurations of <i>D</i> -glucose.	9
1.5	Configurations of <i>D</i> -glucopyranose. (a)Fisher projection of open chain glucose, (b)Haworth projection and (c) 4C_1 Chair conformation of both anomers.	10
1.6	Rotamers exhibited by the three bond 1 \rightarrow 6 glycosidic linkage.	10
1.7	The spherical coordinate system representing the Cremer-Pople puckering parameters for the six membered pyranose rings.	11
1.8	Cremer Pople and Mercator representation representation of glucopyranose ring	12
1.9	Schematic representation of 1 \rightarrow 4 glycosidic bond between two α -glucose residues.	13
1.10	Representative units of (a)Oat-Celotriosyl units, (b)Barley-Celotetrosyl units and (c)Mushroom based motif.	15
1.11	One dimensional constant velocity pulling. The dummy atom is coloured red and SMD atom is coloured purple. As constant velocity is applied on dummy atom, SMD atom experiences the force which is a linear function of distance between both the atoms.	18
2.1	Simulations at different levels of resolutions and their applicability at different time scales.	23
2.2	Schematic of an AFM experiment to measure the force-extension curve of a macromolecule.	26
2.3	Step by step procedure involved from sample preparation to analysis	27
2.4	van der Waals potential graph with and without application of switching function.	28
2.5	Electrostatics potential graph when full electrostatics are used.	29
2.6	Difference between cutoff and pairlist distance.	30
3.1	39
3.2	RMSD plots of oligosaccharides (without Hydrogen).	41
3.3	Dihedral angle (ϕ, ψ) distributions of oligosaccharides.	42

3.5	Polar plot showing the variation of the Cremer-Pople pseudorotation(θ), and phase angles (φ), (in degrees) for the different oligosaccharides under consideration. 1→3 linked (Red); 1→4 linked (Green) and 1→6 linked (Blue)	44
3.4	ω dihedral angle distributions (in degree) for the oligosaccharides having 1→6 glycosidic linkage.	44
3.6	(top)Variation of end-to-end distance per residue (bottom)Variation of Radius of gyration per residue.	45
3.7	Solvent accessible surface areas per residue of the oligosaccharides under consideration.	45
3.8	(A)Intra molecular H-bonding, (B)Inter molecular H-bonding.	46
3.9	Depiction of glycosidic oxygen atoms along oligosaccharide chain	46
3.10	Eigenvalue Scree plot showing the weightage of the different principal components in the overall dynamical space for the oligosaccharides under consideration	47
3.11	Distribution of scores for the 4000 snapshots collected from 40 ns simulation trajectory in the PC1 to PC2 dynamical space for the different variants of oligosaccharides under study.	48
3.13	(a)Pictorial representation of the contribution of each oligosaccharide residue towards PC1. For generating this data, PCA is done using the Cartesian coordinates of the backbone glycosidic oxygen atoms. The colorbar is common to all the different oligosaccharides under consideration and the data is normalized for easy comparison. AGLC and BGLC refer respectively to α or β -D glucopyranoside unit and the number denotes the residue. (b)Loadings of the oligosaccharide residues towards PC1 as obtained from PCA using Cartesian coordinates.	49
3.12	Residue loadings for the different oligosaccharides using internal coordinates toward the first two principal components: PC1 (blue) and PC2 (red). . .	49
3.14	Cross correlation plots as calculated by linear mutual information for all the different oligosaccharides. The non-correlated and anti-correlated movements are both reduced to zero in this approach.	50
3.15	K-means clustering performed on the dynamical space spanned by PC1 and PC2. The conformations closest to the centroid in each cluster are shown. Color-codes for the clusters are as following: cluster-1 (Red); cluster-2 (Green); cluster-3 (Cyan) and cluster-4 (Blue).	51
3.16	Lowest energy conformation of hydrated oligosaccharides under consideration. The oligosaccharides are represented by twister and paper-chain representations to depict the twist along the oligosaccharide chain and the puckering of the glucopyranose ring.	52
4.1	Molecular structures of (A) the polysaccharide (β -glucan) having mixed 1→4/1→3 glycosidic linkages connecting ten units of β -D-glucopyranose; (B) Cholic acid (Ch) and (C) Sodium cholate (NaCh)	58

4.2	Radial distribution functions showing the molecular arrangements in the β -glucan-bile composites. The C_8 , C_2 , O_1 and O_3 atoms are on Ch and NaCh, as depicted in Figure 4.1. O_6 is the hydroxyl oxygen on C_6 of the β -D-glucopyranose residue in the polysaccharide. O_w denotes the oxygen atom of TIP3P water.	59
4.3	Time evolution of the radius of gyration of the assembly of bile components in presence or absence of β -glucan: (Left) considering all the Ch or NaCh molecules in the box; (Right) considering only those Ch molecules which are part of the biggest cluster.	60
4.4	(Left)Time evolution of the coordination number (Right) Normal (solid line) and cumulative (marker) distributions of coordination number of Ch in the biggest cluster in presence and absence of β -glucan.	60
4.5	Snapshots from the simulation trajectory of NaCh (pink, Top panel) and Ch (blue, Bottom panel) in presence of β -glucan (green) strands at different time domains. The ‘starting structure’ marks that at the beginning of the production runs.	61
4.6	Principal components of the moment of inertia along the simulation trajectory. The biggest cluster evolves as a compact asymmetric ellipsoid. I_{Tot} denotes the sum of the three components.	62
4.7	Shape anisotropy of the biggest cluster of Ch molecules as it evolved along the trajectory in presence (Brown) and absence (Blue) of β -glucan. Snapshots of the biggest Ch cluster at different time instants are shown in VDW representation: Carbon (cyan spheres), Hydrogen (white spheres) and Oxygen (red spheres).	62
4.8	Small angle scattering profiles of Ch in presence and absence of β -glucan. Compared with the simulated data are the experimental SAXS profiles of glycoche-nodeoxycholate (GCDC), <i>L</i> -Phe conjugated bile acid, α/β - <i>L</i> -PheC and sodium taurodeoxycholate (NaTDC)[34, 35, 65].	63
4.9	Snapshots isolated from molecular dynamics trajectories subjected to DFT calculations. The protons having a change in NMR chemical shift ($\Delta\delta$) values $> \pm 0.5$ ppm are shown. Protons experiencing downfield shifts (orange); upfield shifts (yellow).	64
4.10	Snapshot from the molecular dynamics trajectory from which smaller assemblies are scooped out and subjected to DFT calculations. Charge distributions are indicated for: (A-C) Ch- β -glucan assemblies; (D-F) Ch-Ch assemblies. The colour bar denotes the extent of the partial charges. The black ellipse in structures A, B and C encircles the disaccharide domain in the molecular assemblies.	65
4.11	Comparison of hydrogen bond distributions in Ch/NaCh in presence and absence of β -glucan. Competition between lipid-lipid (LL), lipid- β -glucan (LO) and lipid-solvent (LS) hydrogen bonding is evident.	66
4.12	Interplay of non-bonding interaction energies (electrostatic and vdW) for different combinations of molecules.	68
5.1	Colour code for various puckering conformations	71

5.2	Starting conformations of the steered molecular dynamics simulations for the different polysaccharide strands.	74
5.3	Extension of the different polysaccharide strands under pulling stress. The extension of a polysaccharide chain is measured per ring as: $\Delta l = (l_f - l_i)/15$, where l_i and l_f , respectively stand for the initial length of the polysaccharide and that at a given time instant.	74
5.4	Conformational transitions for a selected residue (R2) of the different polysaccharides in a particular SMD trajectory. The initial structure is the one obtained from the starting conformation. The final structure is the one reached at ~ 2100 pN force. The percentage increase in glycosidic bond length is given. The glycosidic oxygen atoms, labelled as red vdW spheres, are used to calculate the glycosidic bond length.	75
5.5	Extension of the different polysaccharide strands under pulling stress. Five different starting structures are shown for each system. The extension of a polysaccharide chain is measured in the same way as in Figure 5.3. . . .	75
5.6	Comparison of the extension profiles of different polysaccharides as obtained from AFM studies[38, 39] and SMD simulations from this work. Here, the normalized length of the polysaccharides is defined as: $l = l_t/l_f$, where, l_t stands for the length of the polysaccharide against a given pulling force at a particular time instant. l_f stands for the final length of the polysaccharide that is achieved after 5 ns of SMD simulation. The experimental curve is normalized by making the experimentally observed extension at the highest force reported equal to that observed in SMD simulations at the same force.	76
5.7	Carbohydrate Ramachandran plots of SMD simulations for the dihedral angle (ϕ, ψ) distributions for oligosaccharides containing 15 α or β -D-glucopyranosyl units linked by the different glycosidic linkages at 310 K in water. The plots are globally normalized with respect to population of snapshots and the same color bar is applicable to all. Hence the color distributions for all the plots are comparable to each other.	77
5.8	Carbohydrate ramachandran plots as obtained from equilibrium simulations for the dihedral angle (ϕ, ψ) distributions for oligosaccharides containing 15 α or β -D-glucopyranosyl units linked by different glycosidic linkages. . .	78
5.9	Distribution of the Cremer-Pople puckering angles of the SMD simulations for the different types of polysaccharides. The puckering angles of all the residues for the 15-mer polysaccharide chain along the entire simulation trajectory are considered here. The Mercator representation is used to indicate whether a snapshot belongs to a boat or skew-boat conformation.	79
5.10	Distribution of the Cremer-Pople puckering angles of SMD simulations for the different types of β -polysaccharides. The puckering angles of all the residues for the 15-mer polysaccharide chain along the entire simulation trajectory are tracked here. The conformations are color-coded based on their time of appearance.	80

5.11	Distribution of the Cremer-Pople puckering angles of the SMD simulations for the different types of α -polysaccharides. The puckering angles of all the residues for the 15-mer polysaccharide chain along the entire simulation trajectory are tracked here. The conformations are color-coded based on their time of appearance.	80
5.13	Extension of a β -1 \rightarrow 4 linked glucopyranoside strand under pulling stress.	81
5.12	82
5.14	Conformational transitions for selected residues (R_i) of an α -1 \rightarrow 6 linked glucopyranoside along the simulation trajectory under pulling stress. The time instant (ps) and the force (pN) are denoted. Below each structure, energy (Hartree) and the glycosidic bond length (\AA) are given.	82
5.15	Conformational transitions for selected residues (R_i) of an β -1 \rightarrow 2 linked glucopyranoside along the simulation trajectory under pulling stress. The time instant (ps) and the force (pN) are denoted. Below each structure, energy (Hartree) and the glycosidic bond length (\AA) are given.	83
5.16	Conformational transitions for selected residues (R_i) of an β -1 \rightarrow 4 linked glucopyranoside along the simulation trajectory under pulling stress. The time instant (ps) and the force (pN) are denoted. Below each structure, energy (Hartree) and the glycosidic bond length (\AA) are given.	83
5.17	Extension of three representative classes of β -D-glucopyranoside strands under pulling stress. The force (pN) is depicted beside each strand. The color of each glucopyranose ring denotes the instantaneous conformation as explained in Figure 5.1. The glycosidic linkage involved is given in each panel.	84
6.1	Individual building blocks for the structures generated. The structure and its graphical notation are given for all the monomeric variants part of this study.	88
6.2	Repetitive units used for the construction of the polysaccharide strands.	89
6.3	Carbohydrate ramachandran plot for the dihedral angle (φ, ψ) distributions of oligosaccharides containing 15 residues in the backbone chain (16 in case of gellan) as obtained from equilibrium simulations at 310 k in water. The colour distributions for all the plots are normalised.	91
6.4	Cremer-Pople puckering angle distribution of all the backbone residues for the various oligosaccharides as obtained from equilibrium simulations under consideration. The puckering angles for all the residues along the entire simulation trajectory are considered here.	91
6.5	92
6.6	End-to-end distance of different polysaccharide strand under pulling stress	93
6.7	Comparison of the extension profiles of different polysaccharides as obtained from AFM studies[31, 32] and our SMD simulations. Here, the normalized length of the polysaccharides is defined as: $l = l_t/l_f$, where, l_t stands for the length of the polysaccharide against a given pulling force at a particular time instant. l_f stands for the final length of the polysaccharide that is achieved after 4 ns of SMD simulation. The experimental curve is normalized by making the experimentally observed extension at the highest force reported equal to that observed in SMD simulations at the same force.	93

6.8	Conformational transitions for selected residue (R2) of different oligosaccharides in a particular SMD trajectory. The color code of the conformations is based on Figure 6.9	94
6.9	Colour followed to track the conformations across the simulations	94
6.10	Carbohydrate ramachandran plot for the dihedral angles (φ , ψ) distributions of oligosaccharides containing 15 residues in the backbone chain (16 in case of gellan) as obtained from SMD simulations at 310 k in water.	95
6.11	Cremer pople puckering angles distribution of all residues of all the oligosaccharide variants studied as obtained from SMD simulations at 310 k in water.	95
6.12	Cremer Pople puckering angles distribution of all residues of all the oligosaccharide variants studied as obtained from SMD simulations at 310 k in water. The conformations are color coded based on the time of appearance.	96
6.13	97
6.14	Extension of a pectin strand under pulling stress.	97
6.15	Conformational transitions for selected residues for the chitin strand along the simulation trajectory under pulling stress. The forces in pN corresponding to each residue are denoted. The color code of the conformations is based on Figure 6.9	98
6.16	Conformational transitions for selected residues for the galactose strand along the simulation trajectory under pulling stress. The forces in pN corresponding to each residue are denoted. The color code of the conformations is based on Figure 6.9	98
6.17	Conformational transitions for selected residues for the pectin strand along the simulation trajectory under pulling stress. The forces in pN corresponding to each residue are denoted. The color code of the conformations is based on Figure 6.9	99
6.18	Variation of puckering angle θ with force (in pN) along the simulation trajectory.	99
6.19	Variation of % non-chair forms with force (in pN) for different temperatures in kelvin.	100
7.1	Representation of polysaccharide backbone. This unit is replicated 7 times in order to make the membrane	104
7.2	Tetrameric unit of serine which interlocks the polymeric strands in the current membrane	104
7.3	(left)Initial structure of the membrane, (right)Structure of the membrane after 1.5 ns	105
7.4	Repeating unit showing the non-conventional 3→6 glycosidic linkage and the tetrameric serine units interlocked.	105
7.5	The snapshots of stretched membrane for both the cases at the end of 4 ns.	106

List of Abbreviations

MD	Molecular Dynamics
XRD	X-ray Diffraction
SAXS	Small Angle X-ray Scattering
XPS	X-ray Photoelectron Spectroscopy
DLLS-GPC	Dynamic Laser Light Scattering Gel Permeation Chromatography
SEM	Scanning Electron Microscopy
TEM	Transmission Electron Microscopy
NMR	Nuclear Magnetic Resonance
CG	Coarse Graining
DFT	Density Functional Theory
CHARMM	Chemistry at HARvard Molecular Mechanics
GROMACS	GRoningen MAchine for Chemical Simulations
OPLS	Optimized Potentials for Liquid Simulations
AA	All Atom
B3LYP	the Becke-3 Lee-Yang-Parr density functional
SCFA	Short Chain Fatty Acids
GI	Gastro Intestinal
QM	Quantum Mechanics
SMD	Steered Molecular Dynamics
SASA	Solvent Accessible Surface Area
PBC	Periodic Boundary Conditions
PME	Particle Mesh Ewald
TCL	Tool Command Language
FDA	Food and Drug Administration
EFSA	The European Food Safety Authority

Chapter 1

Introduction

1.1 Introduction to carbohydrates

Living organisms are comprised of biomolecules[1]. Based on the composition, biomolecules can be broadly categorised into four types: Nucleic acids, Proteins, Lipids and Carbohydrates. Each has its own characteristics and is designated to perform specific roles. These biomolecules, solely by interacting with each other, build complex organisms. The diversity coming from the shape and structure furnishes disparity in their functions. Over the years, proteins, lipids and nucleic acids have been studied extensively.

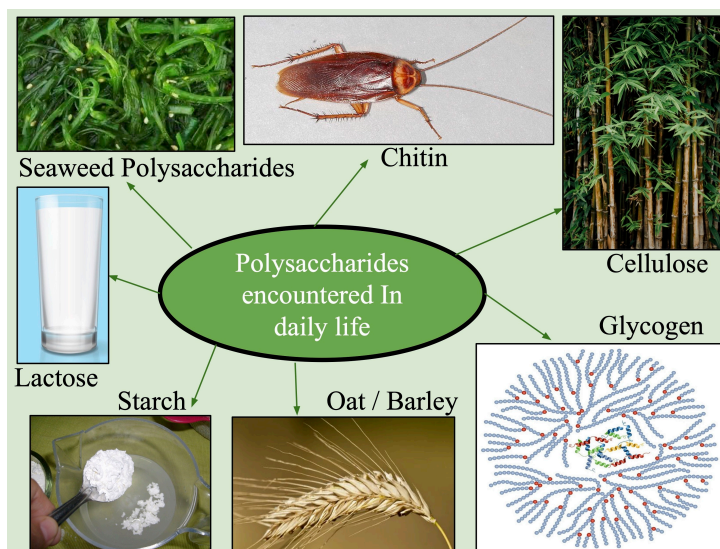


Figure 1.1: Some examples of everyday carbohydrates. Images source: www.lecturio.com, wikipedia.org, www.cnbc.com, www.vectorstock.com

Among all the biomolecules, carbohydrates are the most abundant on earth. They are omnipresent in nature[1, 3]. They constitute a major portion of our daily food intake[4, 5]. The general chemical formula of carbohydrates is $(\text{CH}_2\text{O})_n$. In terms of diet, carbohydrates feature in sugars, fibres and starches. Sugars occur naturally in fruits and vegetables, refined sugars like syrups, cookies and soft drinks. Fibres include whole grain foods such as cereal, bread, oats & barley, nuts, some fruits and vegetables. Starches include potatoes, corn, peas, beans

etc. In non-food items, they can be seen in bark of plants, exoskeleton of arthropods, cell-wall of microorganisms. Figure 1.1 shows examples of some common naturally occurring carbohydrates. Carbohydrates are also crucial in determining our blood group. Specific sugars are attached to the surface lining of red blood cells which differentiate the blood group types[6]. They also play a crucial role in metabolic processes like digestion and excretion[4, 5, 7, 8]. The appearance and application of carbohydrates are manifold in living organisms. Starting from energy storage to structural organization, these macromolecules are truly abundant in nature. However, compared to nucleic acids and proteins, the advancement in carbohydrate research is lagging because of its structural diversity, and functional complexity [1, 9]. Unlike proteins and nucleic acids which can be joined by specific linkage, i.e., peptide or phosphodiester bond respectively, polysaccharides have multiple hydroxyl bonds giving rise to polydispersed polymers without defined molecular

weights. In general, the degree of polymerization varies between a few tens to hundred of thousands.

Polysaccharides comprise of several small units called monosaccharides. These monosaccharide units can exist as open-chain linear form or cyclic form in aqueous solution. In case of cyclic form, they can either exist as 5 membered cyclic structure known as **furanose** or 6 membered cyclic structure called **pyranose**. In nature, the cyclic monosaccharides can exist as dextro-*(D)* or laevo-*(L)* enantiomers, although the *(D)* isomer predominates. Unlike the *(D)* isomer, the *(L)* isomer is not biologically active and but can be synthetically produced in small amounts. Depending on the position of ‘OH’ group on C_1 atom, the anomers are named. If the ‘OH’ group is below the plane, then it is **α -anomer**, where as if the ‘OH’ group is above the plane, it is **β -anomer**. Monosaccharides are stitched together by **O-Glycosidic bond**. This polymeric condensation leads to the formation of highly complex long chains. This glycosidic link is formed by dehydration or condensation of the hemiacetal hydroxy group of one sugar (glycosyl donor) and a hydroxyl group of another sugar unit (glycosyl acceptor). They are found in various living organisms with varied composition. Figure 1.2 shows the formation of 1 \rightarrow 4 linked O-glycosidic bond formation from β -*D*-Glucose units. These glucose units are also known as glucans. In addition, there can also be “N-glycosidic linkage”, “S-glycosidic linkage” and “C-glycosidic linkage” where the ‘O’ of glycosidic bond is replaced by N, S and C respectively. Molecules with N-glycosidic linkage are called glycosyl amines while those with S-glycosidic linkage are called thioglycosides.

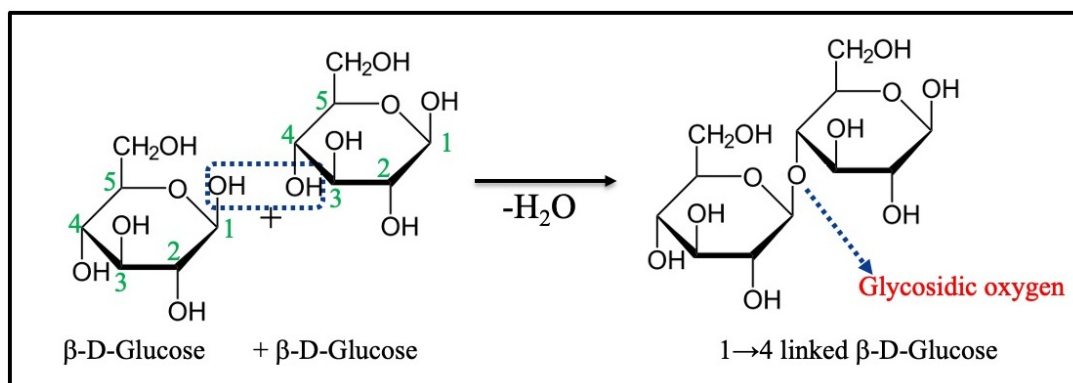


Figure 1.2: Representation of glycosidic bond formation from two β -*D*-glucose monosaccharides. Numbering (in green) is for ring carbons.

The carbonyl carbon of the aldehyde group in linear form becomes anomeric carbon in the cyclic ring. As the anomeric carbon ‘ C_1 ’ is bound to two oxygen atoms, it possesses unique chemical, conformational and structural properties[10]. Polarisation of C-O bonds reduces the σ electron density on the carbon atom. But this is compensated by back donation of

electron density from lone pair of ring oxygen atom to σ^* orbital of the exocyclic C-O bond. The extent to which this occurs depends on the degree of orbital overlap and configuration about C_1 . If the OH group is in axial position, then the donation of lone pair of electrons to this σ^* orbital, lowers the overall energy of the system resulting in more stability. The same is less prominent if the OH group is in equatorial position. This preference of the OH group or the polar groups to take up the axial position is defined as **anomeric effect**. If the anomeric carbon is free and not bound to any other monosaccharide residue, then it is the reducing end whereas if the anomeric carbon is bound to other residue or part of any glycosidic linkage, then it is the non-reducing end.

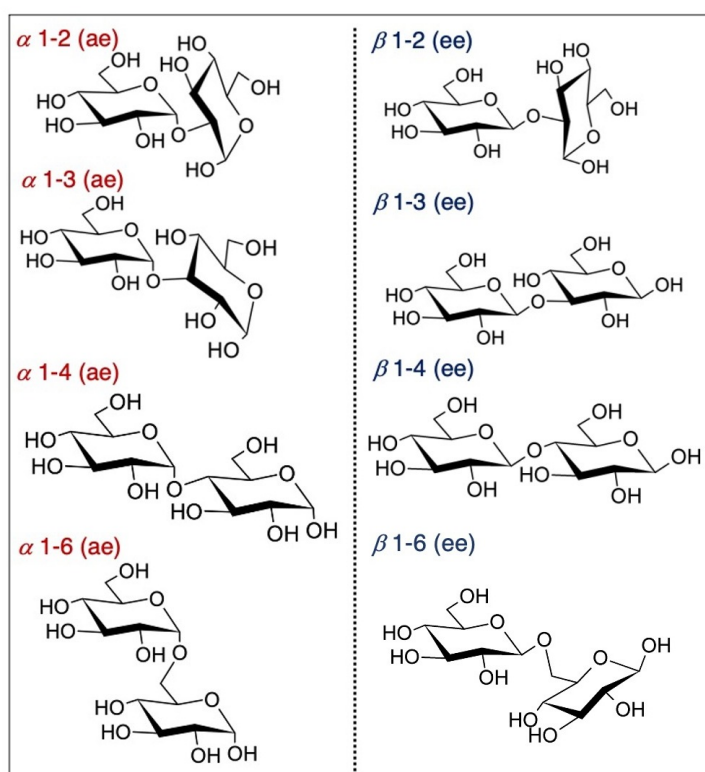


Figure 1.3: Glycosidic linkages formed by α and β glucose molecules.

Each polysaccharide possess unique structural features. These features come up because of the variations in terms of ring size (e.g, 5 membered or 6 membered rings), monosaccharide composition (e.g, glucose, fructose, maltose, galactose, etc.), configuration of the monosaccharide (whether α or β), the glycosidic linkage between the monosaccharides (1 \rightarrow 2, 1 \rightarrow 3, 1 \rightarrow 4, 1 \rightarrow 6 type of linkage), chemical composition (homo-polysaccharides or heteropolysaccharides) of the polymer. Figure 1.3 shows the different glycosidic linkages formed by the anomers of *D*-glucose, which have been used in this work. Apart from these, factors like degree of polymerization, extent of branching and the frequency of branching from the main chain, charged group substitution (carboxylate, sulphate, phosphate group etc.), location of substitution on the ring, molecular weight, three-dimensional arrangement in space, intramolecular hydrogen bonding, nature of the solvent system (pH, ionic strength, temperature) etc. also play a crucial role in controlling the structural features. All these distinct structural and chemical properties pave the way for polysaccharides in exhibiting a wide range of functional properties including rheological properties and solubility. Disaccharides with 1 \rightarrow 3, 1 \rightarrow 4 and 1 \rightarrow 6 type of linkages have received more attention over the years when compared to 1 \rightarrow 2

Each polysaccharide possess unique structural features. These features come up because of the variations in terms of ring size (e.g, 5 membered or 6 membered rings), monosaccharide composition (e.g, glucose, fructose, maltose, galactose, etc.), configuration of the monosaccharide (whether α or β), the glycosidic linkage between the monosaccharides (1 \rightarrow 2, 1 \rightarrow 3, 1 \rightarrow 4, 1 \rightarrow 6 type of linkage), chemical composition (homo-polysaccharides or heteropolysaccharides) of the polymer. Figure 1.3 shows the different glycosidic linkages formed by the anomers of *D*-glucose, which have been used in this work. Apart from these, factors like degree of polymerization, extent of branching

glycosidic linkage. This is primarily because the former glycosidic linkages feature most commonly in nature.

Minor variations in the monomeric unit, configuration of the monomer and the glycosidic linkage will lead to a huge impact on the polysaccharide structural and functional properties. For instance, cellulose and amylose are both naturally occurring homo polysaccharides containing *D*-Glucose units linked by 1→4 O-glycosidic linkage. But the difference lies in their anomericity[11]. Cellulose has β while amylose has α glycosidic linkage. This leads to variation in the arrangement of glycosidic bonds, which would alter their functionalities. In case of cellulose, the strands are linear whereas in case of amylose, the strands are more coiled. Cellulose acts as a structural framework whereas amylose acts as energy storer in plants [12, 13, 14]. They also act as signalling molecules in certain vital biological processes. Biocompatibility, high mechanical strength, good flexibility & elasticity, low toxicity, shear-thinning properties, and ability to swell and hold water enable it to be used in various biomedical applications.

1.2 Extraction of polysaccharides

Naturally occurring polysaccharides usually coexist in nature with other biomolecules which makes the separation process extremely tedious and sometimes even impossible. They can be extracted from plants, animals, fungi, algae etc. Depending on the source of extraction, they can be categorised into plant polysaccharides, animal polysaccharides, algal polysaccharides, microbial polysaccharides, etc. Each of these sources possess a specific glycosidic linkage or is a combination of multiple glycosidic linkages. There are four commonly used techniques for polysaccharide extraction from the most abundant plant sources. They are (i) water extraction (ii) alkaline extraction (iii) acidic extraction and (iv) enzymatic extraction[15]. All these processes are extremely time consuming. Even if β -glucans are extracted with water, several other chemicals have to be employed in order to remove proteins and starch. Presence of proteins or starch even in minor concentration in the extracted polysaccharides might alter the viscosity and in turn its biological efficacy. This in turn elevates the cost of extraction. Hence it is certainly a huge challenge to attain the required compound with high purity as well as high molecular weight.

Owing to their non-volatility and tunable hydrophobicity, ionic liquids (IL) have gained popularity in polysaccharide extraction[16, 17, 18, 19]. For practical implementation of ILs, their “recovery and reuse” is crucial[20]. But, the contamination caused by the reactions in between substrates and ILs can be unfavourable for reuse. Also, the percentage of extraction ranges from 15-80 and varies with the source of extraction, ionic liquid of

choice and conditions employed[16, 17, 18, 19]. Despite the fact that various studies are published to understand the mechanism of polysaccharide isolation and extraction, there is lot more to balance between selectivity and efficiency.

1.3 Synthesis of polysaccharides

In vitro synthesis of polysaccharides has been challenging and tedious as the complexity lies in controlling stereoselectivity and regioselectivity. For instance, between two amino acids, only one dipeptide can be formed but two identical monosaccharides can give up to 13 different disaccharides[21]. Presence of multiple hydroxyl groups with similar pK_a and reactivity is what elevates the complexity. Over the past few decades, carbohydrate chemists have established several glycosylation reactions and several strategies for glycan assembly. Chemical and enzymatic method of oligosaccharide synthesis are obtaining popularity although they are laborious and time consuming.

1.3.1 Chemical synthesis of polysaccharides

Over the years, chemists have developed several novel assembly techniques, protecting group manipulations, glycosylation methods in synthesizing long oligosaccharide chains. In general, three strategies are used for polysaccharide synthesis. They are (i)Poly condensation, (ii)Ring opening polymerization and (iii)Step-wise elongation. The assembly strategy is what determines overall efficiency of the synthesis.

Naturally occurring polysaccharides like cellulose, chitin, xylan, and amylose are all basically 1→4 linked polysaccharides. But their chemical synthesis is extremely tedious. For instance, a degree of polymerization of 60 was obtained in presence of P_2O_5 with the poly condensation of 2,3,6-tri-*O*-phenylcarbamoyl-*D*-glucose. However, this reaction could not accomplish the required stereo and regio selectivity[22]. The challenge of regio specificity is overcome by temporary regio selective protection of hydroxyl groups which do not participate in glycosidic bond formation. Despite the fact that this approach can be accomplished with monosaccharides, it is extremely challenging and time consuming approach for disaccharides, trisaccharides or oligosaccharides. Also, stability of protecting group, attaining a global de-protection, removal of the protecting group under mild conditions without affecting the newly generated glycosidic bond attains a major challenge and affects the overall yield. Recently Joseph and co workers[23] have reported the synthesis of polysaccharide with α -*D*-Glucose with a degree of polymerization of 100 with α 1→6 glycosidic bond.

1.3.2 Enzymatic synthesis of polysaccharides

For the synthesis of natural and synthetic polysaccharides, enzymatic polymerization is known to be a powerful tool. The major advantage being, it does not need protection for hydroxyl groups since the enzymes control both the regio and stereo selectivity of glycosylation reactions by molecular recognition[24]. Apart from this, there are several advantages of using enzymes over chemical methods. They increase catalytic rates, have substrate specificity, most of the enzymes operate at room temperature and at pH 7 in aqueous medium thus avoiding harsh conditions. Their biodegradability and solubility in aqueous solution makes enzymes an eco-friendly option[25].

Enzymatic synthesis can be classified into 4 categories based on type of enzyme used. (i) glycosylases: these form glycosidic linkage in kinetic and thermodynamic approach, (ii) glycosyl transferases: they are involved in Leloir pathway and employ sugar nucleotides as donors, (iii) phosphorylases: they are the non-Leloir pathway and employ sugar-1-phosphate as donors, (iv) artificial glycosynthases: these are mutated glycosylases to curb the hydrolytic activity[24, 25, 26]. Natural polysaccharides such as cellulose and chitin having β 1 \rightarrow 4 glycosidic linkage have been synthesized by an enzyme called hydrolase. The cellulose oligosaccharide and their derivatives are prepared using two step enzymatic reactions[27]. First step involves transfer of methyl β cellobioside as glycosyl acceptor. As the hydroxyl is at axial position, lactosylation occurs exclusively at the glycosyl acceptor forming β 1 \rightarrow 4 glycosidic linkage. In the second step, product gets subjected to enzymatic degalactosylation by β galactosidase giving methyl β cello-tetraoside. This method of stepwise elongation makes it possible to prepare cello oligosaccharides having definite degree of polymerization. In a similar way, poly condensation of α maltosyl fluoride catalysed by α amylase[28] gives malto oligosaccharide with up to 12 glucose units. Chitobiose oxazoline monomer derivative has been used to synthesize chitin using the enzyme chitinase. Unnatural and hybrid polysaccharides with degree of polymerization up to 24 units have been found through MALDI-TOF mass spectroscopy experiments[29].

However, the major drawback of this technique is limited enzyme availability and slightly higher cost of glycosyl donors. The lower solubility of polysaccharides often leads to precipitation, further hindering the formation of polysaccharide with higher degree of polymerization. Although there have been several significant breakthroughs in regulating the stereo and regio selectivity involved in the formation of glycosidic bond, there isn't any generalised route for the synthesis of this diverse class (linear, cyclic, branched, hyper branched etc.) of biomolecules.

1.4 Analysis techniques

Myriad of sugar residues, either natural or synthesized in lab, exhibit a plethora of stereochemistry, configuration, conformation and branching. Hence, unlike proteins, structural elucidation of polysaccharides in attempting to find a generalized pattern becomes a formidable task[30, 31]. Currently, X-ray diffraction studies (XRD)[32], Small angle X-ray scattering (SAXS)[33, 34], X-ray photoelectron spectroscopy (XPS)[35], dynamic laser light scattering-gel permeation chromatography (DLS-GPC)[36], nuclear magnetic resonance (NMR)[37, 38], Mass spectrometry (MS)[39, 40], Scanning electron microscopy (SEM)[38] are the methods to elucidate structure of polysaccharides or polysaccharide based materials. The sample preparation of SEM and TEM is usually complex and needs high vacuum conditions. For XRD, sample should be prepared into film or fibre or crystal. Although XRD can give static structures of mono or disaccharides, it is uncertain if the molecule adopts the same conformation in solution. Further, higher oligosaccharides may not crystallise due to less favourable packing arrangement in solid state. Also, polysaccharides do not have a well characterised secondary or tertiary structure unlike nucleic acids or proteins. The inability of MS to predict the correct anomericity and glycosidic linkage pattern in polysaccharides adds to the problem. In case of NMR, assignment of peaks is highly complicated for higher molecular weight polysaccharides [41]. Although NMR can offer the structure in solution to some extent, it is usually an average of conformers occurring simultaneously[37, 42, 43, 44, 45]. In solution, multiple conformations brought out by glycosidic angle variation exist in equilibrium. This needs appropriate time resolution of spectroscopic methods for the conformational analysis of the molecules. In this scenario, computation plays a vital role to model, simulate and predict intricate structural and dynamical details of this complex class of molecules and is a must have to comprehend the 3D structures in solution[29, 46, 47].

1.5 Simulation studies on saccharides

The micro heterogeneity, i.e., the simultaneous variation in both length and structure of the polysaccharide, hinder the experimental approaches for studying properties of polysaccharides. This void can be filled by molecular dynamic simulations. Since the inception of high performance computing facilities, simulation studies have taken a leap. Advancement in algorithms and technology facilitate in rapid sampling of biomolecular conformations. Simulations can be run for a couple of nanoseconds (ns)[48] and can be extended to microsecond range (μ s) in reasonable amount of time. This is sufficient to account most internal motions of glycans. In the recent years, calculations based on density functional theory (DFT) and force field based molecular dynamics have been used

to analyse the hydrogen bonding, conformational changes, solvent interactions and various other attributes of polysaccharides as well as other biomolecules. Studies are carried out on monosaccharides to oligosaccharides both in all atom (AA) model, coarse grained (CG) model and hybrid models[49, 50, 51, 52]. These studies can be done in vacuum and or in solvent medium. Several force fields are developed to study the properties of carbohydrates. Some of them are CHARMM36[53], GLYCAM-06[54], GROMOS[55] and OPLSAA[56].

1.5.1 Structure and energetics of *D*-glucose

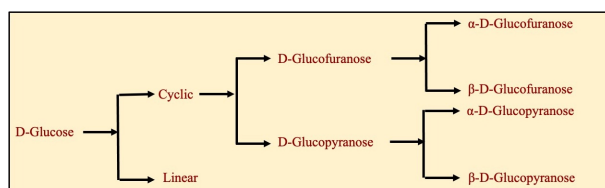


Figure 1.4: Different configurations of *D*-glucose.

Owing to their biological significance, *D*-glucose has been studied extensively among all the carbohydrates. Figure 1.4 shows the different forms of *D*-glucose. *D*-glucose can exist in both linear and cyclic forms. The cyclic ring can either be a furanose or pyranose. Each of these can exist in their respective α/β configurations. To

have a comprehensive understanding of physical and chemical properties of glucose based molecules, one should have a clear idea of their molecular structures, preferred configurations and the energy difference between the two anomers.

Molecular dynamic simulations on β and α glucans were first reported by John W. Brady. The atomic coordinates of glucans for this work are taken from neutron diffraction studies[57, 58]. It has been reported that at 300 K, the energy difference between the chair conformations of the two anomers($\Delta G, \beta \rightarrow \alpha$) of glucose is -0.31 kcal/mol (in aqueous phase) in comparison to the experimental value of 0.33 kcal/mol. This energy difference is a result of intermolecular stabilization through solute-solvent interactions in β anomers[59]. Several calculations of isolated β and α glucose molecules suggests the existence of stable and less stable conformers. In aqueous solution, the equilibrium is towards β -glucopyranose (64%) over α -glucopyranose (36%)[60]. Figure 1.5 shows the different kinds of configurations of *D*-glucopyranose.

Depending on the orientation of the exocyclic $C_6 - O_6$ bond, the conformers can be named as shown in Figure 1.6. If the $C_6 - O_6$ bond is (i) gauche to both $C_5 - C_4$ and $C_5 - O_5$: *gg* rotamer, (ii) trans to $C_5 - C_4$ and gauche to $C_5 - O_5$: *gt* rotamer, (iii) gauche to $C_5 - C_4$ and trans to $C_5 - O_5$: *tg* rotamer. The *gt* and *gg* rotamers have free energy difference close to 0[61], which is in line with NMR measurements[62]. Miura *et al.* have performed the DFT calculations of α and β *D*-glucopyranose.

They have reported the population of *gg*, *gt* and *tg* rotamers as 48:51:1 and 53:46:1 for β -*D*-glucopyranose and α -*D*-glucopyranose respectively[63]. On the other hand, NMR studies by Nishida *et al.* suggests the ratio between these hydroxyl rotamers as 53:45:2 and 56:44:0 for β -*D*-glucopyranose and α -*D*-glucopyranose respectively. Although the numbers obtained from experiment and simulation are close, the small difference could be because of the fact that theoretical work are carried out in gas phase. The furanose and pyranose forms can exist in multiple conformations. These conformations can interconvert among themselves provided the energy requirement is met. Furanose can exist in only two forms which are twist (T) and envelope (E) where as pyranose can exist in five different conformations. They are chair (C), boat (B), skew-boat (S), half-chair (H) and envelope (E). These representations are shown in Figure 1.8 The reactions of polysaccharides are well dependent on the conformation of the ring. Changes in the rotatable ring bonds lead to out of plane bending motions in the flexible ring thus altering its conformation. This phenomenon of distortion of the ring from the ideally planar hexagonal form is called as “ring-puckering”.

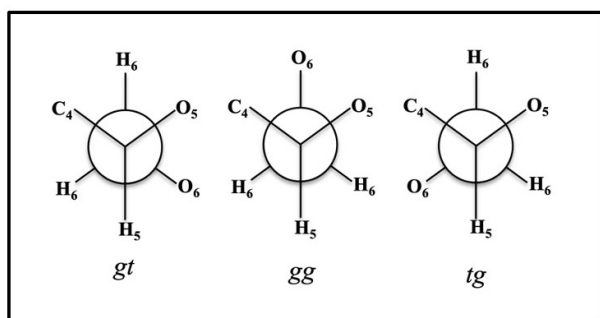


Figure 1.6: Rotamers exhibited by the three bond 1→6 glycosidic linkage.

Pople’s theory based on perpendicular displacement of ring atoms is widely accepted[64]. This method uses $(N-3)$ parameters to describe the geometry of system with N vertices. Thus, for a 6 membered ring, 3 puckering parameters are used to describe the extent of puckering. The generalised ring puckering coordinates can be defined in the following way;

$$q_m \cos \phi_m = \sqrt{\frac{2}{N}} \sum_{j=1}^N z_j \cos \left[\frac{2\pi m(j-1)}{N} \right] \quad (1.1)$$

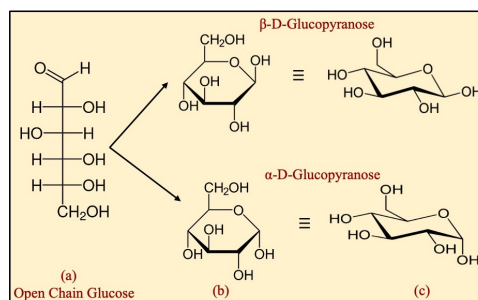


Figure 1.5: Configurations of *D*-glucopyranose. (a)Fisher projection of open chain glucose, (b)Haworth projection and (c) 4C_1 Chair conformation of both anomers.

Wide range of techniques have been developed in order to characterize the extent of puckering in the ring[64, 65, 66, 67, 68]. These approaches are based on perpendicular displacement from mean position by the ring atoms or triangular tessellation of the ring and measure the angle between reference plane and triangular plane or measure of torsion angles. Measure of torsion angle alone is not sufficient as it cannot identify the pseudorotation. D. Cremer and J. A.

$$q_m \sin \phi_m = -\sqrt{\frac{2}{N}} \sum_{j=1}^N z_j \sin \left[\frac{2\pi m(j-1)}{N} \right] \quad (1.2)$$

$$q_{\frac{N}{2}} = N^{-\frac{1}{2}} \sum_{j=1}^N z_j \cos[(j-1)\pi] = N^{-\frac{1}{2}} \sum_{j=1}^N (-1)^{j-1} z_j \quad (1.3)$$

Where N is the number of atoms, z_j is the displacement from the mean plane cartesian coordinate along z -direction, q_m is the part of the puckering parameters which are used to describe the extent of puckering and m is the index of puckering. If the number of atoms in the ring are even and $N > 3$, m takes the value of $2, 3, \dots, N/2$. So for a 6 membered ring, a single amplitude-phase pair (q_2, ϕ_2) and a single puckering coordinate q_3 are used to describe the three puckering degrees of freedom. They represent a set of puckering coordinates with amplitudes q_m (≥ 0) and phase angle ϕ_m ($0 \leq \phi < 2\pi$). These coordinates can alternatively be represented by a “spherical polar set” (Q, θ, ϕ) using the equations 1.4 and 1.5. In the spherical coordinate system, the “total puckering amplitude” is given by Q and the “distortion type” is specified by two angular variables which are θ (psuedorotation angle) and ϕ (phase angle)[69]. Figure 1.7 depicts the spherical coordinate system representing the Cremer-Pople puckering parameters for the six membered pyranose rings. The quantity Q (≥ 0) can be defined as shown in equation 1.4. This coordinate system permits the projection of all types of puckering on the surface of a sphere.

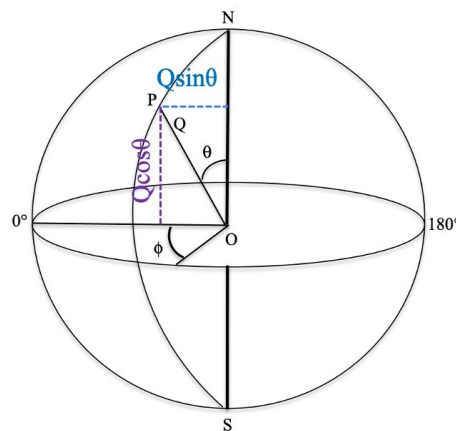


Figure 1.7: The spherical coordinate system representing the Cremer-Pople puckering parameters for the six membered pyranose rings.

$$Q^2 = \sum_m q_m^2 = \sum_{j=1}^N z_j^2 \quad (1.4)$$

$$q_2 = Q \sin \theta; \quad q_3 = Q \cos \theta \quad (1.5)$$

The pyranose ring is considered to be in the most stable chair conformation (4C_1 or 1C_4) for $\theta = 0$ or 180° . For $\theta = 90^\circ$, which denotes the equatorial plane of the sphere, as the phase angle crosses different values from 0 to 360° , the six membered pyranose ring touches six boat ($\phi = 0, 60, 120, 180, 240, 300^\circ$) and six twist boat conformations ($\phi = 30, 90, 150, 210, 270, 330^\circ$). In between for $\theta = 45$ or 135° , envelopes and half-envelopes are observed. The pseudo rotation leads to multiple equivalent conformations. Hence, ring puckers are grouped into different “canonical forms”[68]. For example, the 4C_1 and 1C_4 of the chair

conformation, the ${}^0H_5, {}^4H_5, {}^4H_3, {}^2H_3, {}^2H_1, {}^0H_1, {}^3H_2, {}^1H_2, {}^1H_0, {}^5H_0, {}^5H_4, {}^3H_4$ of the half chair conformation, $E_5, {}^4E, E_3, {}^2E, E_1, {}^0E, E_2, {}^1E, E_0, {}^5E, E_4, {}^3E$ of the envelope conformation, ${}^0S_2, {}^1S_5, {}^1S_3, {}^2S_0, {}^5S_1, {}^3S_1$ of the skew boat conformation and $B_{2,5}, {}^{1,4}B, B_{3,0}, {}^{2,5}B, B_{1,4}, {}^{3,0}B$ of the boat conformation[70] as represented in Figure 1.8.

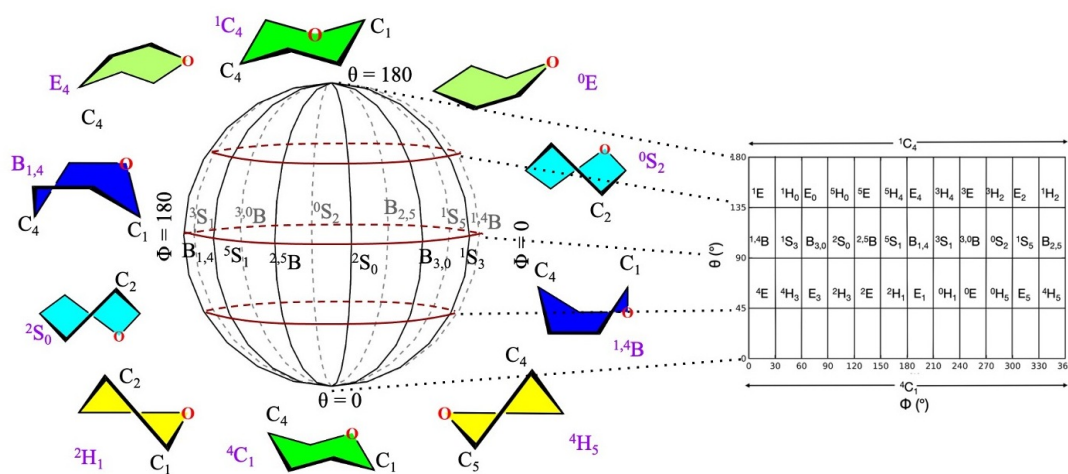


Figure 1.8: Cremer Pople and Mercator representation representation of glucopyranose ring

The dominant 4C_1 arrangement refers to a chair configuration, where the C_4 carbon atom is above the reference plane formed by $(C_2 - C_3 - C_5 - O_5)$ and the C_1 carbon atom is below the plane. In general, for *D*-glucopyranose, 4C_1 conformer and the β -anomers are favoured in aqueous solution. Appell *et al.* reported that electronic energy of 1C_4 chair is 5-10 kcal/mol higher than that of globally stable 4C_1 chair conformation while boat and skew boat are 4-15 kcal/mol higher. They also reported a relative higher energy of *tg* conformer over *gg* and *gt* by 0.4-0.7 kcal/mol using B3LYP/6-311++G** level of theory[71, 72]. The *in vacuo* calculations however favoured α anomer over β anomer by 2.2 kcal/mol in both 4C_1 and 1C_4 conformations which is quite opposite to what is found experimentally in solution. This is because of the inter molecular stabilization of axial OH groups by hydrogen bonding. Anomeric effect is also expected to play some significant role in this case. The hydroxymethyl in *gt* conformation is of lowest energy for both the anomers[71]. For 4C_1 and 1C_4 conformation for β -glucopyranose, barrows *et al.*[73] and csonka *et al.*[74] have reported electronic energy difference of 3-4 kcal/mol using MP2/cc-pVTZ//MP2/cc-pVDZ level of theory. To understand the transition pathway between conformations, Biarnes *et al.* have reported a conformational free energy map. This map has ring distortion as a function of puckering coordinates[75]. In an earlier REMD simulation study by Gnanakaran *et al.* on cellulose fragments comprising β -D-glucopyranoside units linked by 1 \rightarrow 4 glycosidic linkages, it was shown that although 4C_1 is the preferred chair conformation observed in the simulations and about 1-2%

of conformers exhibited non-chair forms. It is noteworthy here that the propensity of formation of non-chair forms increases with the degree of polymerization[76].

On a similar line, Saplin *et al.* have done gas phase acidity studies on both the anomers of *D*-glucose. Using B3LYP functional and 6-31+G(d,p) basis set, they have stated that the anomeric carbon is the most acidic among all the hydroxy groups for both the anomers[77]. The orientation of hydroxyl group on the anomeric carbon is driven by a competition between exo-anomeric effect and negative effect[78]. Preference of anomeric axial or equatorial ring substituents to adopt gauche conformation is “exo-anomeric effect”. While the negative effect is the preference of anomeric substituents in trans orientation. De-protonation of the anomeric hydroxyl group may lead to ring opening or interconversion among the anomers. The most stable conformations of α -*D*-glucopyranose and β -*D*-glucopyranose have same energies and conformation expect for anomeric OH group in axial (α) or equatorial (β) position[79]. This minute change as mentioned earlier is sufficient to trigger variation in physical and chemical properties.

1.5.2 Studies on glucose based disaccharides and beyond

As mentioned earlier, two residues of *D*-glucopyranose are joined by means of a “glycosidic linkage”. Disaccharides are the smallest units representing all the degrees of freedom determining the conformational flexibility of higher saccharides. They take a general formula of $(C_6H_{12}O_5)_n$, where $n \geq 2$. The population of rotamers about this glycosidic linkage is crucial in determining the overall structure of the polysaccharide. Although an individual pyranose ring exhibits some flexibility, there is some limitation in the overall flexibility of the oligosaccharides. This is because of restricted movement in the torsion angles.

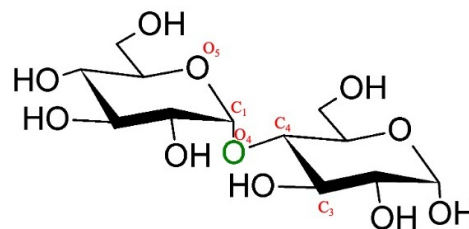


Figure 1.9: Schematic representation of 1→4 glycosidic bond between two α -glucose residues.

For a given (1→*n*) kind of linkage, where $n=2,3,4,6$, the torsion angles φ and ψ can be defined as $(O_5 - C_1 - O'_n - C'_n)$ and $(C_1 - O'_n - C'_n - C'_{n-1})$ respectively. Figure 1.9 shows the glycosidic bond in between two α -*D*-glucose residues. The torsion angles $(O_5 - C_1 - O_4 - C_4)$ and $(C_1 - O_4 - C_4 - C_3)$ are used to represent φ and ψ dihedrals respectively in this case. The φ angle is characterized by high degree of flexibility while ψ presents the restricted motion[80]. For an oligosaccharide, the conformational characteristics can be plotted as φ against ψ in a way similar to proteins known as “**Carbohydrate Ramachandran plot**”[81]. This map differs for all the glycosidic

combinations as they differ in their relative orientation. Pereira *et al.* reported that on a time scale of 50 ns, the complete rotation of the glycosidic dihedral φ is at most once or twice and never for ψ [82]. Additionally, the ω and the ω^* dihedral in 1 \rightarrow 6 linkage, defined as $(O_6 - C_6 - C_5 - O_5)$ and $(O_6 - C_6 - C_5 - O_4)$ respectively[82]. The peaks in ω torsion angle distribution refers to the population of gauche-gauche (*gg*, $\omega \sim 300$), gauche-trans (*gt*, $\omega \sim 60$) and trans-gauche (*tg*, $\omega \sim 180$) rotamers.

Salisbury *et al.* using GLYCAM06 force field have modelled several disaccharides and validated their results by comparing the Ramachandran plot with experimentally obtained results[83]. Over the decades, significant efforts have been made to develop molecular mechanics based force fields[55, 84, 85]. Olgun Guvench *et al.* reported the force field parameters for 1 \rightarrow 1, 1 \rightarrow 2, 1 \rightarrow 3, 1 \rightarrow 4, and 1 \rightarrow 6 glycosidic linkages[86] possible for *D*-glucopyranose in CHARMM format. From simulation point of view, disaccharides are the smallest entities which could validate the force fields and thus aid in the construction of complex saccharides. These parameters were validated against XRD and NMR data. This suggests a significant development in the quality of carbohydrate force field to run MD simulations for determining their thermodynamic and structural properties. These parameters can be used for the modelling of linear, cyclic, branched hexa pyranose glycosidic linkages alone as homogeneous models as well as heterogeneous chains along with proteins and lipids by clubbing with existing CHARMM biomolecular force fields.

Orientation of the glycosidic linkage also has a huge role in reorienting the structure of the oligosaccharide. For instance, the glycosidic 1 \rightarrow 2, 1 \rightarrow 3, 1 \rightarrow 4 and 1 \rightarrow 6 bonds formed between two α anomers are “**axial-equatorial**” in nature. This is because, the OH group on anomeric carbon C_1 is oriented in axial position while all other OH groups are in equatorial position. On the other hand, the glycosidic bonds formed between two β anomers are “**equatorial-equatorial**” in nature as all the OH groups are in equatorial orientation. This property greatly alters the three dimensional structure of oligosaccharide backbone. Thus we can say that the major driving forces governing conformational preference of an oligosaccharide are ring conformation because of puckering, linkage type, glycosidic dihedral angles, steric constraints because of substituents, exoanomeric effect, intramolecular hydrogen bonding and nature of solvent[87].

Hardy *et al.* have reported the conformational behaviour of cello oligomers like cellobiose (*D*-glc- β -1 \rightarrow 4-*D*-glc), cellotetrose and cellooctose. These oligomers exhibit coiled and twisted shape more than what is seen in crystalline cellulose[88]. This is perhaps due to the less constrained structure in solution state. Almond *et al.* have thoroughly investigated the effect of hydrogen bonding in oligosaccharide chains of both the anomers. They have reported that chains with α glycosidic linkage have weak hydrogen bonding while those with β glycosidic linkages have stronger hydrogen bonding[89]. Widmalm *et al.* have done MD simulations on β 1 \rightarrow 4/ β 1 \rightarrow 3 glucose linked decasaccharide[47]. SAXS plots generated

from these MD simulations were in close agreement with experimental data. Feng *et al.* have performed MD simulations of β 1 \rightarrow 3 linked saccharides with chain lengths 6, 12, 18 and 24 inspired from curdlan structure[90]. They have shown that propensity of helix formation does not change with chain length. They have extended their study by using multiple single strands of variable lengths and shown that right handed triple helix to be the thermodynamically most stable arrangement.

1.6 β -glucan bile acid interactions

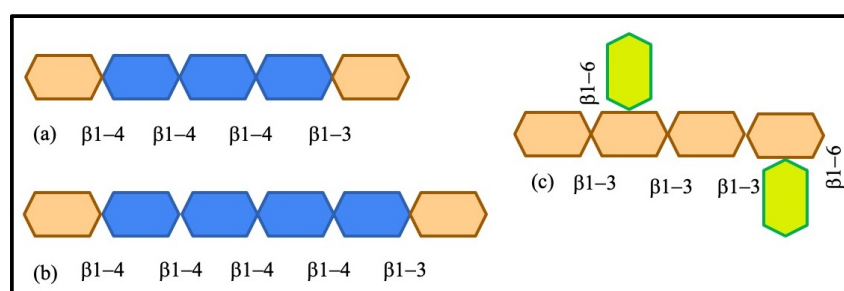


Figure 1.10: Representative units of (a)Oat-Cellotriosyl units, (b)Barley-Cellotetrosyl units and (c)Mushroom based motif.

Certain forms of oligosaccharides called as “ β -glucans”, comprise of β 1 \rightarrow 3, 1 \rightarrow 4 linkages in the main chain and are branched with β 1 \rightarrow 6 linkage. They are proven to benefit human health immensely. They positively influence fat and

sugar metabolism in the body. They are known to alleviate certain chronic diseases like dislipidemia and other cardiovascular disorders (CVD), allergies, obesity, constipation, diabetes mellitus etc[91, 92]. Because of their structure, they interact with innate immunity receptors and also act as dietary fibers in digestive track[93]. Hence the interaction of β -glucans with other dietary components and molecules emerging out of metabolic pathways in the gastrointestinal (GI) tract is attracting widespread attention these days. These are present in the cell walls of fungi, yeast, mushrooms and cereals like oat, barley, wheat and rye. Their structures and molecular weight vary based on the source of extraction. Typically, molecular weight of β -glucans can vary from few tens to thousands of kilodaltons. For instance, oat and barley β -glucans have β 1 \rightarrow 4 linked glucose chains separated by intermediate β 1 \rightarrow 3 glycosidic linkage. Usually, oat β -glucan exists as “cellotriosyl units” i.e., after every three β 1 \rightarrow 4 glycosidic linkages, one β 1 \rightarrow 3 linkage is present as shown in Figure 1.10(a). Whereas, barley β -glucan exists as “cellotetrosyl units” i.e., after every four β 1 \rightarrow 4 glycosidic linkages, one β 1 \rightarrow 3 linkage is present as shown in Figure 1.10(b). Similarly, mushroom based β -glucans have β 1 \rightarrow 3 linked glycosidic bonds as the backbone with small chain β 1 \rightarrow 6 branches as shown in Figure 1.10(c). Cellulose, the most abundant β -glucan, is linear. The molecular weight, chemical structure, solution rheology, extent and rate of dissolution are vital in influencing the physiological function of β -glucans[94].

Recent findings by Jayachandran *et al.* suggested that gut microbiota play a significant role in maintaining healthy life, energy harvest and protection of host from harmful pathogens[95, 96]. The gut microbiota is made up of around 1000 species which varies uniquely for each individual[97]. These mixed linkage β -glucans promote health by the regulation of gut microbiota. Dietary fibre reaching colon gets fermented by local microbiota[8]. Thus, microbiota can be seen as an “additional digestive organ” which has co-evolved with animals and aid in the digestion of selected food components[97]. One of the mechanism behind cholesterol lowering effect of β -glucans is through the production of short chain fatty acids (SCFA) by metabolism of microbiota. Increase in the amount of SCFA decreases cholesterol biosynthesis[99]. There are two forms of β -glucan, soluble and insoluble which can interact with lipids and biliary salts, thus paving a way to reduce cholesterol. Usually, soluble β -glucan fibers have β -(1,3)/(1,6)-*D*-glucose where as insoluble fibers have β -(1,3)/(1,4)-*D*-glucose[100]. Solubility of the most of the oligosaccharides depends on the source of extraction and their molecular weight and it increases with increase in temperature. Due to their high viscosity, the water soluble polysaccharides are believed to trap cholesterol, cholesterol based derivatives, low density lipoproteins thus preventing their absorption. Presence of proteinaceous materials also tend to increase the viscosity in the digestive track, thus influencing the aggregation of β -glucans.

Several experimental studies have been carried on the interaction of β -glucans with bile acids. Meir *et al.* using ^1H - ^{13}C NMR have studied the host-guest interactions of β -(1,3)/(1,4) mixed linkages with bile salts at a pH of 5.3[101]. The effect of β -glucans in reducing cholesterol can also be linked to its molecular weight. Ames *et al.* have reported that high molecular weight β -glucans are more efficient in reducing serum cholesterol[102]. Wilde *et al.* have shown that β -glucan rich unrefined oat based foods are efficient in cholesterol lowering over refined oat based foods[103]. Tosh *et al.* have reported the effect of molecular weight and concentration of β -glucan on the extent of gelation and viscous behaviour[104]. They have shown that β -glucans with low molecular weight tend to gel faster whereas β -glucans with high molecular weight form harder gels which are even resistant to mechanical stress. Till date, several clinical trials have suggested the ability of polysaccharides aid in the reduction of cholesterol by getting bound to bile acids and their aggregates[91, 105, 106, 107].

The complex hierarchical structures of the polysaccharide and mimicking the exact physiological composition of intestinal fluid in vitro are major challenges among others[108, 109]. While it is understandable why molecular details of such interactions are less available, one can focus more on utilizing computation tools to address such problems and fill up the void. In recent times, homology modelling, molecular dynamics simulations, docking and bioinformatics tools are increasingly used to model and study structure dynamics

relationships of complex bio-molecular assemblies[110]. Partay *et al.* have reported the aggregation behaviour of bile salts like sodium cholate and sodium deoxycholate at three different concentrations (30, 90 and 300 mM)[111]. It has been shown that due to their unique molecular structure, which is significantly different from the conventional aliphatic surfactant molecules, the bile salts tend to form soft clusters distinct from the usual spherical micelles. In case of lower concentration, bile acids only formed oligomers where as in case of higher concentration bile ions formed large micelles. Hydrogen bonding together with hydrophobic interactions between the polysaccharide and bile acids play the dominant role in triggering such adsorptions. Li *et al.* have used molecular docking to understand the adsorption of soy-hull polysaccharides on bile acids[112]. Recent work have shown that aggregation of cholesterol is influenced by the presence of β -glucans. β -glucan slows down the cholesterol aggregation by a factor of ~ 2 . This results in the formation of smaller aggregates which are relatively easy for elimination through dietary fibers from our body[113]. In an other work, using well tempered meta dynamics they have shown that oat β -glucans have better wrapping ability over cholesterol aggregates when compared to a fungal β -glucan[114].

1.7 Force spectroscopy of polysaccharides

A set of techniques employed to study the interactions between individual biological molecules is called as "Force spectroscopy"[115, 116]. Optical tweezers, magnetic tweezers and atomic force microscopy are some of the common force spectroscopic techniques in use. Over the last 20 years, tremendous progress has been made in developing these techniques, thus, enabling the force measurements of small molecules to proteins[117, 118, 119, 120]. Simple and rapid sample preparation, ability to conduct measurements on biological molecules in physiological conditions gives AFM an upper hand over other microscopic techniques[115]. AFM technique can measure stretching and deformation in single polysaccharide chains[121, 122, 123, 124, 125, 126, 127]. Force induced conformational transitions are also detectable through AFM which are otherwise not possible through conventional methods[121]. In this method, one end of the molecule under study is attached to a piezo surface and the free end is attached to AFM tip through which force can be applied. The force is measured by tracking the deflection of cantilever. This ability to manipulate biomolecules attached to trapped micro or nanoparticles and thereby measure forces with femtonewton accuracy has opened the way to study various important topics like polymer and nanomaterial characterization, membrane stiffness determination etc[128, 129, 130].

Mechanical properties of polysaccharides are of significant interest[131]. Certain structural polymers help in maintaining body's shape against external mechanical stress[132]. A series of seminal work by the groups of Marszalek and Gaub, exploring the elastic properties of polysaccharides using AFM and steered molecular dynamics simulations (SMD) have already set the stage for the problem[121, 124, 127, 133, 134]. The idea behind SMD simulation is to apply external force on one or more atoms and keep an other set of atoms fixed and study the behaviour of biomolecule. Atoms subjected to external force are called "SMD atoms" while those kept fixed are "fixed atoms". These two combined are the so called "tagged atoms". On time scales accessible to MD simulations, this technique can be used to explore biological processes like unbinding of ligands and conformational changes associated with it. SMD can be broadly categorised into two types, (a) constant velocity pulling and (b) constant force pulling. In case of constant velocity SMD simulation, a dummy atom is attached to SMD atom through a virtual spring. This dummy atom is pulled with constant velocity. On the other hand, in case of constant force pulling, a constant force is experienced by the SMD atom in the direction that defines the vector between SMD atom and fixed atom. Figure 1.11 shows the one dimensional constant velocity pulling.

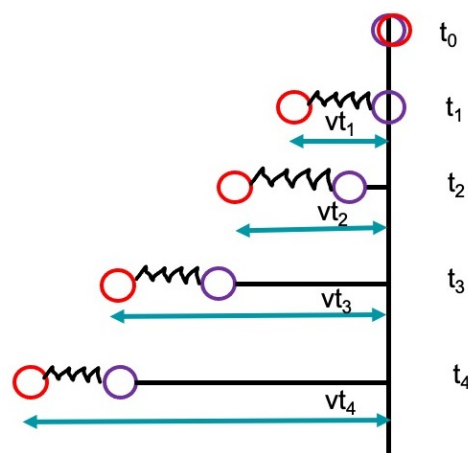


Figure 1.11: One dimensional constant velocity pulling. The dummy atom is coloured red and SMD atom is coloured purple. As constant velocity is applied on dummy atom, SMD atom experiences the force which is a linear function of distance between both the atoms.

Stretching of the polysaccharides are associated with conformational changes. Usually, the conformational transitions associated with the stretching of the polysaccharide can be identified from the characteristic "force-extension (F-E) curves" generated from the AFM studies or SMD simulations. The most common way to address the F-E curves thus explaining the elasticity issue in polysaccharides is in terms of entropic and Hookean regimes[135, 136]. A hump or plateau in the F-E curve would mean that a relatively small force is able to induce extension in the polysaccharide length, thereby decreasing the slope of the curve[137]. This region of smaller force and uncoiling of the polysaccharide is known as the "entropic domain", which on stretching, rotates and orients in the direction of the applied force. Beyond a critical force, marked by the elbow region, the extension usually increases linearly with the applied force, following a Hookean potential. The elastic restoring force generated thereby tries to constrain the possible chain configurations and reduce the configurational entropy. The polymer extends proportionately to the rapidly increasing stress in the high stretch regime, called the "Hookean domain". Finally, as

the polymer reaches its contour length, the chain is fully stretched and has very few configurational options left. In the limit, the entropy reduces to zero when the polymer chain becomes linear[136].

In between the initial entropic and Hookean domain in the later part, there is sometimes an additional region of moderate extension, where the force-extension curve is usually observed to be non-gaussian. In this region, the polysaccharides stretch and transform the chair to boat conformers; the system passes through a high entropy region, as numerous skew boat conformers are possible as intermediates. Experiments reveal that in living systems, certain connective tissues which are exceedingly elastic in nature, like skin, exhibit additional elasticity beyond entropic and Hookean types[132]. This kind of elasticity has a functional role in regulating macroscopic properties of biological materials. Conformational changes originating from the structure of a pyranose can vary in lengths of individual conformation[137]. These force induced conformational changes are also refereed as “clicks”. Transformations between these conformers can be from one chair conformation to other chair conformation (4C_1 to 1C_4), chair conformation to boat and finally to chair (4C_1 to ${}^{1,4}B$ to 1C_4)[126, 134, 138].

With the help of statistical mechanical models of polymer extensibility, like the worm-like chain model (WLC), the freely jointed chain model (FJC) or the extensible versions of them, one can attempt to fit the experimental F-E curves[134, 135]. The worm-like chain (WLC) or freely jointed chain (FJC) models are often used to successfully fit the low-force entropic region of the F-E curve. In an improved version of the WLC model, also known as the extensible worm like chain model (EWLC), the Hookean extension of a polymer chain at higher forces can be fitted with reasonable efficacy. Additionally, the models help estimate the free energy of transformation from a non extended to an extended conformation[137, 139].

1.8 Polysaccharide membranes

Being the structural scaffold in plants (cellulose) and animals (chitin) and due to their immense film-forming abilities, the traditional interest in polysaccharide membranes has been limited along these lines. Of late, glycobiology has been emerging as a challenging new area of research[140]. But developing synthetic carbohydrates like glycoproteins and glycolipids is still a technical challenge[141]. Many reactions in our body take place via some kind of carbohydrate interaction. Seemingly increasing interest in these mainstays of carbohydrate chemistry has been supplemented by a growing appreciation of the importance of the carbohydrate fractions of glycopeptides and glycoproteins in many diverse biological roles. Like recognition processes because of their biocompatibility,

chirality, capacity to form structure and the benign environmental property. These polysaccharide membranes are also part of technologically crucial materials in food industry like biodegradable cutlery, eco-friendly packaging, food coatings to increase the shelf lives therefore manufacturing is also increasing. Some of the crucial characteristics of well defined membrane are resistance to temperature and pH variations, limited permeability to moisture, selective barrier to gasses like O_2 and CO_2 , possess high mechanical strength, tunable transparency, biodegradability.

In food storage and packaging, the excess consumption of non-biodegradable synthetic plastics has been a key cause of environmental pollution. With the soaring demand for high quality fruits and vegetables, there is an increasing demand for the formulation of preserving techniques. A sense of urgency is instigated to develop biodegradable and natural methods of preservation. Biopolymers such as pectin, starch, alginate, xanthan gum and chitosan have been extensively used as edible food coatings. They are used to extend the shelf lives of these. Due to their dense hydrogen bonding ability, polysaccharide membranes act as effective barrier against gases like O_2 and CO_2 [142]. Their natural hydrophilicity limits the moisture barrier properties. Nair *et al.* have reported the edible film/coatings of chitosan and alginate based functionalities. They have shown that these membrane coatings on fruits and vegetables cause high water and moisture retention[143]. Liu et al have studied the selective antibacterial properties, permeability of water and gases in chitosan of three different molecular weights. They have shown that higher molecular weight chitosan has greater stability and has the product quality as packages[144].

Several polysaccharide membranes function as drug delivery systems. Shariatina *et al.* have recently shown the drug delivering abilities of chitosan using MD simulations[145]. Temperature variation analysis showed that at a temperature of 308.15 K, the membrane showed desirable drug delivering ability as it had higher loading capacity. Mohit *et al.* have shown the diffusion of ions through cellulose membranes[146]. In their method, they have shown the relationship between charge on the surface group and diffusion coefficients. Gumbart *et al.* have modelled a peptidoglycan membranes inspired from the cell wall of *Escherichia coli*. They have shown that these membranes poses anisotropic elasticity which arises from orthogonal orientation of the glycan strands and the peptide crosslinks[147]. Comparison of membrane elasticity, pore size and membrane thickness were done to identify membrane closest to native cell wall structure. Recently, Luzhi Zhang *et al.* have shown the ability of peptidoglycan membranes in self healing and bio friendly elastomers for bio integrated electronics[148] at room temperature. This peptidoglycan derives its function from three dimensional network which are uniquely constructed by backbone of alternating heteropolysaccharides which are N-acetylmuramic acid and N-acetylglucosamine. These chains are further cross-linked by peptide side chains.

1.9 Thesis overview

This thesis explores structural, mechanical and dynamical aspects of α and β glucans, their interaction with bile salts and their membrane-forming abilities. **Chapter 2** explains the methodologies imbibed for carrying out the investigations. Details about the modelling of systems, simulation software, force fields and configuration parameters used to perform the simulations are described. In most naturally occurring systems, polysaccharides carry out their functions in aqueous medium. **Chapter 3** specifically gives insight into the structural changes and dynamics spanned by 15 residue α and β -glucans joined by 1 \rightarrow 3, 1 \rightarrow 4 and 1 \rightarrow 6 glycosidic linkages in the aqueous medium. Detailed molecular level investigations such as the extent of inter and intra-molecular hydrogen bonding, end-to-end distance, root mean square deviation, radius of gyration and solvent-accessible surface area add insight into the structural preferences of these oligosaccharides. PCA on glycosidic angles gives insights on the dynamical freedom of individual oligosaccharides. **Chapter 4** gives an account on the influence of 10 residue oat β -glucan on bile salt aggregation. SAXS studies, DFT calculations, gives better appreciation on the aggregation patterns, their compactness and interactions with polysaccharides. **Chapter 5** is the study of mechanical properties of 15 residue α and β -glucopyranosides joined by 1 \rightarrow 2, 1 \rightarrow 3, 1 \rightarrow 4 and 1 \rightarrow 6 glycosidic linkages in the aqueous medium. The force-extension curves give a complete insight into the conformational changes accompanied by stretching the oligosaccharide. Comparison of force-extension curves with experimentally obtained AFM curves after appropriate normalisation validates the MD simulated data. In general, polysaccharides and their derivatives are non-toxic. Thus, they are employed for various food, pharmaceutical and biomedical applications. The work done chapters in 3, 4, 5 are solely based on *D*-glucose units. **Chapter 6** is the study of structural and mechanical properties of oligosaccharide strands inspired from natural species having 1 \rightarrow 4 linkage but varied monomeric units. **Chapter 7** concludes this thesis by pointing out the highlights, drawbacks and future perspectives of the work.

Chapter 2

Methodology

This chapter outlines the general theory, the methods applied for all the simulations performed, and the analysis techniques employed in the following chapters. Specific details pertaining to the simulation setup and methods are described in the respective chapters.

2.1 Molecular Dynamics

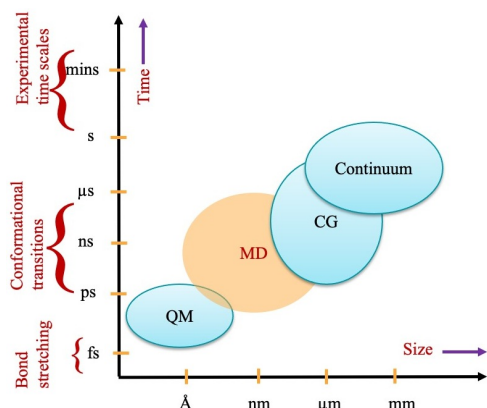


Figure 2.1: Simulations at different levels of resolutions and their applicability at different time scales.

Atoms are in constant motion. This motion involves rapid changes in their bonds, angles and dihedrals giving a possibility of newer interactions and may lead to ceasing of existing interactions. The bond vibrations are featured at a timescale of femtosecond (fs), while several conformational changes can occur in the timescale of nanosecond (ns) to microsecond (μ s). Molecular dynamics (MD) is a technique which gives an insight into this physical motions at atomic scale[1]. It simulates the time dependent behaviour of group of particles[2]. Although the biological processes are experimentally studied, following the inputs from MD simulations one can get a deeper insight of the atomic interactions. MD simulations can handle several thousand atoms unlike Quantum mechanical (QM) calculations which are limited to only few hundreds of atoms. Also there is no grouping of multiple atoms as one like in the case of Coarse graining (CG). Figure 2.1 shows schematic representation of simulations performed at different spatial and temporal levels of resolution. The microscopic details such as atomic positions and velocities are generated in MD simulations using Newtons laws of motions. Using statistical mechanics, this information can be processed to calculate the macroscopic observables like stress tensor, heat capacity, viscosity and other topological properties, structural properties, energetic properties and thermodynamic properties.

$$F_i = m_i a_i = -\frac{dE}{dr_i} \quad (2.1)$$

$$v_i = \frac{dr_i}{dt}; a_i = \frac{dv_i}{dt} \quad (2.2)$$

Where m_i and a_i are the atomic mass and acceleration for the i th particle. F_i as defined in equation 2.1 is the force acting on particle i due to interactions with other atoms. The force on an atom can be calculated as the derivative of energy with respect to change in the position of the atom. This knowledge of force and atomic mass can be used to determine position (r_i), velocity (v_i) and acceleration (a_i) of each atom along a series of small time step dt . For numerical integration of Newtons equations, “Verlet algorithm” is employed[3]. MD simulation is called as “deterministic”, i.e, if the initial set of positions and velocities are known, the subsequent time evolution can be determined from the current state. Apart from the use of classical laws, MD simulations require a description of interaction potential. This is provided in the “force field” (FF). The force fields are

developed based on the “ball and spring” model of atoms which are connected through bonds[4]. The general form of force field is:

$$E(R) = E_{bond} + E_{angle} + E_{dihedral/imp} + E_{LJ} + E_{Coul} \quad (2.3)$$

$$E_{dihedral/imp} = \begin{cases} k_{dihedral/imp}(1 + \cos(n_i\phi_i + \delta_i)) & : \text{if } n_i > 0 \\ k_{dihedral/imp}(\phi_i - \delta_i)^2 & : \text{if } n_i = 0 \end{cases} \quad (2.4)$$

$$E(R) = \sum_b k_{ij}^b (r_{ij} - r_0)^2 + \sum_a k_{ijk}^a (\theta_{ijk} - \theta_0)^2 + \sum_{dih} k_i^{dih} [1 + \cos(n_i\phi_i + \delta_i)] + \sum_i k_i^{constraint} (|\vec{r}_i - \vec{r}_{ref}|)^2 + \sum_i \sum_{j \neq i}^{N-1} 4\epsilon_{ij} \left[\left(\frac{\sigma_{ij}}{r_{ij}} \right)^{12} - \left(\frac{\sigma_{ij}}{r_{ij}} \right)^6 \right] + \sum_i \sum_{j \neq i}^{N-1} \frac{q_i q_j}{\epsilon r_{ij}} \quad (2.5)$$

where $E(R)$ is the potential energy of the molecule as depicted in equations 2.3, 2.4, and 2.5. E_{bond} , E_{angle} , $E_{dihedral}$ and E_{imp} describes the energy terms associated with bond length, bond angle, dihedral and improper angle respectively. These are the bonded interactions and describe harmonic vibrational motion for all the simulations in this thesis. The 2-body spring bond potential describes the harmonic vibrational motion between covalently bonded pair of atoms (i,j). Where $r_{ij} = \|\vec{r}_i - \vec{r}_j\|$ is used to determine the distance between the pair of atoms, r_0 is their equilibrium distance and k_{ij}^b is the spring constant of the bond. The 3-body angular bond potential is used to describe the angular vibrational motion occurring between an (i,j,k) triplet of covalently bonded atoms. Where θ_{ijk} is the angle in radians between $\vec{r}_{ij} = \vec{r}_i - \vec{r}_j$ and $\vec{r}_{kj} = \vec{r}_k - \vec{r}_j$, θ_0 is their equilibrium bond angle and k_{ijk}^a is the angle constant.

The dihedral and improper bonds are used to model the interaction between 4 bonded atoms. The 4-body dihedral angle also known as torsion angle, is used to describe the angular spring formed between the first three and last three atoms of a consecutively bonded (i,j,k,l)-quadruple of atoms. The energy for a dihedral or improper between atoms i,j,k and l is given by 2.4. where n_i is a non-negative integer and indicates periodicity of the bond type, $k_{dihedral/imp}$ is the multiplicative constant, ϕ_i is the calculated angle between the plane formed by atoms (i, j, k) and the plane formed by atoms (j, k, l). δ_i is the phase shift. When $n=0$, the vibrational motion is harmonic in nature and ϕ_i acts as equilibrium angle. If $n>0$, then it belongs to periodic motion. A given set of (i,j,k,l) quadruple atoms can contribute multiple terms to the potential, each with its own parametrization.

$E_{constraint}$ is the harmonic constraint term. Where $k_i^{constraint}$ is the force constant defined for atom i, \vec{r}_i is the current position of atom i and \vec{r}_{ref} is the reference position to which atom i is constrained. E_{Coul} and E_{LJ} i.e., Coulomb and Lennard-Jones potential respectively are energy changes associated with non-bonded interactions. This energy

function is used to calculate energy experienced by a given atom provided the positions of other atoms are known. r_0 and θ_0 are the equilibrium bond length and bond angle respectively. ϵ_{ij} and σ_{ij} are used for defining Lennard-Jones potential well[5]. ϵ_{ij} is a distance dependent dielectric function. It is the depth of energy minimum for a pair of atoms of the same type. On the other hand, σ_{ij} is the finite distance at which energy becomes zero. While, the partial charges q_i, q_j are used for defining Coulombic interactions. These parameters are derived from QM studies or by fitting to experimental quantities[6]. Over the years, several FFs have been developed using various strategies and varying levels of accuracy based on equation 2.5[7, 8, 9]. All the bonding and non-bonding parameters for polysaccharides and bile acids used in this thesis are taken from all atom CHARMM forcefield developed by Alexander Mackerell *et al.*[10, 11, 12, 13]. Water molecules are modelled using TIP3P developed by Jorgensen *et al.*[14, 15]. A.1 and A.2 are the sample input file for running GROMACS and NAMD simulation respectively.

2.2 Steered Molecular Dynamics Simulations

With the advent of massive computational resources, MD technique has been extended to huge systems. Systems with as many as thousands to couple of million atoms reaching the size of most nanomaterials. However, it is not yet possible to reach the typical laboratory timescales beyond few milliseconds. Also, biologically vital reactions are involved in transitions between equilibrium states like binding or dissociation of ligands. But these events involving barrier crossings, cannot be reproduced in MD time scales as they require high energy/temperature, application of external force etc. For this reason, some enhanced-sampling techniques are used which improves the conformational sampling space by providing energy to overcome the barriers separating different states of a system. This is called as “accelerated sampling”. Some of the commonly used accelerated sampling techniques are Replica exchange molecular dynamics (REMD), Metadynamics (METAD), Umbrella sampling, Multiscaling, Steered Molecular Dynamics (SMD) etc. These techniques help in observing conformational changes which are too rare otherwise. These rare states can be converted into highly populated states when the energy landscape is biased by force.

Grubmüller *et al.* and Klaus Schluten *et al.* are among the first few to introduce the applications of steered molecular dynamics (SMD) simulations[16, 17, 18]. It is a method which computationally mimics the use of Atomic Force Microscope (AFM) in estimating the interactions between two objects[17]. Unlike classical molecular dynamics simulation which carries out simulations in equilibrium, SMD is a non-equilibrium simulation. It takes inspiration from single molecule pulling experiments. As the system is forced away from its initial equilibrium conditions, transitions between several energy minima are captured along a specific reaction coordinate in an accelerated manner[19, 20]. Typically,

the range of forces lie between few tens to thousands of pico Newtons (pN). This enhances the sampling path of interest. Brief introduction on SMD is mentioned in section 1.7. In SMD simulations a PDB file has to be supplied which has information of the constrained atoms along with the force constant and the velocity with which they move. In these simulations, the center of mass of tagged atom(s) is allowed to move with constant velocity or constant force. The potential applied on the system with SMD is given by the following equation 2.6[21].

$$U(\vec{r}_1, \vec{r}_2, \dots, t) = \frac{1}{2}k[v t - (\vec{R}(t) - \vec{R}_0(t)) \cdot \vec{n}]^2 \quad (2.6)$$

Where k is the force constant specified in $kcal\ mol^{-1}\ \text{\AA}^{-2}$, v is the velocity specified in $\text{\AA}/(\text{time step})$ in the direction \vec{n} . $t \equiv N_{ts}dt$, where N_{ts} is the number of time steps elapsed in the simulation and dt is the time step size in femtoseconds (fs). Also, $\vec{R}(t)$ is the centre of mass of SMD atoms at the time step and R_0 is the centre of mass of initial position. The SMD simulation is set up as close as possible to AFM experiments. Also, the spring constant should be high enough to sample the local unbinding potential. The pulling velocity is determined based on the required closeness to AFM, the total pulling distance, time step and computer power which is available. Usually, a small velocity is chosen which facilitates long simulations, enough to study all the intermediate unfolding pathways. Apart from the intermediate states, micromechanical and elastic properties of the biomolecule, certain microscopic details missed by the experiments like role of hydrogen bonding and water in unfolding pathway can be explored using this technique. All the SMD simulations are carried out in orthorhombic simulation boxes in thesis.

In this context, it is noteworthy in understanding the stretching of macromolecule using AFM force spectroscopy mode. The molecule being studied is anchored on the surface of substrate which is usually made of gold, mica, silver, silica, pyrolytic graphite, glass, silicon dioxide, zinc oxide, zinc sulphide or calcium oxide. The functionalised AFM cantilever tip picks up the molecule somewhere along its chain. As the cantilever is moved, the molecule gets stretched by the elastic force of the deflecting cantilever. The probe is repeatedly brought towards the surface and then retracted. In this way, the mechanical response of molecule in the force-extension curve can be obtained[22]. The force-extension relation can be measured and calculated under different boundary conditions. Either by fixing the length of the macromolecule and measuring the force required to maintain its length, or apply force and thereby measure the resultant extension of the molecule. Figure 2.2 shows the schematic representation of an AFM experiment to measure the force-extension

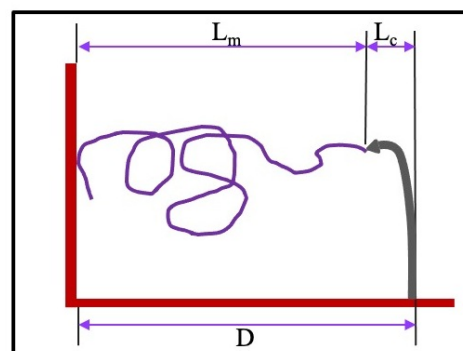


Figure 2.2: Schematic of an AFM experiment to measure the force-extension curve of a macromolecule.

curve. Figure 2.2 shows the schematic representation of an AFM experiment to measure the force-extension

curve. The tip is at a distance D from the surface of anchoring when there is no contact between cantilever tip and the molecule. Once the tip is attached to the molecule, the molecule is stretched to an end-to-end length of L_m . Thus, the cantilever gets deflected by a length of L_c such that $D=L_m+L_c$. L_m is always positive whereas L_c can have any sign. The distance D is adjusted and the resulting tip deflection is measured. This deflection L_c is used for calculation of force using Hooke's law ($F = K_c L_c$) or any other force law. The same can also be studied by deflection of cantilever as a function of piezoelectric surface displacement[23]. In order to apply forces or perform on the fly calculations, Tool Command Language (TCL) is implemented in NAMD analysis[24]. It provides a ready made scripting interface to high performance code written in programming languages like C or C++. It helps in parsing the configuration file for simulations, thus allowing variables and expressions to be used in initially defined options and then to change required options while running simulation. A.3 and A.4 are the sample SMD input files for running the simulations.

Extension profiles of different polysaccharides as obtained from AFM experiments and SMD simulations are compared. Here the normalised length of polysaccharide is defined as $l = l_t/l_f$. Where, l_t stands for length of polysaccharides against a pulling force at a particular time instant. l_f stands for the final length of polysaccharide at the end of 5 ns of SMD simulation. For the AFM data, length of polysaccharide is already in normalised form, so this normalisation is done for SMD data. Further, the abscissa of AFM curves are normalised in such a way that, at highest force of AFM curves, the extension is made equal to that of SMD simulations for the same force.

2.3 Modelling of initial configurations

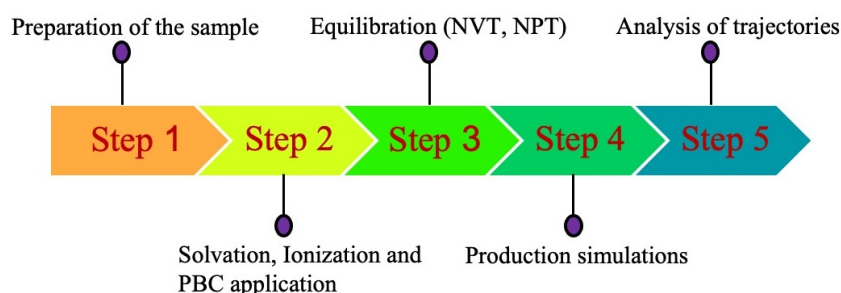


Figure 2.3: Step by step procedure involved from sample preparation to analysis

The starting configurations of all the polysaccharides used in this study were constructed using Glycan reader and Modeler tool of CHARMM-GUI[12, 13]. The initial coordinates of bile acids and bile salts are generated using Ligand reader and Modeler of CHARMM-GUI[25]. The simulation boxes are prepared either by GROMACS editconf & solvate

tools or VMD psfgen[26] & solvate plugin[27] or the Multicomponent Assembler Module of CHARMM-GUI[28]. Figure 2.3 shows the step-by-step procedure involved in running an MD from initial sample preparation to analysis.

2.4 Simulation details

The simulations discussed in this thesis are performed using GROMACS[29] (GROningen MAchine for Chemical Simulations) or NAMD[7] (Nanoscale Molecular Dynamics) simulation engines. The detailed description of configuration parameters is given in (<https://manual.gromacs.org/current/user-guide/mdp-options.html>) for GROMACS and (<https://www.ks.uiuc.edu/Research/namd/2.9/ug/node12.html>) for NAMD simulations. A.1 and A.2 has an example of input configuration file used for GROMACS and NAMD NPT simulations. To simulate a system close to realistic environment and avoid edge artefacts, Periodic Boundary Conditions (PBCs) are employed. These are a set of boundary conditions for approximating large systems using a small replica called “unit cell”. This unit cell can be replicated in space to form an infinite lattice. In the due course of the simulation, as the particles move in the original box, the periodic images move exactly in the same way in the neighbouring boxes. In topological terms, when an object passes through one of the sides of unit cell, it would then reappear exactly on the opposite side with same velocity. If the simulation box is so small as to an atom sees its image, entail of internal correlations occur. So, the size of the simulation box should be large enough to avoid this artefact. PBC is applied for all the simulations studied in this thesis. Simulations involving stretching of polysaccharide chains need simulation box to be long enough to house all the possible conformational transitions.

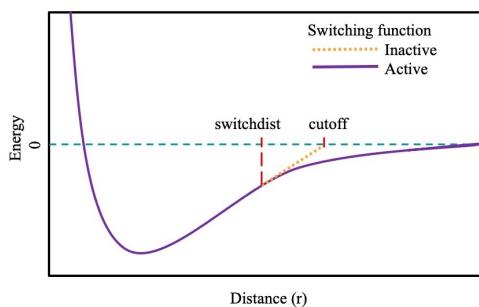


Figure 2.4: van der Waals potential graph with and without application of switching function.

The center of mass drifting is prevented by using ‘COM-pulling’ in GROMACS and ‘COM-motion’ in NAMD as ‘no’. Energy calculation at each integration step is computationally expensive. This is because for a system of N particles, N^2 summations are required. The keyword ‘Cut-off’ distance in GROMACS and ‘cutoff’ distance in NAMD is specified beyond which non-bonding interactions are not calculated. This would enhance the computational efficiency. The cutoff parameter is imposed

only on Lennard-Jones potential as it is fast decaying. It is unlike the Coulombic potential with terms r^{-1} leading to slower decay compared to the former with r^{-6} term[30]. The ‘rvdw’ parameter in GROMACS and ‘switchdist’ in NAMD is used for smooth truncation

of vdW potential at the cutoff distance. Setting this parameter as ‘off’ will lead to abrupt truncation of vdW energy at cutoff distance thus will lead to non-conservation of energy. The values of these parameters are lower than that set for ‘cutoff’ as the smoothing function starts acting well before to bring van der Waals potential to zero at cut off. Figure 2.4 shows the van der Waals potential graph with and without the application of switching function (equation 2.8). The potential is smoothly reduced to 0 keeping the switching function active. On the other hand, truncation point is seen with discontinuity without the switching function. The modified energy function of van der Waals interaction is given by equation 2.7.

$$E_{vdw} = \left(\frac{A}{r_{ij}^{12}} - \frac{B}{r_{ij}^6} \right) S_{vdw}(|\vec{r}_{ij}|) \quad (2.7)$$

where the switching function S_{vdw} is defined as,

$$S_{vdw}(|\vec{r}_{ij}|) = \begin{cases} 1 & : |\vec{r}_{ij}| \leq R_{on} \\ \frac{(R_{off}^2 - r_{ij}^2)^2 (R_{off}^2 + 2|\vec{r}_{ij}|^2 - 3R_{on}^2)}{(R_{off}^2 - R_{on}^2)^3} & : R_{on} < |\vec{r}_{ij}| < R_{off} \\ 0 & : R_{off} \leq |\vec{r}_{ij}| \end{cases} \quad (2.8)$$

Where R_{on} is specified by the parameter ‘switchdist’, R_{off} is specified by the configuration value ‘cutoff’ and r_{ij} is the distance between two atoms.

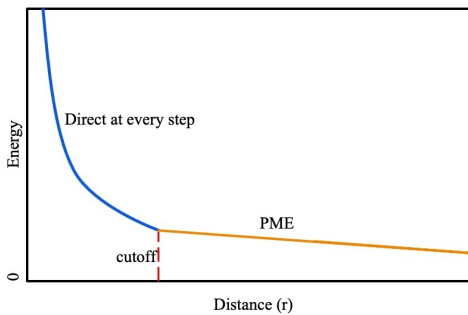


Figure 2.5: Electrostatics potential graph when full electrostatics are used.

There are two cases to consider for electrostatic interactions. The first case is where electrostatics are truncated at a given distance and the second case is where full electrostatics are employed. In the first case, the cutoff parameter represents the local distance up to which the electrostatics are calculated for every time step. Beyond this cutoff distance, the electrostatic interactions are assumed to be zero or ignored. If the switching function is set on, the shift-

ing function is applied to prevent the discontinuity in potential at cutoff distance. In case of full electrostatics, the electrostatic interactions are not truncated at any distance. The cutoff distance parameter in this case represents, the local distance within which electrostatic pairs are calculated for every time step. Beyond this distance, interactions are calculated only periodically. In periodic systems, Particle Mesh Ewald (PME) summation is used for computing long range interactions. It is an efficient method for computing full electrostatics. PME method is used for all the simulations in this thesis. Figure 2.5 shows the electrostatics potential curve when full electrostatics are used. The first portion (represented in blue) is calculated directly for every time step while the second

portion (represented in orange) is calculated using PME. PME full electrostatics are less expensive than large cut off values and is more accurate. Small integer values of grids corresponding to the size of unit cell, is specified. NlogN scaling is employed with fast Fourier transformations for calculations of reciprocal sum and it is more efficient than Ewald summation[31].

Another critical parameter for non-bonded interaction calculations is ‘pairlistdist’. A pair list containing all pairs of atoms for which non-bonding interactions to be calculated is used, to reduce the cost of computation. This search for pairs of atoms with which they have their interactions calculated is quite an expensive operation. So, the pairlist is calculated only periodically. But the atoms move at a faster pace than the updation of this list. So, if the pairlist is to be built including atoms only within cutoff distance, it will be possible for the atoms to drift closer than the cutoff distance during the subsequent time steps and still not have their non-bonded interactions calculated. Thus the parameter pairlist is used to specify distance greater than cutoff distance for the pairs to be part of pairlist. Figure 2.6 shows the difference between pair list distance and cutoff distance. The pair list distance thus specifies a boundary which is slightly larger than the cutoff distance so that pairs of atoms can move in and out of boundary specified by cut off distance and do not hamper energy conservation.

For all the simulations, the intramolecular non-bonding interactions separated by 3 bonds (1-4 interactions) are excluded. The time step chosen has to be smaller than fastest motion in the system. Bond vibrations in general are of the order of femtoseconds, thus restricting the time step to ~ 2 fs. Throughout, a time step of 2 fs is used for the MD simulations reported in this thesis and 1 fs for SMD simulations. A.3 and A.4 have the input files for SMD simulations. SETTLE algorithm[32] for NAMD simulations and LINCS algorithm[33] for GROMACS simulations are used to maintain all water molecules and bonds involving hydrogen as rigid. ‘Noose-Hoover thermostat’ and ‘Parrinello-Rahman barostat’ are used for all GROMACS simulations with a coupling constant of 1 and 2 ps respectively. Langevin dynamics is employed to regulate the temperature and pressure in all NAMD based simulations with a damping coefficient of 5 ps^{-1} .

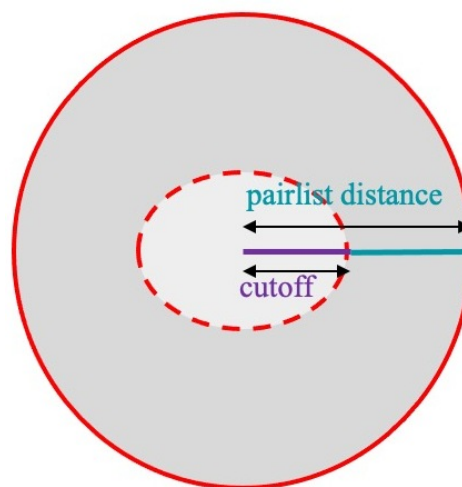


Figure 2.6: Difference between cutoff and pairlist distance.

2.5 Analysis techniques

VMD is used for visualization of simulated trajectories[34]. MATLAB is used for plotting all the graphs. The Ramachandran (φ, ψ) angles and Cremer Pople puckering angles (θ, φ, R) exhibited by individual residues are determined using Plumed[35, 36] scripts. These are calculated using the plumed keyword ‘TORSION’ and ‘PUCKERING’ respectively. The equations behind the calculation of puckering coordinates is briefly explained in section 1.5.1. The root mean square deviation (RMSD), radius of gyration (R_g), end to end distance, inter and intramolecular hydrogen bonding and solvent accessible surface area (SASA) as shown in chapter 3 are calculated using the GROMACS tools “gmX rms”, “gmX gyrate”, “gmX polystat”, “gmX hbond” and “gmX sasa” respectively.

$$RMSD = \sqrt{\frac{1}{n} \sum_{i=1}^n ((r_{ix} - r_{0x})^2 + (r_{iy} - r_{0y})^2 + (r_{iz} - r_{0z})^2)} \quad (2.9)$$

Equation 2.9 is used for calculation of RMSD, where r_i and r_0 are the positions of reference structures and initial or mean position of ‘n’ atoms. This is usually calculated for the backbone atoms. In this case being the C & O atoms and excluded for H atoms. The double cubic lattice method is used in the determination of SASA[37].

$$g(r) = \frac{\langle \rho(r) \rangle}{\rho} \quad (2.10)$$

$g(r)$ given in equation 2.10 is defined as the average local number density of particles at a distance r , to the bulk density of particles ρ . Around a central reference particle, $g(r)$ gives a statistical description of particle density and local packing of the system. The ^1H NMR profiles of bile acid in presence and absence of β -glucan is done using DFT calculations. The inter & intramolecular hydrogen bonding and interaction energies in chapter 4 are calculated using GROMACS tools “gmX hbond” and “gmX energy” respectively. In SMD simulations, the single point energies of conformers at various polysaccharide stretching points is done through DFT calculations using B3LYP functional and 6-311++g (d,p) basis set. “WebPlotDigitizer” (<https://automeris.io/WebPlotDigitizer/>) is used for digitalization of data when and where needed.

2.5.1 Principal component analysis (PCA)

Principal component analysis is a statistical technique used for dimension reduction, feature extraction and data visualization[38, 39]. It aims to transform a high-dimensional dataset into a lower-dimensional space while preserving the most important information or patterns in the data. It involves an orthogonal linear transformation of data to a new coordinate system in such a way that the greatest variance of the data comes to

lie on the first coordinate. This first coordinate is called as first principal component (PC1). The PC1 can be written as the linear combination of variables X_1, X_2, \dots, X_p as given in equation 2.11 where the sum of squares of weights ($a_{11}, a_{12}, \dots, a_{1p}$) is constrained to be 1. The second principal component (PC2) is calculated in such a way that it is uncorrelated/perpendicular to the first principal component. This second greatest variance on second coordinate and this is followed by subsequent ones. This is continued until the total principal components are calculated. In this way, loss of information is minimized. PCA can be performed on any structure database in order to capture and characterize inter-conformer relationships. The number of variables present in the dataset is referred as dimensionality.

$$Y_1 = a_{11}X_1 + a_{12}X_2 + a_{13}X_3 + \dots + a_{1p}X_p = a_1^T X \quad (2.11)$$

$$a_{11}^2 + a_{12}^2 + \dots + a_{1p}^2 = 1 \quad (2.12)$$

The transformation of original variables to matrix form can be written as follows, $Y = XA$. The values within a given row matrix A, are called ‘loadings’ for a particular variable. They describe how much each variable contribute to a particular principal component. If the loadings value is large, then it implies, that particular variable has a strong relationship with that particular principal component.

PCA is sensitive to the scale of variables. So, the data is standardised to have zero mean and unit variance. From the standardised matrix, its covariance is calculated. The covariance between two variables measures their relationship and indicates how they change together. The covariance matrix is diagonalised to obtain eigen vectors (principal component) and corresponding eigen values. The eigenvectors (column vector) represent the directions in the original feature space along which the data vary the most, and the eigenvalues (scalar values) indicate the amount of variance explained by each eigenvector. The relation between variables and principal components is given by correlation values. These values can range from -1 to +1. If the correlation value is -1, then the variables are inversely proportional to each other while if the correlation value is +1, then the variables are directly proportional to each other. If the correlation value is 0, then the variables are not correlated to each other.

The eigen values monotonically decrease from first principal component to the last. These eigenvalues are commonly plotted on a ‘scree plot’. To obtain the new lower-dimensional representation of the data, the standardized data matrix X is projected onto the selected principal components. This is done by taking the dot product of X with the matrix of selected eigenvectors. The resulting matrix represents the transformed data, where each row corresponds to a data point, and the columns represent the principal components. The positions of each observation in this new coordinate system of principal components are called ‘scores’. The overall motion in the dynamical space is explained by different principal components. If the values of all principal components are similar, then the system

is exhibiting diffusive behaviour. If one of the principal component value is dominating, then the system has a discrete behaviour. Principal Component Analysis of dynamical conformational space of glycosidic oxygens of polysaccharides is done using Bio3D[40] on R platform in chapter 3. PCA is done both on the cartesian coordinates and the torsion angles. The dihedral angle PCA is also quite appealing as the other internal coordinates like bond length and bond angle do not undergo large amplitude changes[41].

2.5.2 3x3x3 Simulation cell to account for boundary crossing artefacts of soft clusters

To account for the boundary crossing effects of the portions of the soft aggregate during the course of the simulations in chapter 4, a bigger simulation cell of 3x3x3 dimensions is created from the molecular dynamics trajectory by accounting for the periodic images along $\pm x$, $\pm y$ and $\pm z$ directions. A.5 has the MATLAB script corresponding to big box generation. The coordinates obtained from this ‘big box’ is then used to calculate the radial distribution functions, the coordination number A.6, radius of gyration A.7, moment of inertia, shape anisotropy of the biggest cluster formed at a given time instant along with the scattering profiles. The radial distribution function, $g(r)$, is calculated from post-processing of the simulation trajectory using a FORTRAN code. This ‘big box’ is constructed to ensure proper normalization of $g(r)$.

2.5.3 Moment of inertia and shape anisotropy

$$I = MR_g^2 = (m_1r_1^2 + m_2r_2^2 + \dots + m_nr_n^2) \quad (2.13)$$

The moment of inertia (I) about a given axis of rotation is given as equation 2.13. Where R_g is the radius of gyration, it is the distance between axis of rotation to center of mass of the structure. n is the number of particles and r_1, r_2, \dots, r_n are the perpendicular distances from particle to the axis of rotation and m_1, m_2, \dots, m_n are the mass of corresponding particles. For the same system, different axes of rotation will have different moments of inertia about those axes. All the moment of inertia components can be summarized into a moment of inertia tensor. This matrix is given by the following equation.

$$I = \begin{bmatrix} I_{xx} & -I_{xy} & -I_{xz} \\ -I_{yx} & I_{yy} & -I_{yz} \\ -I_{zx} & -I_{zy} & I_{zz} \end{bmatrix} = \begin{bmatrix} \sum_{k=1}^n m_k(y_k^2 + z_k^2) & -\sum_{k=1}^n m_k x_k y_k & -\sum_{k=1}^n m_k x_k z_k \\ -\sum_{k=1}^n m_k x_k y_k & \sum_{k=1}^n m_k(x_k^2 + z_k^2) & -\sum_{k=1}^n m_k y_k z_k \\ -\sum_{k=1}^n m_k x_k z_k & -\sum_{k=1}^n m_k y_k z_k & \sum_{k=1}^n m_k(x_k^2 + y_k^2) \end{bmatrix} \quad (2.14)$$

The matrix in equation 2.14 is diagonalised. The diagonal components are the principal components of the moment of inertia along xx, yy and zz directions respectively. The square of radius of gyration is determined by dividing the sum principal components of inertia by the total mass of the system. A.7 is the MATLAB script used for calculating the moment of inertia of the biggest cluster and there by its radius of gyration. The relative shape anisotropy can be calculated from the principal moments of inertia using the following expression,

$$\kappa^2 = \frac{3(I_{xx}^4 + I_{yy}^4 + I_{zz}^4)}{2(I_{xx}^2 + I_{yy}^2 + I_{zz}^2)} - \frac{1}{2} \quad (2.15)$$

2.5.4 Small angle scattering profiles

Small angle scattering experiments are an efficient way to characterise the general shape of soft molecular assemblies. The scattering intensity $I(q)$, can be expressed in terms of the total structure factor $S(q)$. The total structure factor $S(q)$, can be estimated from the molecular dynamics trajectories by calculating the atom-atom radial distribution functions of all possible combination of atoms (except H) comprising the soft cluster and using the corresponding atomic scattering functions, f.

$$I(q) \propto S(q) = \sum_i C_i f_i^2 + 4\pi\rho \int_0^\infty \frac{\sin(qr)}{qr} r^2 \sum_{i,j} C_i C_j f_i f_j (g_{ij}(r) - 1) dr \quad (2.16)$$

i and j represent the atomic indices running over all the atoms (except H) in the molecular assembly under consideration.

$$f = \sum_{i=1}^5 a_i e^{-b_i(\frac{q}{4\pi i})^2} + c_i \quad (2.17)$$

The atomic scattering functions is estimated from the work of Waasmaier and Kirfel[42, 43]. Equation 2.17 is used to calculate atomic scattering function of C and O atoms present in the molecule. It is a linear combination of 5 gaussians with 11 parameters. Where a_i, b_i and c_i are the parameters of analytical scattering factor functions. Fourier transformation of the pairwise radial distribution function g_{ij} , is calculated between i^{th} and j^{th} atomic species in solution phase, and is averaged over all orientations. ρ denotes the total number density of the simulation box and C denotes the mole fraction for each atomic type. Each atomic-pair distance r in the molecule contributes $\sin(qr)/qr$ like oscillatory term to the scattering intensity. q is the reciprocal space scattering vector and is represented by,

$$q = \frac{4\pi}{\lambda} \sin \theta \quad (2.18)$$

Here, θ is half the scattering angle and λ is the wavelength of the incident radiation. Equation 2.16 can be written as follows for the bile acids studied in chapter 4.

Where q values range from 0.01 to 2 \AA^{-1} with an interval of 0.01 \AA^{-1} and r values range from 0.25 to 60.25 \AA .

$$I(q) = C_c f_c^2 + C_o f_o^2 + 4\pi\rho \int_0^{\infty} \frac{\sin(qr)}{qr} r^2 [C_c^2 f_c^2 (g_{cc}(r) - 1) + C_o^2 f_o^2 (g_{oo}(r) - 1) + C_c C_o f_c f_o (g_{co}(r) - 1)] \quad (2.19)$$

ρ is determined using the expression,

$$\rho = \frac{\text{number of molecules in system } X \text{ total number of atoms in that molecule}}{(\text{edge length of the box})^3} \quad (2.20)$$

Section [A.8](#) has the MATLAB scripts which is used to calculate the scattering profiles of soft bile acid clusters.

Chapter 3

Relation between glycosidic linkage, structure and dynamics of α and β -glucans in water

This chapter is based on the following paper, Peesapati, S., Sajeevan, K., Patel, S. & Roy, D. Relation between glycosidic linkage, structure and dynamics of α -and β -glucans in water. *Biopolymers*. **112**, e23423 (2021)

url:<https://onlinelibrary.wiley.com/doi/abs/10.1002/bip.23423>

3.1 Introduction

Carbohydrates are integral components of both extracellular and intracellular matrix in living organisms. They exist as mono-, di-, oligo-, or as polysaccharides, when their reducing ends are free and not covalently linked to other molecules. They are also found as glycoconjugates, where the terminal sugar residues form N or O glycosidic linkage to proteins or lipids. Apart from being the predominant source of energy, carbohydrates are essential components of our staple diet. They are the primary macronutrients consumed by humans. They comprise more than 50% of the regular intake. Certain form of this macromolecule, called **β -glucans** have proved immensely beneficial for human health in resisting chronic diseases and modulating/blocking metabolic pathways. These conditions can otherwise be detrimental to health. For instance, in combating dyslipidemia by slowing down cholesterol/low-density lipoprotein (LDL) absorption in the gut[1, 2, 3, 4, 5]. This class of complex polysaccharides, especially those with mixed glycosidic linkages are indeed “super foods,” owing to their hypolipidemic effects[2, 5, 6, 7]. With cardiovascular diseases being the lead cause of death worldwide, the need for such super foods in order to promote the cardiovascular health and cholesterol lowering properties are increasing. Both Food and Drug Administration (FDA) and The European Food Safety Authority (EFSA) have approved the health benefits of β -D-glucans. After various clinical trials, a minimum dosage of 3 g/day of β -glucan as part of diet low in saturated fat and healthy life style was recommended by FDA for successful reduction in blood cholesterol levels[1, 8, 9, 10, 11]. They also exhibit wide spectrum of biological properties like immunostimulant, anti-tumour, anti-ageing and anti-inflammatory.

These β -glucans are natural ingredients of endosperm and aleurone cell walls of fibre rich cereals (e.g., oats, barley, wheat and rye), bacteria and fungi[2]. They significantly vary in chemical and physical diversity, depending on the source of extraction[12]. For example, the endospermic cell walls of food grains like oats, barley and wheat mainly constitute mixed-linkage β -glucans composed of linear polysaccharides in which D-glucosyl residues are linked by 1 \rightarrow 3/ 1 \rightarrow 4 glycosidic bonds. Schematic representation of the same is shown in Figure 1.10. The ratio of these linkage types varies with the source of β -glucan. A major component of the fungal and yeast cell walls and mushrooms like Shiitake is (1 \rightarrow 3)- β -linked glucose polymer with (1 \rightarrow 6)- β -linked side chains. The structures of mushroom and fungal β -glucans are different from the cereal β -glucans and so are their functions and efficiencies. Detailed explorations on their functions can be obtained from some comprehensive clinical level research literature[8, 9]. Mixed β 1 \rightarrow 3/1 \rightarrow 6 D-glucans, derived from baker’s yeast, are also known for their potency as immune-system enhancers[13].

Food scientists have already recognized the beneficial and detrimental effects of carbohydrates on human health, especially in the light of diabetes, obesity, celiac disease, gluten allergy, and so forth. The effect of water-insoluble oligosaccharides/carbohydrates on bowel

movement as purgatives is also explored widely. However, the most interesting property of some water-soluble oligosaccharides containing 1→3/1→4 β -*D*-glucopyranoside linkages with /without 1→6 side chains in lowering the plasma cholesterol/LDL is what is exceedingly fascinating and worth researching further at the molecular level[1, 11, 14]. The effect of β -glucans in reducing serum cholesterol is related to the dissolution and aggregation behaviour of these oligosaccharides in the gut during digestion. The abundance of β -glucan in the digestive tract is believed to create viscous slurries during digestion. This decreases the intestinal uptake of dietary cholesterol resulting in the increase of hepatic conversion of cholesterol into bile acids. So, the cholesterol pools are reduced and plasma LDL removal is facilitated[9]. Electrostatic interaction between bile acid pool and β -glucan aggregate is also considered to play an important role in the process[15, 16].

Usually, polysaccharides are non-toxic in nature. Thus, they are employed for various food, biomedical and pharmaceutical applications. These applications depend on their solubility in solvents. In most naturally occurring systems, polysaccharides function in aqueous medium. This brings up a huge necessity in understanding their structural changes, dynamics spanned, their interaction with other particles of the medium, mechanical features, etc. The relationship between polysaccharide structure and solubility is well established[17, 18, 19]. This present work is attributed in understanding of the structural and dynamical properties of β -glucans. In this context the behaviour of the corresponding anomeric α -series of glucans is equally important to understand what role do stereochemistry and glycosidic linkage pattern play in dictating the structural and dynamical attributes. Apart from just being a comparative benchmark, α -glucans, like starch and glycogen are known for their energy-storing capacity in nature and are worth exploring further.

Physical and chemical properties of these oligosaccharides vary widely depending on the anomericity of the *D*-glucose residue, repeat sequence, molecular weight and linkage pattern[16, 20]. Owing to the conformational constraints imposed by the presence of cyclic monomers and the intramolecular H-bonds, the oligosaccharide chains, especially those linked by 1→3/1→4 glycosidic linkages are fairly stiff in nature. Oligosaccharides having 1→6 linkages, which are actually “three-bond” glycosidic linkages allows extra freedom to the chain. A stiff chain would impart high shear viscosity to the solution[21, 22]. Hence, the structural attributes of the glucan are important factors, which regulate physical properties like water solubility, viscosity, and gelation propensity[23, 24, 25, 26, 27, 28].

Along the same line, the contrasting flexibility imparted to the oligosaccharide chains as the glycosidic linkage type of either the α or β -*D*-glucopyranosyl units are varied is an important physical attribute to calibrate properly. A very good measure of chain flexibility is the persistence length of the oligosaccharides. However, here, as the lengths of oligosaccharides are limited, the decay of the autocorrelation functions for the glycosidic torsion angles are followed to estimate the chain flexibility[28]. Literature survey of

molecular level experimental or computational studies in the current field shows that most reports encompass primarily the di-, some oligo- and few polysaccharides in a systematic way[23, 29, 30, 31, 32, 33]. However, it is still challenging to draw patterns or general conclusion out of the dataset as the structural or dynamical behaviour is very specific and customized for a given oligosaccharide, depending a lot on the residues involved, the degree of polymerization, the glycosidic linkage pattern and the solvent/temperature conditions used. Investigating the structure and/or dynamics of oligosaccharides is especially challenging owing to their numerous degrees of freedom, which make the conformational space highly complex. Thus, this work is an attempt to compare and contrast the two-anomeric glucan series in water, composed of linear polymers having either α or β -*D*-glucopyranosyl residues with various glycosidic bond positions (1→3/1→4/1→6) using molecular dynamics simulations.

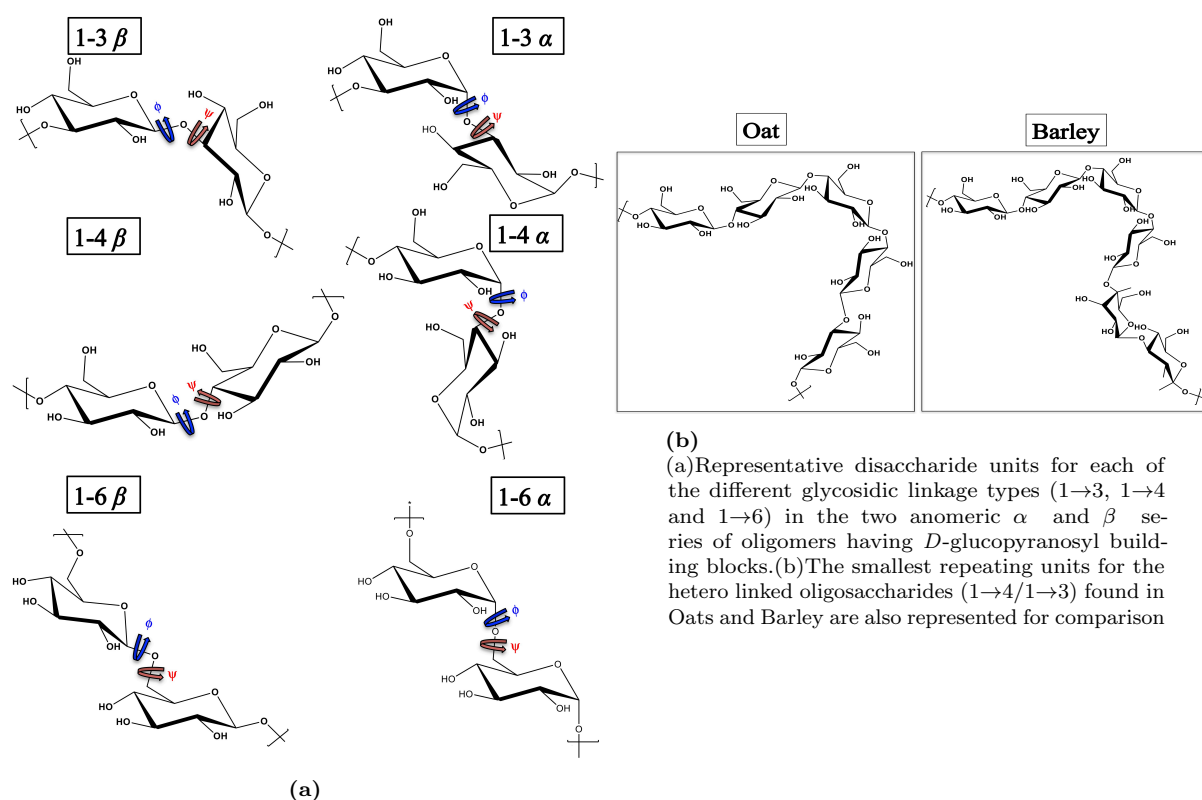


Figure 3.1

3.2 Methodology

3.2.1 Modeling of oligosaccharides

The initial coordinates of the polysaccharides are generated using Glycan Reader and Modeler as available in CHARMM-GUI[34, 35]. Homo oligosaccharides containing only α

or β -D-glucopyranosyl residues having any one of the three different glycosidic linkage patterns, namely 1 \rightarrow 3, 1 \rightarrow 4 and 1 \rightarrow 6 are modeled and solvated with \sim 28,000-31,000 TIP3P water. Each of these polysaccharide strands is composed of 15 residues. Additionally, mixed 1 \rightarrow 4/1 \rightarrow 3 linked β -D-glucopyranosides as found in oat and barley are also modeled as shown in Figure 3.1. Oat and barley fragments have 16 and 20 β -D-glucopyranosyl residues, respectively. Smallest repeating units of oat and barley are shown in Figure 3.1b. The oat fragment has one 1 \rightarrow 3 linkage after three consecutive 1 \rightarrow 4 linkages while the barley chain has one 1 \rightarrow 3 linkage after four consecutive 1 \rightarrow 4 linkages. Final equilibrated cubic simulation boxes have an edge length of \sim 80 to 95 Å. All the systems under consideration correspond to a concentration of \sim 0.5% to 0.7% (wt/wt). Each oligosaccharide is explored with multiple starting structures.

3.2.2 Simulation software, parameters and force fields

All MD simulations in this chapter, have employed GROMACS as the molecular dynamics software[36]. The polysaccharides are modeled following the CHARMM36 force field[37, 38, 39]. The water molecules are explicitly modeled by TIP3P forcefield as incorporated in CHARMM36[39]. In all the simulations reported, a time step of 2 fs is used. The “LINCS” algorithm is used to keep all waters and bonds involving hydrogens rigid. Each of the system is energy minimized using the steepest descent algorithm followed by equilibration in NVT ensemble for about 10 ns. This is followed by 20 ns of equilibration and 90 ns of production runs in NPT ensemble. These simulations are carried out at 310 K and 1.013 bar pressure. Temperature and pressure are kept constant by coupling the oligosaccharides and solvent to a Nose-Hoover thermostat[40, 41] and Parrinello-Rahman barostat[42] with coupling constants of 1 and 2 ps, respectively. Cubic PBC is used along the three directions of the orthogonal simulation box. A cutoff distance of 1.2 nm is used for the non bonded vdW interactions, with the switching of LJ potential starting at 1.0 nm, extending up to 1.2 nm. A pair list distance of 1.2 nm is used for vdW and electrostatic calculations. Coulomb interactions are calculated through the PME method. Intramolecular non-bonded interactions between atoms separated by three bonds (1-4 interaction) are excluded. Visualization of the structures and analysis of the data are done using VMD[43], PLUMED[44, 45], Gromacs analysis tools and MATLAB (R2015b, version 8.0). The principal component analysis is done using Bio3D library in R platform[46]. The H-bonds are estimated within a cutoff distance of 3.5 Å and an Acceptor-Donor-Hydrogen (A-D-H) angle cutoff of 30°.

3.3 Results and discussion

Considering the conventional solvent water, a moderately high temperature of 310 K is used. A first-hand RMSD analysis for the polysaccharides without hydrogen, as calculated with respect to the starting

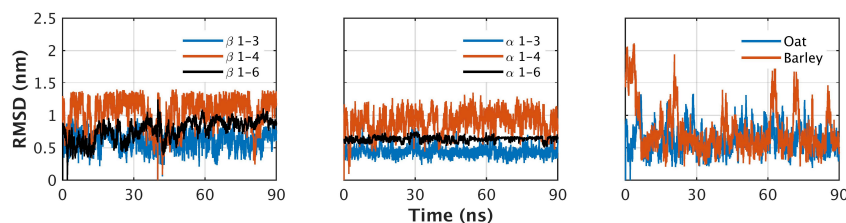


Figure 3.2: RMSD plots of oligosaccharides (without Hydrogen).

structure of the production run trajectory indicates that throughout the simulations, all the systems exhibit significant conformational fluctuation. Figure 3.2 shows the RMSD plots of oligosaccharides part of this study. The reference structure is the starting configuration of the production run trajectory for each system. The fluctuations are especially prominent for the oligosaccharides having only 1→4 glycosidic linkage or mixed 1→3/1→4 linkages as found in oats and barley sequence.

Anomer series	Glycosidic linkage	φ	ψ	ω	References
β	1→3	-72(-69 to -85)	-108(-109 to -162)	-	[31]
	1→4	-75(-71 to -96)	111(110 to 154)	-	[47, 48, 49, 50]
	1→6	-70 (~ -70)	± 178 (~ ± 178)	-66 (gg) -59(gt)	[29]
α	1→3	87 (71-100)	-138 (-90 to -135)	-	[47, 51, 52, 53]
	1→4	98	98	-	
	1→6	66 (64-70)	-170 (-170 to -178)	-63 (gg)	[47, 53]
		66 (59)	78 (94)	62 (gt)	

Table 3.1: Most Probable values of the glycosidic torsion angles for the different linkages in oligosaccharides composed of 15 *D*-glucopyranosyl units

The starting coordinates of glucans is challenging to model, as the 3D structures of most of these complex polysaccharides are still experimentally unattainable. Having said that, one can still attempt to generate a reasonable starting configuration of these complex molecules using algorithms based on heuristics, incorporating information from experimental data to create the three-dimensional structure. The CHARMM-GUI glycan builder is one such tool. Therefore, the starting structures already have a quite close guess to the experimentally observed internal coordinates and overall structural parameters. Hence in our equilibrium simulations, while fluctuations reflecting the extent of rigidity in diverse glucans having varied glycosidic linkages are seen, the overall structures appear not to evolve much. However, outcomes of the simulations have been checked in terms of structural data like the glycosidic dihedral space spanned by the oligosaccharides and

compared with literature, wherever available. References to experimental data are given in Table 3.1.

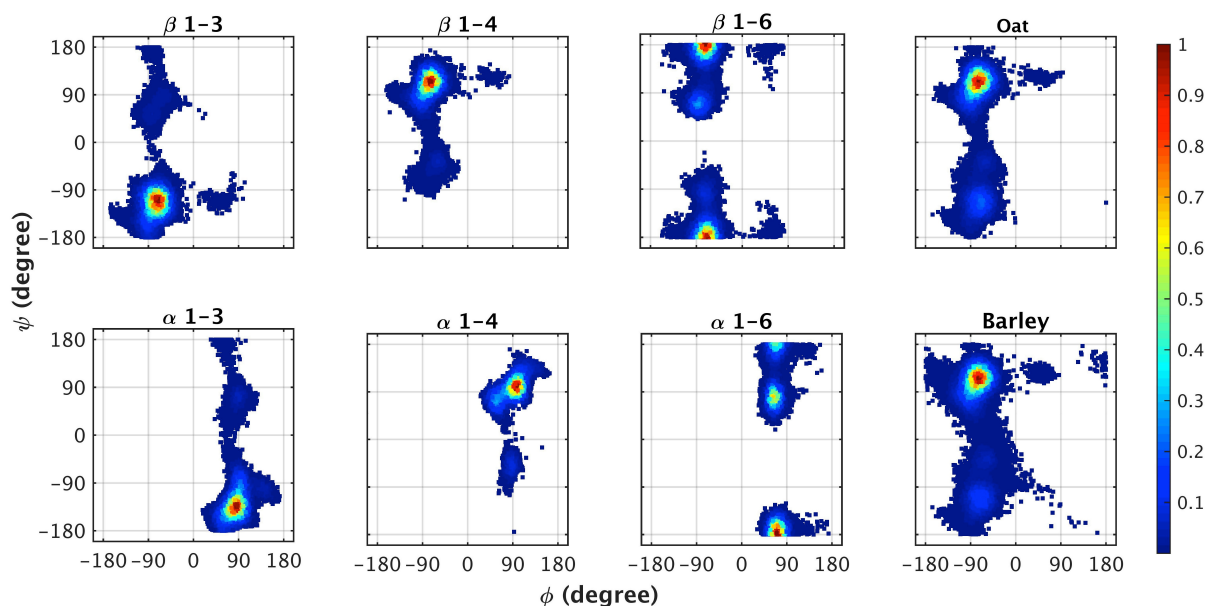


Figure 3.3: Dihedral angle (φ, ψ) distributions of oligosaccharides.

The (1 \rightarrow 3), (1 \rightarrow 4) or (1 \rightarrow 6) glycosidic linkages that feature most predominantly in natural α or β -glucan fibers, like those in starch, oat and barley, have significantly distinctive distributions of the glycosidic torsion angles $\varphi(O_5 - C_1 - O_1 - C'_n)$ and $\psi(C_1 - O_1 - C'_n - C'_{n-1})$ as defined for the (1 \rightarrow n) glycosidic linkage, where n=3, 4 or 6. They are shown in Figure 3.1. Figure 3.3 shows the comparative φ, ψ distributions, the “Carbohydrate-Ramachandran” plots for the oligosaccharides under consideration. The plots are globally normalized and the same color bar is applicable to all. Hence, the color distributions for all the plots are comparable to each other. The heat-maps indicate the region of maximum probability and the inverted nature of the φ glycosidic torsion angles in the two-anomeric series of glucans. It further points to the additional freedom that the 1 \rightarrow 6 linkage provides to the oligosaccharide chain that helps spanning a relatively wider range of torsion angle combinations, with the flexibility appearing to decrease in the order (1 \rightarrow 6) > (1 \rightarrow 3) \approx (1 \rightarrow 4). While barley and oat exhibit mixed linkage patterns of 1 \rightarrow 4 linked cellotetraosyl and cellotriosyl β -D-glucopyranosyl units respectively, intervened by a unit of 1 \rightarrow 3 linked β -D-glucopyranose. This feature shows up explicitly in their torsion angle distributions where the overall plot bears signatures of both (1 \rightarrow 4) and (1 \rightarrow 3) glycosidic linkage patterns. This further points out that the individualistic torsion angle signatures exhibited by a given linkage pattern is reasonably preserved even in the presence of other linkage types.

The most probable values of the (φ, ψ) combination as obtained from the heat map plot as shown in Figure 3.3 for the (1 \rightarrow 3), (1 \rightarrow 4) and (1 \rightarrow 6) linkages are given in Table 3.1.

The results are in line with those obtained from previous experimental and simulation studies[29, 48]. In a detailed NMR and molecular dynamics simulation study involving 1→6 linked oligosaccharides, comprising diverse α or β -*D*-pyranosides, Mackerell and co-workers reported the scanning of the conformational space of the disaccharide made up of α -*D*-Manno-pyranose units linked by 1→6 glycosidic linkage[29]. In accordance with previous reports[54], ϕ prefers an exoanomeric conformation with some transitions to higher energy conformations (anti- ϕ), as noted also in the case of our 1→6 α -*D*-glucopyranosides. In our work, for the α -*D*-linked oligosaccharides (1→3/1→4/1→6), the most probable value of ϕ is 66 to 98°, in agreement to $\sim 70^\circ$ as mentioned by Mackerell and co-workers. It is to be noted that ϕ_{exo} , an exoanomeric conformation is defined by the region $0^\circ < \phi < 120^\circ$ for α -*D*-/ β -*L*-anomeric compounds and $-120^\circ < \phi < 0^\circ$ for β -*D*-/ α -*L*-anomeric compounds. The trans glycosidic NMR coupling constant measurement of $^3J(C_6, H_1)$ validate the preference of exoanomericity[55]. In line with our observations, the studies further observed ~ 80 to 90% of the populations belonging to the anti periplanar ψ conformation given by $120^\circ < \psi < 180^\circ$ or $-180^\circ < \psi < -120^\circ$. Some high energy conformations, centered around 90° ($0^\circ < \psi < 120^\circ$; ψ_{90°) or -90° ($-120^\circ < \psi < 0^\circ$; ψ_{-90°) were observed as well, in accordance to our data. Evidence for the existence of these high-energy conformations (with ψ_{-90°) can be obtained from the NMR and molecular modelling study of Lycknert *et al.*[56]. Further, it is also noted that the deviation of ψ from the preferred anti-periplanar conformation results in the preference of the “*gt*” rotamer as given by the ω angle distributions. This feature clearly shows up in our simulation data as well, where the 1→6 linked α -*D*-glucopyranoside oligomer shows an exceptional preference to the “*gt*” conformer as discussed in Figure 3.4.

From Figure 3.3, it appears that α/β -(1→6) glucans have the most flexibility, but Figure 3.2 indicates that these have the least fluctuation in their RMSD values as compared to their 1→3 and 1→4 counterparts. With respect to the sampling of the glycosidic dihedral angles, the 1→6 glucans have greater freedom because of the extra ‘-CH₂-’ group. This feature is not reflected while considering the overall backbone RMSD. RMSD calculation, reflecting the square root of the number averaged squared distortions from the starting structure, is highly dominated by the motions of the flexible termini. In fact it is observed in several studies involving structure of bio-macromolecules in literature that RMSD is greatly affected by the amplitude of errors, as pointed out in a detailed discussion by Kufareva *et al.*[57]. It appears further that alteration of a few backbone dihedral angles can lead to significant distortion in the global structure and packing. On the other extreme, very similar structures, in terms of RMSD, can sometime have a significant disparity in their dihedral angles. Partial cancellation of these variations, especially if the chain flips or turns, may leave RMSD value relatively unaffected.

For the three bond glycosidic linkage, as observed in 1→6 linked oligosaccharides, along with the two conventional backbone torsion angles ϕ and ψ , there is an additional handle of freedom in terms of the side-chain torsion angle $\omega(O_6 - C_6 - C_5 - O_5)$ and

$\omega^*(O_6-C_6-C_5-C_4)$ to describe the conformations of the hydroxyl group side chain. The peaks in ω torsion angle distribution usually refers to the population of the gauche-gauche (gg , $\omega \sim 300$), gauche-trans (gt , $\omega \sim 60$), and trans-gauche (tg , $\omega \sim 180$) rotamers for the 1 \rightarrow 6 linked oligosaccharides. The details of the definition of the various rotamers as characterized by the values of ω and ω^* can be found in previous reports[29, 48, 58]. Figure 3.4 shows the distribution of the ω torsion angle ($\omega = \omega^* + 120$) for the 1 \rightarrow 6 linked oligosaccharides under consideration[29, 58].

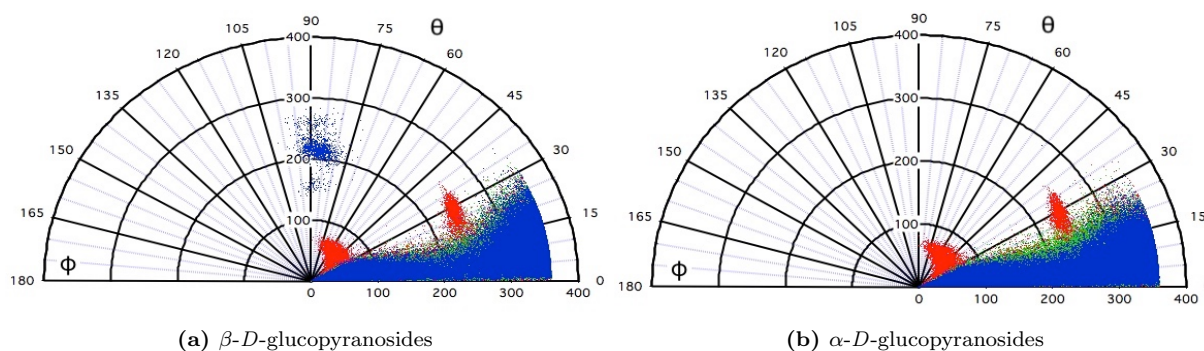


Figure 3.5: Polar plot showing the variation of the Cremer-Pople pseudorotation(θ), and phase angles (ϕ), (in degrees) for the different oligosaccharides under consideration. 1 \rightarrow 3 linked (Red); 1 \rightarrow 4 linked (Green) and 1 \rightarrow 6 linked (Blue)

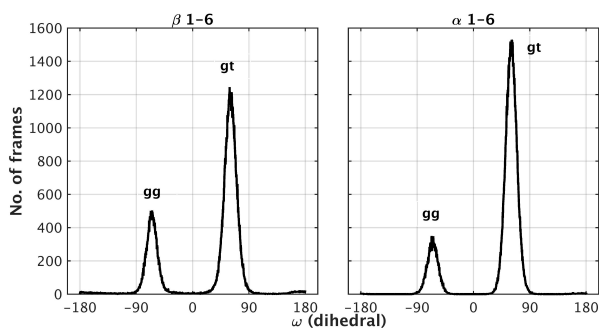


Figure 3.4: ω dihedral angle distributions (in degree) for the oligosaccharides having 1 \rightarrow 6 glycosidic linkage.

The puckering of the rings in such oligosaccharides can be followed by estimating the Cremer-Pople puckering parameters as a spherical polar set (Q , θ , ϕ). A polar plot representing only the variation in the pseudorotation angle(θ), and phase angle(ϕ), is adequate to probe the conformers exhibited by each of the oligosaccharides along the course of the simulations as shown in Figure 3.5. The energy barriers associated with ring flipping is significantly high to be reached in equilibrium simulations at 310 K. However, small distortions from the ideal 4C_1 chair are observed in our simulations in line with some earlier studies[58, 59, 60]. Among the β - D -glucopyranosides, the 1 \rightarrow 6 linked oligomer undergoes the highest puckering. When α - D -glucopyranosides are compared, it is found that the α/β - D -1 \rightarrow 3 and β - D -1 \rightarrow 6 linked oligosaccharides shows some population density around the boat/twist-boat region, along with some envelopes/half-envelopes. The α/β - D -1 \rightarrow 4 linked oligosaccharides show the least distortion from the ideal chair among all. In an earlier REMD simulation study by Gnanakaran *et al.*[58], on cellulose fragments, comprised of β - D -glucopyranoside units linked by 1 \rightarrow 4 glycosidic linkages, it was shown that although 4C_1 is the preferred chair conformation observed in the simulations, \sim 1 to 2% of conformers exhibited non chair forms. It is noteworthy

here that the propensity of formation of non-chair forms increases with the degree of polymerization[58, 60]. It was further noted that the glucose ring in the non-reducing end shows fewer flips than the other rings.

With greater accessibility toward different glycosidic torsion angle combination, arises higher probability of exhibiting conformational variance with respect to end-to-end distance and radius of gyration(R_g). The trends of these two physical attributes are similar across the oligosaccharides studied. The end-to-end distance is calculated as the distance between the two most distant atoms, C_1 of residue 1 and O_6 of the last residue. Figure 3.6 shows the comparison of the end-to-end distance and R_g .

The end-to-end distance and R_g values are normalized per number of residues for the two anomeric series of glucans having different glycosidic linkages. From the figure 3.6 it appears that the 15-meric α/β -1 \rightarrow 6-*D*-glucans have the smallest end-to-end distance and R_g among all oligosaccharides under consideration. The β -1 \rightarrow 4 variant has the highest end-to-end distance and R_g . This implies that among all the oligosaccharides studied, β -1 \rightarrow 4 takes linear form and is less curled.

Figure 3.7 depicts the solvent accessible surface areas for the oligosaccharides, normalized per number of residues. The 1 \rightarrow 3 and 1 \rightarrow 4 α/β -*D*-glucans show a relatively narrow distribution of surface areas, peaked at 1.8 to 2 nm^2 . The α/β -1 \rightarrow 6 glucans assume several conformations with relatively broad distributions (peaked respectively at \sim 1.5 and \sim 1.8 nm^2). The α -1 \rightarrow 3/1 \rightarrow 4 glucans show relatively less solvent exposure than their β -variants.

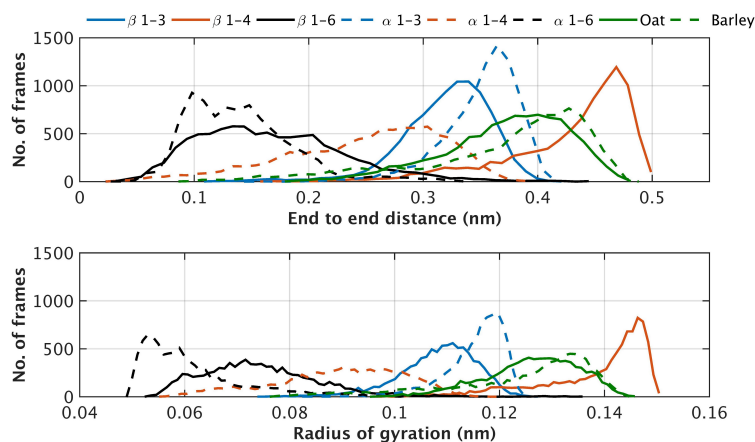


Figure 3.6: (top)Variation of end-to-end distance per residue (bottom)Variation of Radius of gyration per residue.

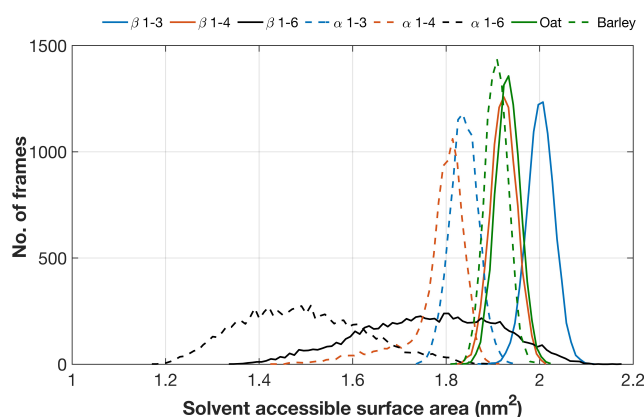


Figure 3.7: Solvent accessible surface areas per residue of the oligosaccharides under consideration.

n The structure of the different glucan variants and their interaction with the aqueous environment are indicated by a comparison of distributions of the intramolecular vs intermolecular H-bonding as shown in Figure 3.8. The donor-acceptor distance cut-off used in the calculation is 3.5 Å and the A-D-H angle cutoff of 30°. Overall, the glucans interact extensively with water through 5-7 H-bonds per residue. It appears from the plots that 1→4 linked *D*-glucans exhibit more intra-molecular H-bonding as compared to their 1→6 counterparts. Among all the oligosaccharide variants studied, 1→4 α -*D*-glucan oligomer showed relatively less intermolecular H-bonds with a concomitant rise in intra-molecular H-bonding propensity. This is further verified from the appearance of organized motifs held by H-bonding network in its lowest energy structure identified from our simulations as discussed later in Figures 3.15 and 3.16. The 1→6 linked oligomers on the other hand have noticeably less intramolecular H-bonds. The structures as given in Figures 3.15 and 3.16, however, shows significant curling up, but low intra-molecular H-bond propensity for these oligomers indicates that the structures are lacking systematic repetition of motifs which interferes with H-bond formation between two parts of an oligosaccharide chain.

Apart from the structural attributes, oligosaccharides behaving like a fluctuating random coil in conventional solvent water have also distinctive dynamical features. However, due to the presence of significant number of degrees of freedom, the overall motion is too complicated to conceive, let alone understand comprehensively. To simplify the dynamical scenario, principal component analysis (PCA) is performed on the glycosidic torsion angles of these several variants of oligosaccharides to understand what effect the different glycosidic links in the two anomeric series of oligosaccharides precisely have on the dynamical freedom.

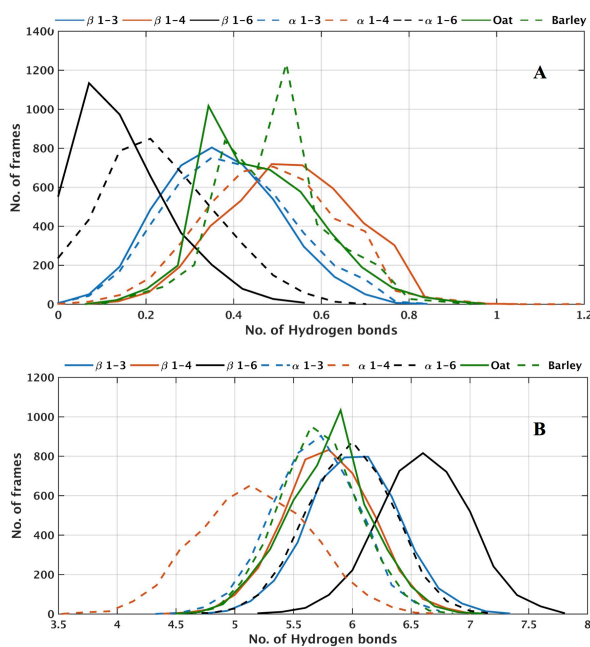


Figure 3.8: (A) Intra molecular H-bonding, (B) Inter molecular H-bonding.

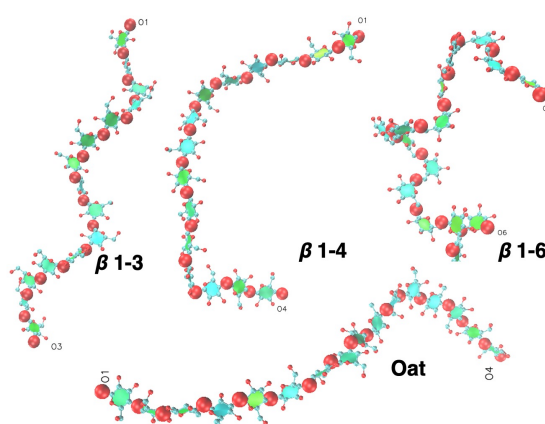


Figure 3.9: Depiction of glycosidic oxygen atoms along oligosaccharide chain

To simplify the problem, only the oxygen atoms participating in the (1→n) glycosidic linkage are considered to be the backbone. Figure 3.9 indicates the backbone atoms considered for principal component analysis of the representative β -D-glucopyranosides under study. It is evident that the choice of glycosidic oxygen atoms (red spheres in vdw representation as incorporated by VMD) as the backbone is not too bad to catch up the overall dynamical intricacies while keeping the overall degrees of freedom at check. Relatively small oligomeric molecules in solution, such as those considered here, exhibits both translation and rotation in addition to vibrational motion, which makes the natural separation between overall motion and internal motion difficult. Thus, the internal coordinates of the backbone torsion angles are subtended between the oxygen atoms of the glycosidic linkage, which reflects only the internal motion of the oligomeric chain as represented in Figure 3.9. This approach is known to reduce statistical noise in the data by evading accentuated correlations between backbone and side-chain atoms[61].

An eigenvalue scree plot as shown in Figure 3.10 can be generated to understand the distribution of the overall oligomer dynamics (in terms of fluctuation of the internal coordinates) into the most relevant principal components (PCs) in the reduced dynamical space. The scree plot shows the respective weightages of the PCs on the total variance of the data. Although the first two PCs could capture just ~ 30 to 50% of the overall dynamics, for simplicity, analysis is restricted to PC1 and PC2. PCA is a relatively difficult analysis to comprehend, especially for big molecules having numerous degrees of freedom. Therefore, the scree plots have rather long tails, which extend to several tens of components. As the total number of principal components would be equal to the number of degrees of freedom available, providing physical interpretation to this entire set becomes very stiff. Thus to keep it understandable only the first two major components are considered. While this approach does not cover the entire scenario, but it does provide the major information, which possibly one would mostly care about.

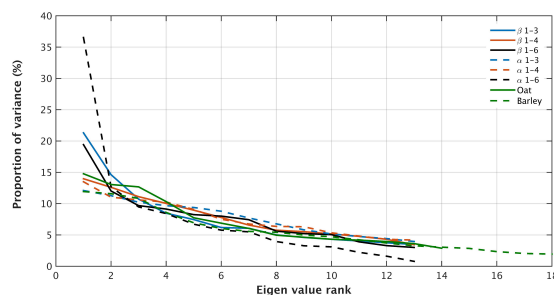


Figure 3.10: Eigenvalue Scree plot showing the weightage of the different principal components in the overall dynamical space for the oligosaccharides under consideration .

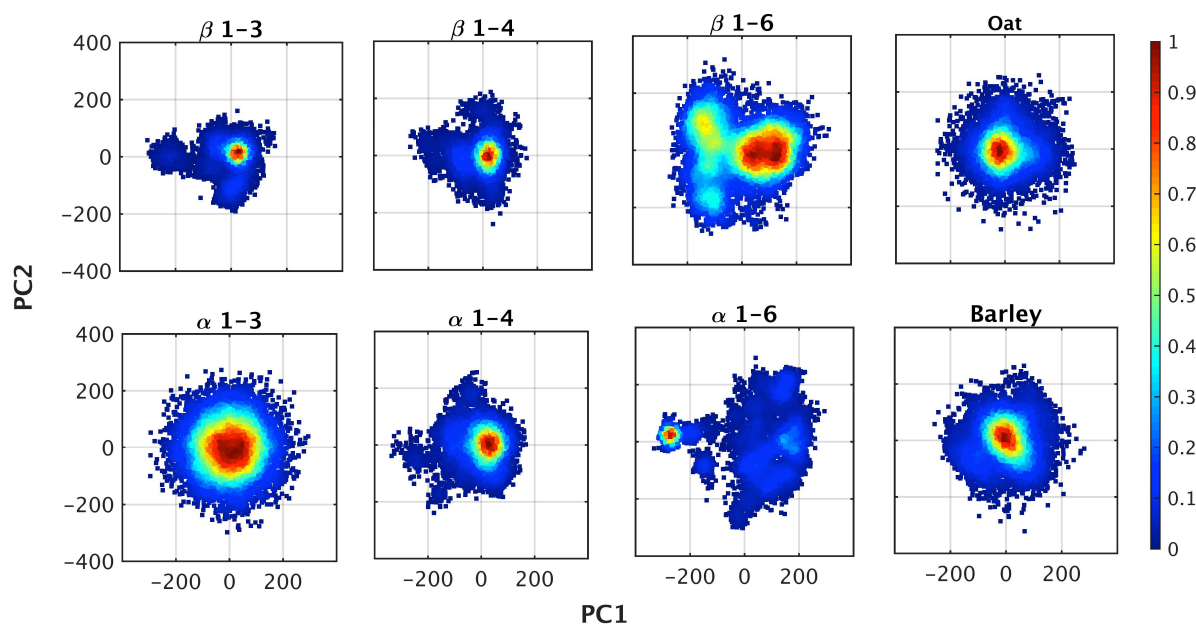


Figure 3.11: Distribution of scores for the 4000 snapshots collected from 40 ns simulation trajectory in the PC1 to PC2 dynamical space for the different variants of oligosaccharides under study.

Figure 3.11 shows the distribution of the snapshots in the PC1 and PC2 dynamical space for all the oligosaccharide variants, bringing out the disparity in dynamics caused principally by the difference in anomericity and glycosidic linkage type. Except Oats and barley, the rest of the oligosaccharides contain exactly the same number of residues of *D*-glucopyranoside type. The plots indicate that in general the dynamics of the oligosaccharides are characterized by low redundancy or correlation in PC1 and PC2 dynamical space. This is indicative of random diffusive motion along the oligosaccharide chains. Among the β -oligomers, the 1 \rightarrow 6 linked oligosaccharide is the most flexible, while it is the 1 \rightarrow 3 and 1 \rightarrow 6 linked oligomers for the α -anomeric series, which show maximum spread in the data. Oligosaccharides bearing the 1 \rightarrow 6 linkage have significantly more dynamical freedom as compared to their 1 \rightarrow 3/1 \rightarrow 4 peers owing to the “3-bond glycosidic linkage” or the additional CH₂ group. The presence of multiple maxima and the asymmetric spread of the PC1 and PC2 distribution for 1 \rightarrow 6 linked oligosaccharides point toward this aspect.

To further understand these features, the loadings of the residues are analysed along the oligosaccharide chains for all the variants in Figure 3.12. While for oligosaccharides of the β -anomeric series, the contribution of PC1 and PC2 toward the dynamics of a given residue follow similar trends, for the α -anomeric series, it appears to be more complementary in nature. For example, in α 1 \rightarrow 3 oligomer, the residues that feature prominently in PC1 (residues 3-6; 9-12) are downgraded in PC2 and vice versa. Interestingly, this complementarity is also prominent in the loading plot of oat. Although they are composed

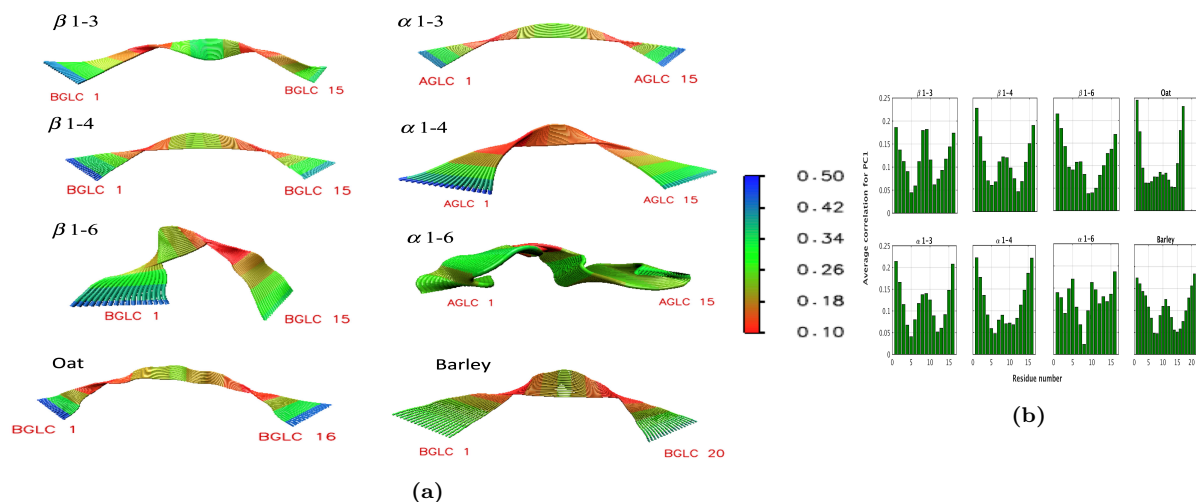


Figure 3.13: (a) Pictorial representation of the contribution of each oligosaccharide residue towards PC1. For generating this data, PCA is done using the Cartesian coordinates of the backbone glycosidic oxygen atoms. The colorbar is common to all the different oligosaccharides under consideration and the data is normalized for easy comparison. AGLC and BGLC refer respectively to α or β -D glucopyranoside unit and the number denotes the residue. (b) Loadings of the oligosaccharide residues towards PC1 as obtained from PCA using Cartesian coordinates.

of β 1 \rightarrow 4/1 \rightarrow 3 linked *D*-glucopyranoside units, barley has higher content of 1 \rightarrow 4 linked units as compared to oat, which is probably the cause of different PC1 and PC2 weightages in the two oligosaccharide chains.

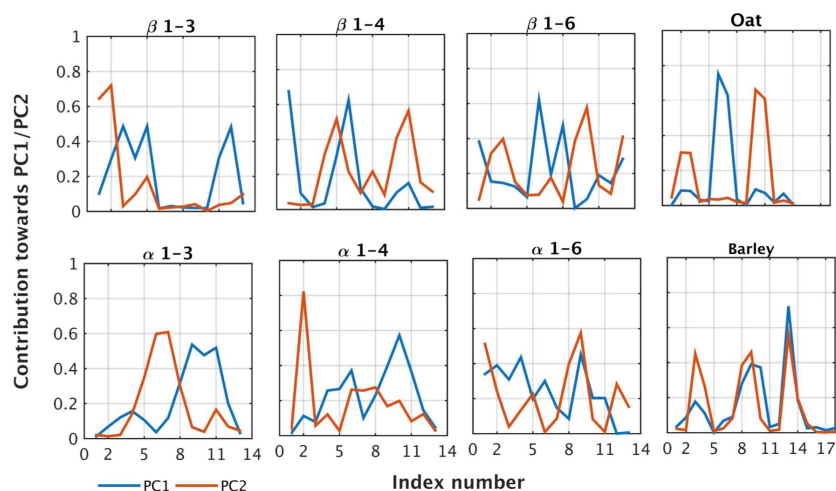


Figure 3.12: Residue loadings for the different oligosaccharides using internal coordinates toward the first two principal components: PC1 (blue) and PC2 (red).

exhibited substantial distortion throughout the length of the oligomeric chain. Compared with oat, barley is observed to have fewer hinges.

To comprehend the dynamical attributes from another perspective, Figure 3.13 shows estimated amplitude of the different regions of the oligosaccharide chain toward PC1, endorsed by the corresponding PC1 loadings corresponding to each residue in Cartesian coordinates. While most of the oligomers showed reduced motions/hinges for non-terminal residues, the α 1 \rightarrow 6 oligomer

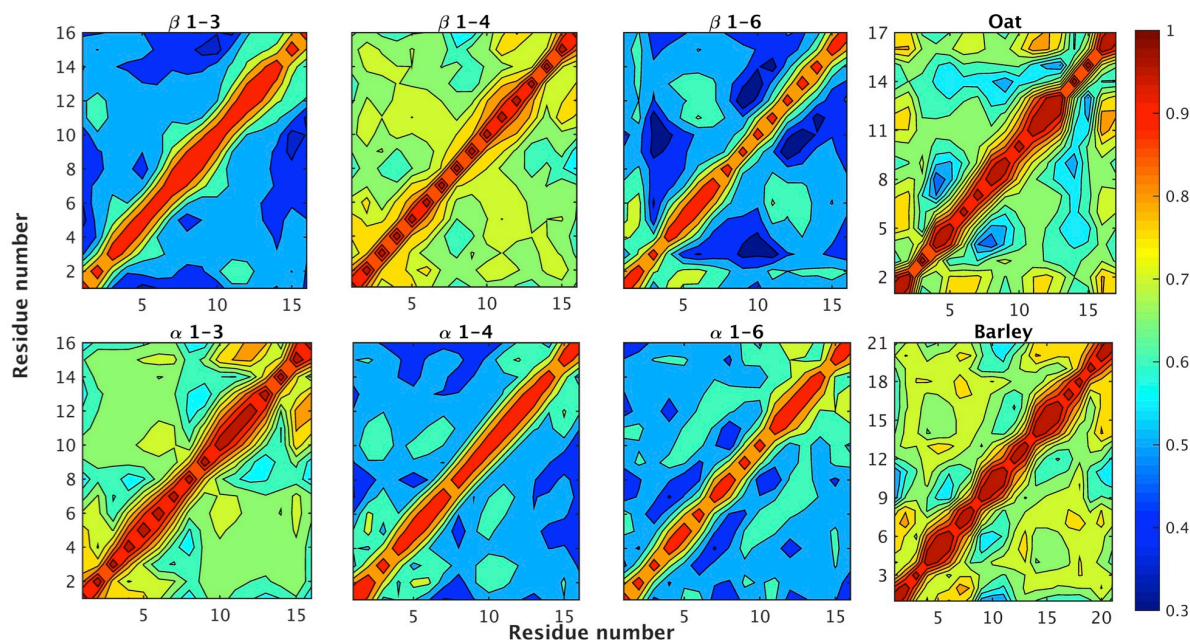


Figure 3.14: Cross correlation plots as calculated by linear mutual information for all the different oligosaccharides. The non-correlated and anti-correlated movements are both reduced to zero in this approach.

While the VMD representations of the overall dynamics of the oligosaccharides and their corresponding residue wise loading plots are indicative of the magnitude of fluctuations observed in a given residue along the chain, no information is obtained regarding the presence of correlated motions, if any. Figure 3.14 shows the cross-correlation plots of the residues in the different variants of oligosaccharides. Here, the data are calculated using linear mutual information theory, which reduces both non-correlated and anti-correlated motions to zero. The plot brings out contrasting features of correlated motions along the chain for the different variants. While β 1 \rightarrow 4 oligomer shows existence of dominant correlated motions, which are indeed visible in oat and barley fragments as well, the α 1 \rightarrow 4 oligomer shows less correlation. Among both α and β -D-glucopyranosides, the 1 \rightarrow 6 linked oligomer shows the highest uncorrelated/anti-correlated movements.

The dynamical space of oligosaccharides spanned by the first two principal components, PC1 and PC2, can be further classified into four clusters by K-means clustering. The minimum number of clusters sufficient to describe the dynamical space is found by the “elbow criterion” as observed in the variation of SSR/SST ratio against number of clusters[62]. In the case of all the oligosaccharides under consideration, an optimum four clusters could refine the dynamical space adequately as depicted in Figure 3.15. This figure shows the variation in the structure of the lowest energy oligosaccharide conformation belonging to each cluster across all the oligosaccharide variants studied. A comparison of Figures 3.14 and 3.15 reveals that correlated movements are lost as the structure of the

oligosaccharide curls up as in the case of α/β 1 \rightarrow 6, α 1 \rightarrow 4 and β 1 \rightarrow 3 linked variants. Correlated movements are relatively high for the straight chain oligosaccharides.

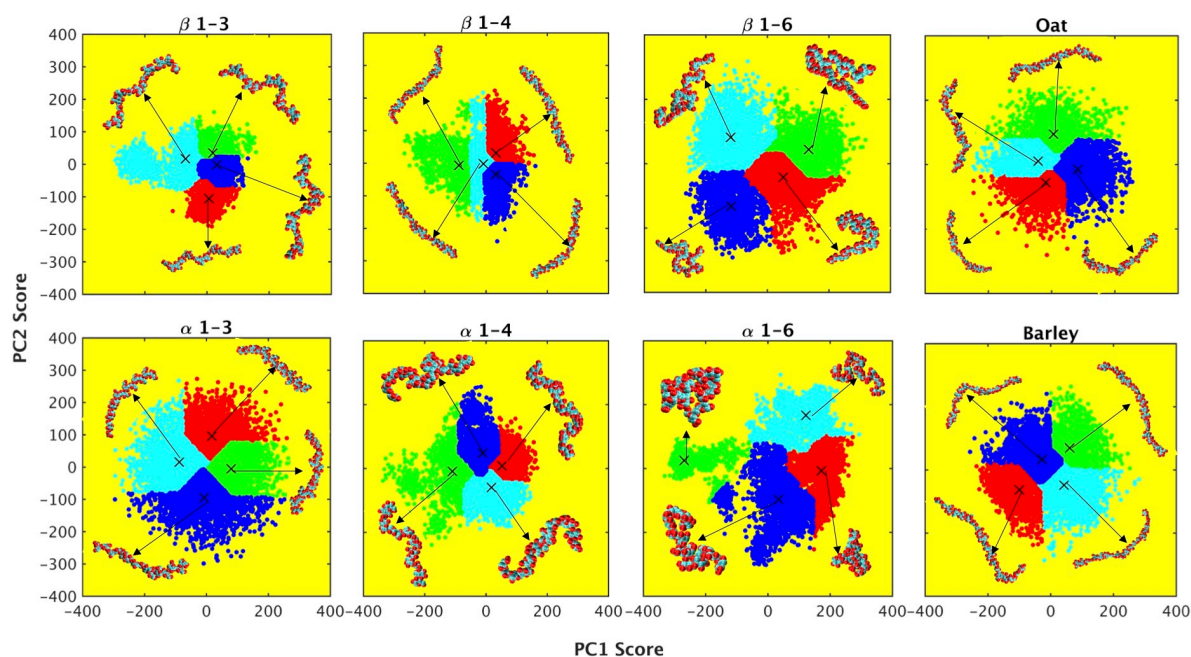


Figure 3.15: K-means clustering performed on the dynamical space spanned by PC1 and PC2. The conformations closest to the centroid in each cluster are shown. Color-codes for the clusters are as following: cluster-1 (Red); cluster-2 (Green); cluster-3 (Cyan) and cluster-4 (Blue).

Lastly, it is important to compare the most stable solvated oligomeric structure obtained in the course of the simulation for all the variants studied. These variants are depicted in Figure 3.16. While the β -1 \rightarrow 3 and 1 \rightarrow 4 oligosaccharides are mostly slender and straight, the 1 \rightarrow 6 variant is zigzag. While α -1 \rightarrow 3 is straight, α -1 \rightarrow 4 and 1 \rightarrow 6 are noticeably curled. Oat is more wrapped up than barley. For the mixed linkage (1 \rightarrow 3, 1 \rightarrow 4)- β -glucans, like oats and barley, the discontinuity induced into the β -(1 \rightarrow 4) linked sequences by intermittent β -(1 \rightarrow 3) linkages usually prevents the oligosaccharides from stacking up forming layers. On increasing the ratio of β -(1 \rightarrow 3)-linkages in the sequence, more kinks are introduced in the structure leading to an open conformation and a water-soluble polymer[63, 64]. In our study the barley sequence has lower β -(1 \rightarrow 3): β -(1 \rightarrow 4) ratio as compared to oats. This is probably the reason why barley chain appears to be straighter and dynamically more labile as compared with oat. The presence of kinks in oat can also be noted in the pictorial representation of the contribution of each oligosaccharide residue toward PC1 in the dynamical PCA map (Figure 3.13a, the red regions are domains of minimal movement in PC1). These structural features are indicative of the lineage that the oligosaccharides carry out of their anomeric type and glycosidic linkage pattern and could prove useful while designing newer motifs.

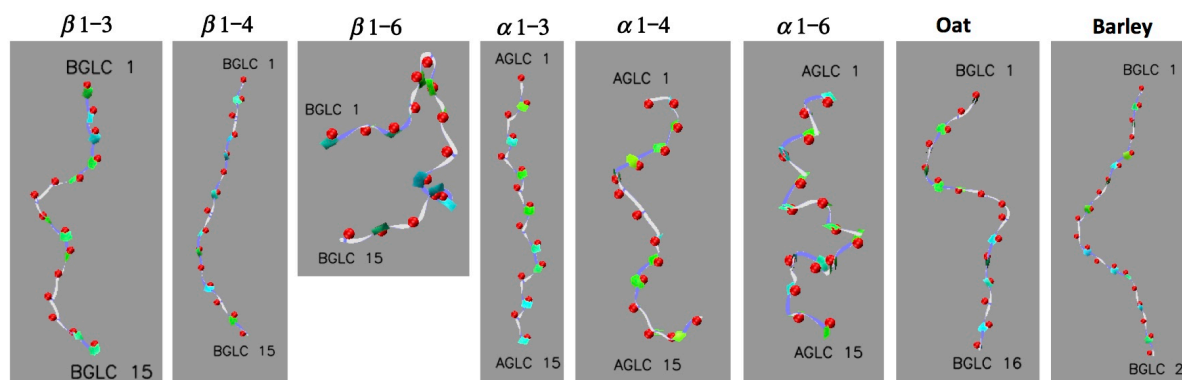


Figure 3.16: Lowest energy conformation of hydrated oligosaccharides under consideration. The oligosaccharides are represented by twister and paper-chain representations to depict the twist along the oligosaccharide chain and the puckering of the glucopyranose ring.

3.4 Conclusion

The present study compares and contrasts the conformational changes and dynamics spanned by 15 residue oligosaccharides belonging to two anomeric series of linear α and β -*D*-glucopyranosides and having varying glycosidic linkages of types 1 \rightarrow 3, 1 \rightarrow 4 and 1 \rightarrow 6. Two mixed linkage β -*D*-glucan fragments comprising 1 \rightarrow 4 and 1 \rightarrow 3 linkages in certain ratio as found in natural fibers of oats and barley are also investigated. The primary aim of the work is to understand how changes in glucopyranose rings as dictated by changes in anomeric nature and glycosidic linkage, forces the oligosaccharides to reveal different structural patterns, H-bond propensity, solvent exposure and the radius of gyration. As structure is affected, it influences critically the dynamical freedom along the chain, exhibited by significantly different score maps in the PC1 and PC2 dynamical space. While some oligosaccharides show diffusive dynamics, the overall motional behaviour of others are more restricted into specific clusters. Overall, the following observations are noted: Firstly, as compared to the α series, the β -oligomers, especially the 1 \rightarrow 3 and 1 \rightarrow 4 linked chains are relatively more slender with higher solvent exposure, high end-to-end distance with concomitant rise in the radius of gyration. The 1 \rightarrow 6 linkage on the other hand attains diverse configurations in solution. β -1 \rightarrow 6-*D*-glucan is especially remarkable in terms of its litheness as evident from the multiple maxima in the score plot in the PC1 and PC2 dynamical space. The significant uncorrelated/anti-correlated motions as indicated by the cross-correlation plot and the uniform loadings across all the residues of the β 1 \rightarrow 6 oligomeric chain further endorse this aspect. Information obtained from this work is intended to help design oligosaccharides, linear or branched, with tunable physical characteristics for specific purposes. For example, for wrapping spherical cholesterol or LDL particles in simulations mimicking physiological disorders like dyslipidemia.

Chapter 4

Structural and spectroscopic details of polysaccharide–bile acid composites from molecular dynamics simulations

This chapter is based on the following paper, Peesapati, S. & Roy, D. Structural and spectroscopic details of polysaccharide–bile acid composites from molecular dynamics simulations. *Journal Of Biomolecular Structure And Dynamics*. pp. 1-13 (2022)
url:<https://www.tandfonline.com/doi/abs/10.1080/07391102.2022.2137242>

4.1 Introduction

Polysaccharides, apart from being integral component of diet, play a vital role in metabolic processes of digestion and excretion[1, 2, 3, 4, 5]. They have both therapeutic and detrimental effects on human health. Hence, the interactions of polysaccharides with other dietary components and molecules emerging out of metabolic pathways in the GI tract is attracting widespread attention these days[6, 7, 8]. Polysaccharides of the form β -glucan, help alleviate some chronic pathological conditions like dyslipidemia, fatty liver, diabetes, gallstones and other metabolic syndromes[9, 10]. These conditions are associated with abnormal lipid metabolism and bile transport.

In this context, it is crucial to understand the structure and types of lipids like bile acids/salts which play a critical role in the metabolism. Diverse bile acids are synthesized from cholesterol in liver[11]. They are also called as ‘primary bile acids’. They belong to a large class of molecules which take the structure of steroids. Chenodeoxycholic acid (CDCA) and cholic acid (Ch) are the common primary bile acids in humans. They are conjugated with taurine or glycine residues to give bile salts. These bile acids are amphiphilic in nature i.e., they have both hydrophobic and hydrophilic regions. These primary bile acids are subjected to bacterial action in colon, thus getting converted to secondary bile acids. The cholic acid gets converted into deoxycholic acid (DCA) and chenodeoxycholic acid gets converted to lithocholic acid (LiCA). The bile acid pool is mostly comprised of cholic acid and chenodeoxycholic acid. Small amounts of deoxycholic acid and lithocholic acid and minute amounts of ursocholic acid can also be present. Increased bile acid usually account for liver damage.

A major fallout in dyslipidemic patients is the raised serum cholesterol levels, subsequently leading to accumulation of surplus cholesterol in various body parts including eyes, arteries, liver etc[12, 13]. Cholesterol although detrimental in excess amounts, is actually vital for several metabolic processes[14]. Unfortunately, the human body often obtains much excess of cholesterol from biosynthesis and by significant absorption through the GI tract. The liver hepatocytes, on the other hand, can only disintegrate cholesterol down to bile. Thus any inhibitory effect on bile production or reabsorption in the GI tract triggers the conversion of cholesterol to bile acids in the liver, in order to maintain the constancy of the biliary pool[15, 16]. The interlink between cholesterol and biliary metabolic pathways is thus well known and is often exploited by therapies to treat dyslipidemic patients.

β -glucans can significantly lower down serum cholesterol levels by binding to bile acids thereby facilitating faecal excretion[3, 5, 17, 18, 19, 20, 21, 22, 23]. A substantial portion of primary and conjugated bile acids, especially the hydrophilic ones like cholic acid, chenodeoxycholic acid and deoxycholic acid are reabsorbed through specific transporters present in the enterocytes[24]. It is noteworthy that polysaccharides constituting the dietary fibres are particularly resistant to enzymatic degradation in the upper GI tract and

help adsorb such bile acids on their surface by hydrophobic interactions. Section 3.1 has a brief discussion of role played by polysaccharide viscosity in prevention of reabsorption of bile acids[25, 26, 27]. Several clinical studies indicate that β -glucans can alternate the microbiome activity in the gut, which has additional direct influence on the host bile acid and cholesterol homeostasis[28, 29, 30].

Numerous clinical studies along with some computational work indicate that polysaccharides have the ability to bind with bile acids and bile salts. But, the molecular details highlighting such interactions are still awaited. The complex hierarchical structures of the polysaccharide and mimicking the exact physiological composition of intestinal fluid in vitro are major challenges among others[31, 32]. Conformations and related properties of polysaccharides are challenging to study experimentally. NMR spectroscopy[31, 33], SAXS[34, 35] and AFM imaging[36] are few techniques used to characterize the binding of bile acids to polysaccharides. Brief introduction on the analysis techniques of polysaccharides given in section 1.4. In a recent work, Zielke *et al*, investigated the bile acid binding capacity of oat β -glucan using asymmetric flow field-flow fractionation (AF4) and NMR assays[31]. Bile acids are seen to affect the density of the undigested β -G aggregates, which further manifests itself in the altered chemical shifts values of carbons as observed through NMR. Another in-vitro assay utilizing low and medium viscosity barley β -glucan having β -(1 \rightarrow 4)/(1 \rightarrow 3) glycosidic linkages and bile salts like glycocholate (GC) and tauro-chenodeoxycholate (TCDC) could detect changes in NMR chemical shifts for both bile salts and β -glucan in the timescale of minutes, indicating evidences of dynamical interactions between the molecules[33]. The stabilization of the bile salt micelles by the barley glucans is found to be pH dependent and likely favoured at pH 5.3[33]. Inter-particle interactions between bile salts and glucans are also noticeable from the changes in the SAXS patterns of bile salt aggregates in presence and absence of β -glucan, as reported by Gunness *et al*,. The extent of interaction and binding depends on several factors, primarily the method of extraction from natural sources, the molecular weight of the β -glucan, the glycosidic linkages available, just to name a few[37].

While it is understandable why molecular details of such interactions are less available, one can focus more on utilizing computation tools to address such problems and fill up the void. In recent times, homology modelling, molecular dynamics simulations, docking and bioinformatics tools are increasingly used to model and study structure-dynamics relationships of complex bio-molecular assemblies. In an earlier report on the aggregation behaviour of two typical bile salts like sodium cholate and sodium deoxycholate. Pàartay *et al* reported that due to their unique molecular structure, which is significantly different from the conventional aliphatic surfactant molecules, the bile salts tend to form soft clusters distinct from the usual spherical micelles[38]. In a recent study, Li and co-workers have used molecular docking to understand the adsorption of soy-hull polysaccharides on bile acids. Hydrogen bonding together with hydrophobic interactions between the polysaccharide and bile acids play the dominant role in triggering such adsorptions[39].

In the present work, molecular dynamics tools are employed to understand atomistic details of a prototypical bile acid and its corresponding sodium salt would potentially interact with strands of a standard decameric β -glucan chain which is inspired by that extracted from oat or barley. Each polysaccharide strand comprises of ten units of β -D-glucopyranose, linked by mixed β -(1 \rightarrow 4)/(1 \rightarrow 3) glycosidic linkages. The bile components are prone to form soft clusters of varying moment of inertia and coordination number. These properties are described in detail in section 4.3. Some spectroscopic signatures, directly comparable to experimental data, like, the small angle scattering profiles and ^1H NMR chemical shifts are estimated to compare with experimental reports.

4.2 Methodology

4.2.1 Modelling of the polysaccharide, cholic acid and sodium cholate

The initial coordinates of the oat polysaccharide are generated using Glycan Reader and Modeler as available in CHARMM-GUI[40, 41]. The oat polysaccharide consists of mixed 1 \rightarrow 4/1 \rightarrow 3 type glycosidic linkages joining ten β -D-glucopyranose residues. The oat-inspired polysaccharide fragment has one 1 \rightarrow 3 linkage after three consecutive 1 \rightarrow 4 linkages. Fifteen such decameric strands are considered for studying the interaction with the bile acid (Ch) and the corresponding sodium salt (NaCh) after solvating with \sim 40,000 TIP3P water[42]. Equilibrated cubic simulation boxes resulted in edge length of \sim 11 nm. The structural and dynamical properties of the polysaccharide are explored with several independent starting structures as reported in previous work[43]. The initial coordinates of cholic acid (CA) and sodium cholate (NaCh) are generated using Ligand Reader and Modeler of CHARMM-GUI[44]. Multicomponent Assembler Module of CHARMM-GUI is used to combine these molecules with the polysaccharide and hydrated with TIP3P water to generate the simulation cell[45].

4.2.2 Simulation parameters and force field

All the molecular dynamic simulations employed GROMACS as the simulation engine[46]. The mutually compatible CHARMM General Force Field and CHARMM all-atom additive force field are used to model the molecules[47, 48]. The water molecules are explicitly modelled by TIP3P force field as incorporated in CHARMM36[42]. A time step of 2 fs is used for the simulations. Each of the systems is minimized using a ‘steep’ integrator followed by equilibration in NVT ensemble (at 310 K) for 2 ns. This is followed by NPT simulation for 300 ns at 310 K and 1 atm. Temperature and pressure are maintained by coupling

the system to a Nose-Hoover thermostat[49, 50] and Parrinello-Rahman barostat[51] with coupling constants of 1 ps and 2 ps respectively. The ‘LINCS’ algorithm[52] is used to keep all waters and all bonds involving hydrogens rigid. Coulomb interactions are treated through the particle mesh Ewald method. Cubic periodic boundary conditions (PBC) are employed along the three directions of the orthogonal simulation box. A cut-off distance of 1.2 nm is used for the non-bonded vdW interactions, with the switching of LJ potential starting at 1.0 nm, extending up to 1.2 nm. A pair list distance of 1.2 nm is used for vdW and electrostatic calculations. Gaussian 09 is employed for the prediction of NMR chemical shifts and surface charge distributions from the structures isolated from molecular dynamics trajectory. The Gauge-Independent Atomic Orbital (GIAO) method and ‘mixed’ option as implemented in Gaussian are used along with B3LYP functional and 6-311G basis set. The structures for the quantum calculations are sampled randomly from the last 10 ns of the 300 ns long MD trajectory. After a snapshot is selected, a disaccharide unit of the polysaccharide in close contact with the bile acid molecule is chopped off and capped with H. The bile acid molecule along with the disaccharide unit is then subjected to the DFT study. Same approach is taken while selecting two bile acid molecules for studying them using DFT.

4.2.3 Software and data analysis

Gaussian 09, VMD (1.9.4a)[53], PLUMED (2.7.2)[54] and MATLAB (R2021b) have been used respectively for the studies using density functional theory (DFT), visualization of the structures and analysis of the data. Radius of gyration, and non-bonding energy have been determined using the GROMACS analysis tools, gyrate and energy respectively. Hydrogen bonds are determined using VMD plugin with distance cut-off of 3 Å and Acceptor-Donor-Hydrogen angle cut-off of 30°. Coordination number, moment of inertia and scattering patterns are determined using in-house MATLAB scripts. 3.5 nm is used as the cut-off distance in coordination number calculation. Moment of inertia and shape anisotropy have been calculated only for the biggest cluster present in the frame.

4.3 Results and discussions

Figure 4.1 shows the structure of Ch, NaCh and the β -Glucan under study. The polysaccharide structure is inspired after those obtained from cereals like oat and barley and consists of a decamer of β -D-glucopyranoside residues linked by mixed β -(1 \rightarrow 4)/(1 \rightarrow 3) glycosidic linkages. Intermittent β -(1 \rightarrow 3) linkages induce discontinuity into the β -(1 \rightarrow 4) linked sequences, which is shown to prevent the polysaccharides from stacking up in layers. As the proportion of β -(1 \rightarrow 3)-linkages increase in the sequence, more kinks get introduced in the polysaccharide structure resulting in an open conformation and better

water-solubility[43, 55, 56]. Bile, on the other hand, is a complex aqueous mixture of several bile acids and salts along with phospholipids, cholesterol and other steroids, with water being the major constituent (95%)[57]. Ch and its sodium salt, NaCh are the major constituents of the biliary pool and are abundant in the GI tract. The concentrations of Ch and NaCh, individually, in the human caecal extract is <1 mM, which is typically below the critical micellar concentration of Ch (8 mM) and NaCh (13 mM) in water at 310 K[58, 59]. In such low concentration range, the bile components do not aggregate and typically gets adsorbed on the food residues. However, Tanaka et al, showed that the total bile acid concentration in rat ileum is often very high and reaches 100–160 mM, large enough to possibly trigger clusterization[60]. Thus, in the present work, a higher concentration of the prototypical bile acid Ch (130mM) and the salt NaCh (140 mM) has been used to observe the possible soft clusterization of such molecules in absence and presence of the β -glucan (20 mM).

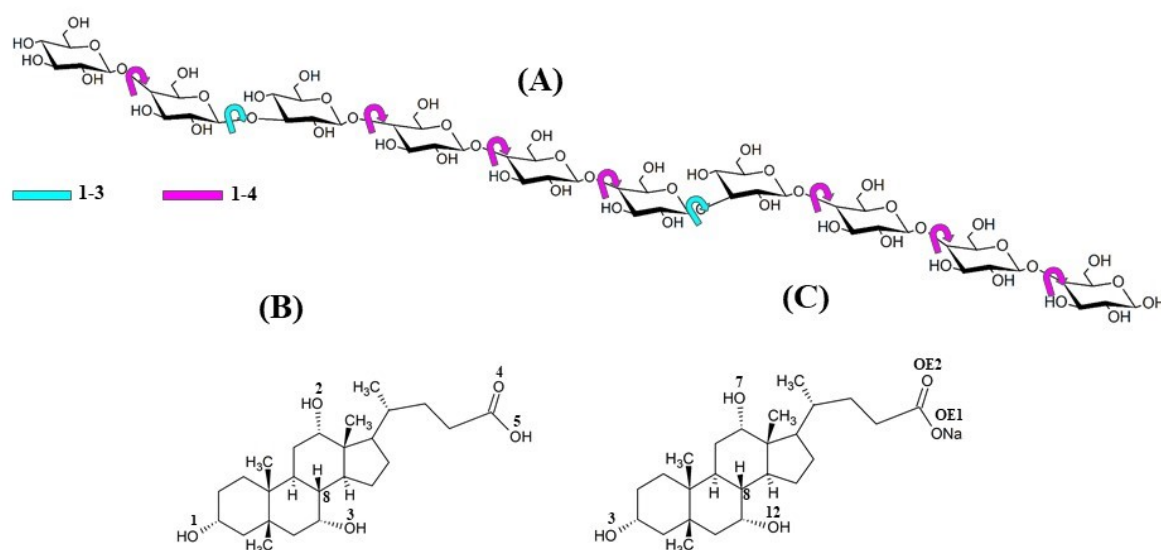


Figure 4.1: Molecular structures of (A) the polysaccharide (β -glucan) having mixed 1→4/1→3 glycosidic linkages connecting ten units of β -D-glucopyranose; (B) Cholic acid (Ch) and (C) Sodium cholate (NaCh)

4.3.1 Molecular arrangements of Ch and NaCh in water and impact of polysaccharide

The problem of studying the interaction of bile components with other dietary elements is of huge clinical interest and it is certainly non-bonding interactions, primarily van der Waals and sometimes electrostatic forces that dominate such complex ensembles. As the simulation data of the aqueous Ch system is compared to those from aqueous Ch in presence of β -glucan (130 mM or 5.3% w/v Ch; 20 mM or 3.2% w/v β -glucan), it becomes

apparent that the aggregation of the Ch molecules proceeds uninterruptedly even in the presence of the polysaccharide.

Figure 4.2 shows the radial distribution functions between some chosen atoms lying either on Ch (C_8 , C_2 , O_1), NaCh (C_8 , C_2 , O_3) or on the β -glucan (C_6 , O_6) to understand the proximal arrangements. For NaCh, which is seen to form relatively smaller aggregates even at 140 mM concentration, the peaks are narrow and interactions with the oxygen atoms of the polysaccharide chain is less dominant than in the case of Ch. This is probably because of the negative charge on cholate, which approaches the carbons of the polysaccharide chain a bit more favourably than Ch, as given by the C_2 - C_6 distributions. The O_1 - O_6 or O_3 - O_6 distributions are comparable for both the bile acid and its salt. NaCh interacts strongly with water as given in the inset. The interactions between two Ch molecules are still preferred in the near vicinity leading to rather unperturbed Ch cluster formation, even in the presence of β -glucan. The polysaccharide chain is more comfortable either coiling around itself or interacting with surrounding water molecules (Figure 4.2,Right).

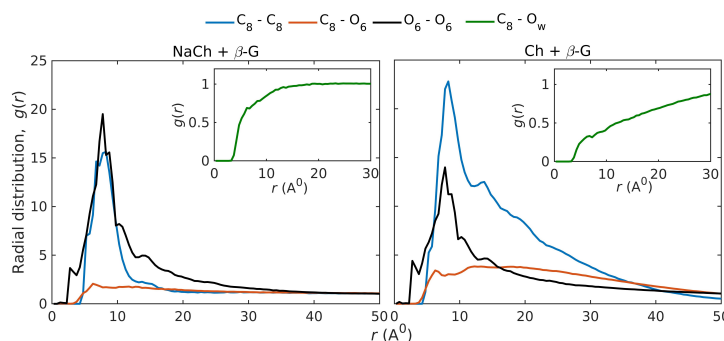


Figure 4.2: Radial distribution functions showing the molecular arrangements in the β -glucan-bile composites. The C_8 , C_2 , O_1 and O_3 atoms are on Ch and NaCh, as depicted in Figure 4.1. O_6 is the hydroxyl oxygen on C_6 of the β -*D*-glucopyranose residue in the polysaccharide. O_w denotes the oxygen atom of TIP3P water.

4.3.2 Time evolution of the shape and size of the bile acid and β -glucan composites

Figure 4.3 shows the impact of the presence of polysaccharide chain on the time evolution of the radius of gyration. The radius of gyration is calculated by considering all the molecules of Ch or NaCh present in the simulation box (Figure 4.3,Left). Additionally, the radius of gyration of the biggest cluster of Ch is also calculated for a given time instant, both in presence and absence of β -glucan (Figure 4.3,Right). The molecular composition of the biggest cluster in a simulation snapshot is estimated from the maximum coordination number that a particular Ch molecule (out of 100 molecules) is exhibiting at a given time instant. The coordination number of a Ch molecule is calculated by considering all neighbouring Ch molecules which are lying within a cut-off radius of 3.5 nm.

The cut-off radius is estimated from the C_8-C_8 radial distribution function plot, where the function decays by one order of magnitude within a distance of 3.5 nm. It is worth mentioning here that determining the cut-off radius for breathing soft clusters like those of Ch is challenging and that such a cut-off can only serve as an upper limit for the radius of gyration.

The presence of the polysaccharide appears to slightly speed up the aggregation of Ch molecules, as given by a faster initial component of the temporal profiles. The formation of the compact cluster is evident from the collapse of the radius of gyration of the Ch molecular ensemble, consisting of 100

molecules along the course of the simulation. NaCh is ionic and hence considerably more hydrophilic than Ch. Thus aggregation is not observed appreciably in these simulations for the bile salt (Figure 4.3,Left), in line with previous reports[59]. As a cut-off of 3.5 nm is used to identify the biggest cluster formed in a given time instant, the radius of gyration of the 100 molecular Ch ensemble starts from 3.4 nm compacting up to 2.1 nm towards the end of the trajectory, when the nearly 100-mer cluster is fully matured and dense (Figure 4.4). No particular interference in the packing of the Ch molecules is noticed in the presence of the β -glucan.

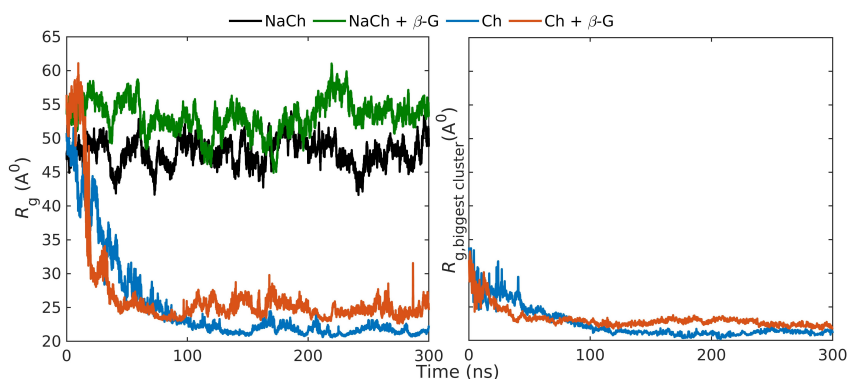


Figure 4.3: Time evolution of the radius of gyration of the assembly of bile components in presence or absence of β -glucan: (Left) considering all the Ch or NaCh molecules in the box; (Right) considering only those Ch molecules which are part of the biggest cluster.

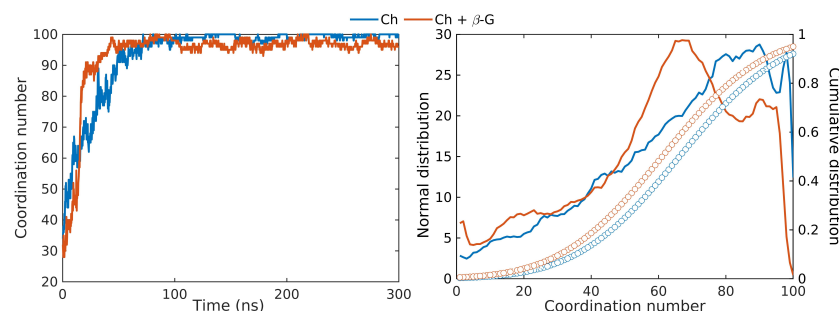


Figure 4.4: (Left) Time evolution of the coordination number (Right) Normal (solid line) and cumulative (marker) distributions of coordination number of Ch in the biggest cluster in presence and absence of β -glucan.

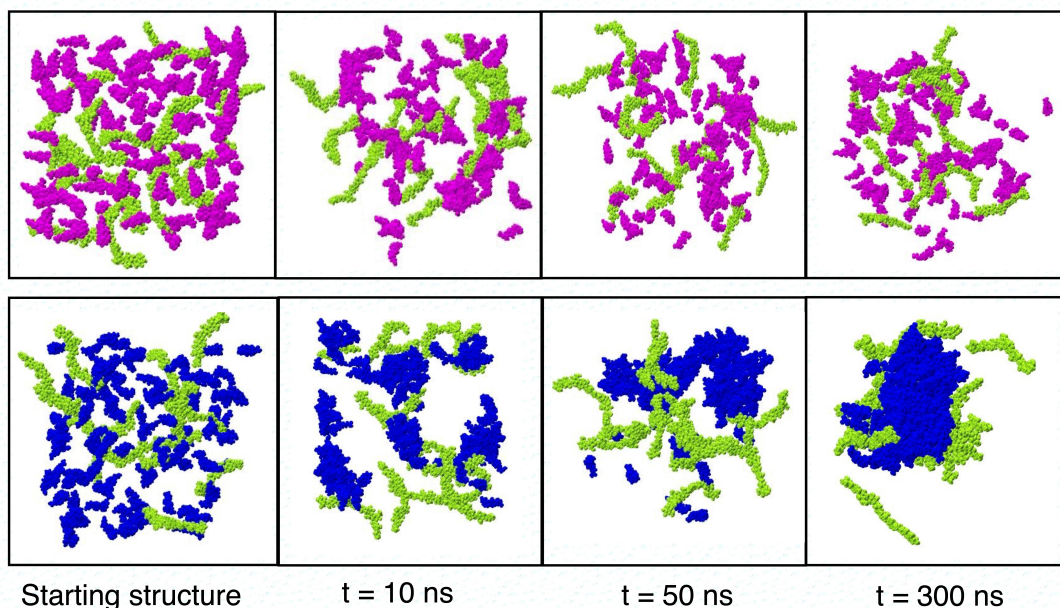


Figure 4.5: Snapshots from the simulation trajectory of NaCh (pink, Top panel) and Ch (blue, Bottom panel) in presence of β -glucan (green) strands at different time domains. The ‘starting structure’ marks that at the beginning of the production runs.

The time evolution of the coordination number of Ch molecules within a cut-off radius of 3.5 nm is plotted in Figure 4.4,Left. The biggest cluster evolved from a coordination number of ~ 30 to 100 within a time window of 100 ns and remained noticeably stable till 300 ns. Figure 4.4,Right shows the normal and cumulative distributions for the same data. Presence of β -glucan does not inhibit the build-up of the compact Ch cluster. Snapshots from varied time instants retrieved from the simulation trajectories of both Ch and NaCh in presence of β -glucan reveal the progress of clusterization (Figure 4.5). The average cluster size after 300 ns of simulation is significantly larger in Ch than those found in NaCh. Figure 4.5 further shows the evolution of the real cluster shape, as obtained from the trajectory being broken up into three domains of clusterization, identified as ‘predominantly monomeric’ denoting cluster size less than trimers, ‘intermediate’ and ‘fully matured’. These snapshots are correlated to the relative shape anisotropy factor, κ^2 as given by Equation 2.15 and Figure 4.7.

4.3.3 Moment of inertia and shape anisotropy

At this point one may like to know about the shape of the biggest cluster formed and follow the breathing of the cluster along with its change in shape as the simulation progresses and the cluster matures. The principal moments of inertia of the biggest cluster of Ch, in presence and absence of the β -glucan is calculated. This is shown in Figure 4.6. It is clear

from the components of the principal inertial moments that $I_{XX} < I_{YY} \approx I_{ZZ}$ pointing to the possible prolate or more aptly, an asymmetric ellipsoidal shape.

The molecular cluster breathes and fluctuates in size. Particularly, in the trajectory analysed, few cholic acid molecules come in and go out, primarily in the x-z plane. This leads to large fluctuations in the x and z components of the inertial moments. The total value of the moment of inertia along the trajectory however remains stable. The inertia tensor can work as a morphological descriptor for the shape of the Ch

aggregates as it fluctuates along the trajectory. The relative shape anisotropy can be calculated from the principal moments of inertia using the expression given in equation 2.15. For a spherical aggregate, $\kappa^2=0$ [61, 62]. Figure 4.7 aptly shows the intuitively expected structure of the 100-mer Ch aggregates, which are neither spherical nor significantly elongated with somewhat symmetric top characteristics. In principle, they are asymmetric top soft clusters with varying degrees of anisotropy.

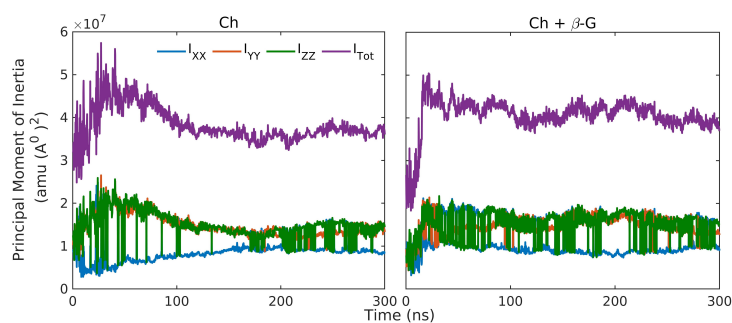


Figure 4.6: Principal components of the moment of inertia along the simulation trajectory. The biggest cluster evolves as a compact asymmetric ellipsoid. I_{Tot} denotes the sum of the three components.

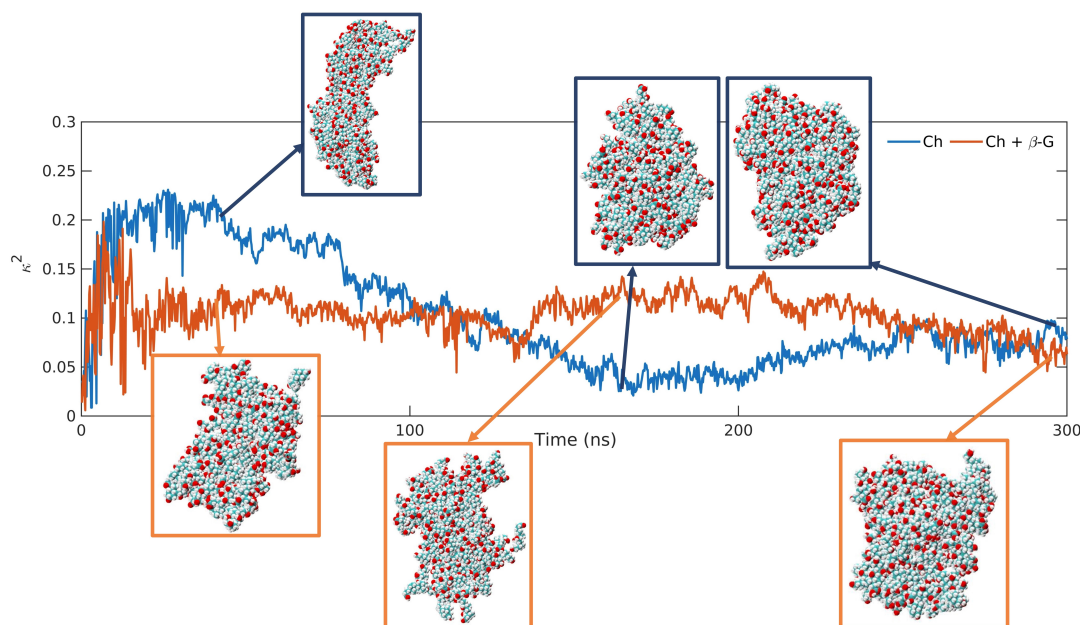


Figure 4.7: Shape anisotropy of the biggest cluster of Ch molecules as it evolved along the trajectory in presence (Brown) and absence (Blue) of β -glucan. Snapshots of the biggest Ch cluster at different time instants are shown in VDW representation: Carbon (cyan spheres), Hydrogen (white spheres) and Oxygen (red spheres).

4.3.4 Small angle scattering profiles of the Ch self-assembly and other biliary components

An efficient way to characterize the general shape of such soft molecular assemblies is through small angle scattering experiments. Substantial experimental data on similar β -glucan and bile components are available for reasonable comparison with the simulated profiles. A compact spheroidal structure leads to smaller values of inter-atom distances and low frequency of the oscillations, which typically dominate the scattering

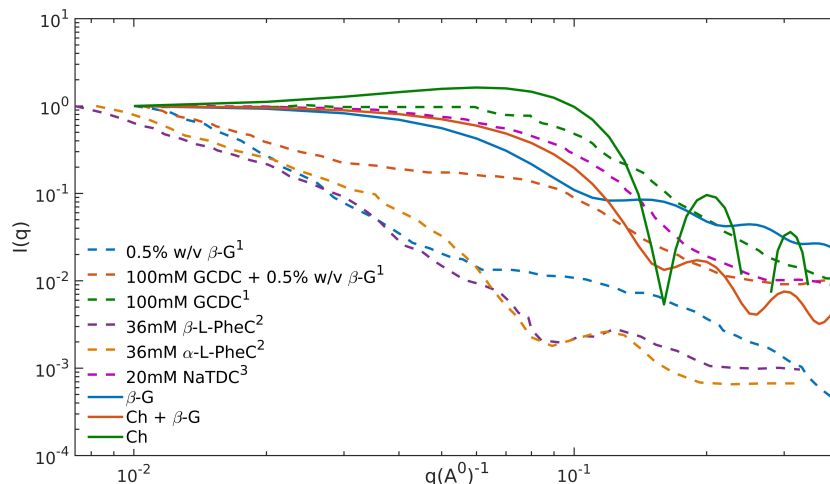


Figure 4.8: Small angle scattering profiles of Ch in presence and absence of β -glucan. Compared with the simulated data are the experimental SAXS profiles of glycoche-nodeoxycholate (GCDC), L -Phe conjugated bile acid, α/β - L -PheC and sodium taurodeoxycholate (NaTDC)[34, 35, 65].

signal at high q values. A relatively loose structure leads to high frequency oscillations appearing pre-dominantly at low q [63, 64]. Scattering patterns of elongated or rod-shaped particles show absence of oscillations at high or low q values. Apart from the oscillatory nature, the scattering profiles of anisometric particles appear to be relatively featureless decaying significantly slowly as compared to that from globular particles[64]. Figure 4.8 shows an encouraging comparison between the simulated scattering profiles of the Ch cluster, β -glucan strands and the Ch/ β -glucan mixed systems. Experimental SAXS data on 1 \rightarrow 4/1 \rightarrow 3 linked barley β -glucan in presence and absence of bile salt glycochenodeoxycholate (GCDC)[35], the L -Phe conjugated bile acids, α/β - L -PheC[65] and sodium taurodeoxycholate (NaTDC)[34] are plotted for comparison to the simulated data. Oscillations at $q > 0.1 \text{ \AA}^{-1}$ is noticeable in the simulated profiles of Ch cluster, with the frequency increasing in the presence of β -glucan, indicating formation of more compact spheroidal assembly. Some of the scattering profiles including those from this simulations for Ch soft assemblies, in presence and absence of β -glucan exhibits the Guinier plateau region at low q values ($< 0.1 \text{ \AA}^{-1}$) with the intensities levelling off. Strong inter-particle interactions leading to aggregation and instrumental artefacts at very low q values can often lead to disappearance of the Guinier plateau[63]. Overall, the scattering profiles simulated in this work mostly indicate existence of spheroidal soft-assemblies.

Proton index in A	$\Delta\delta$ (ppm)	Proton index in B	$\Delta\delta$ (ppm)	Proton index in C	$\Delta\delta$ (ppm)
H4	0.86	H2	0.52	H16	1.06
H6	-0.66	H3	-0.57	H18	1.09
H10	-0.67	H7	-0.55	H30	1.98
H13	-0.74	H16	1.01	H32	0.72
H16	0.90	H18	1.19	H35	1.59
H17	0.69	H29	0.82	H36	-0.69
H19	0.72	H30	0.54	H39	-0.81
H20	-1.23	H31	1.59	H40	-0.88
H26	0.87	H35	0.88		
H27	0.91	H39	-0.99		
H30	1.78				
H31	1.33				
H34	0.65				
H37	0.63				
H40	-0.78				

Table 4.1: Change in ^1H NMR chemical shift of representative protons of Ch molecule in presence of β -glucan from the three structures given in Figure 4.9.

4.3.5 NMR chemical shifts of Ch in absence and presence of β -glucan

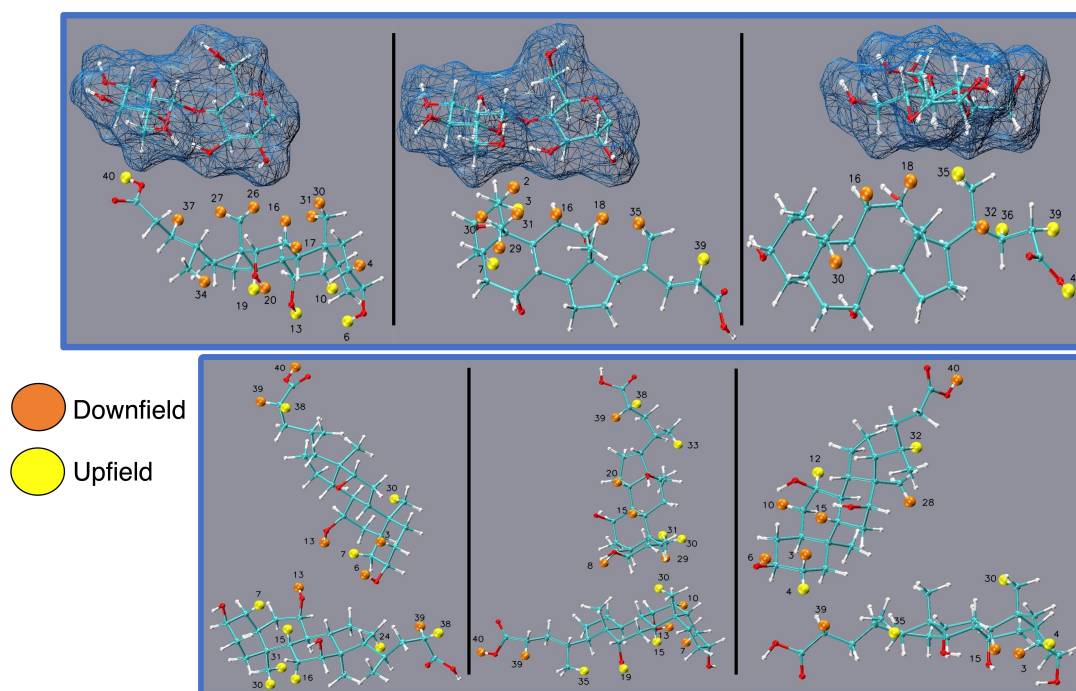


Figure 4.9: Snapshots isolated from molecular dynamics trajectories subjected to DFT calculations. The protons having a change in NMR chemical shift ($\Delta\delta$) values $> \pm 0.5$ ppm are shown. Protons experiencing downfield shifts (orange); upfield shifts (yellow).

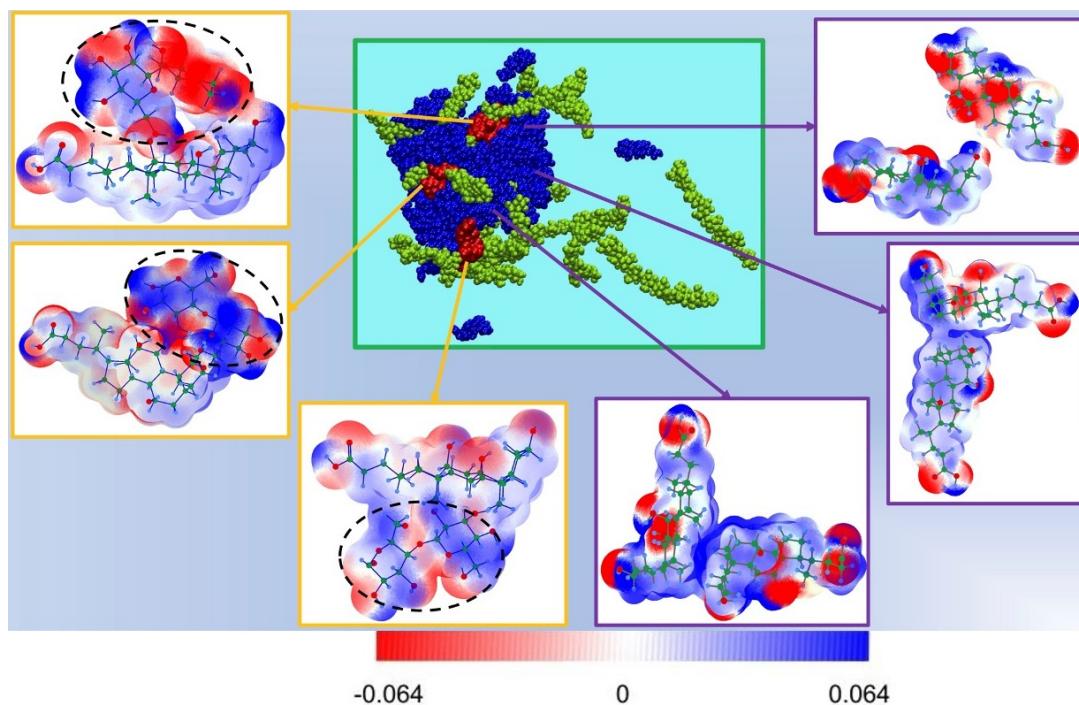


Figure 4.10: Snapshot from the molecular dynamics trajectory from which smaller assemblies are scooped out and subjected to DFT calculations. Charge distributions are indicated for: (A-C) Ch- β -glucan assemblies; (D-F) Ch-Ch assemblies. The colour bar denotes the extent of the partial charges. The black ellipse in structures A, B and C encircles the disaccharide domain in the molecular assemblies.

Literature search further reveals that there are many experimental reports where the interaction between bile components and polysaccharides are investigated using NMR spectroscopic tools[31]. Keeping that in mind, in order to have similar correlations with experiment, snapshots of the Ch aggregate in presence of β -glucan from the simulated trajectory are isolated to prepare structures for DFT calculations (Figures 4.9) in order to estimate a change in the chemical shift values of the protons of Ch[13]. To lessen the computation cost and complexity, in every structure, disaccharide unit is scooped out from the β -glucan chain, which is in close vicinity of a Ch molecule in the cluster. The sampling of the structures from the Ch- β -glucan assembly can be seen in Figures 4.9. Three representative structures with varying relative orientations and the change in the ^1H NMR chemical shifts of some selected protons are shown in Figure 4.9. The change in chemical shift ($\Delta\delta$) for a given proton on Ch molecule in presence of the β -glucan is calculated as following:

$$\Delta\delta = \delta_{\text{Ch}/\beta\text{-G}} - \delta_{\text{Ch}} \quad (4.1)$$

In Figure 4.9, the protons on Ch are coloured based on whether the change in chemical shift, $\Delta\delta$, is positive (up-field shift) or negative (downfield shift). Tables 4.1 and 4.2 respectively list the $\Delta\delta$ (those for whom $|\Delta\delta| > 0.5$ ppm) values of the protons of some representative Ch molecules in close vicinity of another Ch or a disaccharide unit of the

β -glucan, as marked in Figure 4.9. Similar magnitudes of $\Delta\delta$ can be found in the work of Meier and co-workers[33].

In some cases, the DFT calculations further revealed a small extent of charge transfer (1-5%) between a Ch molecule and the disaccharide unit of β -glucan or between two Ch molecules. As a result of this charge transfer, equal and opposite charges develop on the previously uncharged pair of molecules. Figure 4.10 shows the surface charge distributions between the molecular pairs.

Presence of hydrogen bonding type specific interactions between a Ch and the β -glucan molecule is also observed in the simulations. Figure 4.11 helps understand how the competitive H-bond scenario between two Ch or NaCh molecules (lipid-lipid, LL type) and that with solvent (lipid-solvent, LS

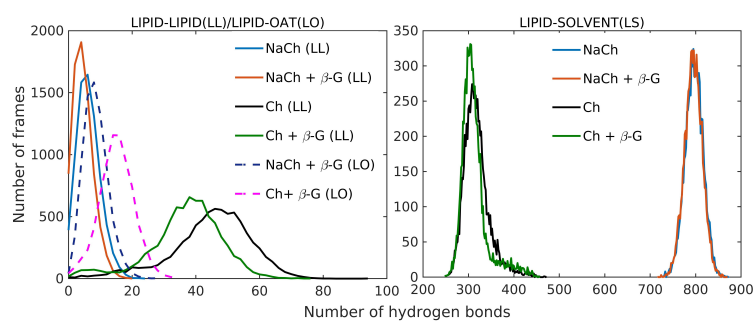


Figure 4.11: Comparison of hydrogen bond distributions in Ch/NaCh in presence and absence of β -glucan. Competition between lipid-lipid (LL), lipid- β -glucan (LO) and lipid-solvent (LS) hydrogen bonding is evident.

type) changes in presence of the β -glucan (lipid-polysaccharide, LO type). It appears that upon addition of the polysaccharide, the possibility of formation of L-O type H-bonds between a Ch or NaCh molecule and the β -glucan chain competitively inhibits the corresponding L-L type H-bonding. H-bonding of Ch or NaCh with solvent water is clearly dominating and is not affected much by the presence of the polysaccharide strands. The non-bonding interactions between the different molecular pairs are documented in Figure 4.12. A significant stabilizing short range vdW interaction is noticed between the lipid and β -glucan strands indicating their close association in solution.

Proton index in D			
Molecule1	$\Delta\delta$ (ppm)	Molecule2	$\Delta\delta$ (ppm)
H3	0.57	H7	-0.98
H6	0.59	H13	0.70
H7	-0.56	H15	-0.74
H13	0.91	H16	-0.56
H30	2.39	H24	-0.67
H38	-0.84	H30	-1.53
H39	0.95	H31	-1.43
H40	0.52	H38	-0.90
		H39	0.64
Proton index in E			
Molecule1	$\Delta\delta$ (ppm)	Molecule2	$\Delta\delta$ (ppm)
H8	0.68	H8	0.71
H15	0.73	H10	1.04
H20	0.88	H13	0.96
H29	0.57	H15	-0.64
H30	-1.41	H19	-0.61
H31	-1.49	H30	-2.46
H33	0.56	H35	-1.55
H38	-0.62	H39	0.86
H39	0.90	H40	0.53
Proton index in F			
Molecule1	$\Delta\delta$ (ppm)	Molecule2	$\Delta\delta$ (ppm)
H3	0.61	H3	0.97
H4	-0.85	H4	-1.11
H6	0.64	H15	1.04
H10	0.73	H30	-1.71
H12	-0.82	H35	-0.92
H15	0.66	H39	0.54
H28	0.61		
H30	-2.06		
H32	-0.58		

Table 4.2: Change in ^1H NMR chemical shift of representative protons of two Ch molecules in close vicinity as obtained from the three structures shown in Figure 4.9.

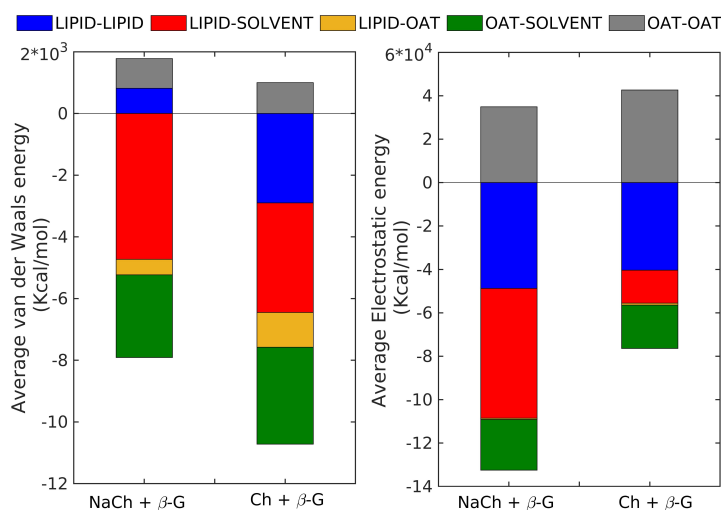


Figure 4.12: Interplay of non-bonding interaction energies (electrostatic and vdW) for different combinations of molecules.

4.4 Conclusion

Simulating the human intestinal fluid, that is known to contain colloidal structures of small molecules in a complex dynamic equilibrium, is a topic of significant challenge and utmost curiosity at the same time. In that ensemble of varied molecules, interactions between molecular assemblies are ubiquitous. Bile acids and salts are predominant constituents of bile with a total concentration in the range 100–160 mM, high enough to trigger aggregation. The bile acid aggregates often interact strongly with other dietary components, majorly polysaccharides that are still left undigested in the GI tract. This work sheds light on the molecular level interactions of a standard dietary β -Glucan motif (β -glucan) with a prototypical bile acid, the cholic acid (Ch) and its corresponding sodium salt (NaCh) by means of molecular dynamics simulations. The bile components are amphiphilic in nature and thus it is important to understand how the Ch- β -glucan soft assembly would organise and remain stable. The simulation data indicates that Ch aggregates use non-bonding, primarily short range attractive van der Waals forces to hold onto the polysaccharide chain. Due to this association, there is a significant change in NMR chemical shifts of the protons on Ch. Some extent of charge transfer interaction is also observed between Ch and polysaccharide or another molecule of Ch. An estimate of the principal moment of inertia and radius of gyration of the Ch- β -glucan composites along the simulation trajectory indicates that they are asymmetric top soft clusters with varying degrees of shape anisotropy. The scattering profiles mostly indicate existence of spheroidal soft-assemblies with prominent Guinier regions at low q values. Small angle scattering patterns and change in ^1H NMR chemical shifts are seen to be in line with the already reported experimental data, indicating non-specific interactions in the Ch- β -glucan composites.

Chapter 5

Control of anomericity and glycosidic linkage on the mechanics of polysaccharides

This chapter is based on the following paper, Peesapati, S. & Roy, D. Control of anomericity and glycosidic linkage on the mechanics of polysaccharides. *Journal Of Chemical Sciences*. **135**, 32 (2023)

url:<https://www.ias.ac.in/describe/article/jcsc/135/0032>

5.1 Introduction

Polysaccharides, the most diverse class of biomolecules, are omnipresent in nature[1, 2]. They offer an incredibly complicated conformational and dynamical space[3, 4, 5]. These conformational variations are undoubtedly translated to a wide array of structural and mechanical properties, which are absolutely important to recognize for various reasons[1, 6, 7]. Their incredible film & sheet forming abilities, gelling abilities deserve thorough investigation as to how the conformational properties of the integral monosaccharide units end up influencing the polysaccharide elasticity[8, 9, 10, 11]. The monosaccharides, which are linked by glycosidic linkages into linear or branched arrays of polysaccharides, dictate the polymer's physical properties to a great extent. As discussed in section 1.1 there are several handles regarding the structure of the monosaccharides and how they control the overall properties of the polysaccharide[3, 12, 13, 14]. Given so many features that can influence polymer elasticity, it is undoubtedly a problem of a significantly large scale and deserves systematic addressing[15, 16, 17, 18, 19].

A series of seminal work by the groups of Marszalek and Gaub, exploring the elastic properties of polysaccharides using atomic force microscopy (AFM) and steered molecular dynamics simulations (SMD) have already set the stage for the problem[15, 16, 17, 20]. Lot of insights can be obtained from these work on how the varied glycosidic linkages found in natural polysaccharides can affect the stretching of the polymer. Conformational transitions involving conversion from chair to boat through intermediate half-chair and skew boat conformers could be identified along the stretching process[16, 19]. Apart from the chair-boat transitions, the force induced conformational flips from a compressed to an extended conformation often lead to helix-sheet transformations, as found in some α -linked polysaccharides[15, 18, 19, 20, 21].

The conformational transitions associated with the stretching of the polysaccharide can be identified from the characteristic force-extension (F-E) curves generated from the atomic force microscopic (AFM) studies or steered molecular dynamics (SMD) simulations. As discussed in section 1.7, the F-E curve is mostly characterised by three regions. The initial plateau is explained as the entropic domain. It is the region of smaller force and low extension in entropic domain. Upon further stretching, the polysaccharide segment orients in the direction of applied force. The domain in which the polysaccharide extends proportionately to the rapidly increasing stress is the Hookean domain. This is usually marked by the elbow region. As the polymer reaches its contour length, the chain is fully stretched and has very few configurational options left. In this limit, the entropy reduces to zero when the polymer chain becomes linear[22]. Apart from the initial entropic and Hookean domain in the later part, there is sometimes an additional region of moderate extension in between, where the force-extension curve is usually observed to be non-Gaussian. In this region, the polysaccharides stretch and the chair is transformed to boat

conformers; the system passes through a high entropy region, as numerous skew boat conformers are possible as intermediates. This can be understood more easily from the Cremer-Pople representation of the possible conformers arising from a β -*D*-glucopyranose moiety as shown in the Figure 1.8, as the 4C_1 chair transcends to boat forms through the flexible boat-skew cycle for aldopyranoses[23]. The colour trend followed by various puckering conformations is shown in Figure 5.1.

Certain polysaccharides can exhibit this extra elastic extensibility, triggered by a conformational change under stress. The chemical structure of the pyranose ring and the glycosidic linkage present in the polysaccharide crucially control whether the polysaccharide would show extra extension. The origin of this lies in the presence of different conformers of varying glycosidic lengths in equilibrium. Typically, a *D*-glucopyranose moiety prefers to be in the 4C_1 chair conformation in the absence of any stress. Thermodynamically, this is more stable than the 1C_4 chair by ~ 8 kcal/mol[24, 25]. Thus, under stress, the monomers may undergo the following transformations: from one chair to another (e.g. 4C_1 to 1C_4), from a chair to a boat, or from a chair to an envelope/half-chair[15, 19, 20, 22].

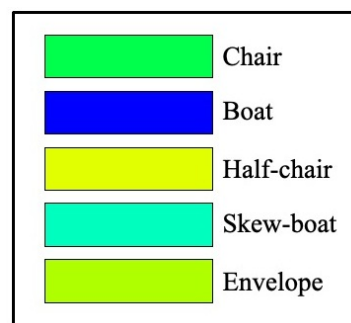


Figure 5.1: Colour code for various puckering conformations

It is important to recognize which pyranose-based polysaccharides would show the extra elongation or stretching as the conformations switch. Further correlating them to the monosaccharide structure and the glycosidic linkage present is vital. The primary criterion to have significant elongation as the pyranose changes conformation from the 4C_1 chair is to have at least one axial glycosidic linkage. One main conformational transition can be observed in amylose in 1(axial)-4(equatorial) glycosidic linked polysaccharide. Conversely, Pectin with 1(axial)-4(axial) glycosidic linkage exhibits two transitions. On the other hand, in cellulose with 1(equatorial)-4(equatorial) glycosidic linkage, no transition is observed[15, 19, 21].

SMD simulation data in the present report endorses some of these previous findings along with newer insights on conformational flips for the α and β -*D*-glucopyranosides with 1 \rightarrow 2, 1 \rightarrow 3, 1 \rightarrow 4 and 1 \rightarrow 6 types of glycosidic linkages. The mechanics of different homopolysaccharides have been compared with an attempt to address the following: (i) The effect of glycosidic linkage type and orientation on the extra elasticity of polysaccharides; (ii) The extent of monosaccharide ring puckering as the conformational transitions are noticed and (iii) whether the conformational flips are synchronous in nature down the polysaccharide chain.

5.2 Simulation methodology

The initial coordinates of the polysaccharide chains are generated using Glycan Reader and Modeler as available in CHARMM-GUI[26]. The generated polysaccharides are linear strands composed of α or β -D-glucopyranosides having any one of the 1 \rightarrow 2, 1 \rightarrow 3, 1 \rightarrow 4, or 1 \rightarrow 6 linkage types. Each strand has 15 residues and is solvated with TIP3P[27] water in a box with dimensions 30x30x150 Å. The SMD runs employed five independent trajectories for each system originating from different starting structures, sampled from molecular dynamics simulations in NPT ensemble at 1 atm and 300 K.

All the molecular dynamics simulations employed NAMD as the simulation engine[28]. The CHARMM36 all-atom additive Force Field is used to model the molecules[29]. The water molecules are described by the TIP3P model as incorporated in the CHARMM force field[27, 30]. A time step of 1 fs is used for the simulations. A cut-off distance of 12 Å is used for the nonbonded vdW interactions, with a switching distance of 10 Å. A pair list distance of 14 Å is used for electrostatic and vdW calculations. The particle mesh Ewald (PME) method is employed to calculate the electrostatics. The starting structures of the SMD runs are picked up from a 20 ns equilibrium simulation trajectory for each system. The long axis of the simulation box is oriented along the z-axis using the orient plugin of VMD[31]. Each starting structure is then subjected to initial conjugate gradient minimization followed by SMD simulations in NVT ensemble for 5 ns at 300 K. In all the SMD simulations of the 15-mer polysaccharide strands, the atom O₄ of the pyranose residue, 15 is kept fixed (fixed atom) while atom O₂ of pyranose residue 1 is pulled (SMD atom).

A constant pulling velocity of 0.1 Å ps⁻¹ is used for all the systems, and the force constant is set to 1 kcalmol⁻¹Å⁻². The nature of unfolding forces of a molecule in SMD simulations often increase with the pulling speed. Here, the magnitude of the pulling velocity and the force constant are optimized based on previous literature reports on similar molecules and the computation cost involved[15, 17, 32]. While SMD simulations do provide microscopic details of the unfolding process for a molecule, the simulated forces and pulling speeds required for unfolding are actually several orders of magnitude larger than those used in a typical AFM experiment (\sim 100-500 nm s⁻¹). SMD simulations, within a reasonable temporal window of a few nanoseconds, tend to induce a desired event under the applied stretching forces. Hence, simulations likely require higher pulling speeds and stronger forces than those observed in an AFM experimental setup. VMD (1.9.4)[31], MATLAB (R2019b) and Plumed (2.7.2)[33, 34] are used for the visualization of the structure, plotting, and analysis of data. Gaussian 09 is employed to predict the single point energies of the pyranose conformers for a chosen monosaccharide residue along the SMD trajectory. For a given polysaccharide, five different residues are picked: three successive residues R3, R4,

and R5, close to the SMD atom, one in the middle (R10), and one close to the fixed atom (R14).

Each of the chosen residues is saved separately and capped with the missing OH/H atoms using Gauss-View. The single-point energy calculations for each of these residues are done using the B3LYP functional and 6-311++g (d,p) basis set, as used in a previous study on the mechanical properties of the polysaccharide, pectin[35]. The color code used to represent the monosaccharide conformers are adapted from the work of Cross *et al*, as implemented in VMD[36].

5.3 Results and discussion

5.3.1 Monosaccharide variants and the glycosidic linkages

Figure 1.3 shows different monosaccharide repeating units along with the respective glycosidic linkages studied in this work. The two anomeric series of α and β -*D*-glucopyranose with either axial-equatorial (ae) or equatorial-equatorial (ee) orientation of the bonds involved in the glycosidic linkage brings substantial differences in their stretching patterns under the influence of an external pulling force. As mentioned in the introduction, the presence of an axial glycosidic bond would help trigger a prominent conformational transition from the 4C_1 chair to 1,4B thereby stretching the pyranose residue and resulting in the extra-elastic domain for the polysaccharide in the F-E curves. A detailed description of the nomenclature and interconversions of the conformational variants of the six-membered aldopyranose ring is available in the report from the IUPAC-IUB Joint Commission on Biochemical Nomenclature (JCBN)[37].

In Figure 5.2, some representative starting structures for each kind of polysaccharide picked up from their respective equilibrium trajectories and used for subsequent SMD runs are depicted to emphasize the difference in the extent of ordering in their 3D structures. All the *D*-glucopyranose residues in a given polysaccharide are in 4C_1 chair conformation at the beginning of the simulation.

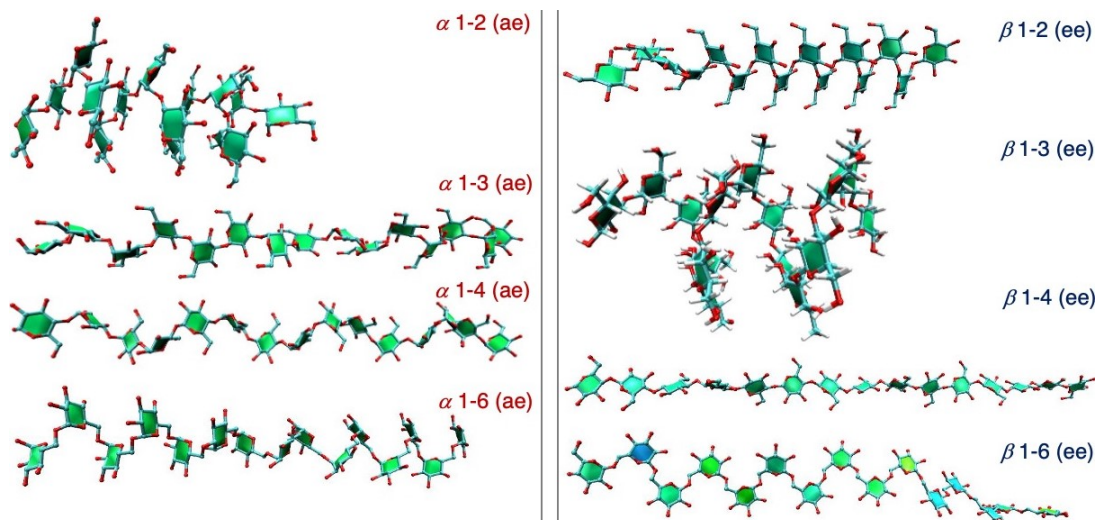


Figure 5.2: Starting conformations of the steered molecular dynamics simulations for the different polysaccharide strands.

5.3.2 Force-extension (F-E) curves: comparison of SMD and AFM data

The force-extension (F-E) curve, as depicted in Figure 5.3, is an output of the SMD runs, which can be compared to those from AFM experiments after appropriate normalization. Some of the polysaccharides exhibit a phenomenon of extra elasticity where a stretch in the polysaccharide strands is noticed in the form of a hump or kink in the F-E curves in between the entropic and Hookean domains, corresponding to intermediate pulling forces of ~ 1000 - 2000 pN. This phenomenon is evident from Figure 5.3. α -D-1 \rightarrow 3 and β -D-1 \rightarrow 3/1 \rightarrow 4 linked glucopyranosides appear to show low elasticity, with the F-E curves transitioning directly from the entropic to the Hookean domain. Further, different starting configurations of the same polysaccharide can exhibit the varying extent of ‘entropic elasticity’, given by the initial linear region at very low forces, depending on the extent of coiling in the structure.

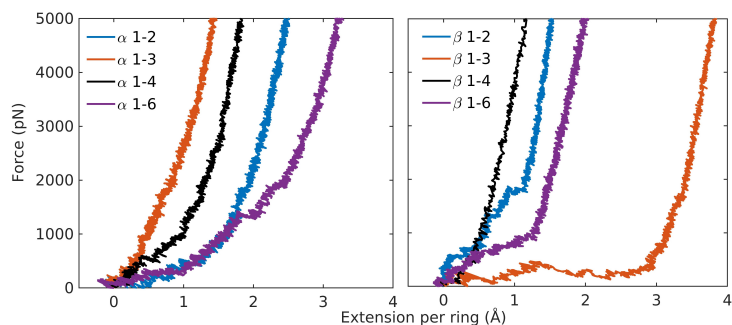


Figure 5.3: Extension of the different polysaccharide strands under pulling stress. The extension of a polysaccharide chain is measured per ring as: $\Delta l = (l_f - l_i)/15$, where l_i and l_f , respectively stand for the initial length of the polysaccharide and that at a given time instant.

Type	Initial	Final	Glycosidic length (Å)
α 1-2			2.95 ↓ 17% 3.46
α 1-3			4.34 ↓ 14% 4.97
α 1-4			4.58 ↓ 25% 5.75
α 1-6			4.36 ↓ 37% 6.01

Type	Initial	Final	Glycosidic length (Å)
β 1-2			2.99 ↓ 27% 3.82
β 1-3			4.70 ↓ 11% 5.22
β 1-4			5.39 ↓ 6% 5.71
β 1-6			4.80 ↓ 27% 6.09

Figure 5.4: Conformational transitions for a selected residue (R2) of the different polysaccharides in a particular SMD trajectory. The initial structure is the one obtained from the starting conformation. The final structure is the one reached at ~ 2100 pN force. The percentage increase in glycosidic bond length is given. The glycosidic oxygen atoms, labelled as red vdW spheres, are used to calculate the glycosidic bond length.

This is clearly observed in the overall conformational organization of the various systems and their different starting structures, e.g., β -1 \rightarrow 3 strand is helically coiled, thereby exhibiting a relatively long entropic domain in the F-E curves. Figure 5.5 shows the starting structure variation of all the systems. Figure 5.4 documents the conformational switches and extensions of the 2nd residue (R2) from the 15-meric strands of the polysaccharides under consideration, which is adjacent to the residue containing the SMD atom. The final

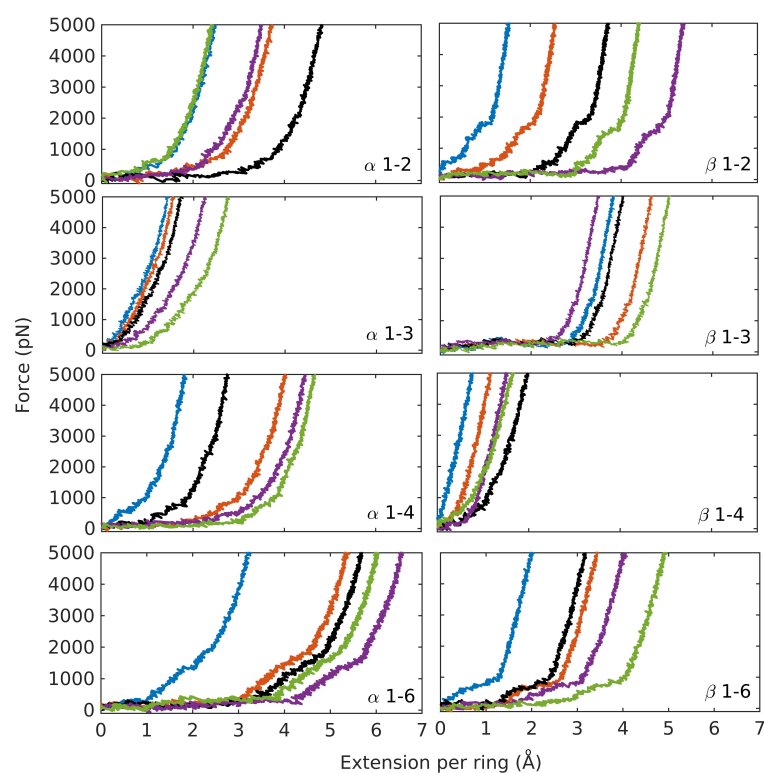


Figure 5.5: Extension of the different polysaccharide strands under pulling stress. Five different starting structures are shown for each system. The extension of a polysaccharide chain is measured in the same way as in Figure 5.3.

structure of the residue corresponds to the one taken from the F-E curve of the corresponding polysaccharide under a stretching force of ~ 2100 pN. The prominent difference in the extent of stretching of the glycosidic linkage, given by the distance between the two glycosidic oxygen atoms is evident in some polysaccharides.

Most of the α -series shows puckering of the 4C_1 chair to intermediate conformations that leads to the prominent extension by ~ 14 - 37% for each residue. The important observation at this point that has gone unreported previously is that some of the members of the β -series, like the β -1 \rightarrow 2 linked polysaccharide, can also undergo puckering and distortion from the conventional chair form, resulting in extra elasticity. This puckering of the monosaccharide rings is evident from the Figures 5.4, 5.10 and 5.11. The length of a polysaccharide chain may affect the stretching profile as the

population of non-chair conformers is shown to depend on it. In an earlier REMD simulation study by Gnanakaran and co-workers on cellulose fragments comprising β -D-glucopyranoside units linked by 1 \rightarrow 4 glycosidic linkages, it was shown that although 4C_1 is the preferred chair conformation observed in the simulations, about 1-2% of conformers exhibited non-chair forms. It is noteworthy here that the propensity of formation of non-chair forms increases with the degree of polymerization[40].

The advantage and usefulness of SMD simulations lie primarily in their ability to generate F-E curves that can be compared to AFM results after appropriate normalization, as mentioned in the legend of Figure 5.6. Hence, it is imminent to validate the simulations against the output from AFM studies reported in the literature. Figure 5.6 compares the F-E curves of some representative trajectories after normalizing them at the maximum

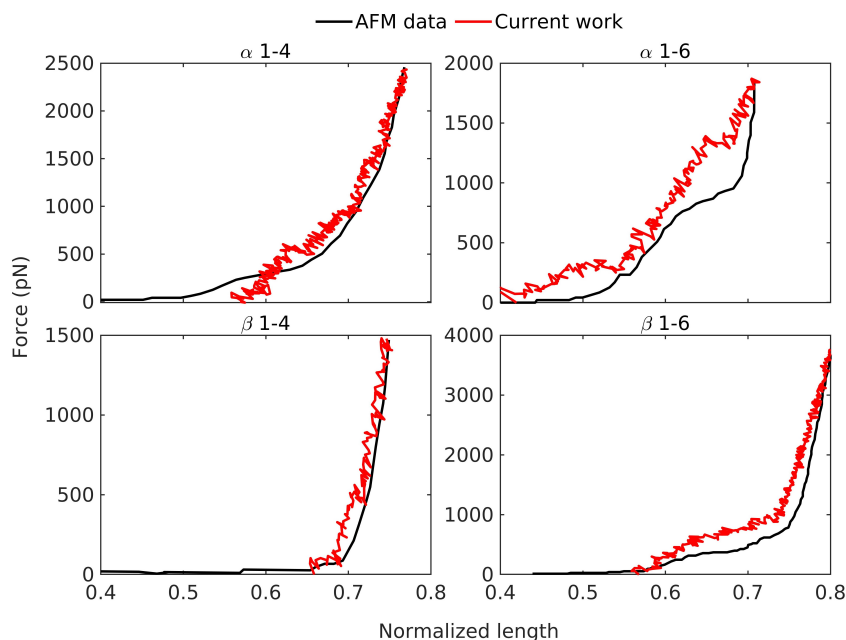


Figure 5.6: Comparison of the extension profiles of different polysaccharides as obtained from AFM studies[38, 39] and SMD simulations from this work. Here, the normalized length of the polysaccharides is defined as: $l=l_t/l_f$, where, l_t stands for the length of the polysaccharide against a given pulling force at a particular time instant. l_f stands for the final length of the polysaccharide that is achieved after 5 ns of SMD simulation. The experimental curve is normalized by making the experimentally observed extension at the highest force reported equal to that observed in SMD simulations at the same force.

force in the available experimental data. Despite the limitations in classical molecular dynamics force fields and artefacts in modeling and simulation, good correspondence between simulated profiles and the experimental F-E curves is found.

5.3.3 Glycosidic dihedrals and Cremer-pople pyranose ring puckering parameters

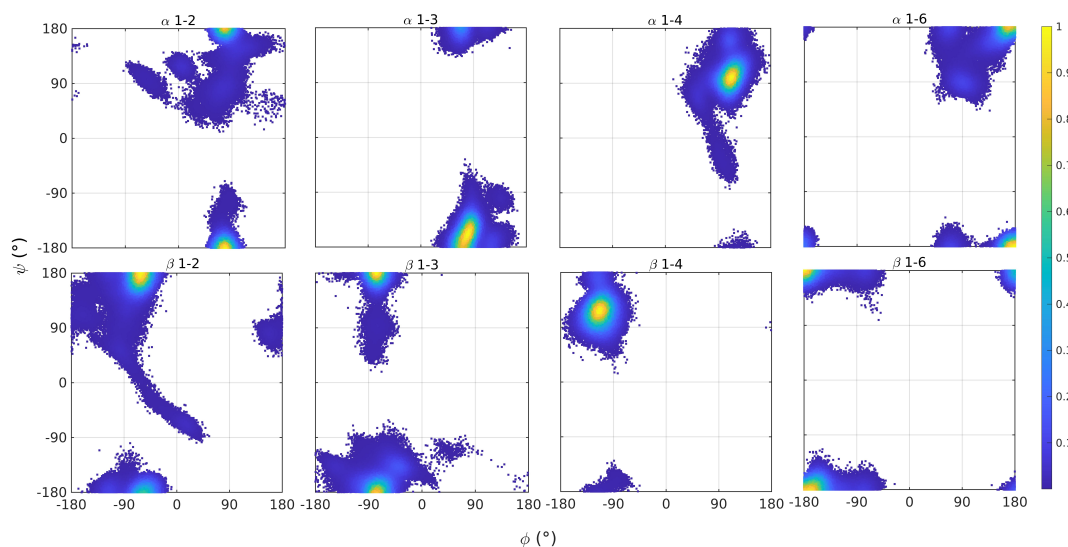


Figure 5.7: Carbohydrate Ramachandran plots of SMD simulations for the dihedral angle (ϕ, ψ) distributions for oligosaccharides containing 15 α or β -D-glucopyranosyl units linked by the different glycosidic linkages at 310 K in water. The plots are globally normalized with respect to population of snapshots and the same color bar is applicable to all. Hence the color distributions for all the plots are comparable to each other.

As the polysaccharides stretch under the influence of the pulling forces, the glycosidic dihedral angles ϕ ($O_5 - C_1 - O'_n - C'_n$) and ψ ($C_1 - O'_n - C'_n - C'_{n-1}$) curve out a phase space, which helps to understand the allowed regions for a polysaccharide with a given glycosidic link. Along with anomericity, this work shows that glycosidic linkages also play a vital role in the extent of stretching, as discussed later in this section. Figure 5.7 shows the carbohydrate ramachandran plots for the various systems constructed by collecting snapshots along the SMD trajectory. The spread in the dihedral angles for α -1 \rightarrow 4 and β -1 \rightarrow 2/1 \rightarrow 3/1 \rightarrow 4 linked D-glucopyranosides is substantial, indicating significant flexibility in this attribute that might lead to twisting of the polysaccharide chains. Also under stretched conditions, the glycosidic dihedral angles show deviation from their unstretched configurations (shown in Figure 5.8). This deviation from equilibrium values is quite notable for 1-6 glycosidic linked system owing to their higher flexibility due to the presence of $-CH_2$ group in the glycosidic linkage. Also, the stretching of polysaccharides facilitates in

coverage of dihedrals which are otherwise not accessible in equilibrium simulations. Along with the glycosidic dihedrals, the puckering of the monosaccharide rings under perturbation is an important attribute to follow. The puckering of the rings in monosaccharides can be followed by estimating the Cremer-pople puckering parameters as discussed in section 1.5.1[41]. This classification has been very useful in distinguishing between the different stable, metastable and transition states along the potential energy surface, as given in Figure 1.8. The color codes given in Figure 5.1 is used in Figures 5.12-5.13 later to track the conformers along a SMD trajectory.

Deviation of θ from 0° indicates distortion from the 4C_1 chair form[42]. The pyranose ring is considered to be in the most stable chair conformation (4C_1 or 1C_4) for $\theta = 0$ or 180° . Out of the two chair conformers, D-glucose has a strong preference towards the 4C_1 chair[43]. For conformers lying in the equatorial plane of the sphere corresponding to $\theta=90^\circ$, as the phase angle (ϕ), crosses different values

from 0 to 360° , the six-membered pyranose ring moves through six boat ($\phi = 0, 60, 120, 180, 240, 300^\circ$) and six twist boat conformations ($\phi = 30, 90, 150, 210, 270, 330^\circ$). In between, for $\theta = 45$ or 135° , envelopes and half-envelopes appear[41, 42].

Figure 5.9 depicts the distributions of the Cremer-Pople angles along the simulation trajectory. It is clear that under the influence of the pulling force, all the α -polysaccharides undergo major puckering of the pyranose ring leading to boat or twist boat conformers. In the β -series, polysaccharides with 1 \rightarrow 2 and 1 \rightarrow 3 linkages exhibit similar distortions. However, the β -1 \rightarrow 4 and 1 \rightarrow 6 linked polysaccharides undergo minimal distortion; hence, no extra elasticity is observed due to the conformational switch in the F-E curves.

The case of β -1 \rightarrow 6 *D*-glucopyranoside is however more interesting, owing to the stretching observed under pulling stress due to the presence of the extra flexible 1 \rightarrow 6 glycosidic linkage (Table 1 and Figures 1-3). Figures 5.10 and 5.11, showing the residue wise variation in the pseudorotation angle and phase angle, for all the residues of some representative polysaccharide strands and colored based on their time of appearance, are important to

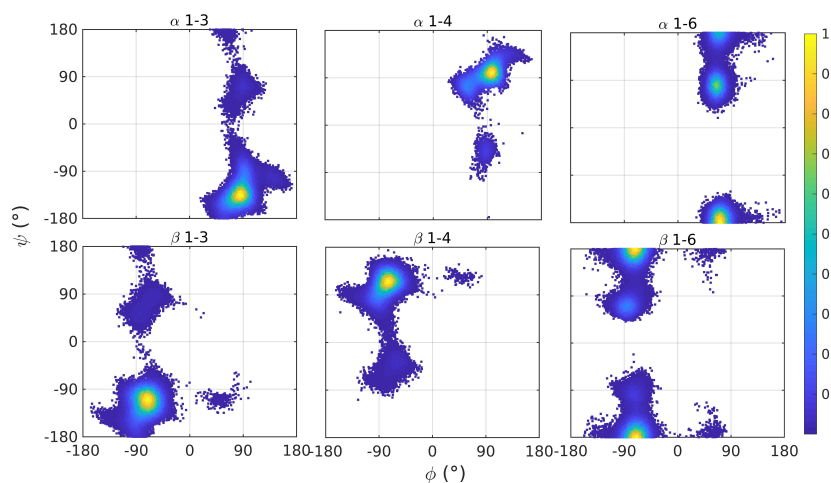


Figure 5.8: Carbohydrate ramachandran plots as obtained from equilibrium simulations for the dihedral angle (ϕ, ψ) distributions for oligosaccharides containing 15 α or β -D-glucopyranosyl units linked by different glycosidic linkages.

understand how the act of distortion proceeds down the polysaccharide chain in the course of the SMD runs. This plot is further intended to show how far along the chain the memory of distortion of a pyranose ring lasts. In the α -series, for most of the polysaccharides except a 1 \rightarrow 2, the residues show transitions from 4C_1 to boat or twist boat-like conformations, which are stable and have long residence times. In some cases, envelopes or half-envelopes are also noted. None of them, however, undergo complete flipping to the 1C_4 chair. Hence, in the F-E curves, all these polysaccharides exhibit a single hump corresponding to a single 4C_1 chair-to-boat/twist boat transition. In the β -series, except β -1 \rightarrow 2 and the SMD residue of the β -1 \rightarrow 3 polysaccharide, none of the other residues show appreciable distortion; at the most, envelopes or half-envelopes are noticed in some cases. This is in line with expectations from the simulated F-E profiles and also validated by AFM signatures.

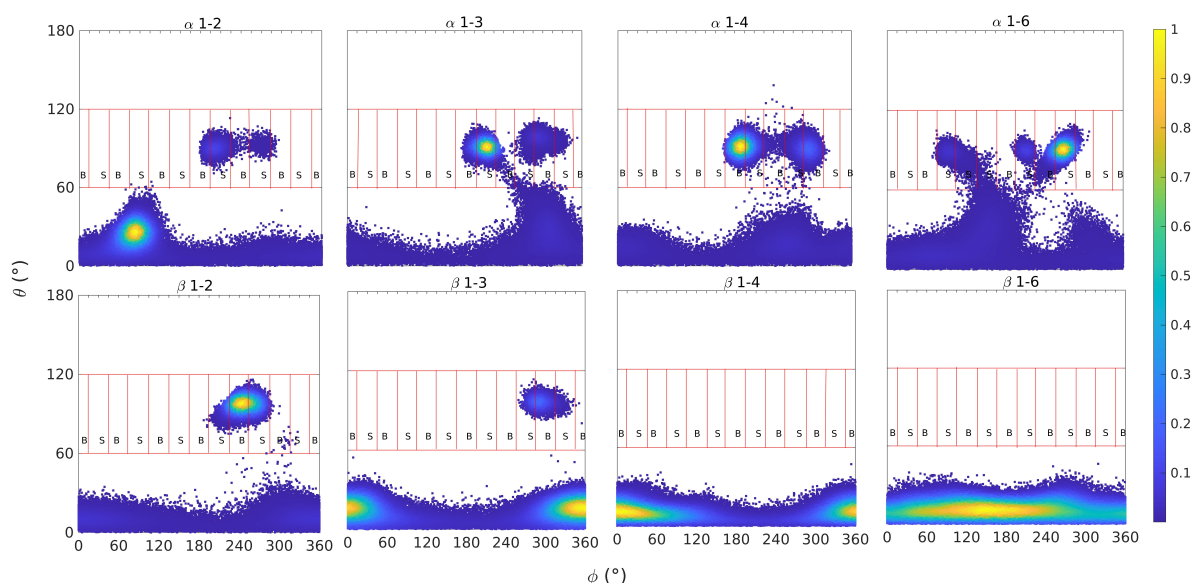
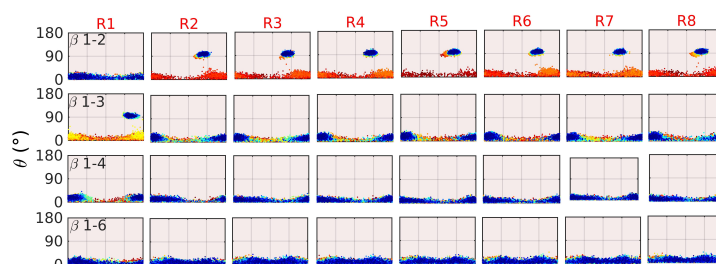


Figure 5.9: Distribution of the Cremer-Pople puckering angles of the SMD simulations for the different types of polysaccharides. The puckering angles of all the residues for the 15-mer polysaccharide chain along the entire simulation trajectory are considered here. The Mercator representation is used to indicate whether a snapshot belongs to a boat or skew-boat conformation.



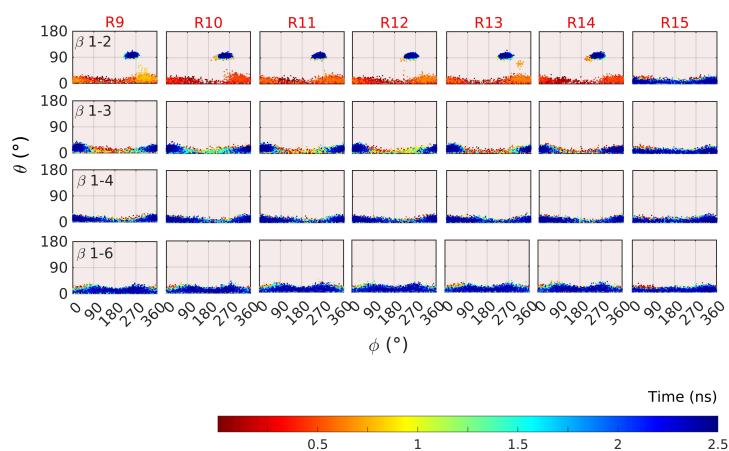


Figure 5.10: Distribution of the Cremer-Pople puckering angles of SMD simulations for the different types of β -polysaccharides. The puckering angles of all the residues for the 15-mer polysaccharide chain along the entire simulation trajectory are tracked here. The conformations are color-coded based on their time of appearance.

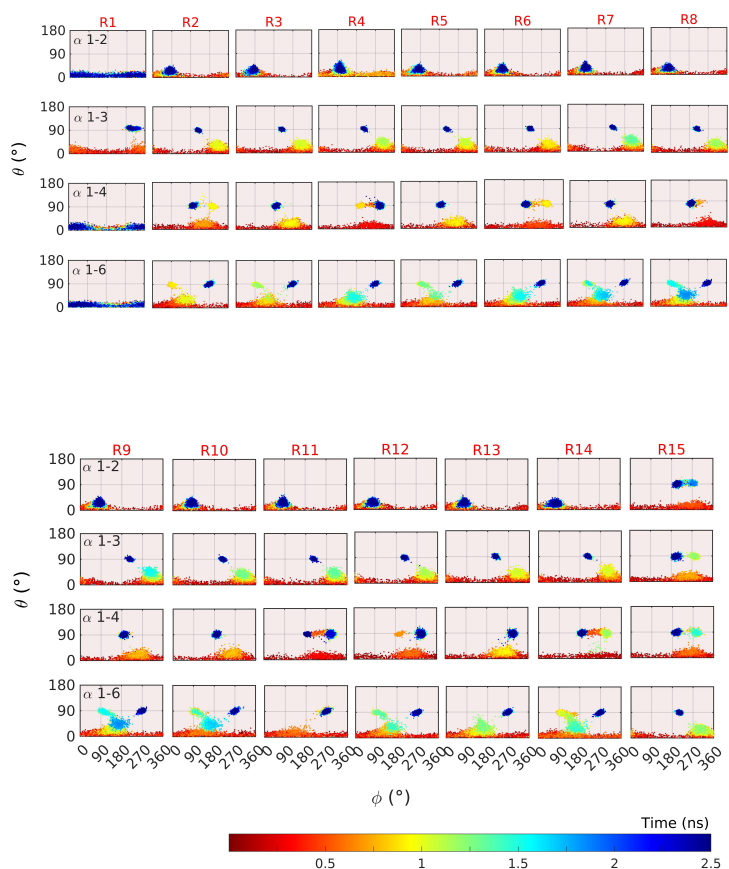


Figure 5.11: Distribution of the Cremer-Pople puckering angles of the SMD simulations for the different types of α -polysaccharides. The puckering angles of all the residues for the 15-mer polysaccharide chain along the entire simulation trajectory are tracked here. The conformations are color-coded based on their time of appearance.

5.3.4 Structure and energetics of the monosaccharide conformers along an SMD trajectory

Figures 5.12, 5.13, 5.14, 5.15 and 5.16 depict the conformers for a given monosaccharide residue along a representative SMD trajectory for three classes of polysaccharides: α -1 \rightarrow 6, β -1 \rightarrow 2 and β -1 \rightarrow 4. While α -1 \rightarrow 6, β -1 \rightarrow 2 polysaccharides are noted for their extra elastic behavior, β -1 \rightarrow 4 shows minimal extension. Figure 5.12a shows upon stretching, a typical residue from a strand of α -1 \rightarrow 6 polysaccharide would start with a 4C_1 chair and gradually evolve into the boat conformer through intermediate half chairs and envelopes. Figure 5.14 shows the fates of some selected residues along the polysaccharide chain, some from the end which is pulled (R3, R4 and R5), one from the middle (R10) and the last one is close to the fixed end (R14). The single point energy of the capped residues as calculated using DFT and the glycosidic bond length are mentioned below each conformation. The time of appearance and the force exerted on the polysaccharide are denoted above the panel. Similar plots for the β -1 \rightarrow 2 polysaccharide also indicate steady and consistent progression from the 4C_1 chair to the boat form. However, for β -1 \rightarrow 4 linked polysaccharides, this kind of transition is not noticed. It is reported in the literature that for cellulose, α,β -1 \rightarrow 4 polysaccharide, the region of ‘extra elasticity’ is minimal[44]. For the 1 \rightarrow 6 linked polysaccharides of both anomeric series, the stretching originates from the dual combination of conformational switch and straightening of the extra-flexible 1 \rightarrow 6 glycosidic bond. Indeed, the flexibility of the extra $-\text{CH}_2$ group in the 1 \rightarrow 6 linkage can help stretch the polysaccharides without a ring conformation switch. This is why the elasticity is maximum for the α 1 \rightarrow 6 polysaccharide, where both of these factors contribute. For the same reason, the corresponding β anomer (β -1 \rightarrow 6) exhibits $\sim 27\%$ extension in glycosidic bond length, although a conformational switch is absent, as seen previously in Figure 5.10.

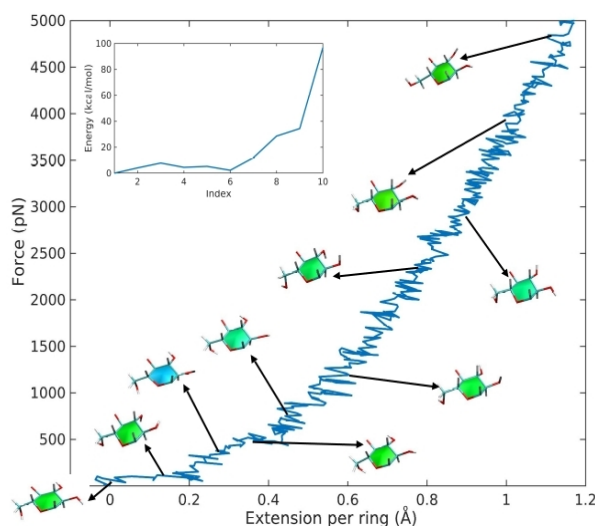


Figure 5.13: Extension of a β -1 \rightarrow 4 linked glucopyranoside strand under pulling stress.

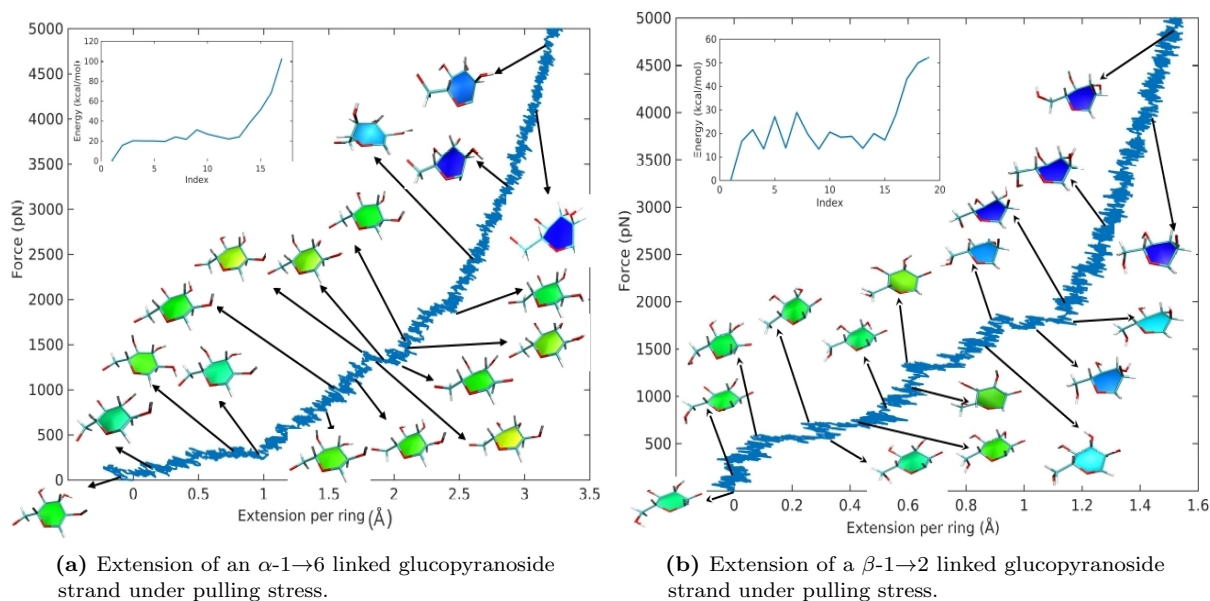


Figure 5.12

Time(ps)/ Force(pN)	0/-	120/266	640/1330	1245/2930	1700/4597
R-3	 -687.94 / 4.4	 -687.36 / 4.4	 -687.34 / 5.1	 -687.31 / 6.4	 -687.28 / 6.5
R-4	 -687.38 / 4.3	 -687.36 / 4.4	 -687.36 / 5.1	 -687.31 / 6.2	 -687.28 / 6.6
R-5	 -687.38 / 4.4	 -687.35 / 4.4	 -687.35 / 5.1	 -687.32 / 6.1	 -687.29 / 6.4
R-10	 -687.39 / 4.4	 -687.36 / 4.6	 -687.36 / 5.5	 -687.33 / 5.9	 -687.29 / 6.5
R-14	 -687.39 / 4.3	 -687.36 / 4.6	 -687.32 / 5.9	 -687.29 / 6.0	 -687.26 / 6.7

Figure 5.14: Conformational transitions for selected residues (R_i) of an α -1 \rightarrow 6 linked glycopyranoside along the simulation trajectory under pulling stress. The time instant (ps) and the force (pN) are denoted. Below each structure, energy (Hartree) and the glycosidic bond length (\AA) are given.

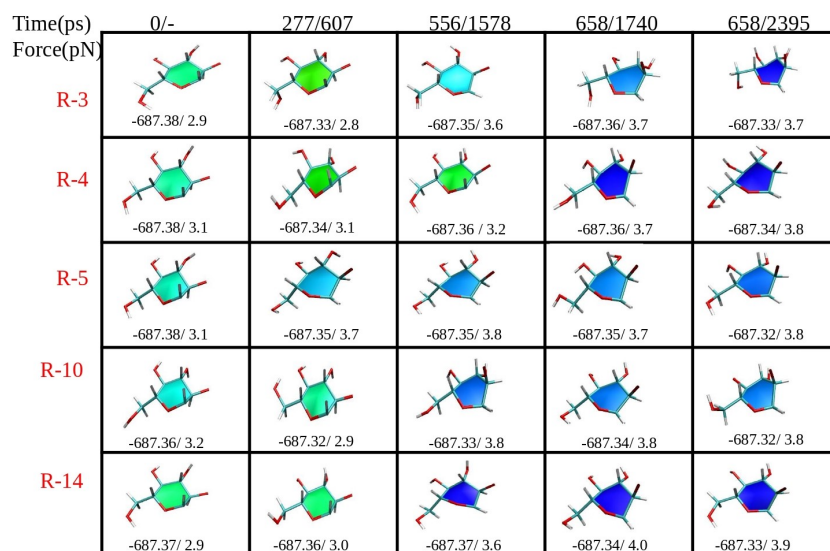


Figure 5.15: Conformational transitions for selected residues (R_i) of an β -1 \rightarrow 2 linked glucopyranoside along the simulation trajectory under pulling stress. The time instant (ps) and the force (pN) are denoted. Below each structure, energy (Hartree) and the glycosidic bond length (\AA) are given.

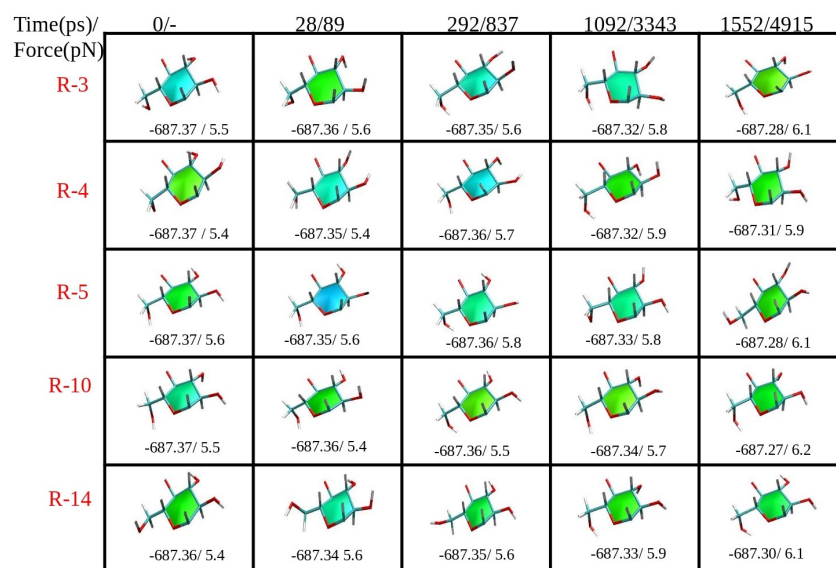


Figure 5.16: Conformational transitions for selected residues (R_i) of an β -1 \rightarrow 4 linked glucopyranoside along the simulation trajectory under pulling stress. The time instant (ps) and the force (pN) are denoted. Below each structure, energy (Hartree) and the glycosidic bond length (\AA) are given.

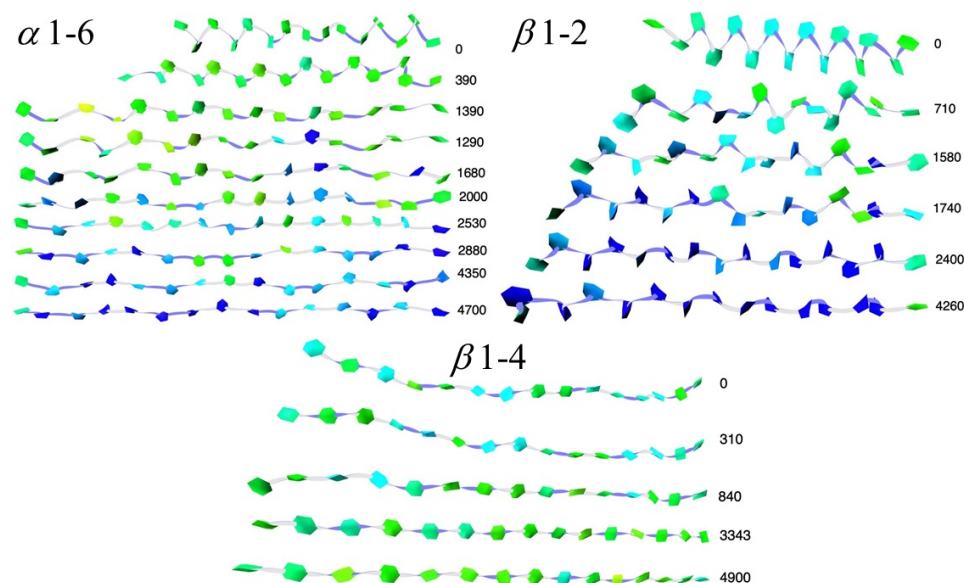


Figure 5.17: Extension of three representative classes of β -D-glucopyranoside strands under pulling stress. The force (pN) is depicted beside each strand. The color of each glucopyranose ring denotes the instantaneous conformation as explained in Figure 5.1. The glycosidic linkage involved is given in each panel.

Figure 5.17 shows time-resolved snapshots depicting the progress of the overall stretching of the polysaccharide strands along the SMD trajectory for representative systems. Each pyranose ring is color-coded based on its conformation, as depicted in Figure 5.1. The gradual evolution from the 4C_1 chair to the intermediate half-chair/ envelope leading to the boat is evident from the snapshots. The conformational switching across the monosaccharides along a polysaccharide chain is not following any apparent synchronous pattern. However, this aspect needs thorough investigation with longer polysaccharide strands before any conclusion can be reached.

5.4 Conclusion

Understanding the mechanics of polysaccharide framework bearing unlimited mechanical potential, is worthy to say the least. Polysaccharides are future must for many applications including the design of non-conventional and bio-conductive membranes. Especially, in the context of the present scenario, where plastics have turned out to be a menace, polysaccharides show great promises to come up with viable alternatives. This study is thus aimed at unfolding the fundamental structural intricacies of some model 15-meric D-glucopyranosides and how the glycosidic linkage patterns and anomeric nature of the monosaccharides affect their mechanics. Steered molecular dynamics simulations and DFT calculations are used to track the changes along a polysaccharide chain as it is

subjected to a wide range of pulling stresses. The transformations from the entropic to the Hookean domain is clearly visible in the force-extension curves generated by SMD and validated by AFM studies from literature for these polysaccharides. The ‘extra-elastic’ region as it appears between the entropic and Hookean domain in the F-E curves of some polysaccharides is correlated to the conformational switch of the aldopyranose ring from the 4C_1 chair to a boat or intermediates like half-chair or envelopes. Wherever possible, the SMD F-E curves are compared to the experimentally obtained AFM curves after appropriate normalization and a reasonably good agreement is noticed. The polysaccharides belonging to α -D-1 \rightarrow 4 and α -D-1 \rightarrow 6 series show significant stretching and so do β -D-1 \rightarrow 2 and β -D-1 \rightarrow 6 series. A special characteristic of polysaccharides bearing 1 \rightarrow 6 linkage is the extra freedom imparted to them by the presence of an additional -CH₂ group in the glycosidic link. This contributes significantly to stretching of the strand under stress, even sometime without any conformational switch, as observed in the β -D-1 \rightarrow 6 strand. In future, temperature dependent SMD runs could be attempted to understand the evolution of the entropic domain of the F-E curves for the different polysaccharides. Additionally, one could also explore polysaccharide sheets consisting of multiple strands of such pyranosides linked by varied glycosidic linkages, with an eye to understand and tune their mechanics.

Chapter 6

Characterizing the mechanical properties of natural polysaccharides through steered molecular dynamics

The contents of the chapter is based on the following paper, Peesapati,S. & Roy, D. Characterizing the mechanical properties of natural polysaccharides through steered molecular dynamics.

(Manuscript under preparation)

6.1 Introduction

The conformational transitions associated with the stretching of α,β -linked glucans has been thoroughly investigated in chapter 5. Current chapter involves detailed study of structure, molecular force-extension behaviour of selected polysaccharides involving α or β 1 \rightarrow 4 glycosidic linkages between their constituent pyranose rings of homo or hetero polymers. These modelled oligosaccharide strands are inspired from the naturally available polysaccharides like acetan, amylopectin, galactose chain, mannose chain, galactomannan, chitin, gellan, pullulan and pectin. Among these gellan, acetan, amylopectin and galactomannan are hetero polysaccharides while rest are homo polysaccharides. All these polysaccharides can be extracted from plants, animals or bacteria and are gaining popularity in food and packaging industries. Acetan is an anionic bacterial hetero-polysaccharide[1, 2]. It is water-soluble in nature. This polysaccharide contains cellulosic backbone with pentasaccharide branching on alternate glucose units[3]. The molecular composition can be quite heterogeneous across species and strains. Acetan and acetan-like polymers have a huge potential for commercial usage in food and pharmaceuticals industries[3].

Amylopectin, a highly branched water-insoluble polysaccharide is composed of α -glucose units[4]. It is one of two major components of starch which is found in plants. It contains large number of residues with irregular branching by 1 \rightarrow 6 glycosidic linkage every after \sim 22 monosaccharide residues[5]. The main function of amylopectin is to store energy in plants. The major sources of amylopectin include rice, wheat, maize, root vegetables like potatoes, casaava etc. Galactomannan is a hetero polysaccharide present in most leguminous seeds and is composed of galactose in the backbone and mannose as the branched unit[6]. Bean gum, guar gum, cluster bean and fenugreek are the most common sources of galactomannan. These polymers are resistant to human digestive secretions and so act as natural fiber[7]. These are commonly used as food additives to increase the viscosity of the water phase. Pectin is a water soluble structural fibre[6]. It is linear polymer with few hundred to thousand galactouranic acid units linked forming the backbone. It is found in the primary cell wall of fruits such as apples, oranges, lemons, etc. Pectin is used in jams, jellies, frozen foods, as an alternative of sugar in low calorie food items[8]. Pectins can be highly methyl substituted, intermediate methyl substituted or de-methyl substituted. This degree of substitution can greatly alter the extent of cross linking, thus altering its properties[9].

Chitin is present in the exoskeletons of arthropods such as crabs and shrimps. It is highly acylated and insoluble in water[6]. It is the second most abundant biopolymer on earth after cellulose. Chitin can be used as edible coatings to extend the shelf life of fresh and frozen food[10, 11]. Pullulan is a linear glucosidic polysaccharide[12]. It is commercially in use for edible films of oral hygiene. It is a water soluble polymer and can replace starch in baked foods[13]. Due to their adhesive properties, pullulan and their derivatives

can be used in wound healing compositions. Pullulan based biofilms are known for their low oxygen, moisture permeability and promising mechanical properties. Esterified and etherified forms of pullulan are water insoluble in nature. Gellan is an anionic polysaccharide that can contains tetrasaccharide repeating units. It can be processed into heat resistant transparent gels[14]. The gellan gum chains can interlock with each other to form a coherent network which can trap high fraction of water[15]. Depending on the degree of acyl substitution, gellans can be categorised as high acyl or low acyl gellan gums. Both of which are insoluble in water. While the former can only be tuned into soft and elastic gells, the later can form strong and brittle gels[16].

These natural polysaccharides, with their ability to form gels and sheets have garnered much attention as valuable alternative to plastics. The diverse range of applications include food, pharmaceuticals and material engineering. For determining suitability for specific application, ‘elasticity’ of polysaccharides plays a crucial role. The conformational properties of the individual monosaccharide units, which constitute polysaccharides, have a profound impact on their overall elasticity[17]. As discussed earlier in section 5.1, conformational properties of monosaccharide units are influenced by several factors including glycosidic linkage, anomeric state and presence of functional substitutions. These factors play a critical role in the spatial arrangement and interactions between adjacent monosaccharide units within the polysaccharide chain.

Understanding the relationship between conformational properties and elasticity is useful in optimizing processing conditions such as pH, temperature, solvent composition, etc. in order to manipulate structure and properties of polysaccharide based films or membranes. The current chapter provides a comprehensive idea on the intricate relation between conformational properties of selected polysaccharides and their elasticity. This knowledge opens up avenues in harnessing in them for the development of innovative applications in various fields.

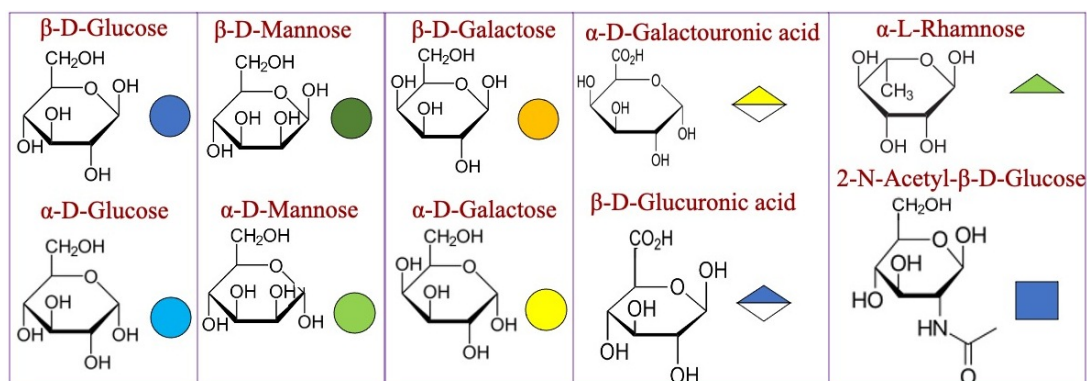


Figure 6.1: Individual building blocks for the structures generated. The structure and its graphical notation are given for all the monomeric variants part of this study.

6.2 Simulation methodology

The initial coordinates of the polysaccharide chains are generated using Glycan Reader and Modeler as available in CHARMM-GUI[18]. The generated polysaccharides are linear or branched strands having 1→4 linkage types in the backbone and branched using 1→6 or 1→2 linkage types. Each strand has 15 residues (except for gellan which has 16 residues) in the backbone chain and is solvated with TIP3P[19] water in a box with dimensions ranging from 30x30x150 to 50x50x150 Å. Figure 6.1 depicts the structures of individual monomers which are used in the generation polysaccharide strands. The graphical notation beside each building blocks is used to illustrate the repetitive units in strands as shown in Figure 6.2.

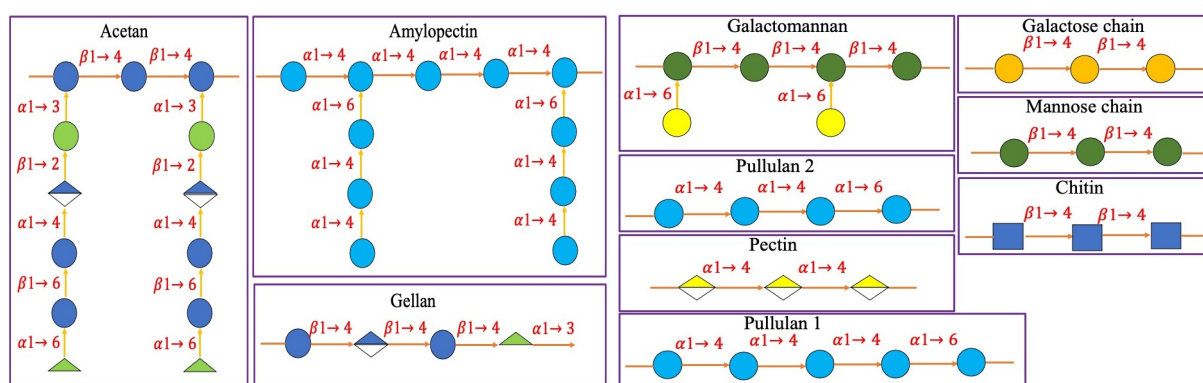


Figure 6.2: Repetitive units used for the construction of the polysaccharide strands.

The acetan chain is composed of β 1→4 linked glucose units in the backbone. Every alternate residue is linked by a side chain from the mannose end using α 1→3 linkage. The branched chain is composed of $-\alpha$ -MAN-2- β -GLCA-4- α -GLC-6- β -GLC-6- α -RHA. Amylopectin is composed of α 1→4 linked glucose units in the backbone chain. Every third residue starting from residue number 2 is branched through α 1→6. The branching side is composed of $-\alpha$ -GLC-4- α -GLC-4- α -GLC. Similarly, the chain galactomannan is composed of β 1→4 linked mannose units in the backbone chain and branched at every alternate residue through 1→6 linkage with α -galactose units. The linear chains of galactose, mannose, chitin and pectin are composed of β 1→4 linked GAL, β 1→4 linked MAN, β 1→4 linked 2-NAGLC (N acetyl substitution in second position) and α 1→4 linked GALA units respectively. Gellan chain is composed of alternating repetitive units of $-\beta$ -GLC- β -4-GLCA- β -4-GLC- α -4-RHA-. Pullulan1 and pullulan2 are linear chain polysaccharides with α 1→4 linked units in the backbone. Pullulan1 has α 1→6 linked after every third 1→4 linkage where as in pullulan2 it is present after second 1→4 linkage. Here, GLC, GLCA, MAN, GAL, GALA, NAGLC, RHA stands for glucose, glucuronic acid, mannose, galactose, galacturonic acid, 2-N-acetyl glucose, rhamnose respective.

All the systems were subjected to NVT equilibration for 2 ns followed by 20 ns of NPT equilibration. This was followed by 80 ns of production run in NPT ensemble at 1

atm and 310 K. Thus obtained 80 ns of production run trajectories are used for the structural analysis. All the molecular dynamics simulations employed NAMD as the simulation engine[20]. The CHARMM36 all-atom additive Force Field is used to model the molecules[21]. The water molecules are described by the TIP3P model as incorporated in the CHARMM force field[19, 22].

SMD simulations were run by picking 3 different starting structures from 80 ns of production runs for each system. The long axis of the simulation box is oriented along the z-axis using the orient plugin of VMD[23]. Each starting structure is then subjected to initial conjugate gradient minimization followed by SMD simulations in NVT ensemble for 4 ns at 310 K. In all the SMD simulations, the atom O₂ of residue 15 (residue 16 in case of gellan) is kept fixed (fixed atom) while atom O₂ of residue 1 is pulled (SMD atom). A time step of 2 fs and 1 fs is used for the equilibrium and SMD simulations respectively. Temperature variation for the SMD simulation is done on chitin, galactose and pectin chains. The temperatures are elevated from 297 K to 447 K with 5 K increase in separate simulations. The choice of these systems is due to the nature of glycosidic linkage i.e., equatorial-equatorial, axial-equatorial and axial-axial in chitin, galactose and pectin respectively.

A cut-off distance of 12 Å is used for the non bonded vdW interactions, with a switching distance of 10 Å. A pair list distance of 14 Å is used for electrostatic and vdW calculations. The particle mesh Ewald (PME) method is employed to calculate the electrostatics. A constant pulling velocity of 0.1 Å ps⁻¹ is used for all the systems, and the force constant is set to 1 kcalmol⁻¹Å⁻². VMD (1.9.4)[23], MATLAB (R2019b) and Plumed (2.7.2)[24, 25] are used for the visualization of the structure, plotting, and analysis of data. Gaussian 09 is employed to predict the single point energies of the pyranose conformers for a chosen monosaccharide residue along the SMD trajectory. For a given polysaccharide, five different residues are picked: three successive residues from the beginning, close to the SMD atom, one in the middle, and one close to the fixed atom. Each of the chosen residues is saved separately and capped with the missing OH/H atoms using Gauss-View. The single-point energy calculations for each of these residues are done using the B3LYP functional and 6-311++g (d,p) basis set[26]. The color code used to represent the monosaccharide conformers are adapted from the work of Cross *et al*, as implemented in VMD[27].

6.3 Results and discussion

6.3.1 Structural properties of the variants

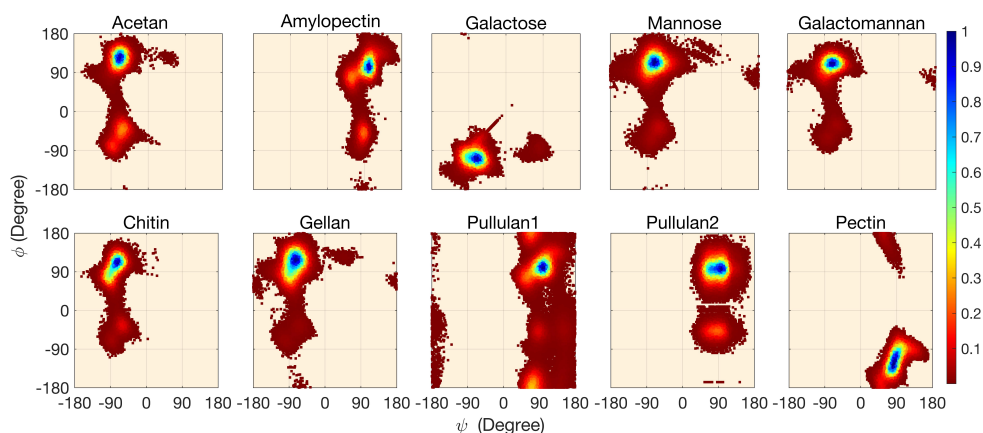


Figure 6.3: Carbohydrate ramachandran plot for the dihedral angle (ϕ, ψ) distributions of oligosaccharides containing 15 residues in the backbone chain (16 in case of gellan) as obtained from equilibrium simulations at 310 k in water. The colour distributions for all the plots are normalised.

Figure 6.3 shows the carbohydrate ramachandran plots for the oligosaccharides under consideration. The heat-maps indicate the region of maximum probability. The inverted nature of α and β anomers is clearly reflected in the dihedral distribution. This pattern is independent of the building block and only based on its anomeric nature. The most probable values of the β and α linkages are in well agreement with previous simulation and experimental studies[28, 29, 30].

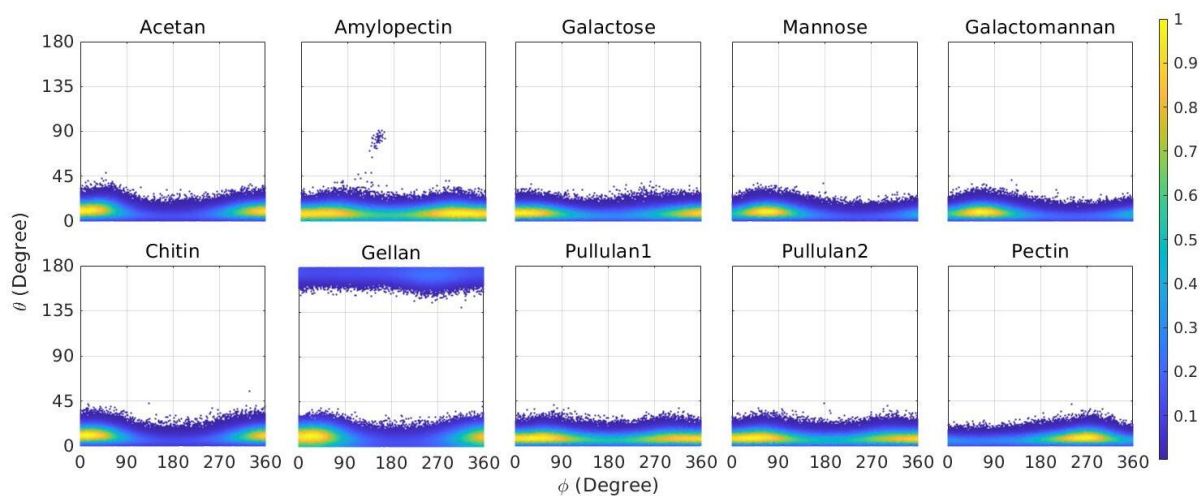


Figure 6.4: Cremer-Pople puckering angle distribution of all the backbone residues for the various oligosaccharides as obtained from equilibrium simulations trajectory under consideration. The puckering angles for all the residues along the entire simulation trajectory are considered here.

Apart from the dihedral angles, the Cremer-Pople puckering angles give a fair idea on the conformations of the residues under study. Cremer-Pople analysis of the oligosaccharide

strands is shown in Figure 6.4. This kind of mercator representation is used to indicate whether a snapshot belongs to chair, boat or inverted-chair conformation. The present data implies that under equilibrium condition at 310 K, all the residues of all oligosaccharides remain in chair or close to conformation, except for gellan. In case of gellan, α -rhamnose exists in inverted chair conformation and so it is reflected in the puckering distribution.

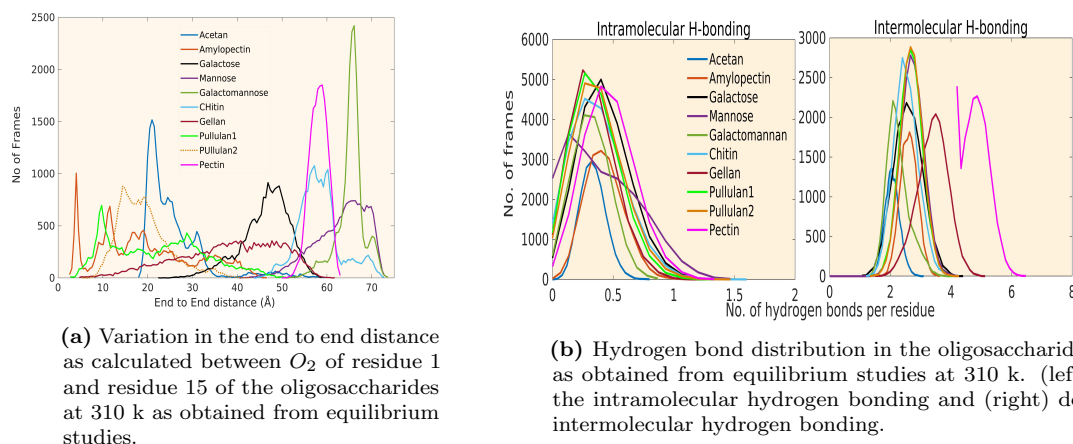


Figure 6.5

Figure 6.5a shows the end-to-end distance of all the oligosaccharide variants. From the figure, it is evident that the oligosaccharide variants with β 1 \rightarrow 4 linkage have higher end to end distance. On the other hand, oligosaccharide variants with α 1 \rightarrow 4 linkage have lower end to end distance and seem to be curled in nature. Among all the variants, galactomannan has the maximum end to end distance, i.e., it exists mostly in linear form while gellan takes the most diverse range of structures. This result is in well agreement with literature values[3]. Another key property for structural elucidation is hydrogen bonding. The hydrogen bond interaction of all the saccharides with themselves and their interaction with aqueous solvent is shown in Figure 6.5b. On an average, acetan and amylopectin based oligosaccharides exhibit less intramolecular and intermolecular hydrogen bonding when compared to others. This can be explained in terms of the additional residues which are part of the backbone through branching which aid in curling up of the system. Pectin on the other hand, exhibits the maximum number of hydrogen bonding with water.

6.3.2 Force-extension curves, comparison of SMD and AFM

The force-extension (F-E) curve, as depicted in Figure 6.6, is an output of the SMD runs, which can be compared to those from AFM experiments after appropriate normalization. Clearly, each of the structure exhibit a different profile. At intermediate pulling forces, some variants show extra elasticity in the form of a hump in between entropic and hookean domain. Galactomannan appears to show low elasticity, with the entropic domain passing

directly into hookean domain. Pectin clearly shows two humps in the curve suggesting the complete flipping of residues.

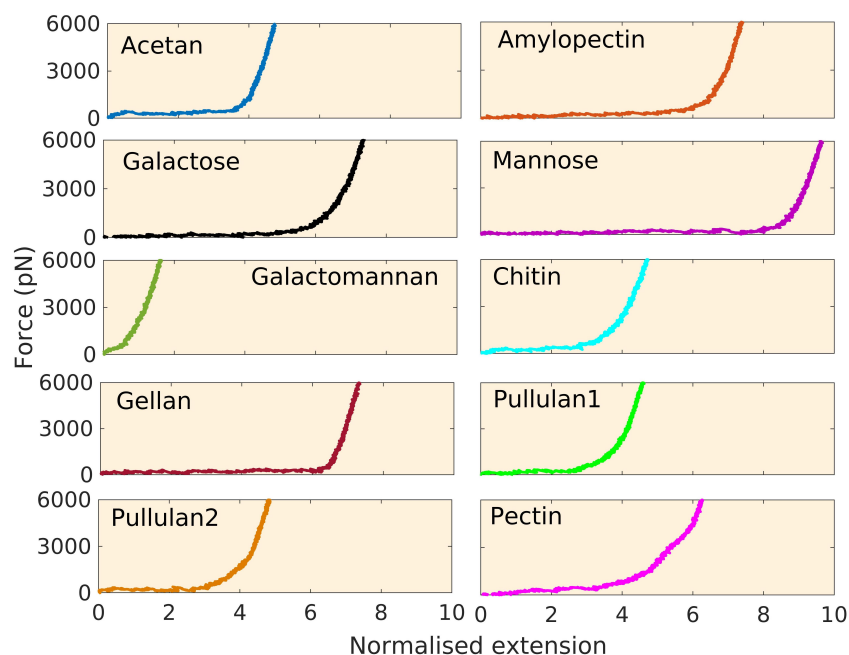


Figure 6.6: End-to-end distance of different polysaccharide strand under pulling stress

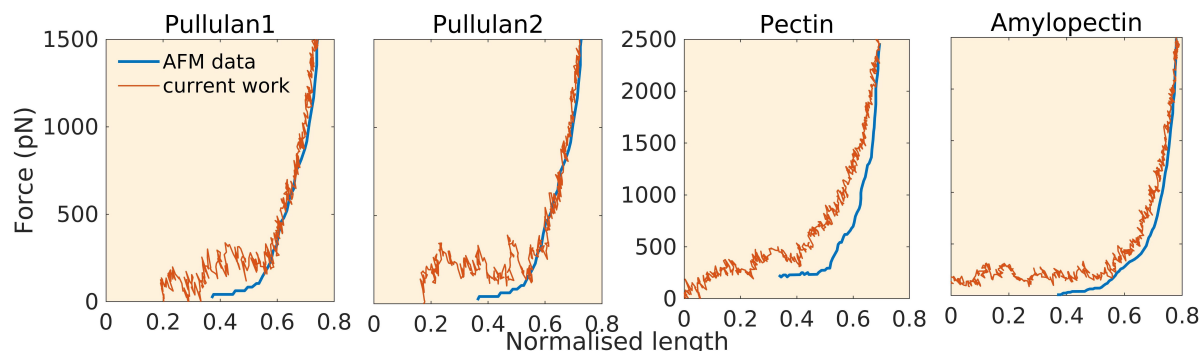


Figure 6.7: Comparison of the extension profiles of different polysaccharides as obtained from AFM studies[31, 32] and our SMD simulations. Here, the normalized length of the polysaccharides is defined as: $l = l_t/l_f$, where, l_t stands for the length of the polysaccharide against a given pulling force at a particular time instant. l_f stands for the final length of the polysaccharide that is achieved after 4 ns of SMD simulation. The experimental curve is normalized by making the experimentally observed extension at the highest force reported equal to that observed in SMD simulations at the same force.

Type	Initial	Final	Glycosidic length (Å)	Type	Initial	Final	Glycosidic length (Å)
Acetan (ee)			5.60 ↓ 5.61 0.06%	Chitin (ee)			5.33 ↓ 5.56 4.3%
Amylopectin (ae)			4.55 ↓ 5.29 16.4%	Gellan			5.61 ↓ 5.66 0.7%
Galactose (ea)			4.68 ↓ 5.38 14.9%	Pullulan1 (ae)			4.52 ↓ 5.27 16.7%
Mannose (ee)			5.53 ↓ 5.75 4%	Pullulan2 (ae)			4.32 ↓ 5.31 22.8%
Galactoman--nan (ee)			5.48 ↓ 5.57 1.7%	Pectin (aa)			4.55 ↓ 5.80 27.3%

Figure 6.8: Conformational transitions for selected residue (R2) of different oligosaccharides in a particular SMD trajectory. The color code of the conformations is based on Figure 6.9

Figure 6.7 compares the F-E curves of pullulan, pectin and amylopectin trajectories after normalizing them at the maximum force in the available experimental data. In spite of the limitations in classical molecular dynamics force fields and artifacts in modelling and simulation good correspondence between simulated profiles and the experimental F-E curves has been seen. It is evident from Figure 6.8 that oligosaccharides with equatorial-equatorial (ee) kind of linking undergo the least extension while those with axial-equatorial (ae) or equatorialaxial (ea) has intermediate extension and those with axial-axial (aa) kind of linkage has the maximum extension. The initial structure is obtained from the starting conformation. The final structure is the one reached at a force of ~ 2100 pN. The percentage increase in glycosidic bond length is given. The glycosidic oxygen atoms, labelled as red vdW spheres, are used to calculate the glycosidic bond length. Pullulan-2 exhibits more stretching when compared to pullulan-1 because of the presence of additional ‘ $-CH_2$ ’ groups in the torsion angle coming from 1 \rightarrow 6 glycosidic linkage.

	Chair
	Boat
	Half-chair
	Skew-boat
	Envelope

Figure 6.9: Colour followed to track the conformations across the simulations

6.3.3 Glycosidic dihedrals and Cremer Pople puckering under stretched conditions

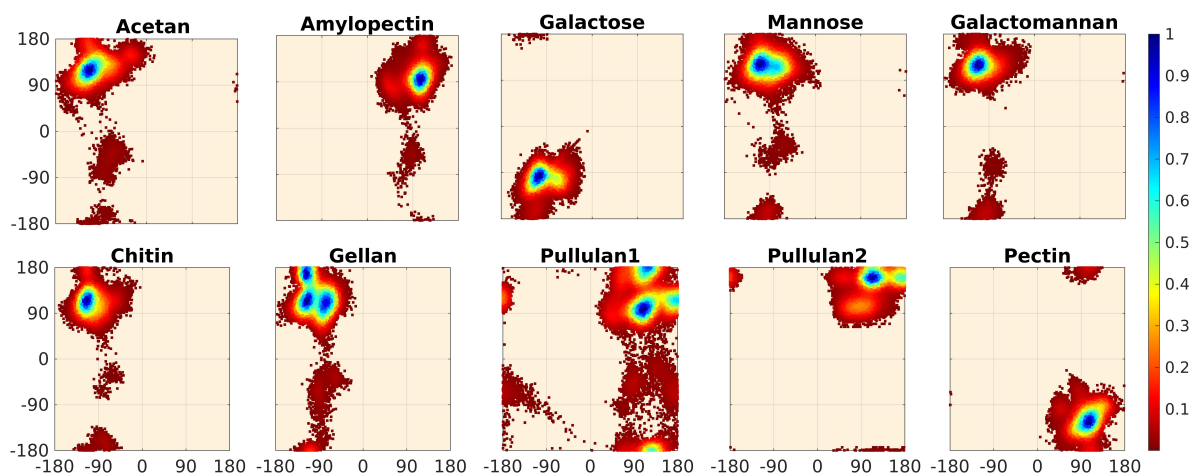


Figure 6.10: Carbohydrate ramachandran plot for the dihedral angles (φ , ψ) distributions of oligosaccharides containing 15 residues in the backbone chain (16 in case of gellan) as obtained from SMD simulations at 310 k in water.

Under the influence external pulling forces, as the oligosaccharides stretch and the glycosidic dihedral angles transcend the confines of ordinary space. This helps in understanding the allowed regions of conformational space for a given set of polysaccharide. Figure 6.10 shows the carbohydrate ramachandran plot for all the variants studied by collecting all the snapshots across the complete trajectory. The spread in case of pullulan1 is maximum suggesting significant stability over oligosaccharides.

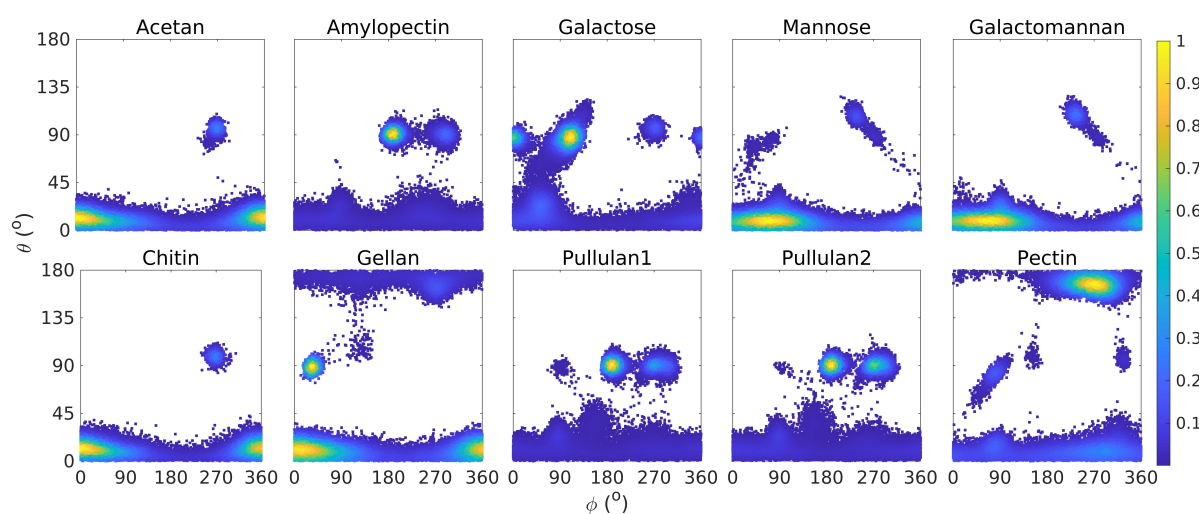


Figure 6.11: Cremer pople puckering angles distribution of all residues of all the oligosaccharide variants studied as obtained from SMD simulations at 310 k in water.

Figure 6.11 shows the puckering angle distribution in all the residues for all oligosaccharides variants. It is clear that under the influence of external pulling, residues undergo conformational flipping. Specifically, pectin undergoes conformational shift from 4C_1 to 1C_4 with boat conformation as an intermediate. Figure 6.12 is used to specifically portray the extent of flipping in individual residue across the backbone. The colouring of the distribution is based on the time of appearance in the trajectory. The oligosaccharides possessing equatorial-equatorial linkage do not undergo much change in conformation. They remain in chair or close to chair kind of conformation. While, the variants with axial-equatorial or equatorial-axial kind of linkage undergo conformational transition from initial 4C_1 to intermediate boat. On the other hand, variant with axial-axial kind of linkage undergoes conformational flip from initial chair to inverted chair through intermediate boat. In the case of gellan, α -rhamnose which initially is in 1C_4 position flipped to boat conformation over time. This phenomenon is clearly evident from the Cremer Pople plot color coded based on time of appearance.

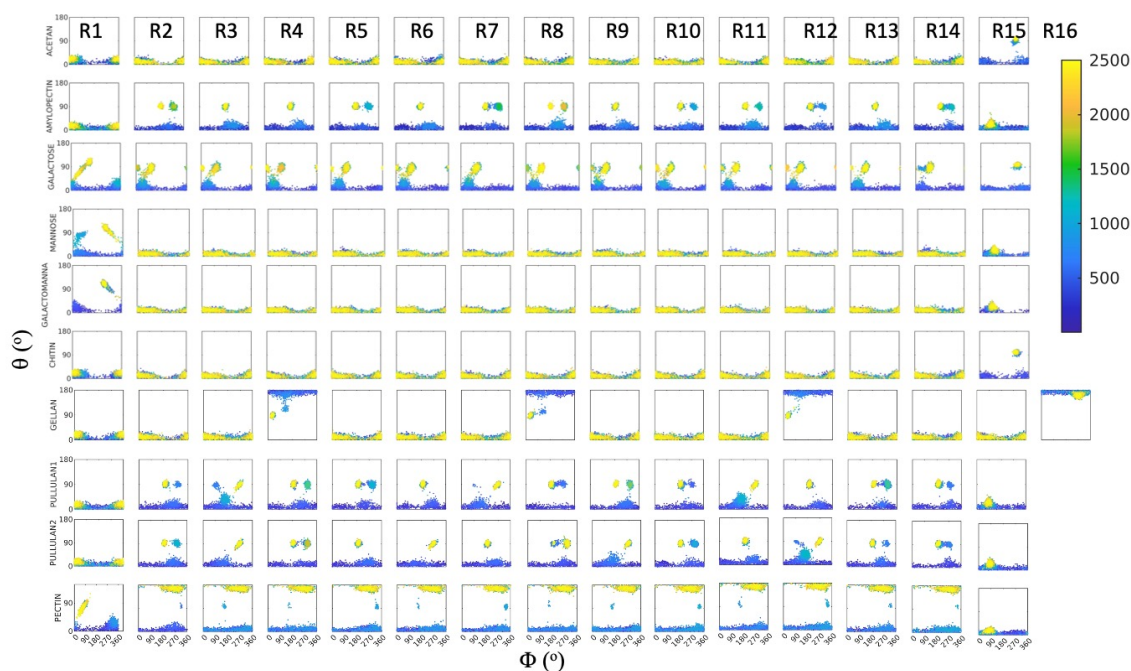
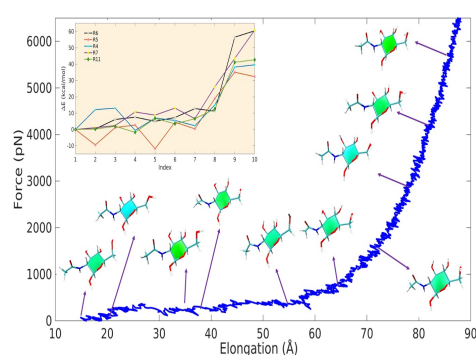
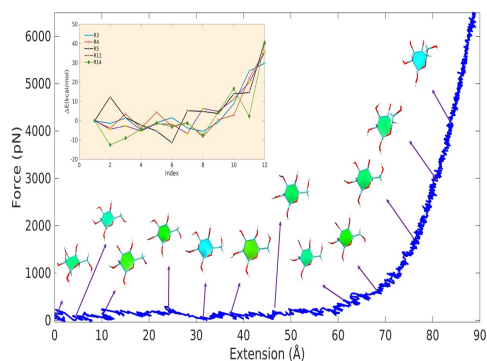


Figure 6.12: Cremer Pople puckering angles distribution of all residues of all the oligosaccharide variants studied as obtained from SMD simulations at 310 k in water. The conformations are color coded based on the time of appearance.

6.3.4 Structure and energetics of the monosaccharide conformers across the SMD trajectory



(a) Extension of a chitin strand under pulling stress.

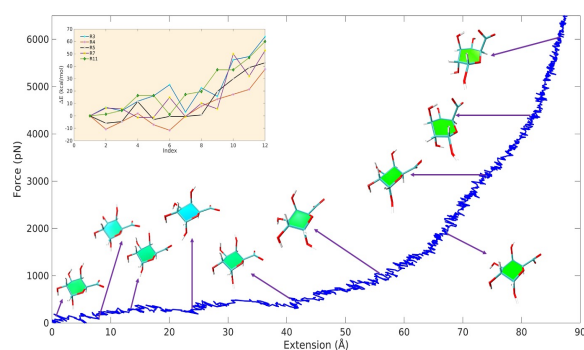


(b) Extension of a galactose strand under pulling stress.

Figure 6.13

Tracking of conformers for selected residues through the course of trajectory has been done on three different variants following their difference in linkages. They are chitin (ee), galactose (ea) and pectin (aa). Figures 6.13 and 6.14 show the force-extension curves of three different systems and the evolution of one of the residue (R3) in the strand. The energy plots are obtained from DFT calculations. At a closer glance, the energy difference between the first and last residue shown here is similar. But, the residues from chitin strand remain close to

4C_1 chair, the residue from galactose chain undergo conformational flip from stable chair to boat or skewed boat forms. But the pectin undergoes complete flipping from chair to inverted chair. This phenomenon suggests that variants with axial-axial kind of linkage would require low amount of energy in order to stretch for longer distances. Figures 6.15, 6.16, 6.17 show the conformational transitions for selected residues along the simulation trajectory under pulling stress for chitin, galactose and pectin respectively.

**Figure 6.14:** Extension of a pectin strand under pulling stress.

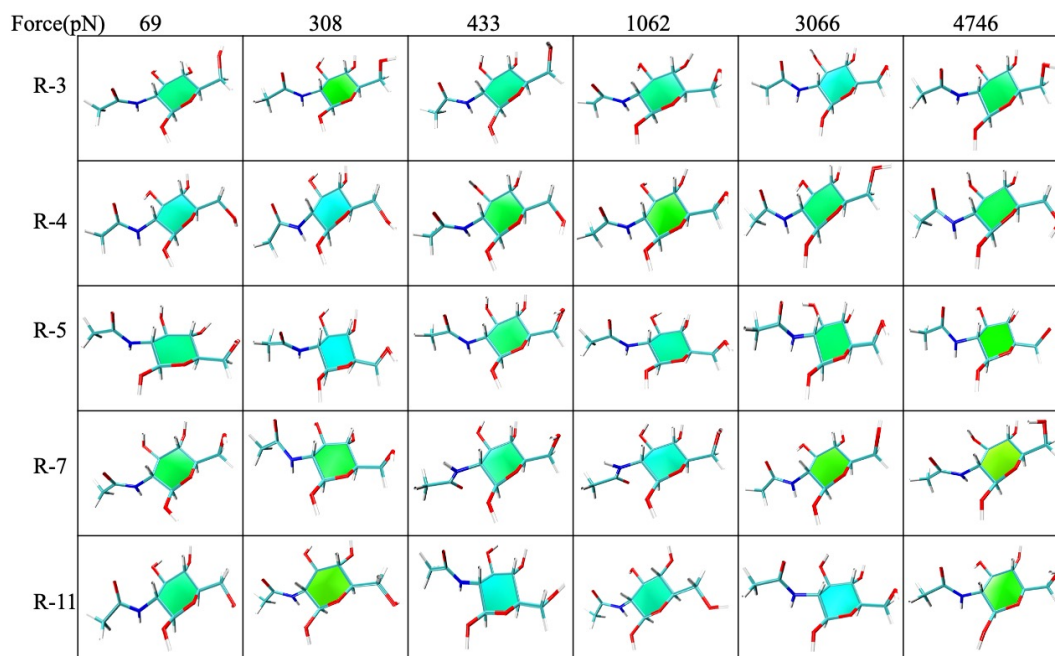


Figure 6.15: Conformational transitions for selected residues for the chitin strand along the simulation trajectory under pulling stress. The forces in pN corresponding to each residue are denoted. The color code of the conformations is based on Figure 6.9

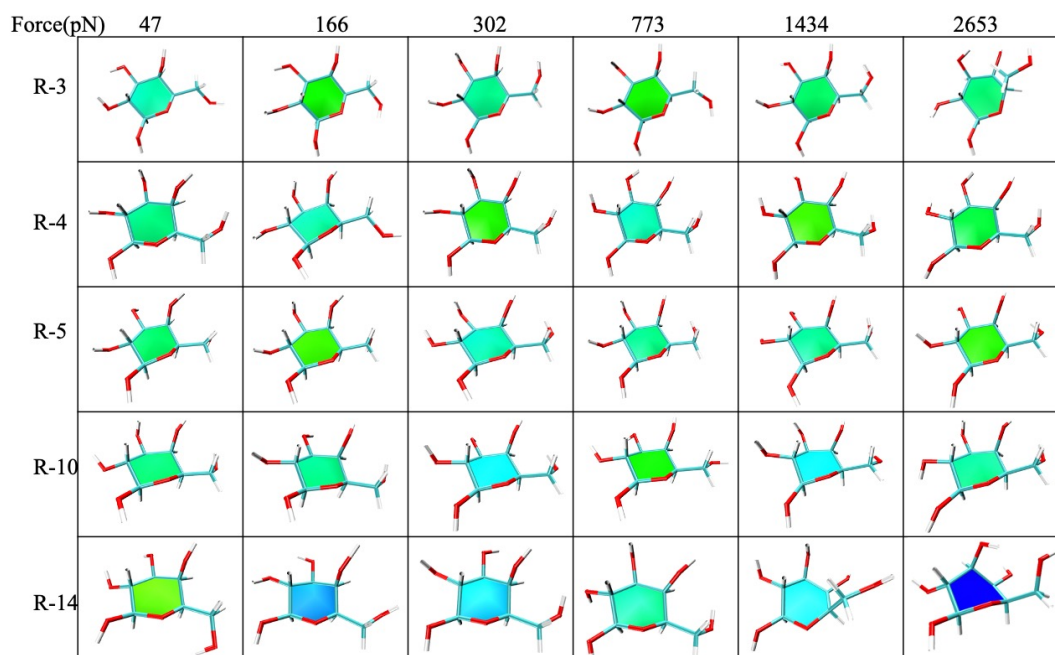


Figure 6.16: Conformational transitions for selected residues for the galactose strand along the simulation trajectory under pulling stress. The forces in pN corresponding to each residue are denoted. The color code of the conformations is based on Figure 6.9

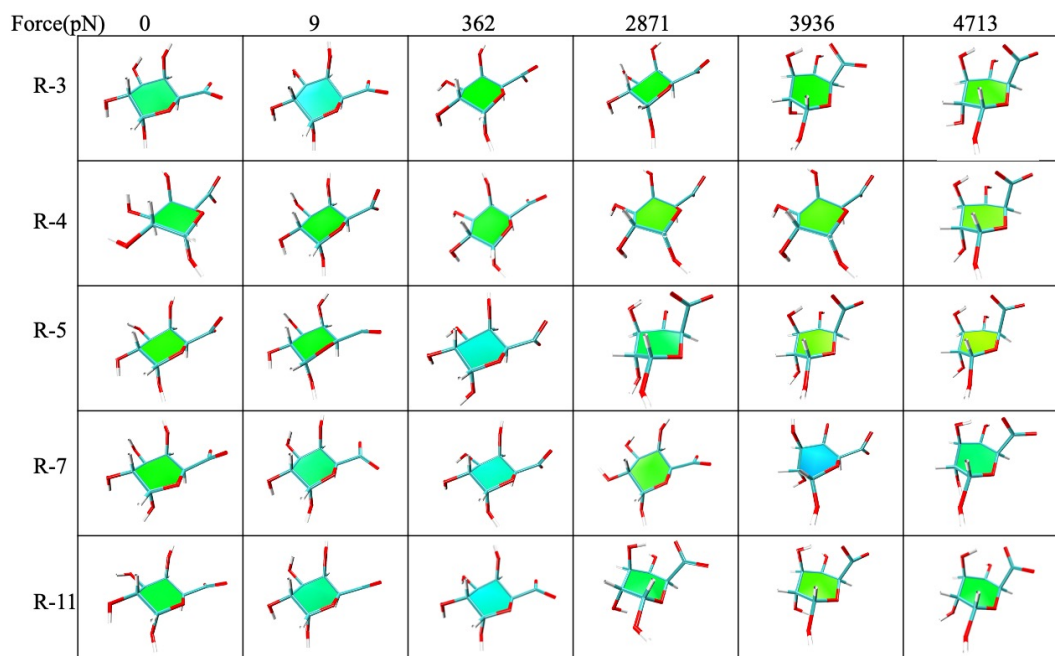


Figure 6.17: Conformational transitions for selected residues for the pectin strand along the simulation trajectory under pulling stress. The forces in pN corresponding to each residue are denoted. The color code of the conformations is based on Figure 6.9

The extent of force required for conformational change varies from residue to residue. This can be determined by plotting the puckering angle θ for selected residues against the pulling forces. Figure 6.18 shows the variation of puckering angle θ with force along the simulation trajectory for three different starting structures. Clearly,

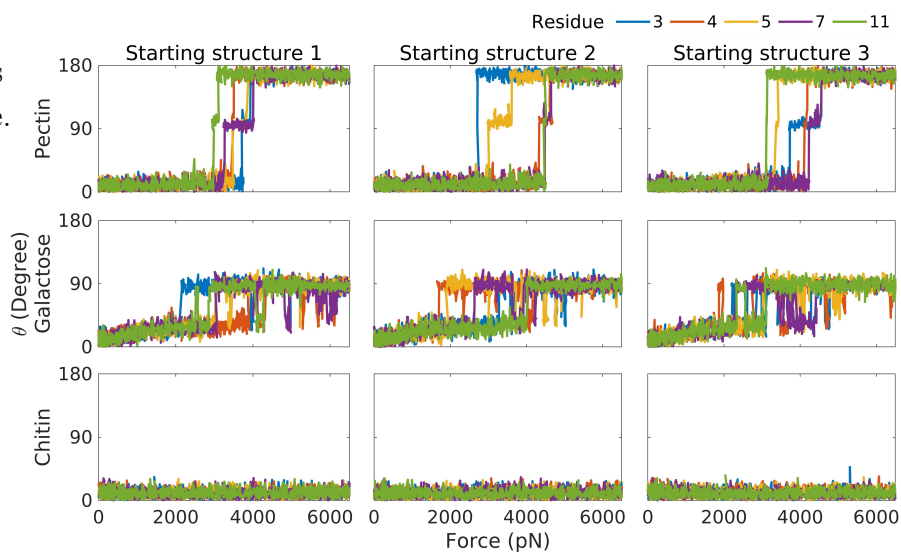


Figure 6.18: Variation of puckering angle θ with force (in pN) along the simulation trajectory.

for no residue of chitin in any of the starting structures, there is a conformational change beyond envelope even at high pulling forces. In the case of galactose, the θ values gradually increase with the pulling force. It requires a minimum of 2000 pN of pulling force for the conformational change to occur. Once the conformational change has happened in

case of most residues, they remain in less stable boat/skew-boat form. Except in case of one/two residues where it tries to come back to stable chair but flips back to less stable conformation with increasing force. In case of pectin, a minimum of 2100 pN is required to flip from stable chair to inverted chair conformation. The amount of time, a given residue spends in the intermediate boat/skew-boat phase is minimum. It flips immediately to inverted chair form.

6.4 Temperature varying SMD simulations of Chitin, Galactose and Pectin

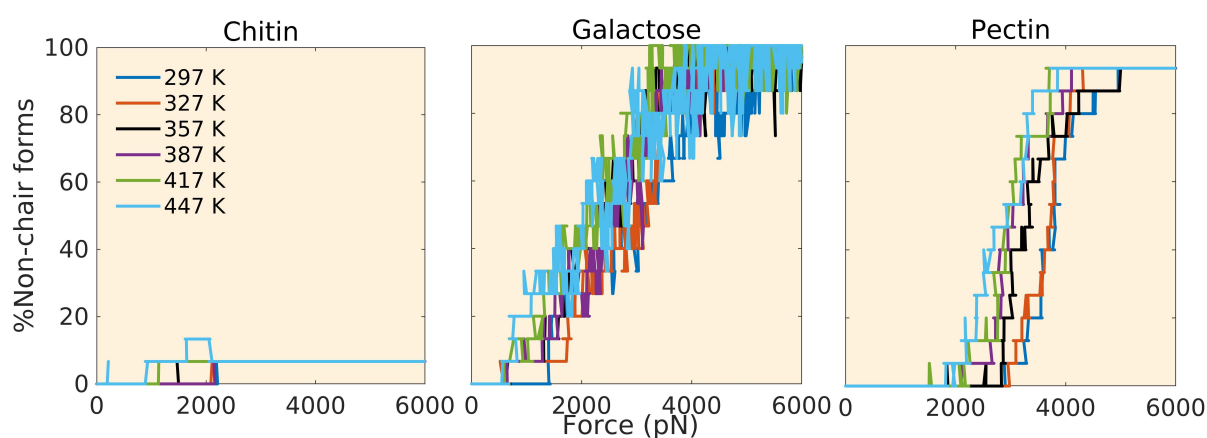


Figure 6.19: Variation of % non-chair forms with force (in pN) for different temperatures in kelvin.

The three systems with different monomeric building unit and different glycosidic linkage have been subjected to different temperatures ranging from 297 K to 447 K with 5 K increment. Figure 6.19 shows the variation of % non-chair forms as a function of force (in pN) for 6 different temperatures. The SMD simulations with higher temperature shows least amount of force required to attain the conformational transitions. In case of chitin, even at 447 K temperatures, there is hardly any deviation from chair form. This suggests that for oligosaccharide variants with (ea)/(ae)/(aa) kind of glycosidic linkage, higher temperature increases the feasibility in conformational changes and thus the stretching.

6.5 Conclusion

With the rising need for lasting materials, understanding the relationship between conformational properties and mechanics of naturally available materials is crucial. To attain this,

the steered molecular dynamics simulations and DFT calculations have been performed to track the changes along selected oligosaccharide variants as they are subjected to a wide range of pulling stresses. This information is highly useful in tuning the properties of polysaccharide membranes. The comparison between SMD force-extension curves and AFM curves show good agreement. The polysaccharides with axial-axial linkage show the maximum elongation while the polysaccharides with equatorial-equatorial linkage shows the least elongation. Comprehending this information can be used for the practical application of polysaccharides with designed structures in various understanding the generation and utilisation of such function might ultimately allow polysaccharides with designed architectures to be utilised in a host of biomimetic soft nanotechnology applications including sensors and advanced materials.

Chapter 7

Conclusions and Future Perspectives

The last 8-10 decades has seen a sharp increase in the utilization of materials derived from conventional fossil fuels for food storage and packaging. With the dearth of non-renewable resources and ever increasing demand, it has become crucial to device renewable alternatives. In this context, materials made out of traditionally popular items like banana leaves, coconut scrap, sugar cane & jute fibres, etc. are gaining the lime-light. Banana leaves, for instance, have been used for centuries in various cultures as natural food wrappers. These leaves possess several desirable properties for packaging, including flexibility, water resistance, and biodegradability. Similarly, coconut scrap, derived from the fibrous husk of coconuts, is known for its robust and resilient nature, making it suitable for packaging applications. Sugar cane and jute fibers, obtained from the cane sugar and jute plant respectively, have long been utilized for their strength, durability, and eco-friendliness, making them suitable for packaging various products. What these materials have in common is their primary composition, which is primarily composed of “polysaccharides.” These materials offer renewable and biodegradable options for packaging applications, thus reducing the reliance on conventional fossil fuel-based materials and contributing to a more environmentally friendly future.

In this context, understanding the primary structure, dynamics and mechanics of α and β polysaccharides, specifically those of glucans is critical. To understand these features, α, β polysaccharides strands have been modelled which are linked with 1 \rightarrow 2, 1 \rightarrow 3, 1 \rightarrow 4, 1 \rightarrow 6 glycosidic linkages and two mixed linkage β -D-glucan fragments comprising 1 \rightarrow 4 and 1 \rightarrow 3 linkages in certain ratio as found in natural fibers of oats and barley in aqueous solution. The influence of anomericity and glycosidic bond is reflected in the hydrogen bonding, end-to-end distance, radius of gyration, dihedrals and puckering of the residue. As the structure is affected, it critically influences the dynamics spanned.

Further, to understand the mechanical strength of these polysaccharides, one of advanced sampling techniques called the “steered molecular dynamics (SMD)” has been employed. Along with DFT calculations, the conformational changes as the polysaccharides strands subjected to an external force have been studied. As the polysaccharide strands are pulled, they undergo transition from initial entropic domain to hookean domain. This phenomenon is clear by studying the force-extension curves. The F-E curves show reasonable agreement with AFM curves after appropriate normalization. The polysaccharide strands of α -D-1 \rightarrow 4, α -D-1 \rightarrow 6, β -D-1 \rightarrow 2 and β -D-1 \rightarrow 6 show significant stretching compared to others.

Furthermore, the mechanical properties of some special polysaccharides like acetan, amylopectin, galactomannan, chitin, pectin, galactose, mannose and pullulan strands have been studied. It has been seen that strands with axial-axial linkage like pectin undergoes maximum stretching with the initial 4C_1 converting to 1C_4 conformation. While, the strands with axial-equatorial linkage exhibits intermediate stretching with chair conformation getting converted to boat form. On the other hand, strand with equatorial-equatorial linkage undergo the least amount of stretching with the initial chair

form remaining in chair or close to chair conformation. This pattern has been seen irrespective of the monomeric building block and side chain variation. These studies provide valuable information in understanding and tuning the mechanics of polysaccharide based membranes.

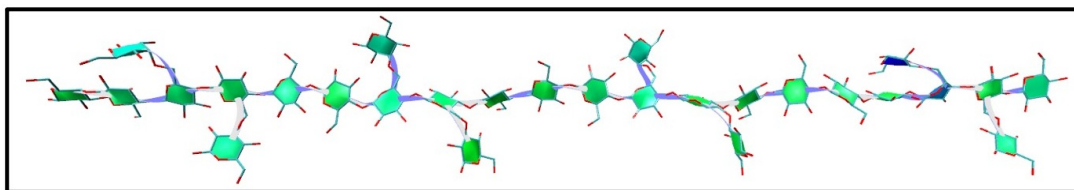


Figure 7.1: Representation of polysaccharide backbone. This unit is replicated 7 times in order to make the membrane

Additionally, research and innovation in the field of polysaccharide-based materials have led to the development of novel biopolymers, blends, and composites with enhanced properties. Polysaccharides are future must for many applications including the design of non-conventional and bioconductive membranes. Biodegradable films and coatings are solid matrices formed by cross-linking between polymers and additives. Especially, in the context of the present scenario, where plastics have turned out to be a menace, polysaccharides show great promises to come up with viable alternatives. By modifying the structure and composition of polysaccharides, their mechanical strength, barrier properties, and biodegradability can be tailored to meet specific packaging requirements. Motivated by sustainability concerns, several groups are striving to fabricate carbohydrate membrane based green technologies[1, 2, 3]. Keeping these applications in mind, a β 1 \rightarrow 4 linked glycopeptide based membrane has been modelled in TIP3 water. Individual strands are cross linked by the amino acid-glucan bond. Serine-Glucose glycopeptide bond in the present context. The membrane is made of β -D-1 \rightarrow 4 linked glucose strand as shown in Figure 7.1.

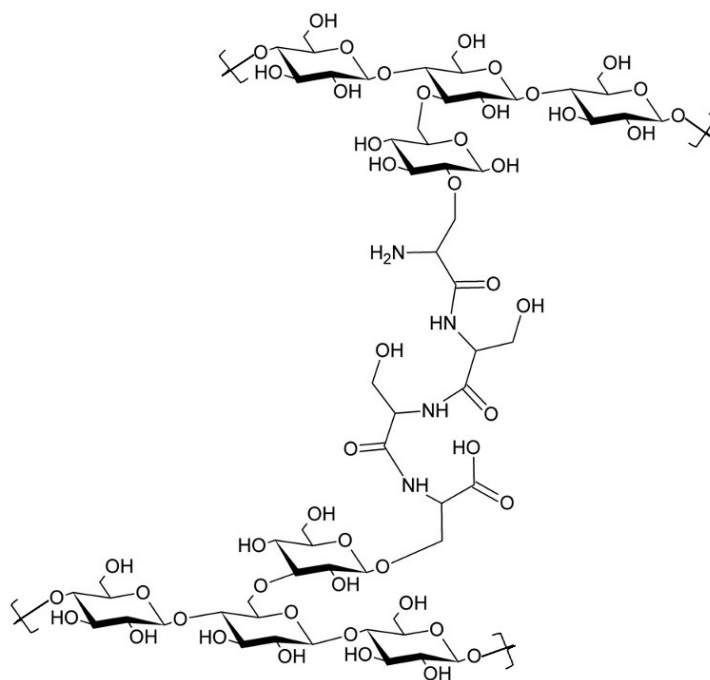


Figure 7.2: Tetrameric unit of serine which interlocks the polymeric strands in the current membrane

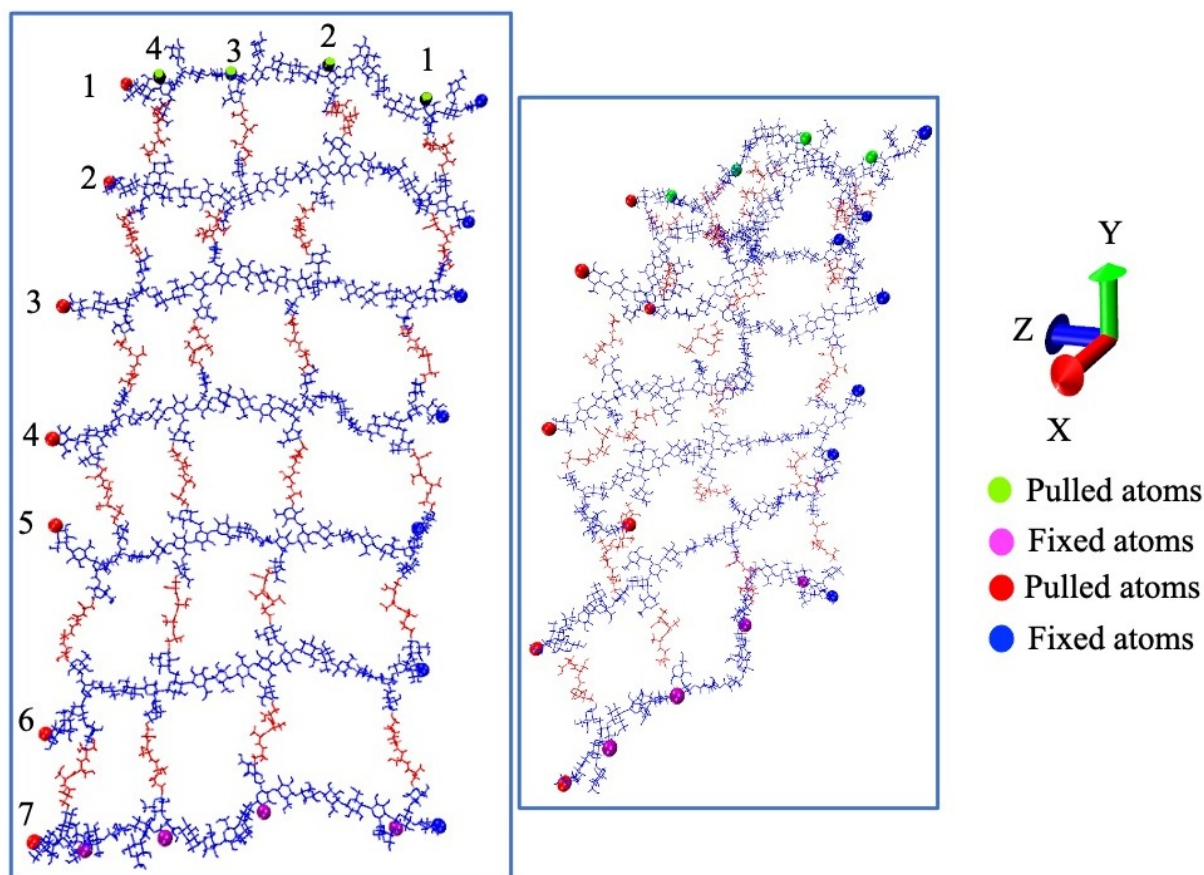


Figure 7.3: (left)Initial structure of the membrane, (right)Structure of the membrane after 1.5 ns

These strands are branched with single glucose unit intermittently through the non-conventional ‘3→6’ glycosidic linkage. The parameters for this particular linkage have been derived from the existing parameters in the CHARMM force-field. This residue is part of the glycopeptide bond. There are 4 serine units in each of the cross linking. Figure 7.2 has the schematic representation of the tetrameric serine interlocked in between polysaccharide backbone. Figure 7.3 shows the representative images of the initial structure and the structure obtained after 1.5 ns of NPT equilibration. In order to study its mechanics, the membrane has been subjected to external pulling in two different directions i.e., along z and y-axis. The SMD simulations were run for 4 ns in both the cases. Along z direction, 7 different atoms are kept fixed (O_4 of the non-reducing end, shown as blue spheres in Figure 7.3(left))

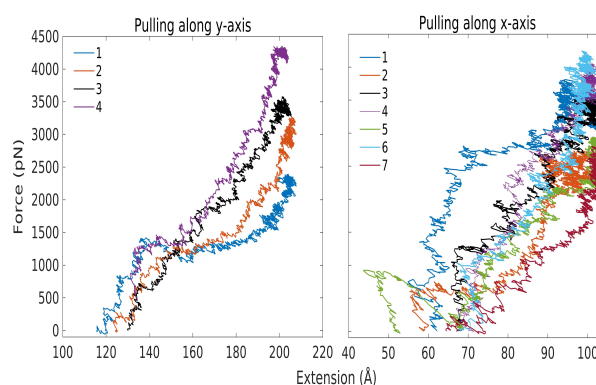


Figure 7.4: Repeating unit showing the non-conventional 3→6 glycosidic linkage and the tetrameric serine units interlocked.

and 7 different atoms are pulled (O_1 of the reducing end, shown as red spheres in Figure 7.3(left)) with constant velocity. Similarly, along y direction, 4 atoms are kept fixed (O_3 atoms of residues 4,8,13 and 19 of chain 7, shown as purple spheres in 7.3) and 4 atoms are pulled (O_2 atoms of residues 3,7,12 and 18 of chain 1, shown as green spheres in 7.3).

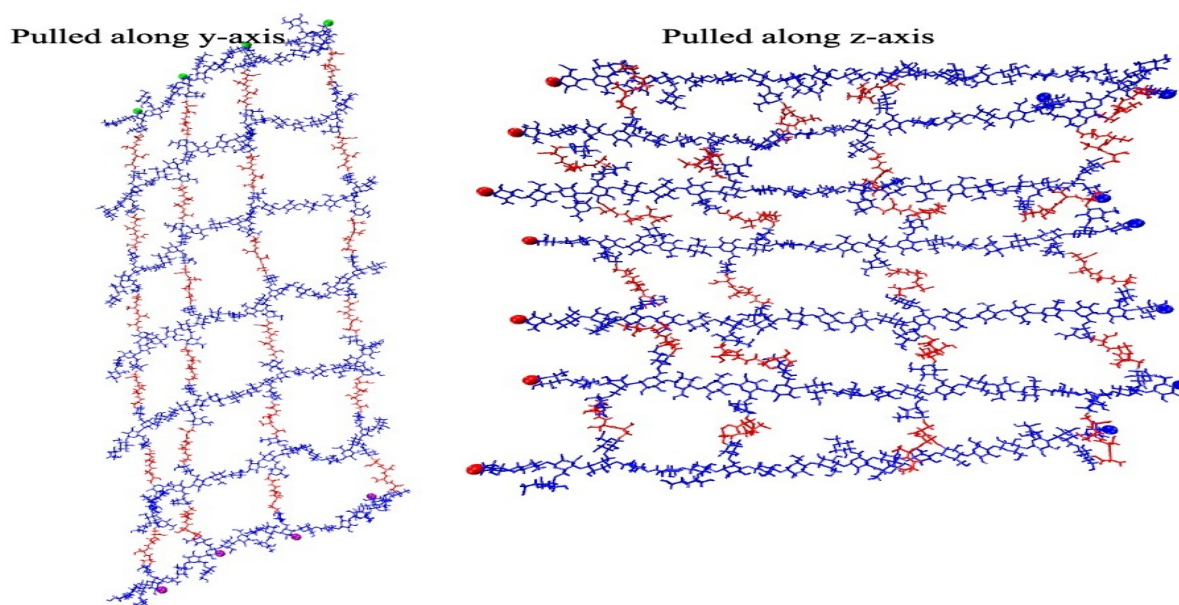


Figure 7.5: The snapshots of stretched membrane for both the cases at the end of 4 ns.

The force-extension plots of the membrane are shown in Figure 7.4. On an average, both the directions exhibit similar extent of stretching for this particular starting structure. The snapshots of the final frame of SMD simulation is shown in Figure 7.5. More thorough investigation has to be made using different starting structures, different amino acids in place of serine, diverse branching. Similar membranes can be modelled based on the application which it will be used. Modeling carbohydrates makes it feasible to study and understand their structures, properties, and interactions without the need for laborious and complex synthesis. Such complex membranes can be modelled first and studied for their properties and synthesized only if the requirements are met. Apart from the mechanics, the penetration of small gas molecules, water vapour can be a worthwhile future study.

To summarise, this thesis is focused on the structure, dynamics, interactions with bile acids and mechanics of α , β sugar units having diverse linkages in aqueous solution. **Chapter 1** gives an introduction to polysaccharides, techniques for their extraction and synthesis, limitations in the chemical synthesis, advantages of modelling over simulations, brief overview of the studies on *D*-glucose anomers and their chains. **Chapter 2** gives a brief introduction to molecular dynamic simulations, importance of advance sampling techniques, details of steered molecular dynamics and its comparison with AFM, methodologies

adopted for their studies, modelling of simulation box and simulation parameters definition. **Chapter 3** studies the structure and dynamics of α and β -*D*-glucopyranosides having varying glycosidic linkages of types 1→3, 1→4, 1→6 and mixed linkage β -*D*-glucan fragments comprising 1→4 and 1→3 linkages in specific ratio in aqueous solution. The changes in structural aspects are correlated with the dynamics spanned by the molecules. It points out the diverse configurations taken by systems with 1→6 linkage because of the additional ‘-CH₂’ group in the glycosidic linkage. **Chapter 4** studies the interaction of β -glucan moieties inspired from oat and barley with that of cholic acid and its salt. Small angle scattering patterns and ¹H NMR chemical shifts are in line with the experimental data. **Chapter 5** studies the mechanics of 15-meric α,β -glucan strands. The force-extension curves are compared with AFM data after appropriate normalisation wherever possible. The polysaccharides belonging to β -1→2, α/β -1→6, α -1→4 show significant extension when compared to others. **Chapter 6** studies the mechanics of oligosaccharide strands inspired from naturally available materials with 1→4 glycosidic linkage in the backbone. Pectin having axial-axial kind of glycosidic linkage is reported to show maximum stretching while the variants with equatorial-equatorial kind of glycosidic linkage show the least stretching. **Chapter 7** points out the possible applications of polysaccharide/glycopeptide based membranes.

Bibliography

Chapter 1

- [1] Seeberger, P. Exploring life's sweet spot. *Nature*. **437**, 1239-1239 (2005)
- [2] Mohammed, A., Naveed, M. & Jost, N. Polysaccharides; classification, chemical properties, and future perspective applications in fields of pharmacology and biological medicine (A review of current applications and upcoming potentialities). *Journal Of Polymers And The Environment*. **29**, 2359-2371 (2021)
- [3] Thomas, B. & Raj, M. B AK; H RM; Joy J.; Moores A.; Drisko GL; Sanchez C. Nanocellulose, A Versatile Green Platform: From Biosources To Materials And Their Applications. *Chemical Reviews*. **118** pp. 11575-11625 (2018)
- [4] Lovegrove, A., Edwards, C., De Noni, I., Patel, H., El, S., Grassby, T., Zielke, C., Ulmius, M., Nilsson, L., Butterworth, P. & Others Role of polysaccharides in food, digestion, and health. *Critical Reviews In Food Science And Nutrition*. **57**, 237-253 (2017)
- [5] Englyst, K., Liu, S. & Englyst, H. Nutritional characterization and measurement of dietary carbohydrates. *European Journal Of Clinical Nutrition*. **61**, S19-S39 (2007)
- [6] Storry, J. & Olsson, M. The ABO blood group system revisited: a review and update. *Immunohematology*. **25**, 48-59 (2009)
- [7] Grundy, M., Edwards, C., Mackie, A., Gidley, M., Butterworth, P. & Ellis, P. Re-evaluation of the mechanisms of dietary fibre and implications for macronutrient bioaccessibility, digestion and postprandial metabolism. *British Journal Of Nutrition*. **116**, 816-833 (2016)
- [8] Capuano, E. The behavior of dietary fiber in the gastrointestinal tract determines its physiological effect. *Critical Reviews In Food Science And Nutrition*. **57**, 3543-3564 (2017)
- [9] Roseman, S. Reflections on glycobiology. *Journal Of Biological Chemistry*. **276**, 41527-41542 (2001)
- [10] Jeffrey, G. & Taylor, R. The application of molecular mechanics to the structures of carbohydrates. *Journal Of Computational Chemistry*. **1**, 99-109 (1980)
- [11] Kajiwara, K. & Miyamoto, T. Progress in structural characterization of functional polysaccharides. *Polysaccharides: Structural Diversity And Functional Versatility*. Marcel Dekker, New York. pp. 1-55 (1998)
- [12] Striegel, A. Influence of anomeric configuration on mechanochemical degradation of polysaccharides: cellulose versus amylose. *Biomacromolecules*. **8**, 3944-3949 (2007)
- [13] Winger, M., Christen, M. & Gunsteren, W. On the conformational properties of amylose and cellulose oligomers in solution. *International Journal Of Carbohydrate Chemistry*. **2009** (2009)
- [14] Xu, J., Sagnelli, D., Faisal, M., Perzon, A., Taresco, V., Mais, M., Giosafatto, C., Hebelstrup, K., Ulvskov, P., Jørgensen, B. & Others Amylose/cellulose nanofiber composites for all-natural, fully biodegradable and flexible bioplastics. *Carbohydrate Polymers*. **253** pp. 117277 (2021)
- [15] Maheshwari, G., Sowrirajan, S. & Joseph, B. Extraction and isolation of β -glucan from grain sources-A review. *Journal Of Food Science*. **82**, 1535-1545 (2017)
- [16] Ornaghi Jr, H., Kerche, E., Neves, R., Monticeli, F. & Agnol, L. A Systematic Review of New Trends in Ionic Liquids Applied to Electrolytes on Polysaccharides. *Polysaccharides*. **3**, 502-514 (2022)

- [17] Lin, X., Jiang, K., Liu, X., Han, D. & Zhang, Q. Review on development of ionic liquids in lignocellulosic biomass refining. *Journal Of Molecular Liquids*. pp. 119326 (2022)
- [18] Taokaew, S. & Kriangkrai, W. Recent Progress in Processing Cellulose Using Ionic Liquids as Solvents. *Polysaccharides*. **3**, 671-691 (2022)
- [19] Shamshina, J. & Abidi, N. Cellulose nanocrystals from ionic liquids: a critical review. *Green Chemistry*. **23**, 6205-6222 (2021)
- [20] Hou, Q., Ju, M., Li, W., Liu, L., Chen, Y. & Yang, Q. Pretreatment of lignocellulosic biomass with ionic liquids and ionic liquid-based solvent systems. *Molecules*. **22**, 490 (2017)
- [21] Soria, A., Brokl, M., Sanz, M. & Martínez-Castro, I. 4.11 - Sample Preparation for the Determination of Carbohydrates in Food and Beverages. *Comprehensive Sampling And Sample Preparation*. pp. 213-243 (2012)
- [22] Huseman, E. & Mueller, G. Synthesis of unbranched polysaccharides. *Macromolecular Chemistry*. **91** pp. 212-230 (1966)
- [23] Joseph, A., Pardo-Vargas, A. & Seeberger, P. Total synthesis of polysaccharides by automated glycan assembly. *Journal Of The American Chemical Society*. **142**, 8561-8564 (2020)
- [24] Kobayashi, S., Sakamoto, J. & Kimura, S. In vitro synthesis of cellulose and related polysaccharides. *Progress In Polymer Science*. **26**, 1525-1560 (2001)
- [25] Gijssen, H., Qiao, L., Fitz, W. & Wong, C. Recent advances in the chemoenzymatic synthesis of carbohydrates and carbohydrate mimetics. *Chemical Reviews*. **96**, 443-474 (1996)
- [26] Ichikawa, Y., Look, G. & Wong, C. Enzyme-catalyzed oligosaccharide synthesis. *Analytical Biochemistry*. **202**, 215-238 (1992)
- [27] Kobayashi, S., Kawasaki, T., Obata, K. & Shoda, S. A novel method for synthesis of cellooligosaccharide derivatives by using enzyme catalyst. *Chemistry Letters*. **22**, 685-686 (1993)
- [28] Okada, G., Genghof, D. & Hehre, E. The predominantly nonhydrolytic action of alpha amylases on α -maltosyl fluoride. *Carbohydrate Research*. **71**, 287-298 (1979)
- [29] Kobayashi, S., Kiyosada, T. & Shoda, S. Synthesis of artificial chitin: irreversible catalytic behavior of a glycosyl hydrolase through a transition state analogue substrate. *Journal Of The American Chemical Society*. **118**, 13113-13114 (1996)
- [30] Agirre, J. & Raaij, M. Carbohydrate structure hits the groove. *Acta Crystallographica Section F: Structural Biology Communications*. **74**, 441-442 (2018)
- [31] Perez, S. X-ray Diffraction and Crystallography of Oligosaccharides and Polysaccharides. *Encyclopedia Of Biophysics; Roberts, GCK, Ed.; Springer: Berlin/Heidelberg, Germany*. pp. 2767-2777 (2013)
- [32] Yu, Y., Tyrikos-Ergas, T., Zhu, Y., Fittolani, G., Bordoni, V., Singhal, A., Fair, R., Grafmüller, A., Seeberger, P. & Delbianco, M. Systematic hydrogen-bond manipulations to establish polysaccharide structure–property correlations. *Angewandte Chemie*. **131**, 13261-13266 (2019)
- [33] Mansel, B., Ryan, T., Chen, H., Lundin, L. & Williams, M. Polysaccharide conformations measured by solution state X-ray scattering. *Chemical Physics Letters*. **739** pp. 136951 (2020)
- [34] Casillo, A., Fabozzi, A., Russo Krauss, I., Parrilli, E., Biggs, C., Gibson, M., Lanzetta, R., Appavou, M., Radulescu, A., Tutino, M. & Others Physicochemical approach to understanding the structure, conformation, and activity of mannan polysaccharides. *Biomacromolecules*. **22**, 1445-1457 (2021)

- [35] Hagberg, A., Rzhepishevskaya, O., Semenets, A., Cisneros, D. & Ramstedt, M. Surface analysis of bacterial systems using cryo-X-ray photoelectron spectroscopy. *Surface And Interface Analysis*. **52**, 792-801 (2020)
- [36] Sathitnaitham, S., Suttangkakul, A., Wonnapijit, P., McQueen-Mason, S. & Vuttipongchaikij, S. Gel-permeation chromatography–enzyme-linked immunosorbent assay method for systematic mass distribution profiling of plant cell wall matrix polysaccharides. *The Plant Journal*. **106**, 1776-1790 (2021)
- [37] Duus, J., Gotfredsen, C. & Bock, K. Carbohydrate structural determination by NMR spectroscopy: modern methods and limitations. *Chemical Reviews*. **100**, 4589-4614 (2000)
- [38] Ji, X., Cheng, Y., Tian, J., Zhang, S., Jing, Y. & Shi, M. Structural characterization of polysaccharide from jujube (*Ziziphus jujuba* Mill.) fruit. *Chemical And Biological Technologies In Agriculture*. **8** pp. 1-7 (2021)
- [39] Bauer, S. Mass spectrometry for characterizing plant cell wall polysaccharides. *Frontiers In Plant Science*. **3** pp. 45 (2012)
- [40] Wang, J., Zhao, J., Nie, S., Xie, M. & Li, S. Rapid profiling strategy for oligosaccharides and polysaccharides by MALDI TOF mass spectrometry. *Food Hydrocolloids*. **124** pp. 107237 (2022)
- [41] Schmidt, R. & Michel, J. Facile synthesis of α - and β -O-glycosyl imidates; preparation of glycosides and disaccharides. *Angewandte Chemie International Edition In English*. **19**, 731-732 (1980)
- [42] Imberty, A. & Pérez, S. Structure, conformation, and dynamics of bioactive oligosaccharides: theoretical approaches and experimental validations. *Chemical Reviews*. **100**, 4567-4588 (2000)
- [43] Wormald, M., Petrescu, A., Pao, Y., Glithero, A., Elliott, T. & Dwek, R. Conformational studies of oligosaccharides and glycopeptides: complementarity of NMR, X-ray crystallography, and molecular modelling. *Chemical Reviews*. **102**, 371-386 (2002)
- [44] Lundborg, M., Fontana, C. & Widmalm, G. Automatic structure determination of regular polysaccharides based solely on NMR spectroscopy. *Biomacromolecules*. **12**, 3851-3855 (2011)
- [45] Kato, K. & Peters, T. NMR in Glycoscience and Glycotechnology. (Royal Society of Chemistry, 2017)
- [46] Guvench, O., Greene, S., Kamath, G., Brady, J., Venable, R., Pastor, R. & Mackerell Jr, A. Additive empirical force field for hexopyranose monosaccharides. *Journal Of Computational Chemistry*. **29**, 2543-2564 (2008)
- [47] Jo, S., Myatt, D., Qi, Y., Douth, J., Clifton, L., Im, W. & Widmalm, G. Multiple conformational states contribute to the 3D structure of a glucan decasaccharide: A combined SAXS and MD simulation study. *The Journal Of Physical Chemistry B*. **122**, 1169-1175 (2018)
- [48] Fadda, E. & Woods, R. Molecular simulations of carbohydrates and protein–carbohydrate interactions: motivation, issues and prospects. *Drug Discovery Today*. **15**, 596-609 (2010)
- [49] Brady, J. Molecular dynamics simulations of α -D-glucose. *Journal Of The American Chemical Society*. **108**, 8153-8160 (1986)
- [50] Brady, J. Molecular dynamics simulations of β -D-glucopyranose. *Carbohydrate Research*. **165**, 306-312 (1987)
- [51] Brady, J. Molecular dynamics simulations of α -D-glucose in aqueous solution. *Journal Of The American Chemical Society*. **111**, 5155-5165 (1989)
- [52] Singh, N. & Li, W. Recent advances in coarse-grained models for biomolecules and their applications. *International Journal Of Molecular Sciences*. **20**, 3774 (2019)

- [53] Zhu, X., Lopes, P. & MacKerell Jr, A. Recent developments and applications of the CHARMM force fields. *Wiley Interdisciplinary Reviews: Computational Molecular Science*. **2**, 167-185 (2012)
- [54] Kirschner, K., Yongye, A., Tschampel, S., González-Outeiriño, J., Daniels, C., Foley, B. & Woods, R. GLYCAM06: a generalizable biomolecular force field. *Carbohydrates. Journal Of Computational Chemistry*. **29**, 622-655 (2008)
- [55] Lins, R. & Hünenberger, P. A new GROMOS force field for hexopyranose-based carbohydrates. *Journal Of Computational Chemistry*. **26**, 1400-1412 (2005)
- [56] Kony, D., Damm, W., Stoll, S. & Van Gunsteren, W. An improved OPLS-AA force field for carbohydrates. *Journal Of Computational Chemistry*. **23**, 1416-1429 (2002)
- [57] Brown, G. & Levy, H. α -D-Glucose: further refinement based on neutron-diffraction data. *Acta Crystallographica Section B: Structural Crystallography And Crystal Chemistry*. **35**, 656-659 (1979)
- [58] Chu, S. & Jeffrey, G. The refinement of the crystal structures of β -D-glucose and cellobiose. *Acta Crystallographica Section B: Structural Crystallography And Crystal Chemistry*. **24**, 830-838 (1968)
- [59] Ha, S., Gao, J., Tidor, B., Brady, J. & Karplus, M. Solvent effect on the anomeric equilibrium in D-glucose: a free energy simulation analysis. *Journal Of The American Chemical Society*. **113**, 1553-1557 (1991)
- [60] Polavarapu, P. & Ewig, C. Ab Initio computed molecular structures and energies of the conformers of glucose. *Journal Of Computational Chemistry*. **13**, 1255-1261 (1992)
- [61] Eijck, B., Hooft, R. & Kroon, J. Molecular dynamics study of conformational and anomeric equilibria in aqueous D-glucose. *The Journal Of Physical Chemistry*. **97**, 12093-12099 (1993)
- [62] Nishida, Y., Ohru, H. & Meguro, H. ¹H-NMR studies of (6r)-and (6s)-deuterated d-hexoses: assignment of the preferred rotamers about C5-C6 bond of D-glucose and D-galactose derivatives in solutions. *Tetrahedron Letters*. **25**, 1575-1578 (1984)
- [63] Miura, N., Taniguchi, T., Monde, K. & Nishimura, S. A theoretical study of α - and β -D-glucopyranose conformations by the density functional theory. *Chemical Physics Letters*. **419**, 326-332 (2006)
- [64] Cremer, D. & Pople, J. General definition of ring puckering coordinates. *Journal Of The American Chemical Society*. **97**, 1354-1358 (1975)
- [65] Pitzer, K. & Donath, W. Conformations and strain energy of cyclopentane and its derivatives. *Journal Of The American Chemical Society*. **81**, 3213-3218 (1959)
- [66] Haasnoot, C. The conformation of six-membered rings described by puckering coordinates derived from endocyclic torsion angles. *Journal Of The American Chemical Society*. **114**, 882-887 (1992)
- [67] Paoloni, L., Rampino, S. & Barone, V. Potential-energy surfaces for ring-puckering motions of flexible cyclic molecules through Cremer-Pople coordinates: Computation, analysis, and fitting. *Journal Of Chemical Theory And Computation*. **15**, 4280-4294 (2019)
- [68] Chan, L., Hutchison, G. & Morris, G. Understanding ring puckering in small molecules and cyclic peptides. *Journal Of Chemical Information And Modeling*. **61**, 743-755 (2021)
- [69] Iglesias-Fernández, J., Raich, L., Ardòvol, A. & Rovira, C. The complete conformational free energy landscape of β -xylose reveals a two-fold catalytic itinerary for β -xylosidases. *Chemical Science*. **6**, 1167-1177 (2015)

- [70] Isbell, H. & Tipson, R. Conformations of the pyranoid sugars. I. Classification of conformers. *Journal Of Research Of The National Bureau Of Standards. Section A, Physics And Chemistry.* **64**, 171 (1960)
- [71] Appell, M., Strati, G., Willett, J. & Momany, F. B3LYP/6-311++G(d,p) study of α - and β -d-glucopyranose and 1,5-anhydro-d-glucitol: chairs and boats, and skew-boat conformations. *Carbohydrate Research.* **339**, 537-551 (2004)
- [72] Momany, F., Appell, M., Willett, J., Schnupf, U. & Bosma, W. DFT study of α - and β -d-galactopyranose at the B3LYP/6-311++G(d,p) level of theory. *Carbohydrate Research.* **341**, 525-537 (2006)
- [73] Barrows, S., Dulles, F., Cramer, C., French, A. & Truhlar, D. Relative stability of alternative chair forms and hydroxymethyl conformations of β -D-glucopyranose. *Carbohydrate Research.* **276**, 219-251 (1995)
- [74] Csonka, G., Éliás, K. & Csizmadia, I. Relative stability of 1C_4 and 4C_1 chair forms of β -D-glucose: a density functional study. *Chemical Physics Letters.* **257**, 49-60 (1996)
- [75] Biarnés, X., Ardevol, A., Planas, A., Rovira, C., Laio, A. & Parrinello, M. The conformational free energy landscape of β -D-glucopyranose. Implications for substrate preactivation in β -glucoside hydrolases. *Journal Of The American Chemical Society.* **129**, 10686-10693 (2007)
- [76] Shen, T., Langan, P., French, A., Johnson, G. & Gnanakaran, S. Conformational flexibility of soluble cellulose oligomers: chain length and temperature dependence. *Journal Of The American Chemical Society.* **131**, 14786-14794 (2009)
- [77] Salpin, J. & Tortajada, J. Gas-phase acidity of d-glucose. A density functional theory study. *Journal Of Mass Spectrometry.* **39**, 930-941 (2004)
- [78] Mulroney, B., Barrie Peel, J. & Traeger, J. Relative gas-phase acidities of glucopyranose from molecular orbital calculations. *Journal Of Mass Spectrometry.* **34**, 544-553 (1999)
- [79] Alonso, J., Lozoya, M., Pena, I., López, J., Cabezas, C., Mata, S. & Blanco, S. The conformational behaviour of free D-glucose—at last. *Chemical Science.* **5**, 515-522 (2014)
- [80] Kony, D., Damm, W., Stoll, S. & Hünenberger, P. Explicit-solvent molecular dynamics simulations of the $\beta(1\rightarrow3)$ - and $\beta(1\rightarrow6)$ -linked disaccharides β -laminarabiose and β -gentiobiose in water. *The Journal Of Physical Chemistry B.* **108**, 5815-5826 (2004)
- [81] Ramachandran, G.N, Ramakrishnan, C., & Sasisekharan, V. Stereochemistry of polypeptide chain configurations. “. *Journal of Molecular Biology.* **7** pp. 95-99 (1963)
- [82] Pereira, C., Kony, D., Baron, R., Müller, M., Gunsteren, W. & Hünenberger, P. Conformational and dynamical properties of disaccharides in water: a molecular dynamics study. *Biophysical Journal.* **90**, 4337-4344 (2006)
- [83] Salisburg, A., Deline, A., Lexa, K., Shields, G. & Kirschner, K. Ramachandran-type plots for glycosidic linkages: Examples from molecular dynamic simulations using the Glycam06 force field. *Journal Of Computational Chemistry.* **30**, 910-921 (2009)
- [84] Homans, S. A molecular mechanical force field for the conformational analysis of oligosaccharides: comparison of theoretical and crystal structures of Man. α . 1-3Man. β . 1-4GlcNAc. *Biochemistry.* **29**, 9110-9118 (1990)
- [85] Ha, S., Madsen, L. & Brady, J. Conformational analysis and molecular dynamics simulations of maltose. *Biopolymers.* **27**, 1927-1952 (1988)

- [86] Guvench, O., Hatcher, E., Venable, R., Pastor, R. & MacKerell Jr, A. CHARMM additive all-atom force field for glycosidic linkages between hexopyranoses. *Journal Of Chemical Theory And Computation*. **5**, 2353-2370 (2009)
- [87] Perić-Hassler, L., Hansen, H., Baron, R. & Hünenberger, P. Conformational properties of glucose-based disaccharides investigated using molecular dynamics simulations with local elevation umbrella sampling. *Carbohydrate Research*. **345**, 1781-1801 (2010)
- [88] Hardy, B. & Sarko, A. Conformational analysis and molecular dynamics simulation of cellobiose and larger cellooligomers. *Journal Of Computational Chemistry*. **14**, 831-847 (1993)
- [89] Almond, A. Towards understanding the interaction between oligosaccharides and water molecules. *Carbohydrate Research*. **340**, 907-920 (2005)
- [90] Feng, X., Li, F., Ding, M., Zhang, R., Shi, T. & Jiang, W. Molecular dynamic simulation: Structural insights of multi-stranded curdlan in aqueous solution. *Carbohydrate Polymers*. **261** pp. 117844 (2021)
- [91] Whitehead, A., Beck, E., Tosh, S. & Wolever, T. Cholesterol-lowering effects of oat β -glucan: a meta-analysis of randomized controlled trials. *The American Journal Of Clinical Nutrition*. **100**, 1413-1421 (2014)
- [92] Anderson, J., Baird, P., Davis, R., Ferreri, S., Knudtson, M., Koraym, A., Waters, V. & Williams, C. Health benefits of dietary fiber. *Nutrition Reviews*. **67**, 188-205 (2009)
- [93] Sima, P., Vannucci, L. & Vetvicka, V. β -glucans and cholesterol. *International Journal Of Molecular Medicine*. **41**, 1799-1808 (2018)
- [94] Wang, Q. & Ellis, P. Oat β -glucan: physico-chemical characteristics in relation to its blood-glucose and cholesterol-lowering properties. *British Journal Of Nutrition*. **112**, S4-S13 (2014)
- [95] Jayachandran, M., Chen, J., Chung, S. & Xu, B. A critical review on the impacts of β -glucans on gut microbiota and human health. *The Journal Of Nutritional Biochemistry*. **61** pp. 101-110 (2018)
- [96] Neis, E., Dejong, C. & Rensen, S. The role of microbial amino acid metabolism in host metabolism. *Nutrients*. **7**, 2930-2946 (2015)
- [97] Tuohy, K., Conterno, L., Gasperotti, M. & Viola, R. Up-regulating the human intestinal microbiome using whole plant foods, polyphenols, and/or fiber. *Journal Of Agricultural And Food Chemistry*. **60**, 8776-8782 (2012)
- [98] Capuano, E. The behavior of dietary fiber in the gastrointestinal tract determines its physiological effect. *Critical Reviews In Food Science And Nutrition*. **57**, 3543-3564 (2017)
- [99] Theuwissen, E. & Mensink, R. Water-soluble dietary fibers and cardiovascular disease. *Physiology & Behaviour*. **94**, 285-292 (2008)
- [100] Barsanti, L., Passarelli, V., Evangelista, V., Frassanito, A. & Gualtieri, P. Chemistry, physico-chemistry and applications linked to biological activities of β -glucans. *Natural Product Reports*. **28**, 457-466 (2011)
- [101] Mikkelsen, M., Cornali, S., Jensen, M., Nilsson, M., Beeren, S. & Meier, S. Probing interactions between β -glucan and bile salts at atomic detail by 1H - 13C NMR assays. *Journal Of Agricultural And Food Chemistry*. **62**, 11472-11478 (2014)
- [102] Wang, Y., Harding, S., Eck, P., Thandapilly, S., Gamel, T., Abdel-Aal, E., Crow, G., Tosh, S., Jones, P. & Ames, N. High-molecular-weight β -glucan decreases serum cholesterol differentially based on the CYP7A1 rs3808607 polymorphism in mildly hypercholesterolemic adults. *The Journal Of Nutrition*. **146**, 720-727 (2015)

- [103] Grundy, M., Fardet, A., Tosh, S., Rich, G. & Wilde, P. Processing of oat: the impact on oat's cholesterol lowering effect. *Food & Function*. **9**, 1328-1343 (2018)
- [104] Brummer, Y., Defelice, C., Wu, Y., Kwong, M., Wood, P. & Tosh, S. Textural and rheological properties of oat beta-glucan gels with varying molecular weight composition. *Journal Of Agricultural And Food Chemistry*. **62**, 3160-3167 (2014)
- [105] Vetvicka, V., Vannucci, L., Sima, P. & Richter, J. Beta glucan: supplement or drug? From laboratory to clinical trials. *Molecules*. **24**, 1251 (2019)
- [106] Rondanelli, M., Opizzi, A., Monteferrario, F., Klersy, C., Cazzola, R. & Cestaro, B. Beta-glucan- or rice bran-enriched foods: a comparative crossover clinical trial on lipidic pattern in mildly hypercholesterolemic men. *European Journal Of Clinical Nutrition*. **65**, 864-871 (2011)
- [107] Queenan, K., Stewart, M., Smith, K., Thomas, W., Fulcher, R. & Slavin, J. Concentrated oat β -glucan, a fermentable fiber, lowers serum cholesterol in hypercholesterolemic adults in a randomized controlled trial. *Nutrition Journal*. **6** pp. 1-8 (2007)
- [108] Korompokis, K., Nilsson, L. & Zielke, C. The effect of in vitro gastrointestinal conditions on the structure and conformation of oat β -glucan. *Food Hydrocolloids*. **77** pp. 659-668 (2018)
- [109] Parrow, A., Larsson, P., Augustijns, P. & Bergström, C. Molecular dynamics simulations on inter individual variability of intestinal fluids: Impact on drug solubilization. *Molecular Pharmaceutics*. **17**, 3837-3844 (2020)
- [110] Chahal, V., Nirwan, S., Pathak, M. & Kakkar, R. Identification of potent human carbonic anhydrase IX inhibitors: a combination of pharmacophore modeling, 3D-QSAR, virtual screening and molecular dynamics simulations. *Journal Of Biomolecular Structure And Dynamics*. **40**, 4516-4531 (2022)
- [111] Pártay, L., Jedlovsky, P. & Sega, M. Molecular aggregates in aqueous solutions of bile acid salts. Molecular dynamics simulation study. *The Journal Of Physical Chemistry B*. **111**, 9886-9896 (2007)
- [112] Wang, Z., Yang, L., Xue, S., Wang, S., Zhu, L., Ma, T., Liu, H. & Li, R. Molecular docking and dynamic insights on the adsorption effects of soy hull polysaccharides on bile acids. *International Journal Of Food Science & Technology*. **57**, 3702-3712 (2022)
- [113] Hazra, R. & Roy, D. Monosaccharide induced temporal delay in cholesterol self-aggregation. *Journal Of Biomolecular Structure And Dynamics*. pp. 1-13 (2022)
- [114] Hazra, R. & Roy, D. Free energy landscape of wrapping of lipid nanocluster by polysaccharides. *Biophysical Chemistry*. pp. 106956 (2023)
- [115] Neuman, K. & Nagy, A. Single-molecule force spectroscopy: optical tweezers, magnetic tweezers and atomic force microscopy. *Nature Methods*. **5**, 491-505 (2008)
- [116] Hoffmann, T. & Dougan, L. Single molecule force spectroscopy using polyproteins. *Chemical Society Reviews*. **41**, 4781-4796 (2012)
- [117] Cluzel, P., Lebrun, A., Heller, C., Lavery, R., Viovy, J., Chatenay, D. & Caron, F. DNA: an extensible molecule. *Science*. **271**, 792-794 (1996)
- [118] Smith, S., Finzi, L. & Bustamante, C. Direct mechanical measurements of the elasticity of single DNA molecules by using magnetic beads. *Science*. **258**, 1122-1126 (1992)
- [119] Greenleaf, W., Woodside, M. & Block, S. High-resolution, single-molecule measurements of biomolecular motion. *Annual Review Of Biophysics & Biomolecular Structure*. **36** pp. 171-190 (2007)

- [120] Zlatanova, J., Lindsay, S. & Leuba, S. Single molecule force spectroscopy in biology using the atomic force microscope. *Progress In Biophysics And Molecular Biology*. **74**, 37-61 (2000)
- [121] Li, H., Rief, M., Oesterhelt, F., Gaub, H., Zhang, X. & Shen, J. Single-molecule force spectroscopy on polysaccharides by AFM–nanomechanical fingerprint of α -(1,4)-linked polysaccharides. *Chemical Physics Letters*. **305**, 197-201 (1999)
- [122] Li, H., Rief, M., Oesterhelt, F. & Gaub, H. Single-molecule force spectroscopy on xanthan by AFM. *Advanced Materials*. **10**, 316-319 (1998)
- [123] Fisher, T., Marszalek, P. & Fernandez, J. Stretching single molecules into novel conformations using the atomic force microscope. *Nature Structural Biology*. **7**, 719-724 (2000)
- [124] Rief, M., Oesterhelt, F., Heymann, B. & Gaub, H. Single molecule force spectroscopy on polysaccharides by atomic force microscopy. *Science*. **275**, 1295-1297 (1997)
- [125] Lee, W., Zeng, X., Yang, W. & Marszalek, P. Mechanics of polysaccharides. *Molecular Manipulation With Atomic Force Microscopy*. (2012)
- [126] Marszalek, P., Li, H., Oberhauser, A. & Fernandez, J. Chair-boat transitions in single polysaccharide molecules observed with force-ramp AFM. *Proceedings Of The National Academy Of Sciences*. **99**, 4278-4283 (2002)
- [127] Marszalek, P. & Dufrêne, Y. Stretching single polysaccharides and proteins using atomic force microscopy. *Chemical Society Reviews*. **41**, 3523-3534 (2012)
- [128] Grier, D. Optical tweezers in colloid and interface science. *Current Opinion In Colloid & Interface Science*. **2**, 264-270 (1997)
- [129] Meiners, J. & Quake, S. Femtonewton force spectroscopy of single extended DNA molecules. *Physical Review Letters*. **84**, 5014 (2000)
- [130] Berthelot, J., Aćimović, S., Juan, M., Kreuzer, M., Renger, J. & Quidant, R. Three-dimensional manipulation with scanning near-field optical nanotweezers. *Nature Nanotechnology*. **9**, 295-299 (2014)
- [131] Furth, A. & Furth, A. Lipids and polysaccharides in biology. (E. Arnold,1980)
- [132] Haverkamp, R., Williams, M. & Scott, J. Stretching single molecules of connective tissue glycans to characterize their shape-maintaining elasticity. *Biomacromolecules*. **6**, 1816-1818 (2005)
- [133] Marszalek, P., Pang, Y., Li, H., Yazal, J., Oberhauser, A. & Fernandez, J. Atomic levers control pyranose ring conformations. *Proceedings Of The National Academy Of Sciences*. **96**, 7894-7898 (1999)
- [134] Marszalek, P., Oberhauser, A., Pang, Y. & Fernandez, J. Polysaccharide elasticity governed by chair–boat transitions of the glucopyranose ring. *Nature*. **396**, 661-664 (1998)
- [135] Haverkamp, R., Marshall, A. & Williams, M. Entropic and Enthalpic Contributions to the Chair-Boat Conformational Transformation in Dextran under Single Molecule Stretching. *The Journal Of Physical Chemistry B*. **111**, 13653-13657 (2007)
- [136] Ortiz, C. & Hadziioannou, G. Entropic elasticity of single polymer chains of poly (methacrylic acid) measured by atomic force microscopy. *Macromolecules*. **32**, 780-787 (1999)
- [137] Haverkamp, R., Marshall, A. & Williams, M. Model for stretching elastic biopolymers which exhibit conformational transformations. *Physical Review E*. **75**, 021907 (2007)
- [138] Lee, G., Nowak, W., Jaroniec, J., Zhang, Q. & Marszalek, P. Molecular dynamics simulations of forced conformational transitions in 1, 6-linked polysaccharides. *Biophysical Journal*. **87**, 1456-1465 (2004)

- [139] Wang, M., Yin, H., Landick, R., Gelles, J. & Block, S. Stretching DNA with optical tweezers. *Biophysical Journal*. **72**, 1335-1346 (1997)
- [140] Mahara, G., Tian, C., Xu, X. & Zhu, J. Breakthrough of glycobiology in the 21st century. (Frontiers,2022)
- [141] Yamamoto, N., Tanabe, Y., Okamoto, R., Dawson, P. & Kajihara, Y. Chemical synthesis of a glycoprotein having an intact human complex-type sialyloligosaccharide under the Boc and Fmoc synthetic strategies. *Journal Of The American Chemical Society*. **130**, 501-510 (2008)
- [142] Freitas, F., Alves, V., Reis, M., Crespo, J. & Coelho, I. Microbial polysaccharide-based membranes: current and future applications. *Journal Of Applied Polymer Science*. **131** (2014)
- [143] Nair, M., Tomar, M., Punia, S., Kukula-Koch, W. & Kumar, M. Enhancing the functionality of chitosan-and alginate-based active edible coatings/films for the preservation of fruits and vegetables: A review. *International Journal Of Biological Macromolecules*. **164** pp. 304-320 (2020)
- [144] Liu, Y., Yuan, Y., Duan, S., Li, C., Hu, B., Liu, A., Wu, D., Cui, H., Lin, L., He, J. & Others Preparation and characterization of chitosan films with three kinds of molecular weight for food packaging. *International Journal Of Biological Macromolecules*. **155** pp. 249-259 (2020)
- [145] Shariatnia, Z. & Mazloom-Jalali, A. Molecular dynamics simulations on chitosan/graphene nanocomposites as anticancer drug delivery using systems. *Chinese Journal Of Physics*. **66** pp. 362-382 (2020)
- [146] Garg, M. & Zozoulenko, I. Ion Diffusion through Nanocellulose Membranes: Molecular Dynamics Study. *ACS Applied Bio Materials*. **4**, 8301-8308 (2021)
- [147] Gumbart, J., Beeby, M., Jensen, G. & Roux, B. Escherichia coli peptidoglycan structure and mechanics as predicted by atomic-scale simulations. *PLoS Computational Biology*. **10**, e1003475 (2014)
- [148] Zhang, L., Liang, J., Jiang, C., Liu, Z., Sun, L., Chen, S., Xuan, H., Lei, D., Guan, Q., Ye, X. & Others Peptidoglycan-inspired autonomous ultrafast self-healing bio-friendly elastomers for bio-integrated electronics. *National Science Review*. **8**,154 (2021)

Chapter 2

- [1] Schneider, R., Sharma, A. & Rai . Introduction to molecular dynamics. *Computational Many Particle Physics*. pp. 3-40 (2008)
- [2] Karplus, M. & Petsko, G. Molecular dynamics simulations in biology. *Nature*. **347** pp. 631-639 (1990)
- [3] Verlet, L. Computer” experiments” on classical fluids. I. Thermodynamic properties of Lennard-Jones molecules. *Physical Review*. **159**, 98 (1967)
- [4] Dinur, U. & Hagler, A. New approaches to empirical force fields. *Reviews In Computational Chemistry*. **2** pp. 99-164 (1991)
- [5] Lennard-Jones, J. On the forces between atoms and ions. *Proceedings Of The Royal Society Of London. Series A, Containing Papers Of A Mathematical And Physical Character*. **109**, 584-597 (1925)
- [6] Jorgensen, W. & Tirado-Rives, J. Potential energy functions for atomic-level simulations of water and organic and biomolecular systems. *Proceedings Of The National Academy Of Sciences*. **102**, 6665-6670 (2005)

- [7] Phillips, J., Braun, R., Wang, W., Gumbart, J., Tajkhorshid, E., Villa, E., Chipot, C., Skeel, R., Kale, L. & Schulten, K. Scalable molecular dynamics with NAMD. *Journal Of Computational Chemistry*. **26**, 1781-1802 (2005)
- [8] Kalé, L., Skeel, R., Bhandarkar, M., Brunner, R., Gursoy, A., Krawetz, N., Phillips, J., Shinozaki, A., Varadarajan, K. & Schulten, K. NAMD2: greater scalability for parallel molecular dynamics. *Journal Of Computational Physics*. **151**, 283-312 (1999)
- [9] Brooks, B., Brooks, C., Mackerell, A., Nilsson, L., Petrella, R., Roux, B., Won, Y., Archontis, G., Bartels, C., Boresch, S. & Others CHARMM: Molecular dynamics simulation package. *J. Comput. Chem.* **30**, 1545-1614 (2009)
- [10] Raman, E., Guvench, O. & MacKerell Jr, A. CHARMM additive all-atom force field for glycosidic linkages in carbohydrates involving furanoses. *The Journal Of Physical Chemistry B*. **114**, 12981-12994 (2010)
- [11] Pastor, R. & MacKerell Jr, A. Development of the CHARMM force field for lipids. *The Journal Of Physical Chemistry Letters*. **2**, 1526-1532 (2011)
- [12] Jo, S., Kim, T., Iyer, V. & Im, W. CHARMM-GUI: a web-based graphical user interface for CHARMM. *Journal Of Computational Chemistry*. **29**, 1859-1865 (2008)
- [13] Park, S., Lee, J., Qi, Y., Kern, N., Lee, H., Jo, S., Joung, I., Joo, K., Lee, J. & Im, W. CHARMM-GUI Glycan Modeler for modeling and simulation of carbohydrates and glycoconjugates. *Glycobiology*. **29**, 320-331 (2019)
- [14] Jorgensen, W. & Jenson, C. Temperature dependence of TIP3P, SPC, and TIP4P water from NPT Monte Carlo simulations: Seeking temperatures of maximum density. *Journal Of Computational Chemistry*. **19**, 1179-1186 (1998)
- [15] Jorgensen, W., Chandrasekhar, J., Madura, J., Impey, R. & Klein, M. Comparison of simple potential functions for simulating liquid water. *The Journal Of Chemical Physics*. **79**, 926-935 (1983)
- [16] Grubmüller, H., Heymann, B. & Tavan, P. Ligand binding: molecular mechanics calculation of the streptavidin-biotin rupture force. *Science*. **271**, 997-999 (1996)
- [17] Izrailev, S., Stepaniants, S., Isralewitz, B., Kosztin, D., Lu, H., Molnar, F., Wriggers, W. & Schulten, K. Steered molecular dynamics. *Computational Molecular Dynamics: Challenges, Methods, Ideas: Proceedings Of The 2nd International Symposium On Algorithms For Macromolecular Modelling, Berlin, May 21-24, 1997*. pp. 39-65 (1999)
- [18] Isralewitz, B., Gao, M. & Schulten, K. Steered molecular dynamics and mechanical functions of proteins. *Current Opinion In Structural Biology*. **11**, 224-230 (2001)
- [19] Park, S. & Schulten, K. Calculating potentials of mean force from steered molecular dynamics simulations. *The Journal Of Chemical Physics*. **120**, 5946-5961 (2004)
- [20] Suan Li, M. & Khanh Mai, B. Steered molecular dynamics a promising tool for drug design. *Current Bioinformatics*. **7**, 342-351 (2012)
- [21] Henin, J., Fiorin, G., Chipot, C. & Klein, M. Exploring multidimensional free energy landscapes using time-dependent biases on collective variables. *Journal Of Chemical Theory And Computation*. **6**, 35-47 (2010)
- [22] Kreuzer, H., Payne, S. & Livadaru, L. Stretching a Macromolecule in an Atomic Force Microscope: Statistical Mechanical Analysis. *Biophysical Journal*. **80**, 2505-2514 (2001)

- [23] Marszalek, P. & Dufre ne, Y. Stretching single polysaccharides and proteins using atomic force microscopy. *Chemical Society Reviews*. **41**, 3523-3534 (2012)
- [24] Ousterhout, J. & Jones, K. Tcl and the Tk Toolkit Second Edition. (1994)
- [25] Kim, S., Lee, J., Jo, S., Brooks III, C., Lee, H. & Im, W. CHARMM-GUI ligand reader and modeler for CHARMM force field generation of small molecules. (Wiley Online Library,2017)
- [26] Gullingsrud, J., Saam, J. & Phillips, J. psfgen User's Guide. *Urbana*. **51** pp. 61801 (2006)
- [27] Fernandes, H., Sousa, S. & Cerqueira, N. VMD Store–A VMD Plugin to Browse, Discover, and Install VMD Extensions. *Journal Of Chemical Information And Modeling*. **59**, 4519-4523 (2019)
- [28] Kern, N. CHARMM-GUI multicomponent assembler for modeling and simulation of complex heterogeneous biomolecular systems. *Biophysical Journal*. **116**, 290a (2019)
- [29] Van Der Spoel, D., Lindahl, E., Hess, B., Groenhof, G., Mark, A. & Berendsen, H. GROMACS: fast, flexible, and free. *Journal Of Computational Chemistry*. **26**, 1701-1718 (2005)
- [30] Saito, M. Molecular dynamics simulations of proteins in solution: artefacts caused by the cutoff approximation. *The Journal Of Chemical Physics*. **101**, 4055-4061 (1994)
- [31] Darden, T., York, D. & Pedersen, L. Particle mesh Ewald: An Nlog (N) method for Ewald sums in large systems. *The Journal Of Chemical Physics*. **98**, 10089-10092 (1993)
- [32] Miyamoto, S. & Kollman, P. Settle: An analytical version of the SHAKE and RATTLE algorithm for rigid water models. *Journal Of Computational Chemistry*. **13**, 952-962 (1992)
- [33] Hess, B., Bekker, H., Berendsen, H. & Fraaije, J. LINCS: A linear constraint solver for molecular simulations. *Journal Of Computational Chemistry*. **18**, 1463-1472 (1997)
- [34] Humphrey, W., Dalke, A. & Schulten, K. VMD: visual molecular dynamics. *Journal Of Molecular Graphics*. **14**, 33-38 (1996)
- [35] Bonomi, M., Branduardi, D., Bussi, G., Camilloni, C., Provasi, D., Raiteri, P., Donadio, D., Marinelli, F., Pietrucci, F., Broglio, R. & Others PLUMED: A portable plugin for free-energy calculations with molecular dynamics. *Computer Physics Communications*. **180**, 1961-1972 (2009)
- [36] Tribello, G., Bonomi, M., Branduardi, D., Camilloni, C. & Bussi, G. PLUMED 2: New feathers for an old bird. *Computer Physics Communications*. **185**, 604-613 (2014)
- [37] Eisenhaber, F., Lijnzaad, P., Argos, P., Sander, C. & Scharf, M. The double cubic lattice method: Efficient approaches to numerical integration of surface area and volume and to dot surface contouring of molecular assemblies. *Journal Of Computational Chemistry*. **16**, 273-284 (1995)
- [38] Jolliffe, I. & Cadima, J. Principal component analysis: a review and recent developments. *Philosophical Transactions Of The Royal Society A: Mathematical, Physical And Engineering Sciences*. **374**, 20150202 (2016)
- [39] Hasan, B. & Abdulazeez, A. A review of principal component analysis algorithm for dimensionality reduction. *Journal Of Soft Computing And Data Mining*. **2**, 20-30 (2021)
- [40] Grant, B., Rodrigues, A., ElSawy, K., McCammon, J. & Caves, L. Bio3d: an R package for the comparative analysis of protein structures. *Bioinformatics*. **22**, 2695-2696 (2006)
- [41] Altis, A., Nguyen, P., Hegger, R. & Stock, G. Dihedral angle principal component analysis of molecular dynamics simulations. *The Journal Of Chemical Physics*. **126**, 244111 (2007)
- [42] Buitrago, C., Bolintineanu, D., Seitz, M., Opper, K., Wagener, K., Stevens, M., Frischknecht, A. & Winey, K. Direct comparisons of X-ray scattering and atomistic molecular dynamics simulations for precise acid copolymers and ionomers. *Macromolecules*. **48**, 1210-1220 (2015)

- [43] Waasmaier, D. & Kirfel, A. New analytical scattering-factor functions for free atoms and ions. *Acta Crystallographica Section A: Foundations Of Crystallography*. **51**, 416-431 (1995)

Chapter 3

- [1] Grundy, M., Quint, J., Rieder, A., Ballance, S., Dreiss, C., Cross, K., Gray, R., Bajka, B., Butterworth, P., Ellis, P. & Others The impact of oat structure and β -glucan on in vitro lipid digestion. *Journal Of Functional Foods*. **38** pp. 378-388 (2017)
- [2] Gilissen, L., Meer, I. & Smulders, M. Why oats are safe and healthy for celiac disease patients. *Medical Sciences*. **4**, 21 (2016)
- [3] Smulders, M., Wiel, C., Broeck, H., Meer, I., Israel-Hoewelaken, T., Timmer, R., Dinter, B., Braun, S. & Gilissen, L. Oats in healthy gluten-free and regular diets: A perspective. *Food Research International*. **110** pp. 3-10 (2018)
- [4] Wang, Y., Harding, S., Eck, P., Thandapilly, S., Gamel, T., Abdel-Aal, E., Crow, G., Tosh, S., Jones, P. & Ames, N. High-molecular-weight β -glucan decreases serum cholesterol differentially based on the CYP7A1 rs3808607 polymorphism in mildly hypercholesterolemic adults. *The Journal Of Nutrition*. **146**, 720-727 (2015)
- [5] Whitehead, A., Beck, E., Tosh, S. & Wolever, T. Cholesterol-lowering effects of oat β -glucan: a meta-analysis of randomized controlled trials. *The American Journal Of Clinical Nutrition*. **100**, 1413-1421 (2014)
- [6] El Khoury, D., Cuda, C., Luhovyy, B. & G. Beta glucan: health benefits in obesity and metabolic syndrome. *Journal Of Nutrition And Metabolism*. **2012** (2012)
- [7] Sima, P., Vannucci, L. & Vetvicka, V. β -glucans and cholesterol. *International Journal Of Molecular Medicine*. **41**, 1799-1808 (2018)
- [8] McCleary, B. & Draga, A. Measurement of β -glucan in mushrooms and mycelial products. *Journal Of AOAC International*. **99**, 364-373 (2016)
- [9] Othman, R., Moghadasian, M. & Jones, P. Cholesterol-lowering effects of oat β -glucan. *Nutrition Reviews*. **69**, 299-309 (2011)
- [10] Wang, Q. & Ellis, P. Oat β -glucan: physico-chemical characteristics in relation to its blood-glucose and cholesterol-lowering properties. *British Journal Of Nutrition*. **112**, S4-S13 (2014)
- [11] Grundy, M., Fardet, A., Tosh, S., Rich, G. & Wilde, P. Processing of oat: the impact on oat's cholesterol lowering effect. *Food & Function*. **9**, 1328-1343 (2018)
- [12] Zhu, F., Du, B. & Xu, B. A critical review on production and industrial applications of beta-glucans. *Food Hydrocolloids*. **52** pp. 275-288 (2016)
- [13] Vetvicka, V., Vannucci, L., Sima, P. & Richter, J. Beta glucan: supplement or drug? From laboratory to clinical trials. *Molecules*. **24**, 1251 (2019)
- [14] Sletmoen, M. & Stokke, B. Higher order structure of (1,3)- β -D-glucans and its influence on their biological activities and complexation abilities. *Biopolymers: Original Research On Biomolecules*. **89**, 310-321 (2008)
- [15] Zielke, C., Kosik, O., Ainalem, M., Lovegrove, A., Stradner, A. & Nilsson, L. Characterization of cereal β -glucan extracts from oat and barley and quantification of proteinaceous matter. *PLoS One*. **12**, e0172034 (2017)

- [16] Zielke, C., Lu, Y., Poinso, R. & Nilsson, L. Interaction between cereal β -glucan and proteins in solution and at interfaces. *Colloids And Surfaces B: Biointerfaces*. **162** pp. 256-264 (2018)
- [17] Whistler, R. Solubility of polysaccharides and their behavior in solution. (ACS Publications,1973)
- [18] Li, S., Xiong, Q., Lai, X., Li, X., Wan, M., Zhang, J., Yan, Y., Cao, M., Lu, L., Guan, J. & Others Molecular modification of polysaccharides and resulting bioactivities. *Comprehensive Reviews In Food Science And Food Safety*. **15**, 237-250 (2016)
- [19] Guo, M., Hu, X., Wang, C. & Ai, L. Polysaccharides: structure and solubility. *Solubility Of Polysaccharides*. **2** pp. 8-21 (2017)
- [20] Lazaridou, A. & Biliaderis, C. Molecular aspects of cereal β -glucan functionality: Physical properties, technological applications and physiological effects. *Journal Of Cereal Science*. **46**, 101-118 (2007)
- [21] Bacic, A., Fincher, G. & Stone, B. Chemistry, biochemistry, and biology of 1 \rightarrow 3 beta glucans and related polysaccharides. (Academic Press,2009)
- [22] Morris, E., Cutler, A., Ross-Murphy, S., Rees, D. & Price, J. Concentration and shear rate dependence of viscosity in random coil polysaccharide solutions. *Carbohydrate Polymers*. **1**, 5-21 (1981)
- [23] Jo, S., Myatt, D., Qi, Y., Douth, J., Clifton, L., Im, W. & Widmalm, G. Multiple conformational states contribute to the 3D structure of a glucan decasaccharide: A combined SAXS and MD simulation study. *The Journal Of Physical Chemistry B*. **122**, 1169-1175 (2018)
- [24] Vaikousi, H., Biliaderis, C. & Izydorczyk, M. Solution flow behavior and gelling properties of water-soluble barley (1 \rightarrow 3, 1 \rightarrow 4)- β -glucans varying in molecular size. *Journal Of Cereal Science*. **39**, 119-137 (2004)
- [25] Tosh, S., Brummer, Y., Wood, P., Wang, Q. & Weisz, J. Evaluation of structure in the formation of gels by structurally diverse (1 \rightarrow 3)(1 \rightarrow 4)- β -D-glucans from four cereal and one lichen species. *Carbohydrate Polymers*. **57**, 249-259 (2004)
- [26] Tosh, S., Wood, P., Wang, Q. & Weisz, J. Structural characteristics and rheological properties of partially hydrolysed oat β -glucan: the effects of molecular weight and hydrolysis method. *Carbohydrate Polymers*. **55**, 425-436 (2004)
- [27] Brummer, Y., Defelice, C., Wu, Y., Kwong, M., Wood, P. & Tosh, S. Textural and rheological properties of oat beta-glucan gels with varying molecular weight composition. *Journal Of Agricultural And Food Chemistry*. **62**, 3160-3167 (2014)
- [28] Tvaroska, I., Ogawa, K., Deslandes, Y. & Marchessault, R. Crystalline conformation and structure of lichenan and barley β -glucan. *Canadian Journal Of Chemistry*. **61**, 1608-1616 (1983)
- [29] Patel, D., Pendrill, R., Mallajosyula, S., Widmalm, G. & MacKerell Jr, A. Conformational properties of α - or β -(1 \rightarrow 6)-linked oligosaccharides: Hamiltonian replica exchange MD simulations and NMR experiments. *The Journal Of Physical Chemistry B*. **118**, 2851-2871 (2014)
- [30] Zerbetto, M., Polimeno, A. & Widmalm, G. Glycosidic linkage flexibility: The ψ torsion angle has a bimodal distribution in α -L-Rha p-(1 \rightarrow 2)- α -L-Rha p-OMe as deduced from ^{13}C NMR spin relaxation. *The Journal Of Chemical Physics*. **152**, 035103 (2020)
- [31] Pereira, C., Kony, D., Baron, R., Müller, M., Gunsteren, W. & Hünenberger, P. Conformational and dynamical properties of disaccharides in water: a molecular dynamics study. *Biophysical Journal*. **90**, 4337-4344 (2006)

- [32] Kony, D., Damm, W., Stoll, S., Van Gunsteren, W. & Hünenberger, P. Explicit-solvent molecular dynamics simulations of the polysaccharide schizophyllan in water. *Biophysical Journal*. **93**, 442-455 (2007)
- [33] Oelschlaeger, C., Cota Pinto Coelho, M. & Willenbacher, N. Chain flexibility and dynamics of polysaccharide hyaluronan in entangled solutions: a high frequency rheology and diffusing wave spectroscopy study. *Biomacromolecules*. **14**, 3689-3696 (2013)
- [34] Jo, S., Kim, T., Iyer, V. & Im, W. CHARMM-GUI: a web-based graphical user interface for CHARMM. *Journal Of Computational Chemistry*. **29**, 1859-1865 (2008)
- [35] Park, S., Lee, J., Qi, Y., Kern, N., Lee, H., Jo, S., Joung, I., Joo, K., Lee, J. & Im, W. CHARMM-GUI Glycan Modeler for modeling and simulation of carbohydrates and glycoconjugates. *Glycobiology*. **29**, 320-331 (2019)
- [36] Berendsen, H., Spoel, D. & Drunen, R. GROMACS: A message-passing parallel molecular dynamics implementation. *Computer Physics Communications*. **91**, 43-56 (1995)
- [37] Guvench, O., Greene, S., Kamath, G., Brady, J., Venable, R., Pastor, R. & Mackerell Jr, A. Additive empirical force field for hexopyranose monosaccharides. *Journal Of Computational Chemistry*. **29**, 2543-2564 (2008)
- [38] Guvench, O., Hatcher, E., Venable, R., Pastor, R. & MacKerell Jr, A. CHARMM additive all-atom force field for glycosidic linkages between hexopyranoses. *Journal Of Chemical Theory And Computation*. **5**, 2353-2370 (2009)
- [39] Jorgensen, W. & Jenson, C. Temperature dependence of TIP3P, SPC, and TIP4P water from NPT Monte Carlo simulations: Seeking temperatures of maximum density. *Journal Of Computational Chemistry*. **19**, 1179-1186 (1998)
- [40] Hoover, W. Canonical dynamics: Equilibrium phase-space distributions. *Physical Review A*. **31**, 1695 (1985)
- [41] Nosé, S. A unified formulation of the constant temperature molecular dynamics methods. *The Journal Of Chemical Physics*. **81**, 511-519 (1984)
- [42] Parrinello, M. & Rahman, A. Polymorphic transitions in single crystals: A new molecular dynamics method. *Journal Of Applied Physics*. **52**, 7182-7190 (1981)
- [43] Humphrey, W., Dalke, A. & Schulten, K. VMD: visual molecular dynamics. *Journal Of Molecular Graphics*. **14**, 33-38 (1996)
- [44] Bonomi, M., Branduardi, D., Bussi, G., Camilloni, C., Provasi, D., Raiteri, P., Donadio, D., Marinelli, F., Pietrucci, F., Broglia, R. & Others PLUMED: A portable plugin for free-energy calculations with molecular dynamics. *Computer Physics Communications*. **180**, 1961-1972 (2009)
- [45] Tribello, G., Bonomi, M., Branduardi, D., Camilloni, C. & Bussi, G. PLUMED 2: New feathers for an old bird. *Computer Physics Communications*. **185**, 604-613 (2014)
- [46] Grant, B., Rodrigues, A., ElSawy, K., McCammon, J. & Caves, L. Bio3d: an R package for the comparative analysis of protein structures. *Bioinformatics*. **22**, 2695-2696 (2006)
- [47] Wormald, M., Petrescu, A., Pao, Y., Glithero, A., Elliott, T. & Dwek, R. Conformational studies of oligosaccharides and glycopeptides: complementarity of NMR, X-ray crystallography, and molecular modelling. *Chemical Reviews*. **102**, 371-386 (2002)
- [48] Salisburg, A., Deline, A., Lexa, K., Shields, G. & Kirschner, K. Ramachandran-type plots for glycosidic linkages: Examples from molecular dynamic simulations using the Glycam06 force field. *Journal Of Computational Chemistry*. **30**, 910-921 (2009)

- [49] Poppe, L., Brown, G., Philo, J., Nikrad, P. & Shah, B. Conformation of sLex tetrasaccharide, free in solution and bound to E-, P-, and L-selectin. *Journal Of The American Chemical Society*. **119**, 1727-1736 (1997)
- [50] Harris, R., Kiddle, G., Field, R., Milton, M., Ernst, B., Magnani, J. & Homans, S. Stable-isotope-assisted NMR studies on ^{13}C -enriched sialyl Lewisx in solution and bound to E-selectin. *Journal Of The American Chemical Society*. **121**, 2546-2551 (1999)
- [51] Homans, S., Pastore, A., Dwek, R. & Rademacher, T. Structure and dynamics in oligomannose-type oligosaccharides. *Biochemistry*. **26**, 6649-6655 (1987)
- [52] Brisson, J. & Carver, J. Solution conformation of asparagine-linked oligosaccharides: $\alpha(1\rightarrow2)$, $\alpha(1\rightarrow3)$, $\beta(1\rightarrow2)$, and $\beta(1\rightarrow4)$ -linked units. *Biochemistry*. **22**, 3671-3680 (1983)
- [53] Evans, J. Biomolecular NMR spectroscopy. (Oxford University Press, 1995)
- [54] Landersjö, C., Stenutz, R. & Widmalm, G. Conformational flexibility of carbohydrates: A folded conformer at the ϕ dihedral angle of a Glycosidic linkage. *Journal Of The American Chemical Society*. **119**, 8695-8698 (1997)
- [55] Olsson, U., Sävén, E., Stenutz, R. & Widmalm, G. Conformational Flexibility and Dynamics of Two (1 \rightarrow 6)-Linked Disaccharides Related to an Oligosaccharide Epitope Expressed on Malignant Tumour Cells. *Chemistry—A European Journal*. **15**, 8886-8894 (2009)
- [56] Lycknert, K., Edblad, M., Imberty, A. & Widmalm, G. NMR and Molecular Modeling Studies of the Interaction between Wheat Germ Agglutinin and the β -d-Glc p NAc-(1 \rightarrow 6)- α -d-Man p Epitope Present in Glycoproteins of Tumor Cells. *Biochemistry*. **43**, 9647-9654 (2004)
- [57] Kufareva, I. & Abagyan, R. Methods of protein structure comparison. *Homology Modeling: Methods And Protocols*. pp. 231-257 (2012)
- [58] Shen, T., Langan, P., French, A., Johnson, G. & Gnanakaran, S. Conformational flexibility of soluble cellulose oligomers: chain length and temperature dependence. *Journal Of The American Chemical Society*. **131**, 14786-14794 (2009)
- [59] Plazinski, W. & Drach, M. The influence of the hexopyranose ring geometry on the conformation of glycosidic linkages investigated using molecular dynamics simulations. *Carbohydrate Research*. **415** pp. 17-27 (2015)
- [60] Plazinski, W., Lonardi, A. & Hünenberger, P. Revision of the GROMOS 56A6CARBO force field: improving the description of ring-conformational equilibria in hexopyranose-based carbohydrates chains. *Journal Of Computational Chemistry*. **37**, 354-365 (2016)
- [61] Sajeevan, K. & Roy, D. Principal component analysis of a conotoxin delineates the link among peptide sequence, dynamics, and disulfide bond isoforms. *The Journal Of Physical Chemistry B*. **123**, 5483-5493 (2019)
- [62] Wolf, A. & Kirschner, K. Principal component and clustering analysis on molecular dynamics data of the ribosomal L11· 23S subdomain. *Journal Of Molecular Modeling*. **19** pp. 539-549 (2013)
- [63] Pérez, S., Kouwijzer, M., Mazeau, K. & Engelsen, S. Modeling polysaccharides: Present status and challenges. *Journal Of Molecular Graphics*. **14**, 307-321 (1996)
- [64] Christensen, N., Hansen, P., Larsen, F., Folkerman, T., Motawia, M. & Engelsen, S. A combined nuclear magnetic resonance and molecular dynamics study of the two structural motifs for mixed-linkage β -glucans: methyl β -cellobioside and methyl β -laminarabioside. *Carbohydrate Research*. **345**, 474-486 (2010)

Chapter 4

- [1] Capuano, E. The behavior of dietary fiber in the gastrointestinal tract determines its physiological effect. *Critical Reviews In Food Science And Nutrition*. **57**, 3543-3564 (2017)
- [2] Englyst, K., Liu, S. & Englyst, H. Nutritional characterization and measurement of dietary carbohydrates. *European Journal Of Clinical Nutrition*. **61**, S19-S39 (2007)
- [3] Grundy, M., Edwards, C., Mackie, A., Gidley, M., Butterworth, P. & Ellis, P. Re-evaluation of the mechanisms of dietary fibre and implications for macronutrient bio accessibility, digestion and postprandial metabolism. *British Journal Of Nutrition*. **116**, 816-833 (2016)
- [4] Lovegrove, A., Edwards, C., De Noni, I., Patel, H., El, S., Grassby, T., Zielke, C., Ulmius, M., Nilsson, L., Butterworth, P. & Others Role of polysaccharides in food, digestion, and health. *Critical Reviews In Food Science And Nutrition*. **57**, 237-253 (2017)
- [5] Walters, R., Baird, I., Davies, P., Hill, M., Drasar, B., Southgate, D., Green, J. & Morgan, B. Effects of two types of dietary fibre on faecal steroid and lipid excretion. *Br Med J*. **2**, 536-538 (1975)
- [6] Nichifor, M., Stanciu, M. & Zhu, X. Bile acids covalently bound to polysaccharides: 2. Dextran with pendant cholic acid groups. *Reactive And Functional Polymers*. **59**, 141-148 (2004)
- [7] Nichifor, M. & Carpov, A. Bile acids covalently bound to polysaccharides 1. Esters of bile acids with dextran. *European Polymer Journal*. **35**, 2125-2129 (1999)
- [8] Song, Q., Wang, Y., Huang, L., Shen, M., Yu, Y., Yu, Q., Chen, Y. & Xie, J. Review of the relationships among polysaccharides, gut microbiota, and human health. *Food Research International*. **140** pp. 109858 (2021)
- [9] Anderson, J., Baird, P., Davis Jr, R., Ferreri, S., Knudtson, M., Koraym, A., Waters, V. & Williams, C. Health benefits of dietary fiber. *Nutrition Reviews*. **67**, 188-205 (2009)
- [10] Whitehead, A., Beck, E., Tosh, S. & Wolever, T. Cholesterol-lowering effects of oat β -glucan: a meta-analysis of randomized controlled trials. *The American Journal Of Clinical Nutrition*. **100**, 1413-1421 (2014)
- [11] Hoofnagle, J. LiverTox: a website on drug-induced liver injury. *Drug-Induced Liver Disease*. pp. 725-732 (2013)
- [12] Elshourbagy, N., Meyers, H. & Abdel-Meguid, S. Cholesterol: the good, the bad, and the ugly-therapeutic targets for the treatment of dyslipidemia. *Medical Principles And Practice*. **23**, 99-111 (2014)
- [13] Soliman, G. Dietary cholesterol and the lack of evidence in cardiovascular disease. *Nutrients*. **10**, 780 (2018)
- [14] Kumar, G. & Chattopadhyay, A. Cholesterol: an evergreen molecule in biology. *Biomedical Spectroscopy And Imaging*. **5**, S55-S66 (2016)
- [15] Joyce, S., Kamil, A., Fleige, L. & Gahan, C. The cholesterol-lowering effect of oats and oat beta glucan: modes of action and potential role of bile acids and the microbiome. *Frontiers In Nutrition*. **6** pp. 171 (2019)
- [16] McRorie Jr, J. & McKeown, N. Understanding the physics of functional fibers in the gastrointestinal tract: an evidence-based approach to resolving enduring misconceptions about insoluble and soluble fiber. *Journal Of The Academy Of Nutrition And Dietetics*. **117**, 251-264 (2017)

- [17] Ellegaard, L. & Andersson, H. Oat bran rapidly increases bile acid excretion and bile acid synthesis: an ileostomy study. *European Journal Of Clinical Nutrition*. **61**, 938-945 (2007)
- [18] Wang, Y., Harding, S., Thandapilly, S., Tosh, S., Jones, P. & Ames, N. Barley β -glucan reduces blood cholesterol levels via interrupting bile acid metabolism. *British Journal Of Nutrition*. **118**, 822-829 (2017)
- [19] Wang, Q. & Ellis, P. Oat β -glucan: physico-chemical characteristics in relation to its blood-glucose and cholesterol-lowering properties. *British Journal Of Nutrition*. **112**, S4-S13 (2014)
- [20] Andersson, M., Ellegaard, L. & Andersson, H. Oat bran stimulates bile acid synthesis within 8 h as measured by 7α -hydroxy-4-cholesten-3-one. *The American Journal Of Clinical Nutrition*. **76**, 1111-1116 (2002)
- [21] Buhman, K., Furumoto, E., Donkin, S. & Story, J. Dietary psyllium increases fecal bile acid excretion, total steroid excretion and bile acid biosynthesis in rats. *The Journal Of Nutrition*. **128**, 1199-1203 (1998)
- [22] Lia, A., Hallmans, G., Sandberg, A., Sundberg, B., Aman, P. & Andersson, H. Oat beta-glucan increases bile acid excretion and a fiber-rich barley fraction increases cholesterol excretion in ileostomy subjects. *The American Journal Of Clinical Nutrition*. **62**, 1245-1251 (1995)
- [23] Marasca, E., Boulos, S. & Nyström, L. Bile acid-retention by native and modified oat and barley β -glucan. *Carbohydrate Polymers*. **236** pp. 116034 (2020)
- [24] Naumann, S., Schweiggert-Weisz, U., Eglmeier, J., Haller, D. & Eisner, P. In vitro interactions of dietary fibre enriched food ingredients with primary and secondary bile acids. *Nutrients*. **11**, 1424 (2019)
- [25] Kim, H. & White, P. Interactional effects of β -glucan, starch, and protein in heated oat slurries on viscosity and in vitro bile acid binding. *Journal Of Agricultural And Food Chemistry*. **60**, 6217-6222 (2012)
- [26] Zielke, C., Kosik, O., Ainalem, M., Lovegrove, A., Stradner, A. & Nilsson, L. Characterization of cereal β -glucan extracts from oat and barley and quantification of proteinaceous matter. *PLoS One*. **12**, e0172034 (2017)
- [27] Zielke, C., Lu, Y., Poinot, R. & Nilsson, L. Interaction between cereal β -glucan and proteins in solution and at interfaces. *Colloids And Surfaces B: Biointerfaces*. **162** pp. 256-264 (2018)
- [28] Golisch, B., Lei, Z., Tamura, K. & Brumer, H. Configured for the human gut microbiota: Molecular mechanisms of dietary β -glucan utilization. *ACS Chemical Biology*. **16**, 2087-2102 (2021)
- [29] Jayachandran, M., Chen, J., Chung, S. & Xu, B. A critical review on the impacts of β -glucans on gut microbiota and human health. *The Journal Of Nutritional Biochemistry*. **61** pp. 101-110 (2018)
- [30] Shi, H., Yu, Y., Lin, D., Zheng, P., Zhang, P., Hu, M., Wang, Q., Pan, W., Yang, X., Hu, T. & Others β -glucan attenuates cognitive impairment via the gut-brain axis in diet-induced obese mice. *Microbiome*. **8** pp. 1-21 (2020)
- [31] Korompokis, K., Nilsson, L. & Zielke, C. The effect of in vitro gastrointestinal conditions on the structure and conformation of oat β -glucan. *Food Hydrocolloids*. **77** pp. 659-668 (2018)
- [32] Parrow, A., Larsson, P., Augustijns, P. & Bergström, C. Molecular dynamics simulations on interindividual variability of intestinal fluids: Impact on drug solubilization. *Molecular Pharmaceutics*. **17**, 3837-3844 (2020)

- [33] Mikkelsen, M., Cornali, S., Jensen, M., Nilsson, M., Beeren, S. & Meier, S. Probing interactions between β -glucan and bile salts at atomic detail by 1H - ^{13}C NMR assays. *Journal Of Agricultural And Food Chemistry*. **62**, 11472-11478 (2014)
- [34] Clulow, A., Parrow, A., Hawley, A., Khan, J., Pham, A., Larsson, P., Bergström, C. & Boyd, B. Characterization of solubilizing nano aggregates present in different versions of simulated intestinal fluid. *The Journal Of Physical Chemistry B*. **121**, 10869-10881 (2017)
- [35] Gunness, P., Flanagan, B., Mata, J., Gilbert, E. & Gidley, M. Molecular interactions of a model bile salt and porcine bile with (1,3:1,4)- β -glucans and arabinoxylans probed by ^{13}C NMR and SAXS. *Food Chemistry*. **197** pp. 676-685 (2016)
- [36] Gao, J., Lin, L., Sun, B. & Zhao, M. Comparison study on polysaccharide fractions from *Laminaria japonica*: structural characterization and bile acid binding capacity. *Journal Of Agricultural And Food Chemistry*. **65**, 9790-9798 (2017)
- [37] Mäkelä, N., Rosa-Sibakov, N., Wang, Y., Mattila, O., Nordlund, E. & Sontag-Strohm, T. Role of β -glucan content, molecular weight and phytate in the bile acid binding of oat β -glucan. *Food Chemistry*. **358** pp. 129917 (2021)
- [38] Pártay, L., Jedlovsky, P. & Sega, M. Molecular aggregates in aqueous solutions of bile acid salts. Molecular dynamics simulation study. *The Journal Of Physical Chemistry B*. **111**, 9886-9896 (2007)
- [39] Wang, Z., Yang, L., Xue, S., Wang, S., Zhu, L., Ma, T., Liu, H. & Li, R. Molecular docking and dynamic insights on the adsorption effects of soy hull polysaccharides on bile acids. *International Journal Of Food Science & Technology*. **57**, 3702-3712 (2022)
- [40] Jo, S., Kim, T., Iyer, V. & Im, W. CHARMM-GUI: a web-based graphical user interface for CHARMM. *Journal Of Computational Chemistry*. **29**, 1859-1865 (2008)
- [41] Park, S., Lee, J., Qi, Y., Kern, N., Lee, H., Jo, S., Joung, I., Joo, K., Lee, J. & Im, W. CHARMM-GUI Glycan Modeler for modeling and simulation of carbohydrates and glycoconjugates. *Glycobiology*. **29**, 320-331 (2019)
- [42] Jorgensen, W., Chandrasekhar, J., Madura, J., Impey, R. & Klein, M. Comparison of simple potential functions for simulating liquid water. *The Journal Of Chemical Physics*. **79**, 926-935 (1983)
- [43] Peesapati, S., Sajeevan, K., Patel, S. & Roy, D. Relation between glycosidic linkage, structure and dynamics of α - and β -glucans in water. *Biopolymers*. **112**, e23423 (2021)
- [44] Kim, S., Lee, J., Jo, S., Brooks III, C., Lee, H. & Im, W. CHARMM-GUI ligand reader and modeler for CHARMM force field generation of small molecules. (Wiley Online Library, 2017)
- [45] Kern, N. CHARMM-GUI multicomponent assembler for modeling and simulation of complex heterogeneous biomolecular systems. *Biophysical Journal*. **116**, 290a (2019)
- [46] Berendsen, H., Spoel, D. & Drunen, R. GROMACS: A message-passing parallel molecular dynamics implementation. *Computer Physics Communications*. **91**, 43-56 (1995)
- [47] Guvench, O., Mallajosyula, S., Raman, E., Hatcher, E., Vanommeslaeghe, K., Foster, T., Jamison, F. & MacKerell Jr, A. CHARMM additive all-atom force field for carbohydrate derivatives and its utility in polysaccharide and carbohydrate-protein modeling. *Journal Of Chemical Theory And Computation*. **7**, 3162-3180 (2011)

- [48] Vanommeslaeghe, K., Hatcher, E., Acharya, C., Kundu, S., Zhong, S., Shim, J., Darian, E., Guvench, O., Lopes, P., Vorobyov, I. & Others CHARMM general force field: A force field for drug-like molecules compatible with the CHARMM all-atom additive biological force fields. *Journal Of Computational Chemistry*. **31**, 671-690 (2010)
- [49] Hoover, W. Canonical dynamics: Equilibrium phase-space distributions. *Physical Review A*. **31**, 1695 (1985)
- [50] Nosé, S. A unified formulation of the constant temperature molecular dynamics methods. *The Journal Of Chemical Physics*. **81**, 511-519 (1984)
- [51] Parrinello, M. & Rahman, A. Polymorphic transitions in single crystals: A new molecular dynamics method. *Journal Of Applied Physics*. **52**, 7182-7190 (1981)
- [52] Hess, B., Bekker, H., Berendsen, H. & Fraaije, J. LINCS: A linear constraint solver for molecular simulations. *Journal Of Computational Chemistry*. **18**, 1463-1472 (1997)
- [53] Humphrey, W., Dalke, A. & Schulten, K. VMD: visual molecular dynamics. *Journal Of Molecular Graphics*. **14**, 33-38 (1996)
- [54] Bonomi, M., Branduardi, D., Bussi, G., Camilloni, C., Provasi, D., Raiteri, P., Donadio, D., Marinelli, F., Pietrucci, F., Broglia, R. & Others PLUMED: A portable plugin for free-energy calculations with molecular dynamics. *Computer Physics Communications*. **180**, 1961-1972 (2009)
- [55] Christensen, N., Hansen, P., Larsen, F., Folkerman, T., Motawia, M. & Engelsen, S. A combined nuclear magnetic resonance and molecular dynamics study of the two structural motifs for mixed-linkage β -glucans: methyl β -cellobioside and methyl β -laminarabioside. *Carbohydrate Research*. **345**, 474-486 (2010)
- [56] Pérez, S., Kouwijzer, M., Mazeau, K. & Engelsen, S. Modeling polysaccharides: Present status and challenges. *Journal Of Molecular Graphics*. **14**, 307-321 (1996)
- [57] Boyer, J. & Soroka, C. Bile formation and secretion: an update. *Journal Of Hepatology*. **75**, 190-201 (2021)
- [58] Hamilton, J., Xie, G., Raufman, J., Hogan, S., Griffin, T., Packard, C., Chatfield, D., Hagey, L., Steinbach, J. & Hofmann, A. Human caecal bile acids: concentration and spectrum. *American Journal Of Physiology-Gastrointestinal And Liver Physiology*. **293**, G256-G263 (2007)
- [59] Pártay, L., Jedlovszky, P. & Sega, M. Molecular aggregates in aqueous solutions of bile acid salts. Molecular dynamics simulation study. *The Journal Of Physical Chemistry B*. **111**, 9886-9896 (2007)
- [60] Tanaka, Y., Hara, T., Waki, R. & Nagata, S. Regional differences in the components of luminal water from rat gastrointestinal tract and comparison with other species.. *Journal Of Pharmacy & Pharmaceutical Sciences*. **15**, 510-518 (2012)
- [61] Jojart, B., Poša, M., Fiser, B., Szőri, M., Farkaš, Z. & Viskolcz, B. Mixed micelles of sodium cholate and sodium dodecylsulphate 1: 1 binary mixture at different temperatures—experimental and theoretical investigations. *PLoS One*. **9**, e102114 (2014)
- [62] Mansfield, M. & Klushin, L. Monte Carlo studies of dendrimer macromolecules. *Macromolecules*. **26**, 4262-4268 (1993)
- [63] Grant, T., Luft, J., Carter, L., Matsui, T., Weiss, T., Martel, A. & Snell, E. The accurate assessment of small-angle X-ray scattering data. *Acta Crystallographica Section D: Biological Crystallography*. **71**, 45-56 (2015)

- [64] Svergun, D. & Koch, M. Small-angle scattering studies of biological macromolecules in solution. *Reports On Progress In Physics*. **66**, 1735 (2003)
- [65] Travaglini, L., D'Annibale, A., Gregorio, M., Schillén, K., Olsson, U., Sennato, S., Pavel, N. & Galantini, L. Between peptides and bile acids: self-assembly of phenylalanine substituted cholic acids. *The Journal Of Physical Chemistry B*. **117**, 9248-9257 (2013)

Chapter 5

- [1] Mohammed, A., Naveed, M. & Jost, N. Polysaccharides; classification, chemical properties, and future perspective applications in fields of pharmacology and biological medicine (a review of current applications and upcoming potentialities). *Journal Of Polymers And The Environment*. **29** pp. 2359-2371 (2021)
- [2] Thomas, B., Raj, M., Joy, J., Moores, A., Drisko, G. & Sanchez, C. Nanocellulose, a versatile green platform: from biosources to materials and their applications. *Chemical Reviews*. **118**, 11575-11625 (2018)
- [3] Peesapati, S., Sajeevan, K., Patel, S. & Roy, D. Relation between glycosidic linkage, structure and dynamics of α - and β -glucans in water. *Biopolymers*. **112**, e23423 (2021)
- [4] Yu, Y. & Delbianco, M. Conformational studies of oligosaccharides. *Chemistry—A European Journal*. **26**, 9814-9825 (2020)
- [5] Pérez, S. & Kouwijzer, M. Shapes and interactions of polysaccharide chains. *Carbohydrates: Structures, Syntheses And Dynamics*. pp. 258-293 (1999)
- [6] Anggara, K., Zhu, Y., Fittolani, G., Yu, Y., Tyrikos-Ergas, T., Delbianco, M., Rauschenbach, S., Abb, S., Seeberger, P. & Kern, K. Identifying the origin of local flexibility in a carbohydrate polymer. *Proceedings Of The National Academy Of Sciences*. **118**, e2102168118 (2021)
- [7] Fittolani, G., Tyrikos-Ergas, T., Vargová, D., Chaube, M. & Delbianco, M. Progress and challenges in the synthesis of sequence controlled polysaccharides. *Beilstein Journal Of Organic Chemistry*. **17**, 1981-2025 (2021)
- [8] Díaz-Montes, E. Polysaccharides: Sources, characteristics, properties, and their application in biodegradable films. *Polysaccharides*. **3**, 480-501 (2022)
- [9] Kong, I., Degraeve, P. & Pui, L. Polysaccharide-Based Edible Films Incorporated with Essential Oil Nanoemulsions: Physico-Chemical, Mechanical Properties and Its Application in Food Preservation—A Review. *Foods*. **11**, 555 (2022)
- [10] Yamazaki, M. & Iijima, K. Fabrication and characterization of polysaccharide composite films from polyion complex particles. *Polymers*. **12**, 435 (2020)
- [11] Rees, D. & Thom, D. Polysaccharide conformation. Part 10. Solvent and temperature effects on the optical rotation and conformation of model carbohydrates. *Journal Of The Chemical Society, Perkin Transactions 2*., 191-201 (1977)
- [12] Sletmoen, M. & Stokke, B. Higher order structure of (1,3)- β -D-glucans and its influence on their biological activities and complexation abilities. *Biopolymers: Original Research On Biomolecules*. **89**, 310-321 (2008)
- [13] Almond, A. & Sheehan, J. Predicting the molecular shape of polysaccharides from dynamic interactions with water. *Glycobiology*. **13**, 255-264 (2003)
- [14] Striegel, A. Influence of anomeric configuration on mechanochemical degradation of polysaccharides: cellulose versus amylose. *Biomacromolecules*. **8**, 3944-3949 (2007)

- [15] Marszalek, P., Pang, Y., Li, H., Yazal, J., Oberhauser, A. & Fernandez, J. Atomic levers control pyranose ring conformations. *Proceedings Of The National Academy Of Sciences*. **96**, 7894-7898 (1999)
- [16] Marszalek, P., Oberhauser, A., Pang, Y. & Fernandez, J. Polysaccharide elasticity governed by chair-boat transitions of the glucopyranose ring. *Nature*. **396**, 661-664 (1998)
- [17] Marszalek, P. & Dufrêne, Y. Stretching single polysaccharides and proteins using atomic force microscopy. *Chemical Society Reviews*. **41**, 3523-3534 (2012)
- [18] Kuttel, M. & Naidoo, K. Glycosidic linkage rotations determine amylose stretching mechanism. *Journal Of The American Chemical Society*. **127**, 12-13 (2005)
- [19] Haverkamp, R., Marshall, A. & Williams, M. Model for stretching elastic biopolymers which exhibit conformational transformations. *Physical Review E*. **75**, 021907 (2007)
- [20] Rief, M., Oesterhelt, F., Heymann, B. & Gaub, H. Single molecule force spectroscopy on polysaccharides by atomic force microscopy. *Science*. **275**, 1295-1297 (1997)
- [21] Haverkamp, R., Marshall, A. & Williams, M. Entropic and Enthalpic Contributions to the Chair-Boat Conformational Transformation in Dextran under Single Molecule Stretching. *The Journal Of Physical Chemistry B*. **111**, 13653-13657 (2007)
- [22] Ortiz, C. & Hadziioannou, G. Entropic elasticity of single polymer chains of poly (methacrylic acid) measured by atomic force microscopy. *Macromolecules*. **32**, 780-787 (1999)
- [23] Pullman, B. & Jortner, J. IUPAC-IUB Joint Commission on Biochemical Nomenclature (JCBN) Abbreviations and Symbols for the Description of Conformations of Polynucleotide Chains. *Nucleic Acids: The Vectors Of Life: Proceedings Of The Sixteenth Jerusalem Symposium On Quantum Chemistry And Biochemistry Held In Jerusalem, Israel, 2-5 May 1983*. pp. 559-565 (1983)
- [24] Barrows, S., Dulles, F., Cramer, C., French, A. & Truhlar, D. Relative stability of alternative chair forms and hydroxymethyl conformations of β -D-glucopyranose. *Carbohydrate Research*. **276**, 219-251 (1995)
- [25] Miyata, T. Reference interaction site model study on the anomeric equilibrium of D-glucose in aqueous solution. *Condensed Matter Physics*. (2007)
- [26] Park, S., Lee, J., Qi, Y., Kern, N., Lee, H., Jo, S., Joung, I., Joo, K., Lee, J. & Im, W. CHARMM-GUI Glycan Modeler for modeling and simulation of carbohydrates and glycoconjugates. *Glycobiology*. **29**, 320-331 (2019)
- [27] Jorgensen, W., Chandrasekhar, J., Madura, J., Impey, R. & Klein, M. Comparison of simple potential functions for simulating liquid water. *The Journal Of Chemical Physics*. **79**, 926-935 (1983)
- [28] Phillips, J., Hardy, D., Maia, J., Stone, J., Ribeiro, J., Bernardi, R., Buch, R., Fiorin, G., Hènin, J., Jiang, W. & Others Scalable molecular dynamics on CPU and GPU architectures with NAMD. *The Journal Of Chemical Physics*. **153**, 044130 (2020)
- [29] Guvench, O., Mallajosyula, S., Raman, E., Hatcher, E., Vanommeslaeghe, K., Foster, T., Jamison, F. & MacKerell Jr, A. CHARMM additive all-atom force field for carbohydrate derivatives and its utility in polysaccharide and carbohydrate-protein modeling. *Journal Of Chemical Theory And Computation*. **7**, 3162-3180 (2011)
- [30] Vanommeslaeghe, K., Hatcher, E., Acharya, C., Kundu, S., Zhong, S., Shim, J., Darian, E., Guvench, O., Lopes, P., Vorobyov, I. & Others CHARMM general force field: A force field for drug-like molecules compatible with the CHARMM all-atom additive biological force fields. *Journal Of Computational Chemistry*. **31**, 671-690 (2010)

- [31] Humphrey, W., Dalke, A. & Schulten, K. VMD: visual molecular dynamics. *Journal Of Molecular Graphics*. **14**, 33-38 (1996)
- [32] Lu, H. & Schulten, K. Steered molecular dynamics simulation of conformational changes of immunoglobulin domain I27 interpret atomic force microscopy observations. *Chemical Physics*. **247**, 141-153 (1999)
- [33] Bonomi, M., Branduardi, D., Bussi, G., Camilloni, C., Provasi, D., Raiteri, P., Donadio, D., Marinelli, F., Pietrucci, F., Broglia, R. & Others PLUMED: A portable plugin for free-energy calculations with molecular dynamics. *Computer Physics Communications*. **180**, 1961-1972 (2009)
- [34] Tribello, G., Bonomi, M., Branduardi, D., Camilloni, C. & Bussi, G. PLUMED 2: New feathers for an old bird. *Computer Physics Communications*. **185**, 604-613 (2014)
- [35] Williams, M., Marshall, A., Anjukandi, P. & Haverkamp, R. Investigation of the effects of fine structure on the nanomechanical properties of pectin. *Physical Review E*. **76**, 021927 (2007)
- [36] Cross, S., Kuttel, M., Stone, J. & Gain, J. Visualisation of cyclic and multi-branched molecules with VMD. *Journal Of Molecular Graphics And Modelling*. **28**, 131-139 (2009)
- [37] Rings, S. Conformational nomenclature for five and six-membered ring forms of monosaccharides and their derivatives. *European Journal of Biochemistry*. **100** pp. 295-298 (1980)
- [38] Marszałek, P. Short Review: Probing Mechanical Properties of Individual Molecules with Atomic Force Spectroscopy. *Prace Instytutu Elektrotechniki*, 7-24 (2018)
- [39] Lee, G., Nowak, W., Jaroniec, J., Zhang, Q. & Marszałek, P. Molecular dynamics simulations of forced conformational transitions in 1,6-linked polysaccharides. *Biophysical Journal*. **87**, 1456-1465 (2004)
- [40] Shen, T., Langan, P., French, A., Johnson, G. & Gnanakaran, S. Conformational flexibility of soluble cellulose oligomers: chain length and temperature dependence. *Journal Of The American Chemical Society*. **131**, 14786-14794 (2009)
- [41] Iglesias-Fernández, J., Raich, L., Ardévol, A. & Rovira, C. The complete conformational free energy landscape of β -xylose reveals a two-fold catalytic itinerary for β -xyylanases. *Chemical Science*. **6**, 1167-1177 (2015)
- [42] Cremer, D. & Pople, J. General definition of ring puckering coordinates. *Journal Of The American Chemical Society*. **97**, 1354-1358 (1975)
- [43] Csonka, G., Éliás, K. & Csizmadia, I. Relative stability of 1C_4 and 4C_1 chair forms of β -D-glucose: a density functional study. *Chemical Physics Letters*. **257**, 49-60 (1996)
- [44] Haverkamp, R., Williams, M. & Scott, J. Stretching single molecules of connective tissue glycans to characterize their shape-maintaining elasticity. *Biomacromolecules*. **6**, 1816-1818 (2005)

Chapter 6

- [1] Ojinnaka, C., Jay, A., Colquhoun, I., Brownsey, G., Morris, E. & Morris, V. Structure and conformation of acetan polysaccharide. *International Journal Of Biological Macromolecules*. **19**, 149-156 (1996)
- [2] Morris, V. Acetan—A new bacterial polysaccharide. *Biotechnology And Bioactive Polymers*. pp. 9-16 (1994)

- [3] Trecek, J., Dogsa, I., Accetto, T. & Stopar, D. Acetan-Like Polysaccharides: Genetics, Biosynthesis, Structure, and Viscoelasticity. *Polymers* 2021, 13, 815. (s Note: MDPI stays neutral with regard to jurisdictional claims in published . . . ,2021)
- [4] Paredes-López, O., Bello-Perez, L. & López, M. Amylopectin: Structural, gelatinisation and retrogradation studies. *Food Chemistry*. **50**, 411-417 (1994)
- [5] Thurn, A. & Burchard, W. Heterogeneity in branching of amylopectin. *Carbohydrate Polymers*. **5**, 441-460 (1985)
- [6] Mudgil, D. The interaction between insoluble and soluble fiber. *Dietary Fiber For The Prevention Of Cardiovascular Disease*. pp. 35-59 (2017)
- [7] Juhász, A., Greff, D., Teutsch, B., Gede, N., Hegyi, P., Horváth, E., Deák, P., Nyirády, P., Ács, N. & Juhász, R. Galactomannan is the most effective soluble dietary fiber in type 2 diabetes: a systematic review and network meta-analysis. *The American Journal Of Clinical Nutrition*. (2022)
- [8] Thakur, B., Singh, R., Handa, A. & Rao, M. Chemistry and uses of pectin—A review. *Critical Reviews In Food Science & Nutrition*. **37**, 47-73 (1997)
- [9] Willats, W., McCartney, L., Mackie, W. & Knox, J. Pectin: cell biology and prospects for functional analysis. *Plant Molecular Biology*. **47** pp. 9-27 (2001)
- [10] Shahidi, F., Arachchi, J. & Jeon, Y. Food applications of chitin and chitosans. *Trends In Food Science & Technology*. **10**, 37-51 (1999)
- [11] Su, L., Feng, Y., Wei, K., Xu, X., Liu, R. & Chen, G. Carbohydrate-based macromolecular biomaterials. *Chemical Reviews*. **121**, 10950-11029 (2021)
- [12] Cheng, K., Demirci, A. & Catchmark, J. Pullulan: biosynthesis, production, and applications. *Applied Microbiology And Biotechnology*. **92** pp. 29-44 (2011)
- [13] Ullah, M., Ul-Islam, M., Khan, T. & Park, J. Recent developments in the synthesis, properties, and applications of various microbial polysaccharides. *Handbook Of Hydrocolloids*. pp. 975-1015 (2021)
- [14] Zhang, Z., Ortiz, O., Goyal, R. & Kohn, J. Biodegradable polymers. *Handbook Of Polymer Applications In Medicine And Medical Devices*. pp. 303-335 (2014)
- [15] Luo, Z., Mu, X. & Zhang, Y. Biomaterials for bioprinting. *Bioprinting*. pp. 51-86 (2022)
- [16] Banerjee, S. & Bhattacharya, S. Food gels: gelling process and new applications. *Critical Reviews In Food Science And Nutrition*. **52**, 334-346 (2012)
- [17] Peesapati, S. & Roy, D. Control of anomericity and glycosidic linkage on the mechanics of polysaccharides. *Journal Of Chemical Sciences*. **135**, 32 (2023)
- [18] Park, S., Lee, J., Qi, Y., Kern, N., Lee, H., Jo, S., Joung, I., Joo, K., Lee, J. & Im, W. CHARMM-GUI Glycan Modeler for modeling and simulation of carbohydrates and glycoconjugates. *Glycobiology*. **29**, 320-331 (2019)
- [19] Jorgensen, W., Chandrasekhar, J., Madura, J., Impey, R. & Klein, M. Comparison of simple potential functions for simulating liquid water. *The Journal Of Chemical Physics*. **79**, 926-935 (1983)
- [20] Phillips, J., Hardy, D., Maia, J., Stone, J., Ribeiro, J., Bernardi, R., Buch, R., Fiorin, G., Hènin, J., Jiang, W. & Others Scalable molecular dynamics on CPU and GPU architectures with NAMD. *The Journal Of Chemical Physics*. **153**, 044130 (2020)

- [21] Guvench, O., Mallajosyula, S., Raman, E., Hatcher, E., Vanommeslaeghe, K., Foster, T., Jamison, F. & MacKerell Jr, A. CHARMM additive all-atom force field for carbohydrate derivatives and its utility in polysaccharide and carbohydrate–protein modeling. *Journal Of Chemical Theory And Computation*. **7**, 3162-3180 (2011)
- [22] Vanommeslaeghe, K., Hatcher, E., Acharya, C., Kundu, S., Zhong, S., Shim, J., Darian, E., Guvench, O., Lopes, P., Vorobyov, I. & Others CHARMM general force field: A force field for drug-like molecules compatible with the CHARMM all-atom additive biological force fields. *Journal Of Computational Chemistry*. **31**, 671-690 (2010)
- [23] Humphrey, W., Dalke, A. & Schulten, K. VMD: visual molecular dynamics. *Journal Of Molecular Graphics*. **14**, 33-38 (1996)
- [24] Bonomi, M., Branduardi, D., Bussi, G., Camilloni, C., Provasi, D., Raiteri, P., Donadio, D., Marinelli, F., Pietrucci, F., Broglia, R. & Others PLUMED: A portable plugin for free-energy calculations with molecular dynamics. *Computer Physics Communications*. **180**, 1961-1972 (2009)
- [25] Tribello, G., Bonomi, M., Branduardi, D., Camilloni, C. & Bussi, G. PLUMED 2: New feathers for an old bird. *Computer Physics Communications*. **185**, 604-613 (2014)
- [26] Williams, M., Marshall, A., Anjukandi, P. & Haverkamp, R. Investigation of the effects of fine structure on the nanomechanical properties of pectin. *Physical Review E*. **76**, 021927 (2007)
- [27] Cross, S., Kuttel, M., Stone, J. & Gain, J. Visualisation of cyclic and multi-branched molecules with VMD. *Journal Of Molecular Graphics And Modelling*. **28**, 131-139 (2009)
- [28] Peesapati, S., Sajeevan, K., Patel, S. & Roy, D. Relation between glycosidic linkage, structure and dynamics of α - and β -glucans in water. *Biopolymers*. **112**, e23423 (2021)
- [29] Pereira, C., Kony, D., Baron, R., Müller, M., Gunsteren, W. & Hünenberger, P. Conformational and dynamical properties of disaccharides in water: a molecular dynamics study. *Biophysical Journal*. **90**, 4337-4344 (2006)
- [30] Wormald, M., Petrescu, A., Pao, Y., Glithero, A., Elliott, T. & Dwek, R. Conformational studies of oligosaccharides and glycopeptides: complementarity of NMR, X-ray crystallography, and molecular modelling. *Chemical Reviews*. **102**, 371-386 (2002)
- [31] Marszałek, P. Short Review: Probing Mechanical Properties of Individual Molecules with Atomic Force Spectroscopy. *Prace Instytutu Elektrotechniki*, 7-24 (2018)
- [32] Marszalek, P., Li, H. & Fernandez, J. Fingerprinting polysaccharides with single-molecule atomic force microscopy. *Nature Biotechnology*. **19**, 258-262 (2001)

Chapter 7

- [1] Vatanpour, V., Gul, B., Zeytuncu, B., Korkut, S., İlyasoğlu, G., Turken, T., Badawi, M., Koyuncu, I. & Saeb, M. Polysaccharides in fabrication of membranes: A review. *Carbohydrate Polymers*. **281** pp. 119041 (2022)
- [2] Ferreira, A., Alves, V. & Coelho, I. Polysaccharide-based membranes in food packaging applications. *Membranes*. **6**, 22 (2016)
- [3] Freitas, F., Alves, V., Reis, M., Crespo, J. & Coelho, I. Microbial polysaccharide-based membranes: current and future applications. *Journal Of Applied Polymer Science*. **131** (2014)

Appendix A

Appendix

A.1 GROMACS input file

The following is a sample configuration file for **GROMACS NPT** simulations

```
integrator          = md
dt                 = 0.002
nsteps             = 1000000
nstxout            = 0
nstvout            = 0
nstfout           = 0
nstcalcenergy     = 5000
nstenergy         = 5000
nstlog            = 5000
cutoff-scheme     = Verlet
nstlist           = 20
rlist             = 1.2
coulombtype       = pme
rcoulomb          = 1.2
vdwtype          = Cut-off
vdw-modifier      = Force-switch
rvdw_switch       = 1.0
rvdw             = 1.2
compressed-x-grps = CARB
energygrps        = CARB SOL_ION
nstxout-compressed = 1000
compressed-x-precision = 1000
tcoupl            = Nose-Hoover
tc_grps           = CARB SOL_ION
tau_t            = 1.0 1.0
ref_t            = 310 310
pcoupl           = Parrinello-Rahman
pcoupltype       = isotropic
tau_p            = 2.0
compressibility   = 4.5e-5
ref_p            = 1.0
constraints       = h-bonds
constraint_algorithm = LINCS
continuation      = yes
nstcomm          = 100
comm_mode        = linear
comm_grps        = CARB SOL_ION
refcoord_scaling = com
```


A.2 NAMD input file

The following is a sample configuration file for **NAMD NPT** simulations

```
structure =step2_solvator.psf
coordinates =chitin_allignzaxis.pdb
set temperature =310
set outputname =chitin_r1
firsttimestep =10010000
binCoordinates = chitin_eq.restart.coor
binVelocities = chitin_eq.restart.vel
extendedSystem = chitin_eq.restart.xsc
paraTypeCharmm = on
parameters =par_all36_carb.prm
parameters =par_tip3p.prm
temperature =temperature
# Force-Field Parameters exclude
1-4scaling =1.0
cutoff =12
switching =on
switchdist =10
pairlistdist =14
# Integrator Parameters
timestep =2.0
rigidBonds =all
nonbondedFreq =1
fullElectFrequency =2
stepspercycle =10
# Constant Temperature Control
langevin =on
langevinDamping =5
langevinTemp =temperature
langevinHydrogen =off
#Periodic Boundary Conditions
cellBasisVector1 =30, 0, 0
cellBasisVector2 =0, 30, 0
cellBasisVector3 =0, 0, 150
cellOrigin = -0.218, -0.021, 0.069
wrapWater = on
wrapAll = on
wrapNearest = off
# PME (for full-system periodic electrostatics)
```

```
PME                =yes
PMEGridSizeX      = 30
PMEGridSizeY      =30
PMEGridSizeZ      =150
useGroupPressure  =no
useFlexibleCell    =no
useConstantArea   =no
outputName        =outputname
restartfreq        =1000000
dcdfreq           = 2000
xstFreq           =1000000
outputEnergies    = 2000
numsteps          =20000000
minimize          =10000
reinitvels        =temperature
```

A.3 SMD input file

The following is a sample configuration file for **SMD** simulations

```
structure           =acetan_allignzaxis_autopsf.psf
coordinates         = f6634.pdb
outputName         =acetan_s1
set temperature    =310
paraTypeCharmm     =on
parameters         =par_all36_carb.prm
parameters         =par_tip3p.prm
temperature        =$temperature
# Force-Field Parameters
exclude            =scaled1-4
1-4scaling         =1.0
cutoff             =12.0
switching          = on
switchdist        =10.0
pairlistdist       =13.5
# Integrator Parameters
timestep           = 1.0
rigidBonds         = all
nonbondedFreq     = 1
fullElectFrequency =2
stepspercycle      = 10
```

```
# Constant Temperature Control
langevin                = on
langevinDamping         = 1
langevinTemp            = $temperature
langevinHydrogen       = no
wrapWater               = on
wrapAll                 = on
wrapNearest             = off
#periodic boundary conditions CellBasisVector1 = 30, 0, 0
CellBasisVector2       = 0, 30, 0
CellBasisVector3       = 0, 0, 150
CellOrigin              = -0.2077, -0.0217, 0.0406
PME                     = yes
PMEGridSizeX           = 30
PMEGridSizeY           = 30
PMEGridSizeZ           = 150
# Output
binaryoutput           = no
# dcdfreq as tclfreq (50)
dcdfreq                = 2000
outputEnergies         = 2000
tclForces              = on
tclForcesScript        = smd_s1.tcl
minimize               = 2000
#run                   = 5000000
```

A.4 SMD tcl script

The following is a sample **TCL script** used for SMD simulations

```
# Atoms selected for force application
# "BH" is molecule name (probably "PEP" or "PROO")
set id1 [atomid CARB 15 O2]
set grp1
lappend grp1 $id1
set a1 [addgroup $grp1]
set id2 [atomid CARB 1 O2]
set grp2
lappend grp2 $id2
set a2 [addgroup $grp2]
# set the output frequency, initialize the time counter
```

```
set Tc1freq 2000
set t 0
# constraint points
# these should closely match actual positions.
# a13 gives a distance via VMD of 19.61
set c1x 22.26001
set c1y -2.73
set c1z -3.214
set c2x 12.926
set c2y 0.388
set c2z 14.454
# force constant (kcal/mol/A2)
set k 1
# pulling velocity (A/timestep)
set v 0.0001
set outfile s1_acetan_smd.out
open $outfile w
proc calcforces
global Tc1freq t k v a1 a2 c1x c1y c1z c2x c2y c2z outfile
# get coordinates
loadcoords coordinate
set r1 $coordinate($a1)
set r1x [lindex $r1 0]
set r1y [lindex $r1 1]
set r1z [lindex $r1 2]
set r2 $coordinate($a2)
set r2x [lindex $r2 0]
set r2y [lindex $r2 1]
set r2z [lindex $r2 2]
# calculate forces
set f1x [expr $k*($c1x-$r1x)]
set f1y [expr $k*($c1y-$r1y)]
set f1z [expr $k*($c1z-$r1z)]
lappend f1 $f1x $f1y $f1z
set f2x [expr $k*($c2x-$r2x)]
set f2y [expr $k*($c2y-$r2y)]
set f2z [expr $k*($c2z+$v*$t-$r2z)]
lappend f2 $f2x $f2y $f2z
# apply forces
addforce $a1 $f1
addforce $a2 $f2
```

```

# output
set foo [expr $t
if { $foo == 0 } {
set outfile [open $outfile a]
set time [expr $t*1/1000.0]
# MODIFIED to provide units in pN
# 1 kcal/mol A = 69.48 pN
# also because r1z is not 0.0, need to find true distance
puts $outfile "$time [expr $r2z - $r1z] [expr $f2z * 69.48]"
# puts $outfile "$time $r2z $f2z"
close $outfile
}
incr t
return
}

```

A.5 Matlab script for ‘big-box’ calculation

Following is the MATLAB script for **Big-Box** calculation

```

clc
clear
a      = importdata('r1_150_chdjoin_f1_100.txt');
b      = a.data;
c      = a.textdata;
d      = load('chd100_nojoin_f1_100.dat');
q      = importdata('line1.txt');
r      = importdata('line2.txt');
q1     = q.textdata;
r1     = r.textdata;
l1     = table2cell(table(q1,186300,186300,186300));
l2     = table2cell(table(r1,2,2,2));
frames_all = [ ]
for i   = 1:100
e(1,1) = d(i,5)-d(i,2);
e(1,2) = d(i,6)-d(i,3);
e(1,3) = d(i,7)-d(i,4);
t      = (i-1)*6900+1;
disp(i)
c1     = c(t:t+6899,:);

```

```

    coor    = b(t:t+6899,:);
    c_xp    = [ ];
    c_xn    = [ ];
    c_yp    = [ ];
    c_yn    = [ ];
    c_zp    = [ ];
    c_zn    = [ ];
    for k    = 1:6900
    xp      = coor(k,1)+e(1,1);
    xn      = coor(k,1)-e(1,1);
    yp      = coor(k,2)+e(1,2);
    yn      = coor(k,2)-e(1,2);
    zp      = coor(k,3)+e(1,3);
    zn      = coor(k,3)-e(1,3);
    c_xp    = vertcat(c_xp,xp);
    c_xn    = vertcat(c_xn,xn);
    c_yp    = vertcat(c_yp,yp);
    c_yn    = vertcat(c_yn,yn);
    c_zp    = vertcat(c_zp,zp);
    c_zn    = vertcat(c_zn,zn);
    end
    xyz     = table2cell(table(c1,coor(:,1),coor(:,2),coor(:,3)));
    xpyz    = table2cell(table(c1,c_xp,coor(:,2),coor(:,3)));
    xnyz    = table2cell(table(c1,c_xn,coor(:,2),coor(:,3)));
    xypz    = table2cell(table(c1,coor(:,1),c_yp,coor(:,3)));
    xynz    = table2cell(table(c1,coor(:,1),c_yn,coor(:,3)));
    xyzp    = table2cell(table(c1,coor(:,1),coor(:,2),c_zp));
    xyzn    = table2cell(table(c1,coor(:,1),coor(:,2),c_zn));
    xpypz   = table2cell(table(c1,c_xp,c_yp,coor(:,3)));
    xpynz   = table2cell(table(c1,c_xp,c_yn,coor(:,3)));
    xnypz   = table2cell(table(c1,c_xn,c_yp,coor(:,3)));
    xnynz   = table2cell(table(c1,c_xn,c_yn,coor(:,3)));
    xpyzp   = table2cell(table(c1,c_xp,coor(:,2),c_zp));
    xpyzn   = table2cell(table(c1,c_xp,coor(:,2),c_zn));
    xnyzn   = table2cell(table(c1,c_xn,coor(:,2),c_zn));
    xnyzp   = table2cell(table(c1,c_xn,coor(:,2),c_zp));
    xypzp   = table2cell(table(c1,coor(:,1),c_yp,c_zp));
    xypzn   = table2cell(table(c1,coor(:,1),c_yp,c_zn));
    xynzn   = table2cell(table(c1,coor(:,1),c_yn,c_zn));
    xynzn   = table2cell(table(c1,coor(:,1),c_yn,c_zn));
    xynzp   = table2cell(table(c1,coor(:,1),c_yn,c_zp));

```

```

xnynzn    = table2cell(table(c1,c_xn,c_yn,c_zn));
xpypzp    = table2cell(table(c1,c_xp,c_yp,c_zp));
xnypzp    = table2cell(table(c1,c_xn,c_yp,c_zp));
xnynzp    = table2cell(table(c1,c_xn,c_yn,c_zp));
xnypzn    = table2cell(table(c1,c_xn,c_yp,c_zn));
xpypzn    = table2cell(table(c1,c_xp,c_yp,c_zn));
xpynzp    = table2cell(table(c1,c_xp,c_yn,c_zn));
xpynzn    = table2cell(table(c1,c_xp,c_yn,c_zp));
frames_all = vertcat(l1,l2,xyz,xpyz,xnyz,xypz,xynz,xyzp,xyzn,
                    =xpypz,xpynz,xnypz,xnynz,xpyzp,xpyzn,xnyzn,xnyzp,
                    =xypzp,xypzn,xynzn,xynzp,xnynzn,xpypzp,xnypzp,xnynzp,
                    =xnypzn,xpypzn,xpynzp,xpynzn);

writecell(frames_all,'chd100_joinchd_bb_f1_100.txt','WriteMode','append','Delimiter',' ',' ')

end

```

A.6 Coordination number calculation

Following is the MATLAB script for the calculation of coordination number of every bile acid and extraction of highest coordinate in a frame.

```

clc
clear
a          = load('chd100_joinchd_bb_c24.xyz');
alldist    = [];
allmatrix  = [];
coordallframe = [];
for i      = 1620001:2700:2430000
disp(i)
b          = a(i:i+2699,:);
alldist_perframe = [];
for j      = 1:2700
d          = [];
for k = 1:2700
x = b(j,1)-b(k,1);
y = b(j,2)-b(k,2);
z = b(j,3)-b(k,3);
dist = x2 + y2 + z2;

```



```
c = sqrt(dist);
d = vertcat(d,c);
end
alldist_perframe = horzcat(alldist_perframe,d);
end
for row = 1:2700;
for column =1:2700;
if alldist_perframe(row,column) ≤ 40;
e(row,column) = 1 ;
else
e(row,column) = 0 ;
end
end
end
allmatrix = vertcat(allmatrix,e);
sum_frame = [ ] ;
for f = 1:2700 ;
sum1 = 0 ;
for g = 1:2700 ;
sum1 = sum1 + e(f,g) ;
end
sum_frame = vertcat(sum_frame,sum1);
end
alldist = vertcat(alldist,alldist_perframe);
coordallframe = horzcat(coordallframe,sum_frame);
end
csvwrite('chd100_bb_alldist3.csv',alldist)
csvwrite('chd100_bb_coordination_allframes3.csv',coordallframe)
maxvalx = idx ;
csvwrite('chd100_bb_idx3.csv',idx);
csvwrite('chd100_bb_all_matrix3.csv',allmatrix) ;
% to get the maximum cluster in a given frame
max_coord = max(coordallframe) ;
csvwrite('chd100_bb_max_coord3.csv',max_coord)
% to get the average cluster coordination per frame
% avg_coord = sum(coordallframe)/100 ;
% csvwrite('chd100_bb_avg_coord.csv',avg_coord);
%repeation of each cluster size
% s1 = reshape(coordination_allframes,1,750100);
% int = 0.5
% gyrat_min=min(s1);
```

```
% gyrat_max=max(s1);
% bin=gyrat_min:int:gyrat_max
% k=hist(s1,bin)
% plot(bin,k)
```

A.7 Radius of gyration of the biggest cluster

Following is the MATLAB code for calculation of **Radius of gyration** of the biggest cluster

```
clc
clear
for i          = 1:100
    maxcoord(i) = 1;
end
coor_allframe1 = load('f7496_onlycoord.xyz');
rg             = [ ];
g             = load("chd_mass.xvg");
eigval_allframe = [ ];
for k3        = 1:2700:4050000;
    disp(k3)
    mass_all   = [ ];
    coor_all   = [ ];
    for t      = k3:k3+99;
        s     = t-1;
        m     = [ ];
        coor  = [ ];
        if maxcoord(t) == 1
            m   = g(1:69) ;
            coor = coor_allframe1(69*s+1:69*s+69,:);
        else
            m1  = 0;
        end
        mass_all = vertcat(mass_all,m);
        coor_all = vertcat(coor_all,coor);
    end
    xcg_allframe = [ ];
    ycg_allframe = [ ];
    zcg_allframe = [ ];
    mt           = sum(mass_all);
```

```

xcg = sum(mass_all.*coor_all(:,1))/mt;
ycg = sum(mass_all.*coor_all(:,2))/mt;
zcg = sum(mass_all.*coor_all(:,3))/mt;

                                ig = [0, 0, 0;
                                        0, 0, 0;
                                        0, 0, 0];
                                (A.1)

```

```

w      = size(coor_all);
for i7 = 1:w(1,1) ;
x_1    = coor_all(i7,1) - xcg ;
y_1    = coor_all(i7,2) - ycg ;
z_1    = coor_all(i7,3) - zcg ;
m_1    = mass_all(i7);

    ig = ig + m_1 * ((z_1).^2 + (y_1).^2), -m_1 * x_1 * y_1, -m_1 * x_1 * z_1;
        - m_1 * y_1 * x_1, m_1 * ((z_1).^2 + (x_1).^2), -m_1 * y_1 * z_1;
        - m_1 * z_1 * x_1, -m_1 * y_1 * z_1, m_1 * ((y_1).^2 + (x_1).^2);
                                (A.2)

```

```

end
ee      = eig(ig);
ee_rg   = sqrt(sum(ee(:,1))/mt);
eigval_allframe = horzcat(eigval_allframe, ee);
rg      = vertcat(rg, ee_rg);
end

```

A.8 Scattering profile calculation

```

clc
clear
% load the gofr values of cc,oo and co combination
gofr_cc = load('f1_100/out_CC_cutoff60');
gofr_oo = load('f1_100/out_OO_cutoff60');
gofr_co = load('f1_100/out_CO_cutoff60');
x = (0.25:0.5:60.25)'% for bw05;
%coefficients are taken from Acta Cryst. (1995). A51,416-431
ca = [2.657506,1.078079,1.490909,-4.241070,0.713791];
cb = [14.780756,0.776775,42.086843,-0.000294,0.239533];
cc = 4.297983;

```

```

oa = [2.960427,2.508818,0.637853,0.722838,1.142756];
ob = [14.182259,3.936858,0.112726,34.95844,0.390240];
oc = 0.027014;

s_q = [ ]
for q = 0.01:0.01:2
s = q/(4*pi);
t = s*s;
%scattering factor for c,o
s_f_c = 0 ;
s_f_o = 0 ;
for i = 1:5
f_c = ca(:,i)*exp(-(cb(:,i))*t);
s_f_c = s_f_c + f_c ; %sum of all exponents
f_o = oa(:,i)*exp(-(ob(:,i))*t);
s_f_o = s_f_o + f_o ;
end
sum_f_c = s_f_c + cc ; %sum of exponents plus constant c
sum_f_o = s_f_o + oc ; %q value for each value of r
q4 = [ ] ;
for r=1:121
a1 = (0.352*0.352)*(sum_f_c*sum_f_c)*(gofr_cc(r,2)-1);
a2 = (0.0735*0.0735)*(sum_f_o*sum_f_o)*(gofr_oo(r,2)-1);
a3 = (0.352*0.0735)*(sum_f_o*sum_f_c)*(gofr_co(r,2)-1);
a = a1 + a2 + a3;
aa = sin(q*gofr_cc(r,1)) ;
q1 = aa*(gofr_cc(r,1)*gofr_cc(r,1))*a/(q*gofr_cc(r,1));
q4 = vertcat(q4,q1);
end
q2 = trapz( x,q4);
q3 = (0.352*pow2(sum_f_c)) + (0.0735*pow2(sum_f_o)) + (4*pi*7.562*0.001*q2) ;
s_q = vertcat(s_q,q3)
end
csvwrite('ca100_f1_100.csv',s_q)

```

List of Publications

1. **Peesapati, S.** & Roy, D. Control of anomericity and glycosidic linkage on the mechanics of polysaccharides. *Journal Of Chemical Sciences.* **135**, 32 (2023)
2. **Peesapati, S.** & Roy, D. Structural and spectroscopic details of polysaccharide–bile acid composites from molecular dynamics simulations. *Journal Of Biomolecular Structure And Dynamics.* pp. 1-13 (2022)
3. **Peesapati, S.**, Sajeevan, K., Patel, S. & Roy, D. Relation between glycosidic linkage, structure and dynamics of α -and β -glucans in water. *Biopolymers.* **112**, e23423 (2021)
4. **Peesapati, S.** & Roy, D. Structural and Dynamical Disparity in D-Glucopyranose Oligomers Having Diverse Glycosidic Linkages. *Proceedings Of International Conference On Drug Discovery (ICDD).* (2020)

List of Conferences

1. **Peesapati, S.** and Roy D. “Effect of Anomericity and Glycosidic Linkage on Polysaccharide Mechanics.” Convergence of Chemistry and Materials, 2023, Birla Institute of Technology and Science, Hyderabad.
2. **Peesapati, S.** and Roy D. “Effect of Anomericity and Glycosidic Linkage on Polysaccharide Mechanics.” ,Molecular Materials and Functions, 2022, Indian Institute of Technology, Madras .
3. **Peesapati, S.** and Roy D. “Molecular Modelling, Simulations and Principal Component Analysis of Linear 1→3,1→4,1→6 β -Glucans.” International Conference on Drug Discovery (ICDD), 2020, Birla Institute of Technology and Science, Hyderabad.
4. **Peesapati, S.** and Roy D. “Computer-Aided drug discovery and Biologics.” 2019, Schrodinger, Bangalore.
5. **Peesapati, S.** and Roy D. “Molecular Dynamic Simulations of α and β -glucans.” Indian Peptide Symposium (IPS), 2019, Birla Institute of Technology and Science, Hyderabad.

Biography

Brief Biography of the Candidate

Sruthi Peesapati is a Ph.D. Scholar in the Department of Chemistry, Birla Institute of Science and Technology, Pilani, Hyderabad Campus since August 2018. She is guided by Prof. Durba Roy. She has explored the structural, dynamical and mechanical aspects of α, β glucans during her Ph.D. tenure. She has done Integrated MSc in General Chemistry (2012 - 2017) from University of Hyderabad (UOH), Hyderabad. She has worked on 'Potential Energy Surface and Topographical Features of Few Bimolecular Reactive Systems and State-to-State Dynamics Study of H-exchange Reaction' in MSc Project, in UOH, Hyderabad, under the guidance of Prof. Susanta Mahapatra.

Brief Biography of the Supervisor

Prof. Durba Roy is an Associate Professor at the Department of Chemistry, Birla Institute of Technology and Science-Pilani, Hyderabad Campus. She completed her PhD under the supervision of Professor Kankan Bhattacharyya from the Indian Association for the Cultivation of Science (IACS), Kolkata in 2008. Her Ph.D. work was based on ultrafast chemical dynamics involving laser induced fluorescence spectroscopy. After completing her doctoral research, she joined Pennsylvania State University, USA, as a postdoctoral researcher to work under the supervision of Professor Mark Maroncelli, Department of Chemistry (2009-2011), where she learned how to create realistic simulation models of complex liquids and organized assemblies. She worked for a year (2011 - 2012) with Professor Tamar Schlick at New York University to learn Chromatin Folding simulations using Monte Carlo technique. Currently, her research interest revolves around structure, function, dynamics and mechanical properties of polysaccharides, bile acids and proteins and to compare the results obtained from simulations with that of experiments.